ROLES OF MYOPODIN IN ACTIN CYTOSKELETON REMODELING AND CANCER CELL MIGRATION

by

FuiBoon Kai

Submitted in partial fulfilment of the requirements
for the degree of Doctor of Philosophy

at

Dalhousie University
Halifax, Nova Scotia
March 2013

DALHOUSIE UNIVERSITY

DEPARTMENT OF MICROBIOLOGY AND IMMUNOLOGY

The undersigned hereby certify that they have read and recommend to the Faculty of Graduate Studies for acceptance a thesis entitled "ROLES OF MYOPODIN IN ACTIN CYTOSKELETON REMODELING AND CANCER CELL MIGRATION" by FuiBoon Kai in partial fulfilment of the requirements for the degree of Doctor of Philosophy.

Date: 27 March 2013

External Examiner: _____

Research Supervisor: _____

Examining Committee: _____

_____

_____

Departmental Representative: _____

DALHOUSIE UNIVERSITY

DATE: 27 March 2013

AUTHOR: FuiBoon Kai

TITLE: ROLES OF MYOPODIN IN ACTIN CYTOSKELETON REMODELING AND CANCER CELL MIGRATION

DEPARTMENT OR SCHOOL: Department of Microbiology and Immunology

DEGREE: PhD CONVOCATION: May YEAR: 2013

_____

Signature of Author

WRITTEN IN MEMORY OF

MY BELOVED FATHER

TIENSIAK KAI

(1948-1999)

&

BROTHER

HEEHOW KAI

(1981-2002)

TABLE OF CONTENTS

LIST OF TABLES

LIST OF FIGURES

ABSTRACT

Loss of myopodin expression correlates with the transition from indolent to metastatic prostate cancer. However, the mechanisms underlying this correlation and the roles of myopodin in normal cell function have not been determined. Contradictory findings on whether myopodin suppresses or promotes prostate cancer cell migration, and the recent identification of different myopodin isoforms further complicate our understanding of myopodin function. To address these deficits, I ectopically expressed the five different myopodin isoforms in PC3 prostate cancer cells. Transwell migration and invasion assays indicated myopodin isoforms alter the response of PC3 cells to different external stimuli, either increasing or decreasing cell migration depending on the stimulus while having little direct affect on cell invasion. Under the same external stimulus, myopodin isoforms differentially induced and colocalized with distinct actin structures in the cell body. Impairing formation of these myopodin-induced actin structures inhibited myopodin-stimulated cell migration. Subsequent studies revealed that myopodin expression increases RhoA activation, and the actin structures, tail retraction and enhanced cell migration associated with myopodin expression were all diminished by inhibiting the Rho/ROCK pathway. Although non-muscle myosin II (NMII) is a downstream effector of RhoA and is essential for cell migration, inhibiting NMII had no affect on myopodin-enhanced cell migration. Interfering with NMII activity did, however, inhibit the appearance of actin bundles in the cell body of myopodin-expressing cells. Timecourse analysis using serum-starvation to synchronize cells and inhibitors of Arp2/3 complexes and NMII indicated myopodin promotes Arp2/3-dependent lamellipodia formation and Arp2/3-independent actin bundle formation, and myopodin colocalizes with the actin fibers in these protrusions. The formation of lamellipodia and filopodia by myopodin does not require NMII-dependent FA maturation but myopodin does, either directly or indirectly, promote formation of FAs. Live cell imaging further showed the actin fibers generated in the protrusions are subsequently integrated into the stress fibers in the cell body by NMII contraction. Thus, myopodin enhances cell migration by stimulating actin bundle formation at the leading cell edge resulting in the formation of membrane protrusions and FA formation, and the prominent actin bundles formed within the cell body are an incidental effect of myosin contraction.

LIST OF ABBREVIATIONS USED

Abi	Abl interactor 1
ABP	Actin-binding protein
ADP	Adenosine diphosphate
ARP2/3	Actin-related protein 2/3
ATP	Adenosine triphosphate
ATPase	Adenosine triphosphatase
BPH-1	Benign prostatic hyperplasia
BSA	Bovine serum albumin
CaMKII	Ca^{2+}/calmodulin-dependent kinase II
C_c	Critical concentration
CFP	Cyan fluorescent protein
CH-ILKBP	Calponin-homology-domain-containing ILK-binding protein
CM	Conditioned medium
CP	Capping protein
CRIB	Cdc42/Rac interactive binding
DAD	Diaphanous autoregulatory domain
DAPI	4′, 6-diamidino-2-phenylindole
DID	Diaphanous inhibitory domain
DTT	Dithiothreitol
ECL	Enhanced chemiluminescent
ECM	Extracellular matrix
FA	Focal adhesion
F-actin	Filamentous actin
FAK	Focal adhesion kinase
FBS	Fetal bovine serum
FH	Formin homology
FMNL	Formin-like
FRET	Fluorescent resonance energy transfer
G-actin	Globular actin

GAP	GTPase activating protein
GBD	GTPase binding domain
GDP	Guanine diphosphate
GEF	Guanine nucleotide exchange factor
GFP	Green fluorescent protein
GTP	Guanine diphosphate
H_20	Water
HRP	Horseradish peroxidase
ILK	Integrin-linked kinase
INF	Inverted formin
IRSp53	Insulin receptor substrate p53
LB	Luria-Beranti
LIMK	LIM domain kinase
RLC	Regulatory light chain
Mena	Murine enabled
mDia	Mammalian Diaphanous
MHC	Myosin heavy chain
MLCK	Myosin light chain kinase
MMP	Metalloproteinase
MYO	Myopodin
NM II	Non-muscle myosin II
NPF	Nucleation promoting factor
ORF	Open reading frame
PAGE	Polyacrylamide gel electrophoresis
PBD	p21-binding domain
PBS	Phosphate-buffered saline
PC	Prostate cancer
PCR	Polymerase chain reaction
PEI	Poly(ethylenimine)
PINCH	Particularly interesting new cysteine-histidine-rich protein
PKA	Protein kinase A

PSA	Prostate-gland-specific antigen
PVDF	Polyvinylidene difluoride
RFP	Red fluorescent protein
RBD	Rho binding domain
RIPA	Radioimmunoprecipitation assay buffer
ROCK	Rho-associated protein kinase
RT-PCR	Reverse transcription polymerase chain reaction
SD	Standard Deviation
SDS	Sodium dodecyl sulphate
SEM	Standard error of the mean
TBS	Tris-buffered saline
TM4	Tropomyosin-4
UTR	Untranslated region
VASP	Vasodilator-stimulated phosphoprotein
WASP	Wiskott–Aldrich syndrome protein
WAVE	Wiskott–Aldrich syndrome protein family Verprolin-homologous
WH2	Wiskott–Aldrich syndrome protein-homology 2
YFP	Yellow fluorescent protein

ACKNOWLEDGEMENTS

I am deeply indebted to my mother, SiatYuen Chong, for her constant strength and support. She has always believed in my decisions and done everything possible to enable me to realize my dreams. She held our family together through tough times and never let me give up. A young daughter could have no better role model. I also thank my brother, HeeSin Kai, who always makes me smile and has helped to support me in a foreign country and my family back home for all these years. Without the support of my family nothing I have accomplished would have been possible.

I thank my supervisor, Dr. Roy Duncan, who encouraged me endlessly and had the faith in me to let me to pursue a project that diverged from the core areas of the lab. He always challenges me to look at things differently and delves deeply into my results. My projects would have surely stalled without his critical eye. I also want to thank Roy for his tireless editing and presentation suggestions. I believe my communication skills have improved enormously under his tutelage.

I thank Kaitlyn Tanner and Caroline King, my two summers/co-op students. Without these two talented young scientists it would have been impossible for me to have success. I wish them luck in their futures and hope that they can forgive me for all the late nights and weekends.

I would like to thank all my committee members, Dr. Craig McCormick, Dr. Catherine Too, and Dr. Graham Dellaire. This group provided many useful suggestions and coaxed me to get organized at least twice a year. I also want to acknowledge Dr. Dellaire who identified the MYO4 isoform, and Dr. James Fawcett, who trained and assisted me in the use of his confocal microscope. I thank the trainee awards received from the Beatrice Hunter Cancer Research Institute with funds provided by The Terry Fox Foundation Strategic Health Research Training Program in Cancer Research at CIHR. I also thank all Duncan lab members, especially Dr. Roberto de Antueno, JingYun Shou, and Nichole McMullen. Roberto always seemed to have a tool or protocol stuffed in his drawers that he would pull out to help me troubleshoot an experiment. I thank JingYun and Nichole, our past and current lab managers, for tolerating my frequent, and often last minute, purchase requests. I also thank the balance of the Duncan lab (Marta, Hiren, Tim, Jolene, and Nandini), who have been great friends in and outside the lab.

Finally, I would like to thank my husband Dr. Andrew Leidal. He has always been there for me at work and home. Thank you for making me laugh and learning to embrace Thai chilies in everything we eat. He is by far the best lab partner I have ever had. To all aforementioned people, my PhD would never have been possible without you.

CHAPTER 1: INTRODUCTION

1.1. Overview And Rationale

Prostate cancer is the most commonly diagnosed cancer and the second leading cause of cancer death among North American men. Cancer metastasis is generally associated with poor clinical outcome and is the major cause of cancer-related death. Therefore, patients diagnosed with prostate cancer usually proceed immediately with invasive treatments as a precaution against developing aggressive tumors. However, the diagnostic tool for prostate cancer, the prostate gland specific antigen (PSA) assay, has a false positive rate of 75% and does not provide an indication of the metastatic potential of prostate cancer (Schroder et al., 2009). As the vast majority of prostate cancer cases remain indolent and do not display clinical symptoms during their lifetime, the patient's quality of life is often compromised by over-diagnosis and over-treatment (Schroder et al., 2009). A ten-year follow-up study of prostate cancer patients also revealed that radical prostatectomy does not reduce mortality rate, as compared with watchful waiting (Wilt et al., 2012). Patients undergoing watchful waiting also suffer from the risks of developing metastatic prostate cancers. Hundreds of tissue biomarkers, such as Ki67 and BCL2, have been identified but none are reliable to help patients make informed decisions about their treatment selections (Kachroo and Gnanapragasam, 2013). Therefore, it is crucial to identify a reliable prognosticator that can predict the metastatic potential of prostate cancer.

Myopodin was recently identified as such an invasive prostate cancer biomarker. As compared to non-invasive prostate cancer cases, metastatic cancer cells frequently have decreased myopodin expression levels. A genome-wide screen discovered that more than 80% of invasive prostate cancer cases contain partial or complete deletion of the myopodin gene but only 7% of minimally invasive tumors contain such deletions (Lin et al., 2001). Furthermore, a complete loss of myopodin expression also correlates with a significantly elevated clinical relapse rate of 86% (Yu et al., 2006). Besides prostate cancer, myopodin has also been implicated in other cancer types. For example, hypermethylation-dependent silencing of myopodin expression is strongly correlated with the poor clinical outcome of bladder and colorectal cancers (Cebrian et al., 2008; Esteban et al., 2012). These clinical studies strongly suggest that myopodin could be a reliable

prognosticator of invasive cancers. Although a strong inverse correlation is found between myopodin expression and cancer aggressiveness, few studies have attempted to determine how myopodin influences tumor development. My Ph.D. research was therefore focused on determining the role of myopodin in cellular processes and tumorigenesis.

To understand how myopodin regulates cancer metastasis, it is important to understand the factors that affect the invasive properties of cancer cells. Although the genetic profiles of cancer cells from a tumor or different cancer types are very diverse, the cellular and molecular steps of cancer metastasis are relatively similar (Bogenrieder and Herlyn, 2003). Disseminating cancer cells digest the extracellular matrix surrounding tissues, intravasate into the blood circulation, extravasate into another organ, and establish themselves at a distant site. Several key transforming or mesenchymal traits need to be acquired by malignant cancer cells prior to intravasation, including the loss of cell-cell contact, increased proliferation, elevated matrix metalloproteinase (MMP) expression, and increased cell motility. Recent reports showed that myopodin affects some of these traits, including cell proliferation, cell-cell adhesion, cell motility, and invasion (De Ganck et al., 2009; Jing et al., 2004; Yu and Luo, 2006). Ectopic expression of myopodin suppresses invasive PC3 prostate cancer cell proliferation, invasion and colony formation *in vitro*, and it decreases prostate tumor growth, metastasis and mortality in xenografted SCID mice (Jing et al., 2004). These findings are consistent with a tumor suppressor role for myopodin. Perplexingly, siRNA knockdown studies of myopodin suggested otherwise, with downregulation of myopodin expression enhancing PC3 cell adhesion, motility, and invasion (De Ganck et al., 2009), suggesting that myopodin may function as a tumor promoter. These contradictory results highlight a possibly complex role for myopodin in tumorigenesis.

In addition to the prostate cancer studies, myopodin was also discovered as a differentiation-dependent actin-binding protein in murine muscle cells (Weins et al., 2001). The actin cytoskeleton network is an important structural and functional system within eukaryotic cells involved in a diverse range of activities that affect such processes as maintaining cell morphology, cell-cell adhesion, motility, and protein trafficking. To perform these distinct duties, other actin regulator or actin-binding proteins (ABPs) are

required to modulate the functions of actin in a cell. Cell motility is a critical determinant of cancer cell metastasis, driven mainly by the highly regulated rearrangement of the actin cytoskeleton. In recent years, evidence in support of the roles of ABPs in tumor invasion has also been accruing. Since the actin cytoskeleton is such an important factor in cell migration, I was interested in determining whether human myopodin, like its murine counterpart, binds to actin and regulates cytoskeletal dynamics, and if so whether this actin-regulatory activity of myopodin contributes to cancer cell migration and invasion.

Before describing what is known about myopodin and how it might be involved in the complicated pathways that affect actin cytoskeleton remodeling, I will first provide some background on the pathways and ABPs that control rearrangement of the actin cytoskeleton during cell migration. Of note, other than the actin regulators and ABPs mentioned below, many other proteins are important for actin cytoskeleton remodeling and cell migration. For instance, microtubules are another component of the cytoskeleton and are as dynamic as the actin cytoskeleton during cell migration. Crosstalk between the pathways regulating microtubules and the actin regulators are also essential to maintain directional cell migration (Kaverina and Straube, 2011). However, as myopodin is an actin-binding protein, I will focus on how myopodin may regulate cancer metastasis from the actin cytoskeleton perspective.

1.2. Actin-Rich Compartments And Actin Cytoskeleton Remodelling In Migrating Cells

The actin cytoskeleton is part of the molecular machinery that drives cell migration, an important process that regulates diverse cellular activities, such as embryogenesis, wound repair, cell division, and immune responses. Diverse ABPs or actin regulators are designated to orchestrate actin cytoskeleton rearrangement. Generally, cells in migration mode display a fan-like shape that is composed of actin-rich cellular compartments (Fig. 1). For simplification, I divided a fan-shaped migrating cell into three actin-rich compartments: (1) the lamellipodium, a region of protruding membrane at the leading cell edge that also contains smaller membrane protrusions such

as filopodia; (2) the lamellum; and (3) the rest of the cell that includes the cell body and trailing end.

1.2.1. Membrane Protrusions

Membrane protrusions at the leading edge of a migrating cell are composed of the lamellipodium, the lamellum, and filopodia (Fig. 1A & B; grey box a). The lamellopodium is a broad, sheet-like membrane extension at the leading edge of a migrating cell. The actin cytoskeleton within this region is very dense and is present as either a highly branched actin network or linear actin bundles (Abercrombie et al., 1970; Small, 1981). The dendritic or branched actin network is formed in a very organized manner. Newly-synthesized F-actin is polymerized at a 70° branching angle from the pre-existing F-actin, with the assistance of an actin nucleator, the actin-related protein 2/3 (Arp2/3) complex (Mullins et al., 1998). Arp2/3 complexes bind to the sides of pre-existing actin microfilaments and initiate nucleation of new F-actin filaments on the sides of the "mother" filaments. Embedded within the branched actin network, linear F-actin bundles are arranged perpendicular to the leading edge. When the linear F-actin bundles protrude out of the lamellipodium, the membrane extensions are called filopodia. Filopodia are rod-shaped protrusions filled with parallel F-bundles that function as exploratory probes to sense the microenvironment of the cell. The linear F-actin bundles are polymerized by a subset of formin family proteins, another type of actin nucleators (Yang et al., 2007). The actin nucleators, the Arp2/3 complex and the formin family of proteins, will be discussed in detail later in section 1.2.6.

The lamellum is located immediately behind the lamellipodium and is sometimes considered as a chronologically older part of the lamellipodium (Fig. 1A & B; grey box a). Recent studies demonstrate that the actin network within the lamellum is biochemically, kinetically, and functionally different from that in the lamellipodium (DesMarais et al., 2002; Ponti et al., 2004). Lamellipodia are enriched with Arp2/3 complexes but little, if any, Arp2/3 is detected in the lamellum. Instead, the lamellum is enriched with tropomyosin, a filamentous actin-binding protein. Tropomyosin binding to the actin cytoskeleton prevents Arp2/3 dendritic nucleation (Blanchoin et al., 2001) and promotes the recruitment of myosin motor proteins to the actin bundles (Tojkander et al.,

2011). Therefore, rather than having a branched actin network, the lamellum is filled with mostly linear actin bundles that are crosslinked by myosin and lie perpendicular or parallel to the membrane. The actin bundles are also called stress fibers or actomyosin bundles and a more detailed description of these actin structures will be discussed later in section 1.2.12. Assembly and disassembly of the actin network in the lamellum is less dynamic than what occurs in lamellipodia as tropomyosin functions to stabilize and prevent the depolymerization of actin microfilaments (Tojkander et al., 2011). Productive cell advancement requires both a functional lamellipodium and the lamellum that play distinct yet interrelated roles in cell migration. The lamellipodium is important for random membrane protrusions and retractions while the lamellum is required to maintain the persistent advancement of cells (Giannone et al., 2007; Ponti et al., 2004).

1.2.2. Cell Body and Cell Rear.

The compartment located behind the lamellum is considered as the cell body and the trailing end (Fig. 1A & B; grey box b). The cell body comprises the nucleus, organelles, and relatively stable, linear actin cytoskeleton networks. Actin microfilaments within this region are also crosslinked by myosin motor proteins but the actin fibers are much thicker than those present at the leading edge. Myosin motor contractions in the cell body translocate the cell body immediately after the membrane protrusions. The cell rear is tethered to the substratum via adhesion structures called mature focal adhesions. While the cell front is moving, the cell rear needs to catch up. Myosin contraction produces mechanical tension and drives tail retraction (Crowley and Horwitz, 1995). In addition, proteolytic cleavage of the mature adhesion structures by calpain or actin depolymerization also helps to retract the cell rear (Huttenlocher et al., 1997; Mseka and Cramer, 2011). If the cell rear fails to detach, the posterior part of the cell appears as a drawn-out tail. As tail retraction is one of the key steps in cell movement, tail retraction defects can impair cell migration. Interestingly, recent studies demonstrated that tail retraction in fish keratinocytes may not be the consequence, but instead the cause, of membrane protrusions. Fluorescent speckle microscope analysis showed that the first sign of front-rear polarity, the increased centripetal flow of filamentous actin towards the

prospective axis of movement, is observed at the prospective cell rear and perinuclear region, followed by membrane protrusions at the leading edge (Yam et al., 2007).

1.2.3. G-actin and F-actin

The building block of the cytoskeleton is monomeric globular actin (G-actin), which self-associates and polymerizes into double helical filamentous actin (F-actin) (Revenu et al., 2004; Wegner, 1976). F-actin is in turn rapidly depolymerized. The balance between actin polymerization and depolymerization allows the dynamic remodeling of the actin cytoskeleton during cell migration. F-actin polymerization begins with a rate-limiting lag phase, in which G-actin dimerizes or trimerizes to form an actin nucleus. These small actin nuclei are thermodynamically unstable and tend to disassemble. Stabilization of these nuclei is therefore important for F-actin elongation, which occurs asymmetrically. The addition of G-actin generally happens at one end of an actin flament (barbed-end or (+)-end) while G-actin dissociation occurs at the other end (pointed-end or (-)-end). F-actin polymerization eventually reaches a steady state where the rate of G-actin addition equals the dissociation rate. During steady state, the length of actin filaments is maintained although the addition/removal of G-actin is still occurring at both ends of the filament. This process is called actin treadmilling (Neuhaus et al., 1983).

To polymerize F-actin, the concentration of soluble actin monomers first needs to reach a critical concentration (C_c), where the concentration of G-actin is in equilibrium with F-actin (Carlier and Pantaloni, 1997). In other words, G-actin concentrations below or above C_c lead to F-actin depolymerization or polymerization, respectively. What makes F-actin assembly asymmetric is that G-actin has nucleotide binding and adenosine triphosphatase (ATPase) activities. The reactant and the product of the hydrolysis reaction have different C_c. The C_c of ATP-bound G-actin is much lower than that of ADP-bound G-actin, which leads to polymerization of ATP-bound, but not ADP-bound, actin monomers. Instead, ADP-bound actin monomers tend to depolymerize because the C_c is much higher. The ATP hydrolysis reaction happens only after G-actin is incorporated into F-actin. Therefore, the temporal regulation of ATP hydrolysis eventually leads to formation of an asymmetric F-actin structure with a gradient of ATP-bound G-actins at the barbed end and ADP-bound G-actins at the pointed end.

Within migrating cells, diverse actin regulators or ABPs precisely govern F-actin assembly. F-actin can further be organized into more complicated structures by ABPs, such as when actin microfilaments are woven into branched actin networks or aligned into parallel F-actin bundles. The following section discusses several of the more important actin regulators or ABPs that are responsible for actin cytoskeleton reorganization. General functions of the important actin regulators discussed below are also listed in the Table 1.

1.2.4. Rho GTPases

The Rho GTPases are a family of signal transduction proteins that function as molecular switches to control various cellular activities, such as gene expression and actin cytoskeleton rearrangement (Vega and Ridley, 2008). The function of Rho GTPases is switched on or off when bound to the nucleotides GTP or GDP, respectively. The nucleotide binding status of Rho GTPases is regulated by guanine nucleotide exchange factors (GEFs) and GTPase activating proteins (GAPs). GEFs catalyze the exchange of GDP to GTP, thereby activating the Rho protein, while GAPs activate the GTPase activity of Rho GTPases, converting GTP to GDP and inactivating the Rho protein. Rac1, Cdc42, and RhoA are the three best studied Rho GTPases that contribute to actin cytoskeleton remodeling at different actin-rich compartments in the cell. Generally, Rac1 is responsible for lamellipodia formation, Cdc42 promotes filopodia formation, and RhoA stimulates actin bundle formation in the cell body and tail retractions (Kozma et al., 1995; Ridley and Hall, 1992; Ridley et al., 1992; Vega and Ridley, 2008) (Fig. 1A). However, the functional division of Rho GTPases in these compartments is oversimplified as recent studies demonstrate that such compartmental segregation of the Rho GTPases is not absolute, as will be discussed in more detailed in a later section.

1.2.5. G-Actin Binding Proteins

Within a cell, G-actin does not polymerize freely. Several actin monomer-binding proteins, including thymosin β4 and profilin, sequester G-actin from polymerization (Mockrin and Korn, 1980; Safer et al., 1991). Thymosin β4 sequesters G-actin present in either the ADP- or ATP-bound form. In contrast, not only can profilin sequester G-actin,

profilin is also the only protein that can catalyze the exchange of ATP for ADP, priming G-actin for the next barbed end polymerization cycle (Mockrin and Korn, 1980). Furthermore, profilin can interact with several other actin nucleators, such as formin, to supply actin monomers for actin polymerization (Paul and Pollard, 2008).

1.2.6. Actin Nucleators

Formation of stable actin nuclei is the rate-limiting step of actin assembly. Several proteins, including the Arp2/3 complex and the formin family, are able to promote actin assembly by enhancing actin nucleus formation. Generally, actin nucleators promote *de novo* synthesis of F-actin by forming an actin nucleus. Two common mechanisms employed by these nucleators are based on structurally mimicking actin nuclei or positioning actin monomers in close proximity to facilitate actin polymerization.

The Arp2/3 complex is a heptameric macromolecule that is composed of two actin-like subunits (Arp2 and Arp3), as well as five other core subunits (ARPC1, ARPC2, ARPC3, ARPC4, and ARPC5). As suggested by its name, Arp2 and Arp3 are structurally similar to actin. Arp2 and Arp3 imitate the structure of an actin dimer, acting as a template for the subsequent elongation of helical F-actin (Kelleher et al., 1995). One unique feature of Arp2/3-mediated nucleation is that the new F-actin emanates from the side of the pre-existing actin filament at a 70° Y-branch angle (Amann and Pollard, 2001; Mullins et al., 1998). At the branchpoint, Arp2 and Arp3 bind to the pointed end of daughter F-actin while the other subunits face the mother filament (Mullins et al., 1998). During F-actin elongation, the Arp2/3 complex remains at the branchpoint and has no effect on the rate of F-actin elongation (Mullins et al., 1998). The actin nucleation ability of Arp2/3 is inefficient and is significantly promoted by the presence of nucleation promoting factors (NPFs; see below). Other subunits of the Arp2/3 complex are essential for its nucleation function but remain understudied (Balcer et al., 2010; Gournier et al., 2001).

The formin family proteins are actin nucleators that are conserved among animal, plant, and fungal species. The human formin family comprises at least 15 formins, including mammalian Diaphanous proteins (mDia1, mDia2, mDia3), formin-like proteins (FMNL1, FMNL2, FMNL3), inverted formins (INF1, INF2), and others (Schonichen and

Geyer, 2010). All human formins have the conserved formin-homology (FH) domains, FH1 and FH2, which are sufficient to promote actin nucleation *in vitro* (Pruyne et al., 2002). Protein crystallography revealed that FH2 domains are present as a homodimer, forming a closed ring structure (Xu et al., 2004). Further analysis of the structure in the presence of actin indicates that the FH2 homodimer ring structure encircles two actin monomers (Otomo et al., 2005). As disruption of this domain completely abolishes formation of the homodimer and the actin nucleus as well as actin elongation, it is thought that the formins enhance actin polymerization by stabilizing actin nuclei (Otomo et al., 2005; Pruyne et al., 2002). The FH1 domains of formins recruit profilin-bound G-actin to increase the local concentration of actin monomers, thereby facilitating FH2 actin polymerization (Romero et al., 2004). The amino-terminus of formins also has a GTPase-binding domain (GBD) that can bind Rho, Rac, and Cdc42 GTPases.

The formins and Arp 2/3 complex actin nucleators function very differently. First, formins accelerate actin nucleation by bringing two G-actin monomers into close proximity via their FH1-FH2 domains while the Arp2/3 complex mimics the structure of an actin dimer (Otomo et al., 2005). Second, formins nucleate unbranched F-actin while the Arp2/3 complex nucleates branched actin formation (Pruyne et al., 2002). Third, rather than remaining at the initiation site of actin nucleation like the Arp2/3 complex, formins are always found at the barbed end of the elongating microfilaments and polymerize F-actin processively (Pruyne et al., 2002). Therefore, not only do formins promote actin nucleus formation, they also increase the elongation rate of F-actin polymerization.

Several other classes of actin nucleators were recently identified, including Spire, Cordon-blue, and leiomodin (Qualmann and Kessels, 2009). All of these recently identified actin nucleators contain at least two Wiskott-Aldrich syndrome protein (WASP)-homology 2 (WH2) domains that bind actin monomers. Spire, for instance, contains four WH2 domains consecutively, and it is thought that these domains promote actin nucleation by bringing G-actin into close proximity (Quinlan et al., 2005).

1.2.7. Regulators of Actin Nucleators

Arp2/3-mediated nucleation is relatively inefficient in the absence of nucleation promoting factors (NPFs). NPFs are the proteins that function to activate the nucleation activity of the Arp2/3 complex. Many NPFs have been identified, including Wiskott-Aldrich syndrome protein (WASP) family members (WASP and N-WASP) and WASP family Verprolin-homologous protein (WAVE) family members (WAVE-1, WAVE-2 and WAVE-3) (Takenawa and Suetsugu, 2007) (Fig. 2A). I will refer to members of these two families in the singular (i.e. WAVE and WASP). WAVE and WASP are the two best-studied NPFs that promote Arp2/3-mediated actin nucleation (Machesky et al., 1999; Miki et al., 1998; Pollitt and Insall, 2009). WASP and WAVE both contain a carboxy-terminal WCA (WASP-homology, basic connector sequence, acidic stretch) domain that binds to the Arp2/3 complex. WASP has low inherent NPF activity because it is auto-inhibited by intramolecular interaction between the amino-terminus and the carboxy-terminal WCA domain. The inactive structure of WASP is relieved by the binding of GTP-bound Cdc42 and phospholipids (Rohatgi et al., 1999), suggesting that activation of WASP happens in close proximity to membranes. Cdc42 binds to the Cdc42/Rac-interactive binding (CRIB) domain of WASP, which in turn exposes the Arp2/3 binding site of WASP (Kim et al., 2000).

In contrast to WASP, WAVE is trans-inhibited by a multiprotein complex that includes Nap1/Nap125, Sra-1/Pir21, HSPC300, and Abl interactor (Abi). This inactive WAVE multiprotein complex is essential to target WAVE to the tips of membrane protrusions (Steffen et al., 2004). The activation of WAVE requires simultaneous interactions with lipidated Rac-GTP and phospholipids to dissociate the inhibitory complex from WAVE (Lebensohn and Kirschner, 2009). Of note, since WAVE does not have a CRIB domain, Rac1 GTPase cannot interact with WAVE directly. Instead, Rac1 binds to the trans-inhibitory multiprotein complex of WAVE to activate WAVE function (Eden et al., 2002).

Similar to WASP, the prototypic formins are also auto-inhibited due to intramolecular interaction between the carboxyl-terminal Diaphanous-autoregulatory domain (DAD) and the amino-terminal Diaphanous inhibitory domain (DID). The binding of RhoA, Rac1, or Cdc42 relieves the auto-inhibited conformation of formins and allows formin homodimer formation (Lammers et al., 2008; Lammers et al., 2005) (Fig.

2A). Structural analysis of the activated formin mDia1 by RhoC suggests that the Rho GTPase induces conformational changes of the GTPase-binding domain (GBD) adjacent to the DID domain, leading to the release of the DAD-DID autoinhibitory interaction (Nezami et al., 2006). The GBD interaction with Rho GTPase is quite specific. For instance, the GBD of mDia1 binds exclusively to Rho (RhoA, B, and C) while those of mDia2 and mDia3 bind to Rac1 and Cdc42 (Lammers et al., 2008) (Fig. 2A). Importantly, all formins are not necessary composed of GBD, DID, and DAD domains because formin is characterized by the presence of FH-FH2 domains. This difference may lead to distinct cellular functions of different formins. Furthermore, some formins have functions other than actin polymerization. For instance, the INF-1 formin controls actin cytoskeleton dynamics at multiple levels, including actin polymerization, depolymerization, and severing (Chhabra and Higgs, 2006).

1.2.8. Actin Capping and Anti-capping Proteins

In the absence of actin regulators, actin filaments continue to polymerize immediately after the lag phase as long as the G-actin concentration is sustained. In cells, this burst of actin polymerization needs to be tightly regulated. Other than using mechanisms to regulate the concentration of free actin monomers in the cytoplasm, cells also regulate actin polymerization by adopting strategies to cap and decap the barbed ends of actin filaments. The binding of capping proteins, such as the heteordimer capping protein (CP) and gelsolin, to the barbed ends of microfilaments prevents spontaneous addition or removal of G-actin (Wear et al., 2003). However, when actin polymerization is necessary, capping proteins need to be replaced by anti-capping proteins, such as vasodilator-stimulated phosphoprotein (VASP) (Barzik et al., 2005; Bear et al., 2002). VASP is a member of the Ena/VASP protein family that comprises three proteins, murine enabled (Mena), VASP, and EVL. Ena/VASP family members are associated with the actin structures in the cell body, tips of filopodia and the leading edge of lamellipodia. The functions of Ena/VASP remain controversial as these proteins can either positively or negatively regulate actin-dependent processes (Krause et al., 2002). Ena/VASP can also polymerize actin filaments or function as an anti-capping protein under certain ionic strength buffer (Hansen and Mullins, 2010), suggesting that Ena/VASP is a

multifunctional protein. The actin nucleator, formin, also exhibits anti-capping function by occluding the barbed end thereby inhibiting the binding of capping proteins during microfilament assembly (Yang et al., 2007).

1.2.9. Actin Depolymerizing and Severing Proteins

Depolymerization of F-actin at the pointed end is also essential for cell migration as the dissociated G-actin monomers can be recycled for use in polymerization at the barbed ends. Spontaneous actin depolymerization at the pointed end is generally not quick enough to maintain the concentration of actin monomers required for actin polymerization. Cofilin, an actin depolymerizing protein, is needed to promote the rate of actin dissociation at the pointed end and the turnover rate of microfilaments (Carlier et al., 1997; Lappalainen and Drubin, 1997). Cofilin has the highest affinity for ADP-bound actin monomers, therefore cofilin can preferentially bind to the pointed end of chronologically older regions of the actin microfilaments to promote F-actin turnover. Cofilin also binds to the middle of actin filaments, leading to actin severing. Electron microscopy shows that the binding of cofilin twists the helical F-actin structures, leading to breakage at the cofilin-binding site (Maciver, 1998; McGough et al., 1997). The severing activity of cofilin is important for actin polymerization because the F-actin fragments that are generated contain free barbed ends that promote lamellipodia formation (Chan et al., 2000) , thus bypassing the rate-determining actin nucleation step. The generation of free barbed ends of actin filaments also facilitates dendritic nucleation by the Arp2/3 complex. Branch formation mediated by the Arp2/3 complex is regulated by the ATP-bound state of the actin filament: the Arp2/3 complex preferentially forms branches at the barbed end over the pointed end (Amann and Pollard, 2001; Ichetovkin et al., 2002). Hence, the severing activity of cofilin increases the quantity of newly polymerized barbed ends to support dendritic nucleation by the Arp2/3 complex. Conversely, binding of cofilin to the branched F-actin can dissociate the Arp2/3 complex from the side of mother filaments leading to a decrease in branched actin filaments (Chan et al., 2009). Cofilin activity is regulated by its phosphorylation status on Ser3 (Fig. 2B). LIM kinase (LIMK) is a downstream effector of Rho-associated kinase (ROCK) (Yang et al., 1998), the kinase activity of which is in turn activated by RhoA GTPase (Maekawa et

al., 1999). Phosphorylation of cofilin by ROCK inactivates the severing activity of cofilin, thus stabilizing the actin cytoskeleton network. Conversely, dephosphorylation of cofilin by slingshot phosphatase reactivates cofilin-severing function (Niwa et al., 2002). Interestingly, cofilin can also stabilize the actin microfilaments under certain conditions. At a high stoichiometric ratio of cofilin to actin, cofilin binds F-actin co-operatively and leads to formation of cofilin-saturated non-dynamic actin bundles (Bamburg and Bernstein, 2010). The opposing effects of cofilin on F-actin assembly demonstrate the versatile functions of cofilin in actin cytoskeleton rearrangements.

1.2.10. Actin Crosslinkers

F-actin is usually organized by diverse actin crosslinkers into high order actin assemblies. These crosslinkers can differentially generate networks with distinct morphologies as well as biophysical properties. Branched actin networks or parallel actin bundles are the two most common types of actin structures found in cells. Branched actin networks are found within lamellopodia while parallel F-actin bundles are usually observed in filopodia or stress fibers (Fig. 1A). Alpha-actinin, filamin, and fascin are just a few examples of the actin-crosslinkers identified so far. Fascin crosslinks F-actin into straight, stiff actin bundles and the rigid structure is important for membrane protrusions beyond the leading edge of the cell. In contrast, α-actinin bundles actin into more flexible actin bundles, like those found in stress fibers (Honda et al., 1999). Filamin is present as a V-shaped homodimer, which tends to crosslink neighboring microfilaments at an high angle (Honda et al., 1999). Of note, actin crosslinkers can usually generate multiple types of actin structures. For instance, a low concentration of filamin is able to crosslink filamentous actin into a high-angle actin meshwork but high concentration leads to parallel actin bundle formation (Schmoller et al., 2009). Actin crosslinkers do not only function as scaffolding proteins to construct actin cytoskeleton networks. For instance, the presence of the actin crosslinker, α-actinin, is essential for the formation of stress fibers, which is required for focal adhesion maturation (Oakes et al., 2012).

1.2.11. Myosin Motor

Myosins, a superfamily of actin-dependent motor proteins with ATPase activity, convert chemical energy into mechanical work during cell movement. Many myosins have been implicated in different steps of cell migration. For instance, myosin X, a motor that localizes to the tip of filopodia, is critical for filopodia formation (Sousa and Cheney, 2005). However, I have focused this discussion on non-muscle myosin II (NM II) since this class of myosin plays a crucial role at the area where myopodin localizes in motile cells. During cell migration, NM II binds to and exerts forces on F-actin. The tension generated by myosin on actin is essential for stress fiber formation, cell body translocation, tail retraction, and focal adhesion maturation during cell migration (Vicente-Manzanares et al., 2009).

A functional NM II dimer comprises a pair of myosin heavy chains (MHCs), a pair of regulatory light chains (RLCs), and a pair of essential light chains (ELCs) (Fig. 3). The MHC is composed of head, tail, and neck domains. The head domain formed by the amino-terminus of the MHC binds to actin and has ATPase activity. The carboxy-terminal tail of the MHC forms a coiled-coil rod domain that mediates NM II dimerization. On each MHC, the neck domain is bound by the ELC and the RLC. The RLC is a phosphorylation-dependent regulator of NM II activity while the ELC stabilizes the heavy chain structure (Alberts et al., 2008). ATP hydrolysis fuels myosin movement along the actin cytoskeleton toward the barbed end by changing the head domain conformation and affinity of the head group for actin microfilaments. Functional NM II motor protein complexes that drive cell migration form an anti-parallel bipolar homodimer, in which NM II monomers self-associate via their rod domains and position the head domains at both ends. Using the rod domains, NM II homodimers can further multimerize with other homodimers to form NM II bipolar thick filaments.

The subcellular location of actomyosin bundles is spatially regulated. NM II is usually undetectable in membrane protrusions even though filopodia and lamellipodia contain actin bundles. Strong NM II staining is found between the boundary of the lamellipodium and the lamellum, within the lamellum and in the cell body (Conrad et al., 1993). Since myosin plays such an important role in cell migration, its contractibility is tightly regulated. Unphosphorylated NM II is folded into a compact inactive conformation that has its actin-binding site buried. Phosphorylation of the RLCs at Ser19

and Thr18 allows linearization of NM II and exposes the actin-binding sites in the globular heads (Jung et al., 2008) (Fig. 3). Both phosphorylation of RLC and actin binding are required to activate the ATPase activity of NM II (Sellers et al., 1982; Umemoto et al., 1989). Numerous protein kinases have been documented to directly phosphorylate RLC to activate NM II activity, such as ROCK and myosin light chain kinase (MLCK) (Vicente-Manzanares et al., 2009). ROCK regulates actomyosin bundle formation and actomyosin ATPase activity at multiple levels (Fig. 2B). First, ROCK directly phosphorylates RLC to relieve the compact conformation of NM II so that NM II can bind actin and form thick filaments. Second, ROCK phosphorylation of RLC activates NM II ATPase activity. Third, ROCK phosphorylates and thereby inactivates RLC phosphatase, which is responsible for dephosphorylating RLC. Lastly, ROCK maintains stress fiber formation by phosphorylating LIMK, which in turn phosphorylates cofilin and inactivates its actin severing and depolymerization functions (Yang et al., 1998).

1.2.12. Actomyosin Bundles (or Stress Fibers)

Within a cell, bipolar NM II multimers bind and bundle 10-30 actin microfilaments to form actomyosin bundles (Cramer et al., 1997), the force-generating cellular contractile machinery within a migrating cell. Actin and NM II are not the only components in these bundles. Immunofluorescence microscopy indicates actin-crosslinking proteins, such as α-actinin, also stain along the actomyosin bundles (Weber and Groeschel-Stewart, 1974), Actomyosin bundles are sometimes referred to as stress fibers. The original stress fibers were first described in non-motile cells and are NM II-containing actin bundles. However, similar actomyosin bundle structures, although less prominent, are also present in motile cells. Thus, stress fibers and actomyosin bundles are considered identical in this thesis unless noted otherwise. Several types of actin stress fibers have been identified in migrating cells, including graded polarity, ventral, dorsal, and tranverse actin bundles (Fig. 4A & B). The types of actomyosin bundles that dominate in the cell body are dependent on the cell type. For instance, graded polarity stress fibers are the dominant actomyosin bundles found in chicken heart fibroblasts

while the other three types are found in U2OS human osteosarcoma cells (Cramer et al., 1997; Hotulainen and Lappalainen, 2006).

Even though the actomyosin bundles in motile and in stationary cells are morphological similar under immunofluorescence staining, electron microscopic analysis using myosin S1 decoration shows that the polarity of the stress fibers in non-motile cells is different from that in migrating cells. Stress fibers in non-motile cells comprise short, overlapping actin bundles (0.25-2 μm long) that exhibit alternating filament polarity. The alternating filament polarity is similar to the sarcomeric unit of muscle cells, where each block of actin arrays has opposite polarity to the following block (Fig. 4C, left image). As myosin moves toward the barbed ends, the gaps between the two blocks of actin arrays diminish and therefore lead to actomyosin bundle contraction. In contrast, stress fibers in motile chicken heart fibroblast cells consist of predominantly long, overlapping bundles (average 13-30 μm long) that consecutively span the length of the cell (Cramer et al., 1997). Because the orientation of the stress fibers is organized in a graded manner along the direction of cell movement, this type of stress fibers is called graded polarity stress fibers (Fig. 4C, right image).

Graded polarity actin bundles are derived from actin bundles at the leading cell edge. Electron microscopy and photobleaching analyses indicate that actin bundles within filopodia and small amounts of lamellipodia actin bundles, with the assistance of myosin contraction, seed the formation of new graded polarity bundles in lamella (Anderson et al., 2008). The graded polarity bundles have uniform polarity at each end (Fig. 4C, right image), with the barbed ends of the filaments facing out toward the cell membrane. Conversely, the filament polarities become mixed in the center of the overlapping actin bundles. The middle region of graded polarity actin bundles is similar to the sarcomeric arrangement in muscle cells, and myosin contraction allows the actin filaments to slide along each other. One key difference between sarcomeric units and graded polarity bundles is that the actin cytoskeleton of the latter becomes interleaved during contraction (Pellegrin and Mellor, 2007). Actomyosin contraction in the middle of graded polarity stress fibers can help the cell body translocate. The graded polarity actomyosin bundles are established prior to fibroblast cell polarization and cell migration, suggesting that the

organization of graded polarity bundles may contribute to cell polarization or movement (Mseka et al., 2009).

Dorsal, ventral, and transverse stress fibers are classified based on their subcellular localization and orientation within the cell (Hotulainen and Lappalainen, 2006; Pellegrin and Mellor, 2007) (Fig. 4B). Transverse stress fibers, or transverse arcs, are actin bundles found beneath the dorsal membrane of migrating cells and are oriented parallel to the cell edge. The ends of the transverse arcs are not attached to focal adhesions (FAs), and it remains unclear if these fibers physically attach to the dorsal surface of the plasma membrane. Transverse stress fibers originate from the Arp2/3 complex-mediated actin networks and contain mixed polarity bundles, and can thus potentially contract. The formation of transverse stress fibers is dependent on NM II activity. It is thought that NM II molecules at the boundary of the lamellipodium and the lamellum bind to Arp2/3 complex-nucleated actin bundles in the lamellipodium and integrate the bundles endwise into transverse stress fibers (Fig. 5A). During cell migration, transverse stress fibers flow centripetally and disassemble in the cell body or contribute to ventral stress fiber formation.

The second type of stress fibers, dorsal stress fibers, are bundles of actin found close to the leading edge. One end of dorsal stress fibers is attached to FAs while the other end is attached to transverse stress fibers (Fig. 5B). Dorsal stress fibers are assembled in a Rac1- and mDia1-dependent manner from FAs (Hotulainen and Lappalainen, 2006; Kovac et al., 2012). Initial formation of dorsal stress fibers at FAs also requires the presence of α-actinin and is independent of NM II activity, consistent with observations that dorsal stress fibers are crosslinked by α-actinin and have no detectable myosin (Fig. 5B) (Hotulainen and Lappalainen, 2006; Kovac et al., 2012). However, as actin elongation continues, α-actinin is displaced by myosin when the bundles are connected to the transverse stress fibers (Hotulainen and Lappalainen, 2006). Dorsal stress fibers are uniform polarity actin bundles that have barbed ends facing the cell front and pointed ends facing the cell body. As uniform stress fibers do not have contractibility, it is thought that transverse stress fibers may provide tension to the dorsal stress fibers via their physical interaction (Hotulainen and Lappalainen, 2006). The

contraction of transverse stress fibers may help FA maturation at the tip of the dorsal stress fibers.

The third type of stress fibers is ventral stress fibers, which are located at the base of the cell (Fig. 5C). Ventral stress fibers are composed of overlapping actin bundles with their barbed ends connected to FAs and their pointed ends oriented towards the centre of the cell. Ventral stress fibers are similar to the graded polarity actin bundles except that ventral bundles do not span the entire length of the cell and are usually observed with the presence of dorsal or ventral stress fibers.

These three types of stress fibers are dynamically connected to one another. Studies on live cells reveal that the transverse and dorsal stress fibers directly contribute to the formation of ventral stress fibers, which are constructed by two dorsal stress fibers at the opposing end and transverse stress fibers in the center (Fig. 5C) (Hotulainen and Lappalainen, 2006).

1.2.13. Focal Adhesions

Focal adhesions (FAs) comprise highly dynamic multiprotein complexes that mediate communication between the actin cytoskeleton and the extracellular matrix (ECM). At focal adhesion sites, integrin molecules, transmembrane proteins that are the core component of FAs, multimerize and form a focal contact with the ECM. The extracellular domains of integrins interact with the ECM whereas their cytoplasmic tails bind to the actin cytoskeleton via numerous adaptor proteins. Using these specialized multi-protein structures, cells can sense the composition and organization of the ECM, and respond to the microenvironment by reorganizing the intracellular actin cytoskeleton network. Furthermore, FAs function as an anchor point to allow cells to exert traction forces on the ECM to drive cell migration. FAs consist of at least 150 proteins, including integrin-linked kinase (ILK), zyxin, paxillin, talin, vinculin, and α-actinin (Wehrle-Haller, 2012). Based on their protein profile, size, and subcellular localization, FAs can be divided into several categories: nascent adhesions, focal complexes, mature adhesions, and fibrillar adhesions (Huttenlocher and Horwitz, 2011). It is important to note that FAs function as anchor points for the cell to pull itself forward. Therefore, these structures, if they are not turned over, are stationary relative to the ECM although cell advancement is

happening. As the cell advances, nascent adhesions and focal complexes either disassemble or become elongated, which eventually turn into mature adhesions at the trailing ends. The dissolution of mature adhesions at the trailing end of the cell is necessary to complete cell migration.

Actin assembly and Rho GTPase signaling pathways regulate the formation of nascent adhesions and focal complexes. Actin dynamics within lamellipodia and activated Rac GTPase promote the formation of nascent adhesions and focal complexes, respectively. Nascent adhesions appear as tiny dot-like structures within lamellipodia. If nascent adhesions (<0.25 μm diameter) do not disassemble, they grow into stronger, elongated FAs. The maturation of nascent adhesions into elongated FA is dependent on crosslinked actin filaments but is independent of myosin ATPase activity (Choi et al., 2008). Focal complexes (<1 μm diameter) are formed at the boundary between the lamellipodium and the lamellum (Giannone et al., 2007). The maturation of focal complexes is dependent on the tension generated by NM II contraction, which is activated by the RhoA-ROCK signaling pathway (Rottner et al., 1999). In the presence of tension exerted by myosin, elongated FAs at the leading edge further grow into mature adhesions (1-5μm diameter) (Pelham and Wang, 1997). Mature adhesions appear in a more elongated morphology and are physically linked to actomyosin bundles. As mature adhesions are very stable, they allow actomyosin bundles to exert great force to translocate the cell body. Fibrillar adhesions are the largest FAs and are usually found at the trailing end of a migrating cell. As fibrillar adhesions are very stable, they can transmit great intracellular force to remodel the extracellular matrix (Pankov et al., 2000). Due to the stability of the fibrillar adhesions, they are usually not found in highly motile cells. To complete cell movement, the stable fibrillar adhesions or mature adhesions at the trailing end need to be disassembled so the tail can be retracted, a process that may require the proteolytic activity of calpain (Huttenlocher et al., 1997).

1.2.14. Integrated View of Cell Migration

Previous sections introduced the key players involved in regulated actin cytoskeleton rearrangement. This section will discuss how these proteins are envisioned to spatially participate in actin cytoskeleton remodeling at different cellular actin-rich

compartments (Fig. 6). Briefly, the lamellipodium is the actin assembly factory in migrating cells as most of the actin polymerization occurs within this area. The actin network in the lamellipodium contributes to filopodia and actomyosin bundle formation while actin bundles from filopodia can later be recycled and contribute to stress fiber formation in the cell body.

1.2.14.1 Actin Assembly within the Lamellipodium

Within immotile cells, the barbed ends of actin microfilaments are usually protected by capping proteins to prevent actin polymerization and depolymerization (Fig. 6A). Diverse extracellular signals, such as epidermal growth factor, can trigger cell migration by activating actin regulators, such as Rho GTPases. Activation of RhoA, Cdc42, and Rac1 is spatially coordinated at membrane protrusions (Machacek et al., 2009). Although RhoA activation has long been known to trigger prominent stress fiber formation (Ridley and Hall, 1992), its important role at the leading cell edge has recently become better recognized. Activated RhoA at the leading edge promotes formin nucleation, leading to the polymerization of linear actin microfilaments. Ena/VASP (the anti-capping protein) and profilin (G-actin binding protein) cooperate with formin to mediate actin cytoskeleton assembly at the tips of lamellipodia (Lebrand et al., 2004; Sarmiento et al., 2008; Watanabe et al., 1999). On the other hand, Cdc42 and Rac1 are activated ~2 μm behind the leading cell edge and activate WASPs and WAVEs, respectively, whose activation requires simultaneous interactions with phosphoinositides and prenylated Rho GTPases (Higgs and Pollard, 2000; Lebensohn and Kirschner, 2009). Activated WAVEs and WASPs can then promote Arp2/3 complex nucleation activity. Single molecule imaging analysis shows that WAVE, along with the Arp2/3 complex, diffuse laterally along the plasma membrane and are incorporated into actin networks (Millius et al., 2012). Activated Arp2/3 complexes nucleate daughter microfilaments at the sides of mother microfilaments, providing free barbed ends for actin polymerization. The Arp2/3 complex, in conjunction with WAVEs, also forms an inhibitory complex with formin within lamellipodia (mDia2 specifically) to spatially inhibit local filopodia formation (Beli et al., 2008). As Rac1 and RhoA GTPases are well documented to be antagonists of one another (Burridge and Wennerberg, 2004; Sander et al., 1999), RhoA

activity is decreased further away from the leading edge of lamellipodia. This low level of active RhoA decreases ROCK activity and phosphorylation of LIMK, and therefore increases the severing activity of cofilin. As a consequence, high cofilin activity within lamellipodia generates more free barbed ends for actin assembly (Ichetovkin et al., 2002). Cofilin also helps to depolymerize actin microfilaments from the pointed end, thereby replenishing free G-actin and further facilitating barbed end actin polymerization.

Actin assembly at the leading edge is not sufficient to promote membrane protrusions. Instead, actin microfilaments polymerizing at the leading edge flow backward with respect to the substratum due to plasma membrane resistance. This process is called the retrograde flow of F-actin (Fig. 6B). Although the actin cytoskeleton flow backs centripetally, membrane protrusions may happen when the rate of retrograde flow reduces. FAs and NM II are the key players to spatially regulate the rate of retrograde flow. At the leading edge, the retrograde flow of the cytoskeleton is interrupted by the formation of nascent adhesions that anchor the actin filaments to the substratum and allow the polymerizing ends to advance against membrane tension (Alexandrova et al., 2008). The formation of nascent adhesions is dependent on the presence of actin bundles crosslinked by α-actinin and is independent on NM II activity (Choi et al., 2008). Upon engagement of nascent adhesions with the actin cytoskeleton, fast retrograde flow turns into slow flow, which in turn enhances membrane protrusions. However, when actin microfilaments reach the boundary of the lamellipodium and the lamellum, retrograde flow is enhanced when NM II binds to the actin filaments and contracts (Oakes et al., 2012). Myosin contraction also leads to periodic retraction of the membrane protrusions and this contraction directly promotes the maturation of focal adhesions. Sometimes, the tension exerted by NM II is strong enough to break the F-actin microfilaments (Giannone et al., 2007), leading to the integration of the actin microfilaments into actomyosin bundles behind the leading edge (Hotulainen and Lappalainen, 2006). Under the retrograde flow and force exerted by myosin, Arp2/3-nucleated and formin-nucleated actin filaments are eventually integrated into transverse and dorsal stress fibers, both of which eventually combine to form ventral stress fibers.

1.2.14.2 Actin Assembly in Filopodia

Two models of filopodia formation, convergent elongation and *de novo* nucleation, have been proposed. The convergent elongation model suggests that filopodia formation is dependent on reorganization of Arp2/3-nucleated actin networks into linear actin bundles, followed by the elongation of the bundles by formin. This model is supported by studies showing that depletion of formin or disruption of Arp2/3 complex impairs both lamellipodia and filopodia formation (Spillane et al., 2011; Yang et al., 2007). In contrast, the *de novo* nucleation model suggests that actin bundles within filopodia are Arp2/3-independent and are derived from *de novo* nucleation of the actin filaments by formin since knockdown of formin, but not the Arp2/3 complex, inhibits filopodia formation (Nicholson-Dykstra and Higgs, 2008). However, it is possible that the residual Arp2/3 complex within knockdown cells is sufficient for filopodia formation or that other unidentified actin nucleation proteins are present. So far, growing evidence supports the convergent elongation model while only a handful of studies support the *de novo* nucleation model (Yang and Svitkina, 2011). Nonetheless, it is also possible that both models contribute to filopodia formation since the two models are not necessarily mutually exclusive.

Regardless of their origin, the proper formation of filopodia is mediated by activation of RhoA, Cdc42 and Rac1 because all these Rho GTPases are required to activate formin activity (Fig. 2A). The formation of filopodia requires the dissociation of formin from the Arp2/3 and WAVE complexes (Beli et al., 2008). The elongation of actin filaments is facilitated by the actin crosslinker fascin (Fig. 6A). Fascin localizes along the entire length of the filopodia shaft and is essential to maintain its stiff morphology (Vignjevic et al., 2006). The stiff configuration allows the actin filaments to resist membrane tension and to protrude. During filopodia formation, Ena/VASP, formin, and actin-bound profilin are associated with the barbed ends of filopodia to facilitate actin polymerization and membrane protrusions. Ena/VASP, other than functioning as an anti-capping protein, also binds to profilin and crosslinks actin microfilaments into bundles at the barbed ends to facilitate filopodia formation (Applewhite et al., 2007). As the cell front advances, fascin present in the actin bundles within the filopodia is displaced by α-actinin within lamellipodia. As the base of the bundles reach the

lamellum, NM II is incorporated and interdigitates with α-actinin (Schafer et al., 2010). NM II ATPase activity can then promote the integration of the bundles into lamellar stress fibers (Nemethova et al., 2008).

1.2.14.3. Stress Fiber Assembly Behind the Leading Edge

Stress fibers can be derived from the leading cell edge. Dorsal stress fibers are nucleated from FAs within lamellipodia in an mDia1- or mDia2-, α-actinin-, and Rac1-dependent manner (Hotulainen and Lappalainen, 2006; Kovac et al., 2012; Oakes et al., 2012). Transverse stress fibers are formed from two independent actin filament pools; the Arp2/3 complex-nucleated actin filaments crosslinked by α-actinin and mDia2-nucleated, tropomyosin-decorated actin filaments (Hotulainen and Lappalainen, 2006; Tojkander et al., 2011). Live imaging analysis shows that fascin-rich filopodia can also enter the lamellum and integrate into dorsal and transverse stress fibers (Nemethova et al., 2008). Ventral stress fibers are formed when two dorsal stress fibers anneal endwise or via interaction of transverse stress fibers between two dorsal stress fibers.

The other way to make stress fibers is the bundling of pre-existing actin filaments. RhoA activation induces prominent stress fiber formation but triggers low actin polymerization, suggesting that Rho-induced actin assembly might be due to activation of ROCK and NM II actin crosslinking activity (Machesky and Hall, 1997). ROCK activation suppresses the severing activity of cofilin and leads to formation of long actin microfilaments spanning the cell body. NM II binds to actin cytoskeleton meshwork at the base of the lamellipodium and transmits force via the microfilaments from the lamellum to the lamellipodium. Thus, although NM II is physically absent from lamellipodia, distal actomyosin contraction promotes nascent adhesion maturation in lamellipodia. Actomyosin contraction also promotes disassembly of mature FAs and therefore leads to tail retraction of the cell (Vicente-Manzanares et al., 2007).

Actin regulators spatially orchestrate actin cytoskeleton rearrangements to facilitate cell migration. It is important to note that although these actin regulators or ABPs are enriched in the indicated compartments, strong staining is frequently found in other compartments and their functions remain largely unknown. For instance, the filopodia actin crosslinker fascin is also enriched in actomyosin bundles (Yamashiro-

Matsumura and Matsumura, 1986) but the biological significance of fascin in actin cytoskeleton assembly in this region remains to be investigated.

As actin regulators are intimately linked to one another, disruption of one may lead to aberrant actin cytoskeleton rearrangement or cell metastasis. Myopodin, as an actin-binding protein, may play such a critical role in actin cytoskeleton rearrangement. The following sections are a summary of the myopodin literature and the potential roles of myopodin in this complicated actin cytoskeleton remodeling network.

1.3. Myopodin In Cell Migration

Downregulation of myopodin expression strongly correlates with the aggressiveness and recurrence rate of prostate cancer, suggesting that myopodin is a good prognosticator of invasive prostate cancer (Lin et al., 2001; Yu et al., 2006). Subsequent overexpression studies also showed that myopodin is a tumor suppressor because ectopic expression of myopodin suppresses tumor growth and cancer metastasis both *in vivo* and *in vitro* (Jing et al., 2004). However, depletion of endogenous myopodin isoforms also decreases cancer cell invasion and migration (De Ganck et al., 2009). These data suggest that myopodin may have unexpected roles in cancer metastasis.

The studies of myopodin become more complicated with the emergence of multiple alternative splicing variants. Before I started the myopodin project in 2008, ΔN-MYO1 was the only known human myopodin isoform. Three additional isoforms (MYO1, MYO2, and MYO3) were later identified that arise as splice variants of a single transcript (De Ganck et al., 2008) (Fig. 7). I also recently validated the expression of a fifth myopodin isoform, MYO4, which is discussed in Chapter 3 (Fig. 7B). Although multiple myopodin isoforms have been discovered, all previous studies defining myopodin as a tumor suppressor used the shortest and the first identified isoform ΔN-MYO1 (Jing et al., 2004; Lin et al., 2001; Yu and Luo, 2006; Yu and Luo, 2011; Yu et al., 2006). It is therefore of interest to investigate if all myopodin isoforms differentially regulate cancer metastasis. Different research groups investigating myopodin in different cell types and from different species further complicate the situation. For instance, fesselin is a chicken myopodin homologue that shares 60% sequence identity and 72% sequence similarity to human ΔN-MYO1 (Schroeter et al., 2008) and several fesselin

studies have provided useful insights into myopodin functions in smooth muscle cells (Beall and Chalovich, 2001; Pham and Chalovich, 2006; Schroeter and Chalovich, 2004; Schroeter and Chalovich, 2005). Similarly, investigations into the roles of murine myopodin in skeletal muscle development might be germane to how myopodin affects cancer cell migration and invasion. Hence, one of the goals of my research was to reconcile the myopodin literature and to exploit this information to interrogate how myopodin might affect cancer metastasis. The following sections summarize our current understanding of myopodin.

1.3.1. Synaptopodin Family Members

Myopodin is also referred to as synaptopodin-2 based on its similarity to members of the synaptopodin-1family. Synaptopodin-1 proteins are expressed in kidney podocytes, brain cells, and hippocampal neurons in a differentiation-dependent manner (Mundel et al., 1997). The synaptopodin-1 family consists of three splice variants, including renal synaptopodin-long (903 a.a.), neuronal synaptopodin-short (685 a.a.), and synaptopodin-T (181a.a.) (Asanuma et al., 2005). The first 670 amino acids of synaptopodin-short are identical to synaptopodin-long and synaptopodin-long has another 234 amino acids at the caboxy-terminus. Synaptopodin-T is identical to the last 181 amino acids of the carboxy-terminus of synaptopodin-long. The founding members of the synaptopodin-1 and synaptopodin-2 families are synaptopodin-short and ΔN-MYO1, respectively, which are proline-rich proteins with 13% or 20% proline residues distributed evenly within the amino acid sequence, respectively (Mundel et al., 1997; Weins et al., 2001). Sequence alignment of synaptopodin-short and ΔN-MYO1 reveals an overall 46% sequence similarity, with the highest degree (34%) of similarity in the carboxy-terminal sequences (469-683 a.a.) (Weins et al., 2001). Due to the similarity in amino acid sequence, myopodin is classified as synaptopodin-2 family.

Synaptopodin-1 is important for proper actin cytoskeleton rearrangement in kidney podocytes, cells that form a barrier around the glomerulus for blood filtration to retain large protein molecules. Synaptopodin-1 interacts with the actin crosslinker α-actinin and regulates the actin crosslinking activity of α-actinin (Asanuma et al., 2005). Truncation analysis identified four α-actinin interaction sites within the synaptopodin-long sequence; two sites are located in the sequence shared with synaptopodin-short and

two are located in the sequence shared with synaptopodin-T. Overexpression of α-actinin, but not synaptopodin-1, induces short, branched actin bundle formation in HEK-293 cells that have no endogenous synaptopodin-1 or α-actinin. Interestingly, the combination of synaptopodin-1 (synaptopodin-long, synaptopodin-short) and α-actinin leads to the formation of longer, branched actin bundles (Asanuma et al., 2005), suggesting that synaptopodin-1 possesses actin-remodeling ability.

In addition, several studies demonstrated that synaptopodin-1 is involved in regulation of RhoA and Cdc42 GTPases. Undifferentiated kidney podocytes lack synaptopodin-1, have low levels of total RhoA, and high levels of Cdc42 and Rac1 (Asanuma et al., 2006). In contrast, differentiated podocytes exhibit high levels of synaptopodin-1 and RhoA, prominent stress fibers, and a high synaptopodin-1-mediated migration phenotype. Overexpression of synaptopodin-1 in undifferentiated podocytes is also able to increase RhoA levels and induce stress fiber formation, suggesting that synaptopodin-1 may regulate stress fiber formation via RhoA stabilization. Immunoprecipitation analysis showed that RhoA either binds to synaptopodin-1 or ubiquitin ligase Smurf1, suggesting that the binding of synaptopodin-1 to RhoA inhibits Smurf-1-mediated ubiquitin conjugation of RhoA and therefore stabilizes RhoA and promotes stress fiber formation. Synaptopodin-1 is also involved in regulation of the Cdc42 GTPase pathway. Yeast two hybrid assays using the carboxy-terminus of synaptopodin-long as bait identified insulin receptor substrate p53 (IRSp53) as an interacting partner of synaptopodin-1 (Yanagida-Asanuma et al., 2007). Truncation analysis identified two IRSp53-binding sites in synaptopodin-1, one in the carboxy-terminus of synaptopodin-long or synaptopodin-T that is absent from myopodin isoforms and the other at the carboxy-terminus of synaptopodin-short, the region showing the highest similarity (34%) between synaptopodin-1 and -2. Synaptopodin-1 functions as a filopodia suppressor by excluding IRSp53 from the filopodia-inducing, IRSp53-Cdc42-Mena complex. Synaptopodin-1 appears to be a multifunctional protein by promoting RhoA-dependent stress fiber formation and the inhibition of Cdc42-induced filopodia formation.

Due to the sequence similarity to synaptopodin-1, myopodin belongs to the synaptopodin-2 family. Proteins that interact with synaptopodin-1, such as α-actinin, are

also known to interact with myopodin (Linnemann et al., 2010). The synaptopodin-1 literature may provide useful insights into myopodin-mediated cancer metastasis. However, myopodin is expressed abundantly in striated and smooth muscle cells, prostate (primarily in prostate epithelium), and small and large interstine, but is undetectable in the glomerulus, except in the smooth muscle cells of the glomerular arterioles (Lin et al., 2001; Weins et al., 2001). Because of the relatively low sequence similarity and distinct tissue distribution of myopodin, the potential relevance of the synaptopodin-1 literature to myopodin has been underappreciated in the myopodin field.

1.3.2. Human Myopodin Alternative Splicing Variants

Investigations of the role of myopodin in cancer cell metastasis became complicated because of the discovery of two alternate promoters that regulate myopodin gene transcription and the alternative splicing of pre-mRNAs that gives rise to a total of five human myopodin transcript variants (Fig. 7A). For simplification, the myopodin isoforms hereafter are referred to as MYO1 (GenBank accession number NP_001122405), ΔN-MYO1 (GenBank accession number CAZ66141), MYO2 (GenBank accession number NP_001122406), MYO3 (GenBank accession number NP_597734), and MYO4. MYO1 consists of exons 2, 3, 4, and 5 (Fig. 7A). Transcription from an alternate promoter located in exon 4 generates a 5' truncated transcript that encodes the ΔN-MYO1 isoform, which contains part of exon 4 and all of exon 5. The first AUG start site in the ΔN-MYO1 transcript is in the same open reading frame (ORF) as in the MYO1 transcript. Therefore, the resultant ΔN-MYO1 is identical to MYO1 but lacks 395 amino acids at the amino-terminus. A splice donor site located in exon 5 prior to the stop codon (indicated by the asterisk in Fig. 7A) combined with splice acceptor sites in exons 6 or 7 generates the MYO2 or MYO3 isoforms, respectively. MYO4, a new isoform reported in the AceView transcriptome database, is largely identical to MYO3 except MYO4 has a unique exon at the 5' end (i.e. exon 1) and lacks 186 bp at the 3' end of exon 5 (Fig. 7A). Detailed validation of MYO4 expression is described in the Result section of Chapter 3. These five transcripts encode myopodin proteins of 1093, 698, 1109, 1261, or 1172 residues (MYO1, ΔN-MYO1, MYO2, MYO3 and MYO4, respectively). Although each isoform contains a distinct combination of amino- and/or carboxy-termini, all isoforms share a conserved sequence encoded by exon 5.

Interestingly, all of the MYO transcripts have very long 3' untranslated regions that might play a regulatory role in myopodin gene expression.

1.3.3. Interacting Partners Of Myopodin

Fesselin, the chicken homologue of myopodin, is a natively unfolded (or intrinsically disordered) protein (Khaymina et al., 2007). Natively unfolded proteins provide an efficient mechanism to allow interaction with multiple partner proteins (Fink, 2005), which may explain why myopodin contains multiple sites for interaction with numerous interacting partners. Fig. 8 illustrates the identities of known myopodin interacting proteins and the locations within myopodin of the regions that affect these interactions, if available. These studies were conducted with human ΔN-MYO1 or with its mouse or chicken homologues. Overall, three categories of myopodin interacting partners have been identified: (1) FA-associated proteins; (2) actin and ABPs; and (3) proteins that regulate nucleo-cytoplasmic shuttling of myopodin.

1.3.3.1. Focal Adhesion-Associated Proteins

A yeast two-hybrid screen of a human prostate cDNA library using the amino- or carboxy-termini of ΔN-MYO1 as bait revealed that myopodin directly interacts with integrin-linked kinase (ILK) (myopodin residues 82-157) or with zyxin (myopodin residues 606-624), respectively (Yu and Luo, 2006; Yu and Luo, 2011). ILK and zyxin are both FA-associated proteins, suggesting that FA dynamics might play an important role in myopodin-mediated cancer cell metastasis. ILK was originally identified as a kinase that phosphorylates different proteins, such as integrin β1, a subunit of the α/β integrin heterodimer present in FAs (Hannigan et al., 1996). Expression of a myopodin truncation mutant containing a 75-residue deletion of the ILK interaction motif or myopodin expression within cells depleted of ILK by siRNA eliminates the ability of myopodin to suppress PC3 cell growth and migration, suggesting that the interaction with ILK is necessary for the tumour suppression activity of myopodin (Yu and Luo, 2011). Aside from interacting with ILK, in vitro kinase studies using purified GST-tagged ILK and the amino-terminus of ΔN-MYO1 (9-194 a.a.) confirmed that ILK directly phosphorylates myopodin (Yu and Luo, 2011). The exact phosphorylation sites within myopodin by ILK remain to be determined. Although having kinase activity, ILK

predominantly regulates cell adhesion via its role as an adaptor protein that couples the actin cytoskeleton to FAs. Coupling of the actin cytoskeleton to FAs is important for force transmission between the ECM and the intracellular compartments, which directly affect cell migration behavior (Huttenlocher and Horwitz, 2011). ILK forms a ternary protein complex with particularly interesting new cysteine-histidine-rich protein (PINCH) and calponin homology-containing ILK-binding protein (CH-ILKBP). The formation of this complex is necessary for ILK recruitment to FAs (Zhang et al., 2002). As ILK directly interact with integrins and actin-binding proteins, such as CH-ILKBP and paxillin, ILK functions as an adaptor to couple the actin cytoskeleton to FAs (Nikolopoulos and Turner, 2001; Tu et al., 2001; Wu and Dedhar, 2001). The interaction of myopodin with ILK may be another example of FA-actin cytoskeleton coupling, although this has not been shown. While the interaction between myopodin and ILK is important for the migration-inhibitory activity of myopodin, it remains unknown if the ILK-mediated phosphorylation of myopodin is also essential.

Zyxin is another myopodin interacting partner. Deletion of the 18-residue zyxin interaction motif within the carboxy-terminus of myopodin or siRNA knockdown of zyxin impairs the suppression function of myopodin in PC3 cell migration (Yu and Luo, 2006). Zyxin is absent from the early nascent focal adhesion complexes but is recruited later when FAs become mature (Zaidel-Bar et al., 2003). Subcellular localization of zyxin in FAs is highly dynamic and is sensitive to mechanical forces. Disruption of mechanical forces by inhibition of actomyosin contraction or laser incision of stress fibers dissociates zyxin from FAs (Hirata et al., 2008). Conversely, application of an external uniaxial stretch force on cells, even at low actomyosin activity, relocalizes zyxin to FAs and along the stress fibers (Hirata et al., 2008; Yoshigi et al., 2005). The localization of zyxin along stress fibers is essential for the recruitment of other actin regulatory machineries to reinforce stress fiber formation (Hoffman et al., 2012). For instance, the recruitment of α-actinin and Ena/VASP by zyxin is important for stress fiber maintenance under mechanical or pharmacological stresses as interruption of these interactions accelerate the rate of stress fiber demise (Hoffman et al., 2012; Hoffman et al., 2006). VASP is generally known to be an anti-capping protein that promotes barbed end polymerization at the leading cell edge. However, Ena/VASP can also crosslink or bundle actin filaments

because VASP contains a F-actin binding site and can form tetramer (Gentry et al., 2012), which may contribute to stress fiber reinforcement under mechanical forces. Other than stress fiber reinforcement, zyxin also facilitates actin polymerization at FA sites (Hirata et al., 2008). It remains unclear how zyxin mediates this process. One possibility is that zyxin may recruit Ena/VASP, which was recently shown to also possess actin polymerase activity under certain conditions (Fradelizi et al., 2001; Hansen and Mullins, 2010).

As myopodin interacts with FA-associated proteins, the function of myopodin in cell metastasis might be linked to FA dynamics and/or actin cytoskeleton remodeling mediated by FAs. For example, zyxin might exploit the actin-binding activity of myopodin to reinforce stress fiber formation. Similarly, since fesselin studies show that myopodin can promote actin polymerization and nucleation, it is possible that myopodin contributes to zyxin-facilitated actin assembly. So far, no studies have examined the molecular mechanisms of how myopodin regulates FA dynamics.

1.3.3.2. Actin, Actin-Binding Proteins, and Actin Assembly

Myopodin is an actin binding protein that stains periodically along the F-actin fibers at the early stage of C2C12 myoblast differentiation (Leinweber et al., 1999; Weins et al., 2001). Similar to synaptopodin-1, mouse myopodin also has actin-bundling activity as ectopic expression of a GFP-tagged myopodin construct in C2C12 mouse muscle cells induces actin bundle formation (Weins et al., 2001). Truncation analysis revealed that a 168-residue sequence contains an atypical actin-binding domain (Fig. 8; 356-524 a.a.). Actin-bundling activity requires at least one actin-binding site and the ability to multimerize, or more than one actin binding site within a protein. It remains unknown if myopodin possess a multimerization domain or several actin-binding sites within a molecule to bundle actin filaments. In fully differentiated C2C12 myotubes, myopodin colocalizes with α-actinin at Z-discs, and co-immunoprecipitation indicates myopodin interacts with α-actinin (Linnemann et al., 2010; Pham and Chalovich, 2006). Interestingly, truncation mapping analysis showed that myopodin contains three independent α-actinin binding sites (86-268 a.a., 269-521 a.a., and 506-698 a.a.) that span almost the whole protein. Yeast two-hybrid screens with a human skeletal muscle cDNA

library also identified the middle sequence of ΔN-MYO1 (269-521 a.a.) as an interacting partner for another actin-crosslinker, filamin (Linnemann et al., 2010). Interactions of myopodin with these, and possibly other, actin-crosslinking proteins, suggest a potentially important role for myopodin in actin cytoskeleton dynamics. Nonetheless, no one has ascribed any biological significance to the actin-binding/bundling activities of myopodin to cancer metastasis.

Aside from binding to actin and actin crosslinkers, *in vitro* actin polymerization studies show the chicken homologue of myopodin can also enhance the rate of actin polymerization. In the presence of very low levels of fesselin (75 nM), the lag phase of actin polymerization is abrogated and the rate of actin elongation is enhanced by 3-fold (Beall and Chalovich, 2001; Leinweber et al., 1999), suggesting fesselin may stabilize actin nuclei to facilitate actin polymerization. In vitro studies further showed that the rapid actin polymerization activity of fesselin is regulated by its interacting proteins calmodulin and smooth muscle α-actinin. Calcium-bound calmodulin, but not free calmodulin, eliminates the actin polymerization activity of fesselin (Schroeter and Chalovich, 2004). A column binding assay demonstrated that Ca^{2+}-calmodulin inhibits fesselin binding to G-actin but has no effect on fesselin interaction with F-actin, suggesting that calmodulin may inhibit fesselin-mediated actin polymerization by interrupting the binding of fesselin and G-actin. Binding of α-actinin to fesselin also attenuates its actin polymerization activity (Pham and Chalovich, 2006). Fesselin also binds to F-actin competitively with the subfragment S1 of smooth muscle myosin. Interestingly, fesselin also interacts with smooth muscle myosin with low affinity and inhibits its actin-activated ATPase activity, suggesting that fesselin may directly regulate actomyosin contractibility (Schroeter and Chalovich, 2005). Since human myopodin shares 72% sequence similarity with fesselin, the fesselin studies provide useful information on how myopodin might affect actin dynamics. However, the actin polymerization function of human myopodin has not been investigated, and no studies have examined the significance of actin binding and bundling by myopodin in a full cell context.

1.3.3.3. Regulators of the Nucleo-Cytoplasmic Trafficking of Myopodin.

In normal prostate tissues, myopodin predominantly localizes to the nucleus. However, within those invasive prostate cancer cells in which myopodin expression is not completely inactivated, myopodin is depleted in the nucleus and accumulates in the cytoplasm (Yu et al., 2006). As redistribution of ΔN-MYO1 from the nucleus to the cytoplasm in prostate cancer cells is frequently observed in invasive but not in benign tumor cells, the understanding of myopodin nuclear import pathways might provide insights into how myopodin affect tumorigenesis.

Mouse myopodin was first discovered as a differentiation-dependent and stress-dependent nucleo-cytoplasmic shuttling protein during muscle cell differentiation (Weins et al., 2001). Subsequent studies focused mainly on the mechanisms of nucleo-cytoplasmic trafficking of murine ΔN-MYO1 in C2C12 cells. Murine myopodin is phosphorylated by protein kinase A (PKA) and Ca^{2+}/calmodulin-dependent kinase II (CaMKII), and dephosphorylated by calcineurin at Ser225 and Thr272 residues in murine ΔN-MYO1 (Faul et al., 2007; Faul et al., 2005). However, only the Thr272 residue (i.e. Thr215 in human ΔN-MYO1 in Fig. 8) is conserved between human and mouse ΔN-MYO1. Phosphorylation of these sites recruits the 14-3-3 protein, allowing exposure of nuclear localization signals in myopodin and the binding of importin-α and importin-β (Faul et al., 2005; Liang et al., 2008). Dephoshorylation of these sites by calcineurin inhibits the nuclear import of myopodin (Faul et al., 2007). Interestingly, 14-3-3 and α-actinin bind competitively to myopodin in C2C12 cells (Faul et al., 2007). These data suggest that myopodin might be sequestered in the cytoplasm of differentiated muscle cells due to the increased expression of α-actinin at the later stages of differentiation, thereby inhibiting 14-3-3 binding and nuclear import (Faul et al., 2007). Although the nucleo-cytoplasmic shutting ability of myopodin is well documented in mouse muscle cells, no similar studies have been conducted on human prostate cancer cells. Instead, most studies on human ΔN-MYO1 in prostate cancer cells have found that myopodin localizes exclusively to the perinuclear and cytoplasmic regions (De Ganck et al., 2008; Yu and Luo, 2006). It remains to be investigated if other myopodin isoforms differentially localize to distinct cellular compartments.

All the interacting proteins listed above bind to regions in myopodin encoded by exon 5, the conserved region present in all myopodin isoforms from different species. The other larger myopodin isoforms contain multiple exons at the 5' end that encode another ~390 residues. My motif scan analysis (scansite.mit.edu/motifscan_seq. phtml) and other studies (De Ganck et al., 2008) revealed that this region contains a putative PDZ domain (Fig. 7A, green line; 7-85 a.a.), a common protein-protein interaction motif, suggesting that this region might be an important binding site for other proteins. Furthermore, the roles of the distinct carboxy-terminal sequences of all myopodin isoforms remain unknown.

1.4. Hypothesis And Objectives

While myopodin was discovered over a decade ago, the mechanisms of myopodin-regulated tumor development remain elusive. Clinical studies clearly suggest that myopodin is a tumor suppressor since downregulation of myopodin expression directly correlates with the invasiveness of different cancer types (Alvarez-Mugica et al.; Lin et al., 2001; Sanchez-Carbayo et al., 2003; Yu et al., 2006). However, *in vitro* and *in vivo* studies provide contradictory findings (De Ganck et al., 2009; Jing et al., 2004). Because both overexpression and knockdown of myopodin suppress cell migration and invasion, the controversy of the *bona fide* roles of myopodin remains unresolved. Therefore, my first objective was to resolve these contradictory findings and examine the effects of myopodin in cell migration and invasion. The results of these studies are presented in Chapter 3.

The recent discovery of multiple myopodin isoforms could provide an explanation for these contradictory findings. Overexpression studies found that ΔN-MYO1 suppresses cell migration (Jing et al., 2004; Yu and Luo, 2006; Yu and Luo, 2011) while knockdown reports demonstrated that depletion of all myopodin isoforms suppresses cell migration (De Ganck et al., 2009). It was therefore possible that different myopodin isoforms differentially affect cell migration and invasion. Strikingly, even though all recently discovered isoforms contain a putative PDZ domain, no studies have been conducted to investigate if these new myopodin isoforms function differently from ΔN-MYO1. Therefore, my second objective was to determine if different myopodin isoforms

differentially affect cell migration and invasion. The results of these studies are also presented in Chapter 3.

The final and major objective of my graduate research was to obtain a more detailed understanding of the molecular mechanisms of myopodin-regulated cell migration. Several pieces of information from ΔN-MYO1 homologues from other species or from the synaptopodin-1 family have provided useful insights into the potential roles of myopodin in cell migraton and invasion: (1) Synaptopodin-1 possesses actin remodeling ability and directly regulates several Rho GTPases (Asanuma et al., 2006; Yanagida-Asanuma et al., 2007), suggesting that myopodin may alter actin cytoskeleton dynamics by regulating Rho GTPase activity; (2) Fesselin promotes actin nucleation and elongation, and regulates myosin ATPase activity (Beall and Chalovich, 2001; Schroeter and Chalovich, 2005), suggesting that myopodin might modulate cell migration by regulating actin polymerization machinery at the leading edge or actomyosin contraction activity of the stress fibers; (3) Interactions of myopodin with zyxin and ILK further suggest that myopodin may regulate focal adhesion assembly or turnover (Yu and Luo, 2006; Yu and Luo, 2011). In view of these results, I focused the latter part of my research on investigations into how human myopodin affects cytoskeleton remodeling and focal adhesion maturation. The results of these studies are presented in Chapters 4 and 5.

Table 1. Summary of the Functions of Actin Regulators

Actin regulators	Functions	Examples
Actin nucleators	Nucleate actin filaments	Formins, Arp2/3 complex, Spire
Capping Proteins	Prevent barbed end F-actin polymerization	Capping Protein (CP), CapG
Anti-capping proteins	Allow barbed end F-actin polymerization	Ena/VASP
Actin-severing proteins	Promotes F-actin depolymerization or dissociation	Cofilin
Actin crosslinkers	Crosslink actin filaments	Filamin, α-actinin, Fascin
Motor proteins	Crosslink actin filaments and trigger actomyosin contraction	Myosin II
Focal adhesions	Provide linkage between the actin cytoskeleton and extracellular matrix	Paxillin

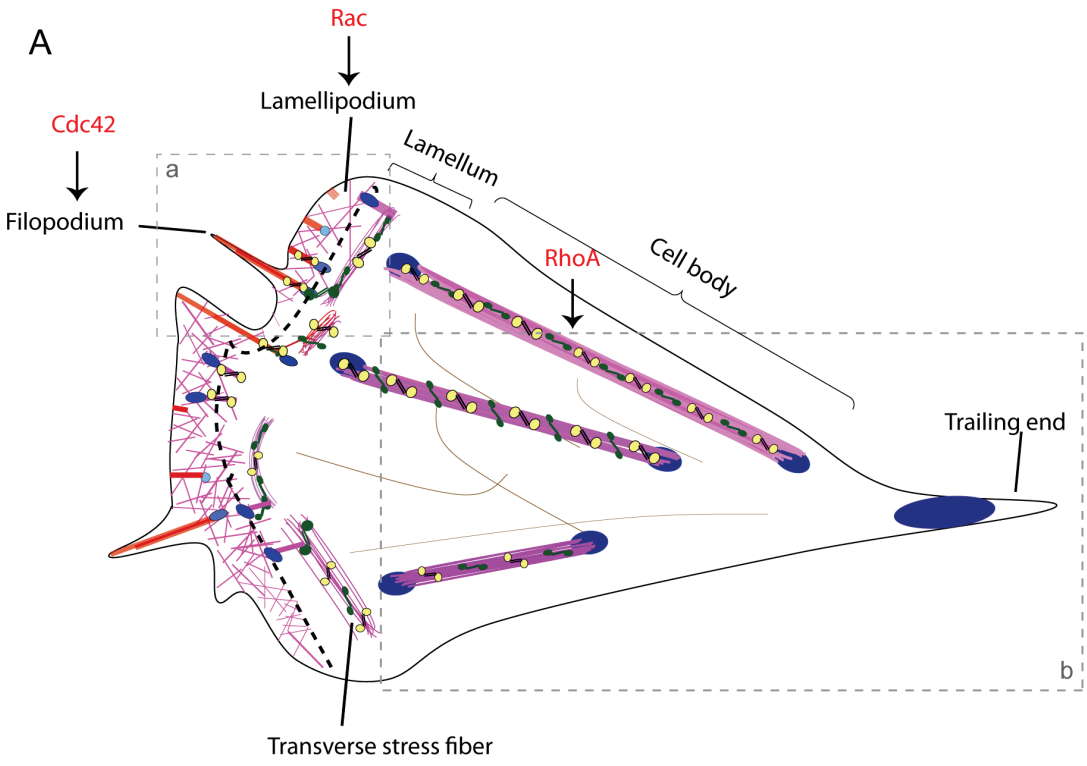
A
Rac
Lamellipodium
Cdc42
Filopodium
a
Lamellum
Cell body
RhoA
Trailing end
b
Transverse stress fiber

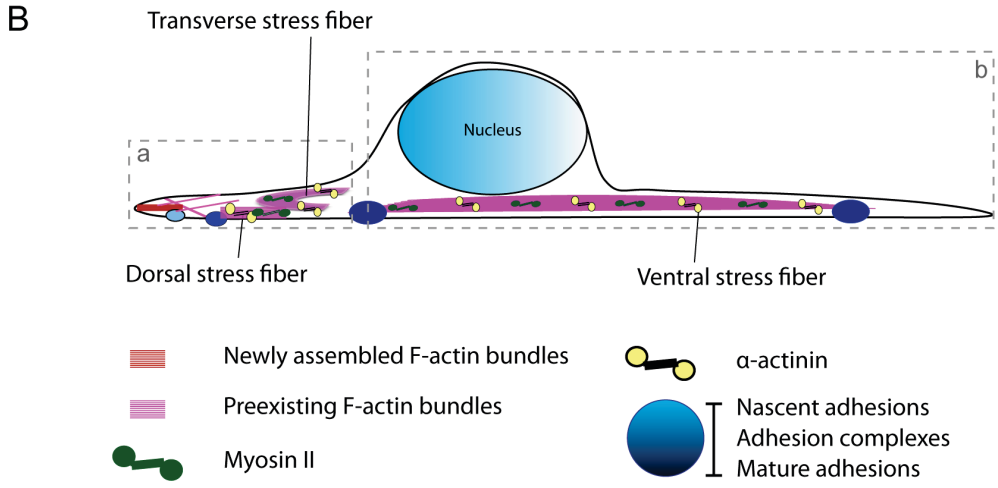
B
Transverse stress fiber
b
Nucleus
a
Dorsal stress fiber
Ventral stress fiber
Newly assembled F-actin bundles
Preexisting F-actin bundles
Myosin II
α-actinin
Nascent adhesions
Adhesion complexes
Mature adhesions

Figure 1. Rho GTPases regulate actin cytoskeleton rearrangement at distinct cellular actin-rich compartments. Top view **(A)** and side view **(B)** of a migrating cell. Essential actin-rich compartments of a migrating cell are illustrated, including filopodia, the lamellipodium, the lamellum, the cell body, and the trailing end. Filopodia, the lamellipodium, and the lamellum (grey box a) constitute the region of membrane protrusion, with the contraction modules of the cell located in the cell body and trailing end (grey box b). Generally, activation of Rac1, Cdc42, and RhoA GTPases are responsible for the formation of lamellipodia, filopodia, and stress fibers, respectively. Filopodia, the lamellum, and the cell body are composed of parallel actin bundles while the lamellipodium comprises both branched and parallel actin networks. Three types of stress fibers (dorsal, ventral, and transverse stress fibers), which are crosslinked by α-actinin and myosin, can be found in a migrating cell. Aside from tranverse stress fibers, most of the stress fibers are physically attached to various focal adhesions (FAs), depicted by different sizes and shade of blue as indicated in the figure legend.

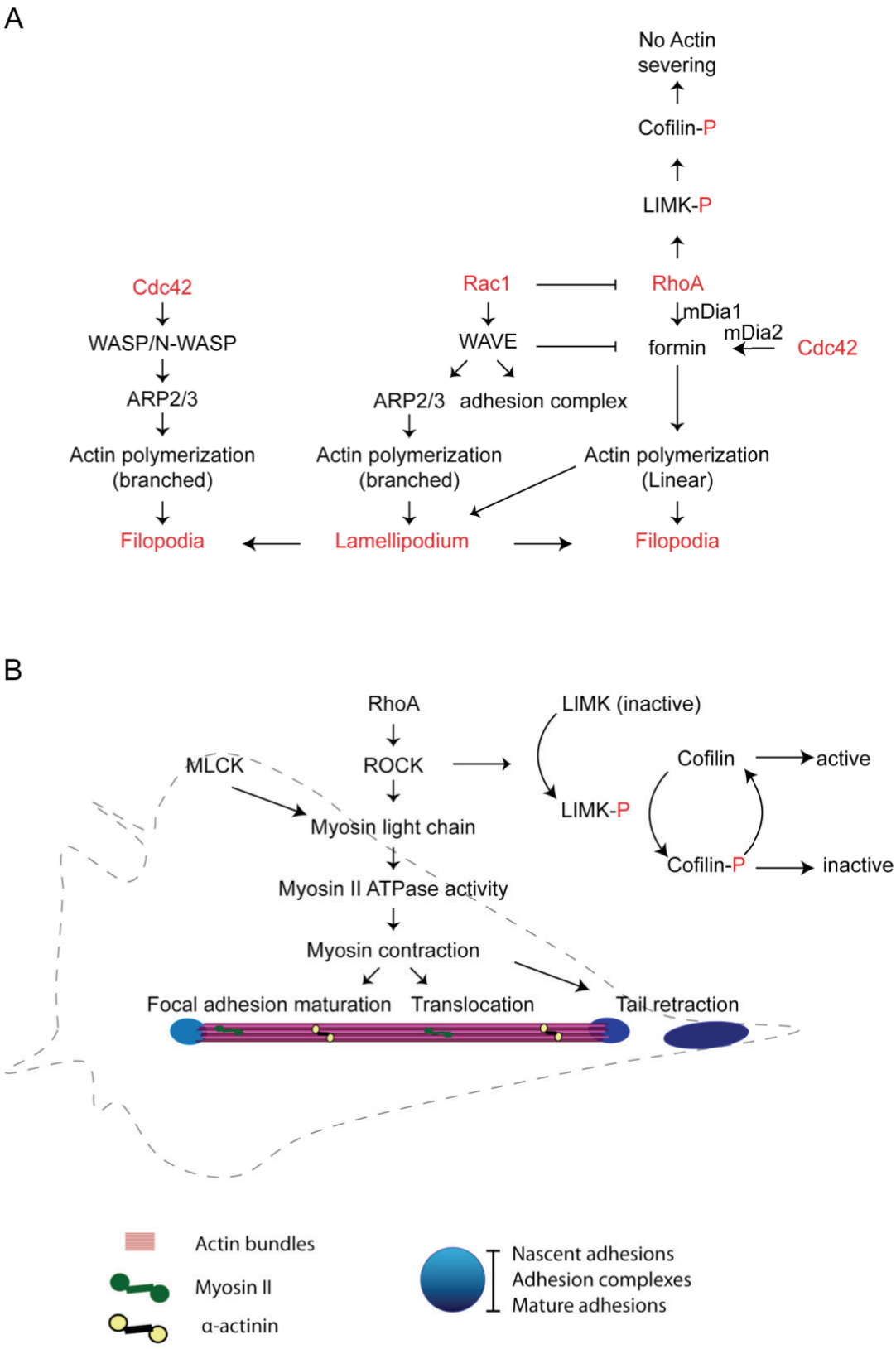
A
No Actin severing
Cofilin-P
LIMK-P
Cdc42
Rac1
RhoA
mDia1
mDia2
WASP/N-WASP
WAVE
formin
Cdc42
ARP2/3
ARP2/3
adhesion complex
Actin polymerization (branched)
Actin polymerization (branched)
Actin polymerization (Linear)
Filopodia
Lamellipodium
Filopodia
B
RhoA
LIMK (inactive)
MLCK
ROCK
Cofilin
active
LIMK-P
Myosin light chain
Cofilin-P
inactive
Myosin II ATPase activity
Myosin contraction
Focal adhesion maturation
Translocation
Tail retraction
Actin bundles
Myosin II
α-actinin
Nascent adhesions
Adhesion complexes
Mature adhesions

Figure 2. Signaling pathways regulated by Rho GTPases and actin regulators. (A) At the leading cell edge, RhoA, Rac1, and Cdc42 are spatially activated. RhoA and Cdc42 activate mDia1 and mDia2 to promote linear actin polymerization, respectively. Cdc42 and Rac1 activate WASPs and WAVEs, respectively, which in turn activate the ARP2/3 complex. Activation of the ARP2/3 complex leads to branched actin network formation. Rac1 can also stimulate nascent focal adhesion formation and Rac1 inhibits localized RhoA activation, resulting in local LIMK suppression leading to activation of cofilin actin severing and depolymerizing activities, thereby generating more free barbed ends for actin polymerization. **(B)** In the cell body, RhoA activity is high. Activated RhoA activates LIMK and thus inactivates the actin depolymerizing function of cofilin, thereby promoting actin polymerization. RhoA can also activate ROCK, which in turn phosphorylates myosin RLC. RLC can also be phosphorylated by MLCK. Phosphorylation of RLC promotes myosin ATPase activity, leading to actomyosin contraction. This contraction can promote cell body translocation and tail retraction. Tensions exerted by the contraction can also distally promote focal adhesion maturation at the cell front.

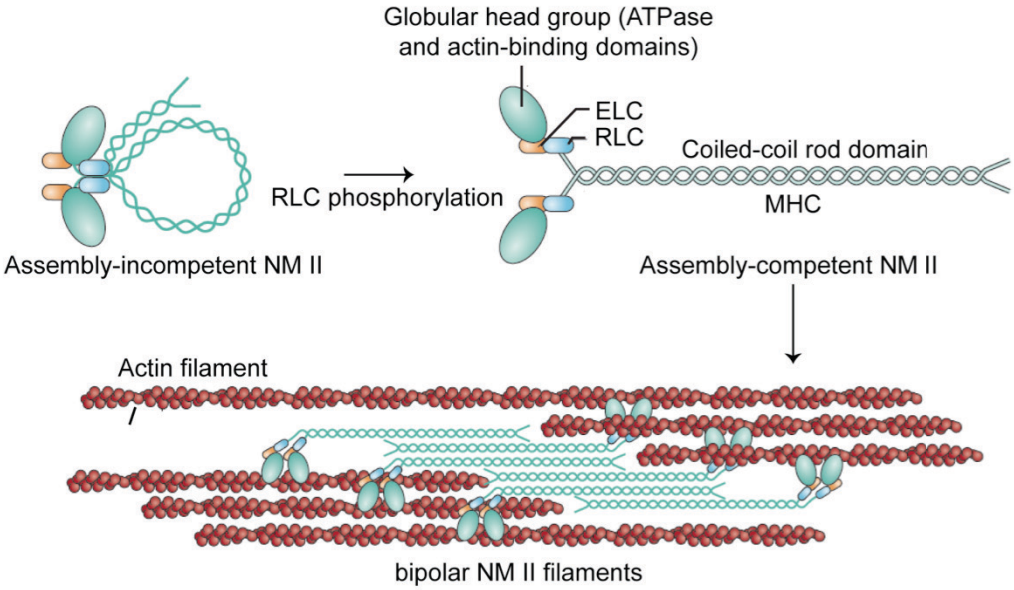

Figure 3. Formation of NM II-containing actin bundles (actomyosin bundles). Figure adapted from Vicente-Manzanares, et al. (Vicente-Manzanares et al., 2009). An assembly-competent NM II homodimer comprises a pair of essential light chains, a pair of regulatory light chains, and a pair of heavy chains. Each heavy chain is composed of a globular head group that has ATPase and actin-binding activities, a carboxy-terminal dimerization domain, and a neck region that connects the head group and the dimerization domain. In the absence of RLC phosphorylation, NM II is present in a compact assembly-incompetent form. Upon RLC phosphorylation, NM II compact structure is relieved. Several NM II molecules can multimerize through the coiled-coil rod domain to form a bipolar myosin filament, which is composed of anti-parallel arrays of myosin molecules.

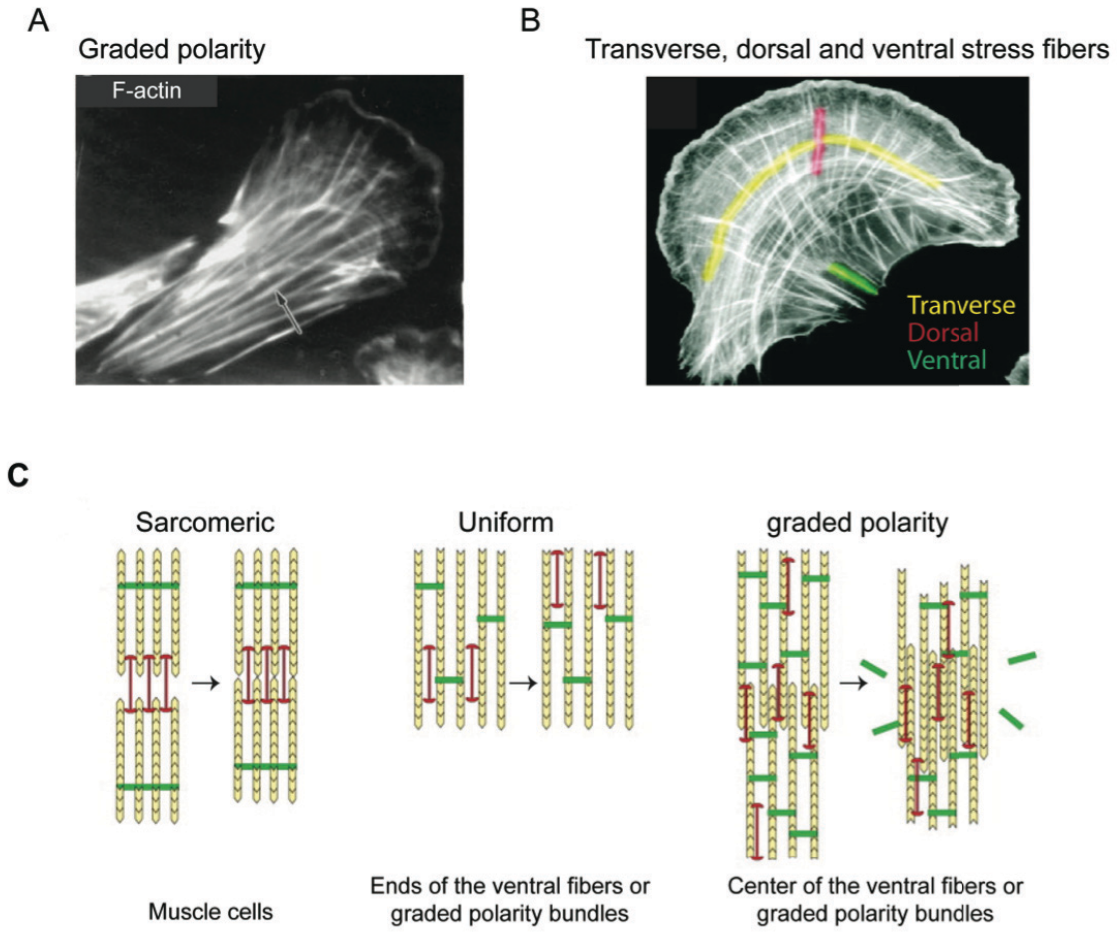

Figure 4. Distinct types of actin stress fibers and actin stress fiber structures. Adapted from Cramer *et al.* (Cramer et al., 1997) (Originally published in *JOURNAL of Cell Biology*. doi: 10.1083/jcb.136.6.1287), Tojkander, *et al.* (Tojkander et al., 2012), and Pellegrin, *et al.* (Pellegrin and Mellor, 2007). **(A)** Graded polarity actin bundles usually span the entire length of the cell (arrow). **(B)** Transverse, ventral and dorsal stress fibers frequently appear with one another. **(C)** Three types of stress fiber organization (sarcomeric, uniform, and graded polarity) found within distinct stress fibers. Actin filaments (yellow blocks) are crosslinked by α-actinin (green) and myosin (red). Sarcomeric stress fibers (left) are composed of blocks of actin that have alternating polarity. Myosin is located between two actin blocks. During contraction, myosin pulls the actin filaments toward one another and closes the gap. Uniform stress fibers (middle) are filaments with the same orientation bundled together and therefore myosin cannot slide F-actin filaments along one another. Instead, myosin can walk along the F-actin filaments. Graded polarity actin fibers (right) contain actin bundles with mixed polarity, thus myosin can slide the filaments leading to interleaved actin structures. Alpha-actinin is displaced when F-actin invades the region between two F-actin filaments.

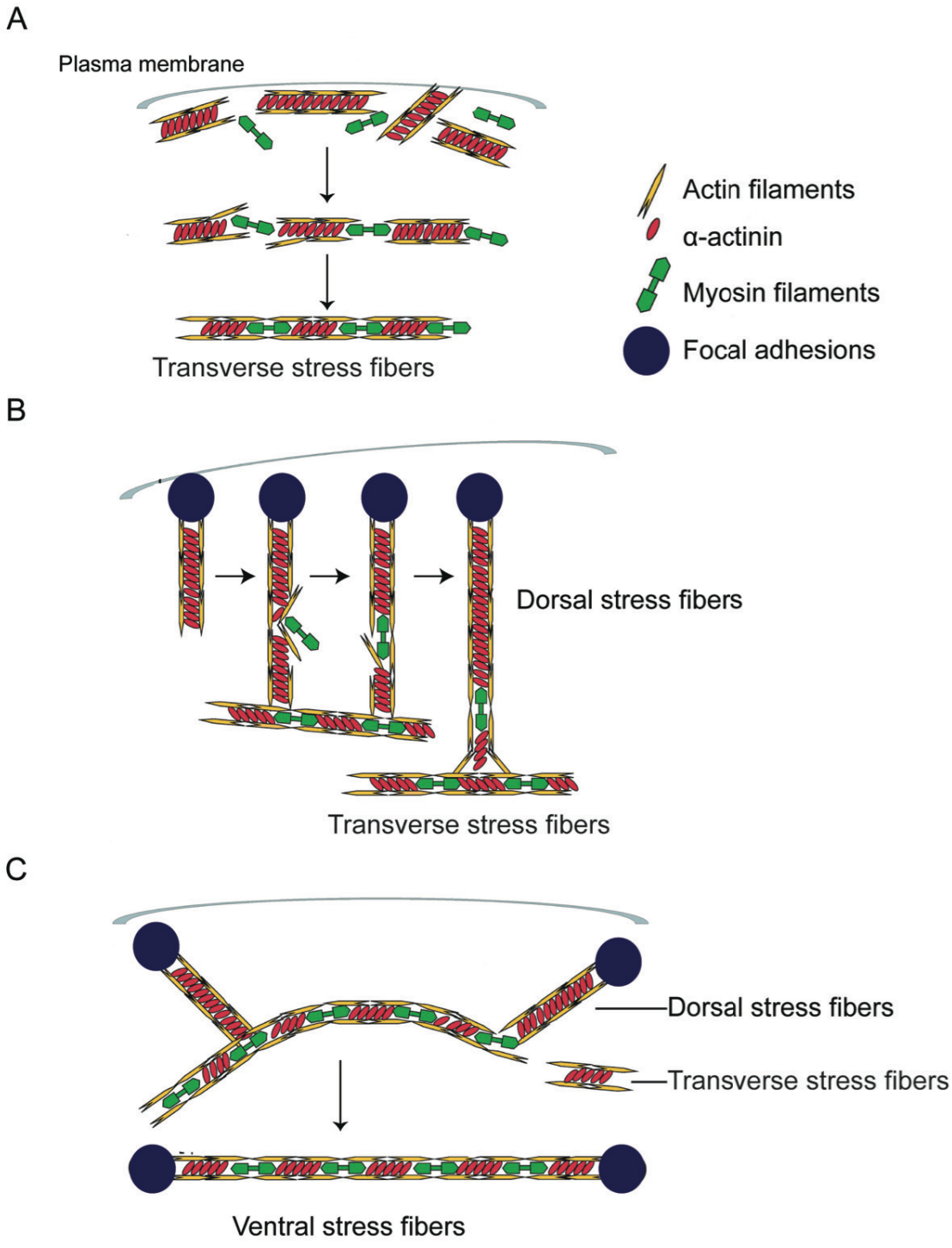
A
Plasma membrane
Actin filaments
α-actinin
Myosin filaments
Focal adhesions
Transverse stress fibers
B
Dorsal stress fibers
Transverse stress fibers
C
Dorsal stress fibers
Transverse stress fibers
Ventral stress fibers

Figure 5. Model of transverse, dorsal, and ventral stress fiber formation. Adapted from Hotulainen and Lappalainen (Hotulainen and Lappalainen, 2006) (Originally published in *JOURNAL of Cell Biology*. doi: 10.1083/jcb.200511093). **(A)** Myosin crosslinks actin filaments endwise to form transverse stress fibers that are parallel to the leading edge and are not physically attached to FAs. **(B)** Elongating dorsal stress fibers nucleated from FAs only contain α-actinin. Myosin is integrated into dorsal stress fibers when dorsal and transverse stress fibers coincide. **(C)** Two dorsal stress fibers and one (or multiple) transverse stress fibers in the middle coalesce into ventral stress fibers. Ventral stress fibers are attached to FAs at both ends.

A

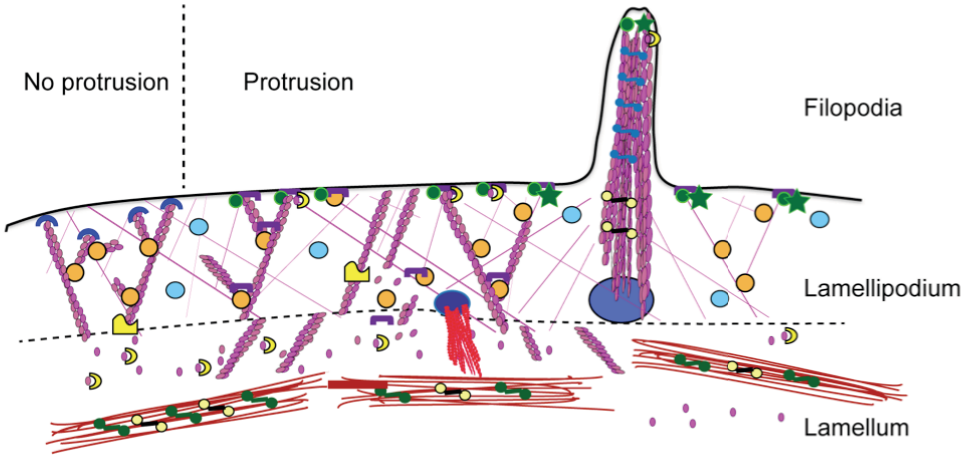
No protrusion
Protrusion
Filopodia
Lamellipodium
Lamellum

B

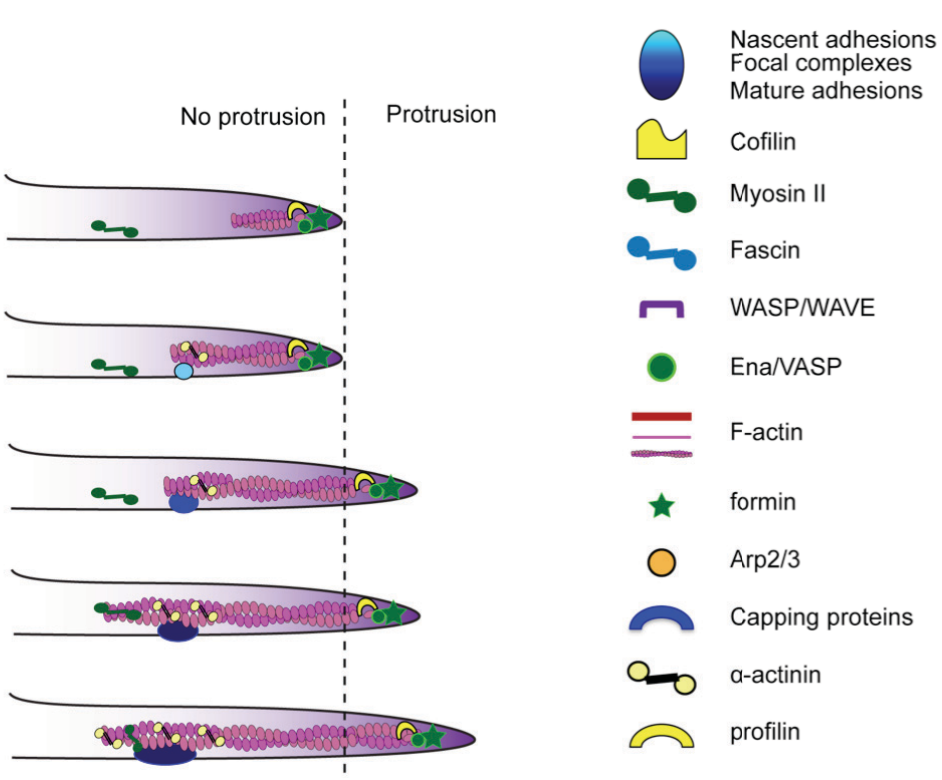
No protrusion
Protrusion
Nascent adhesions
Focal complexes
Mature adhesions
Cofilin
Myosin II
Fascin
WASP/WAVE
Ena/VASP
F-actin
formin
Arp2/3
Capping proteins
α-actinin
profilin

Figure 6. Side and top views of membrane protrusions. **(A)** In this side view, the barbed ends of actin filaments are protected by capping proteins and therefore have no actin polymerization. Extracellular signals activate WASPs and WAVEs, which activate Arp2/3 complexes that nucleate the branched actin filaments. Formins nucleate the linear actin filaments in lamellipodia or parallel actin bundles that are crosslinked by fascin in filopodia. Ena/VASP recruits F-actin-bound profilin and functions as an anti-capping protein to promote actin polymerization at the barbed ends. Cofilin depolymerizes the actin filaments at the pointed end to replenish the G-actin pool to generate more barbed ends for actin polymerization. **(B)** This top view of the leading cell edge (vertical dotted line) shows no productive protrusions are formed during actin polymerization due to high membrane resistance, leading to retrograde flow of F-actin (top two panels). Actin polymerization promotes nascent adhesion formation (light blue circle) and α-actinin is required for its maturation. Maturing FAs anchor F-actin to the ECM and promote membrane protrusions (middle panel). The further maturation of FA (dark blue ellipsoids) is promoted by tension exerted by myosin contraction.

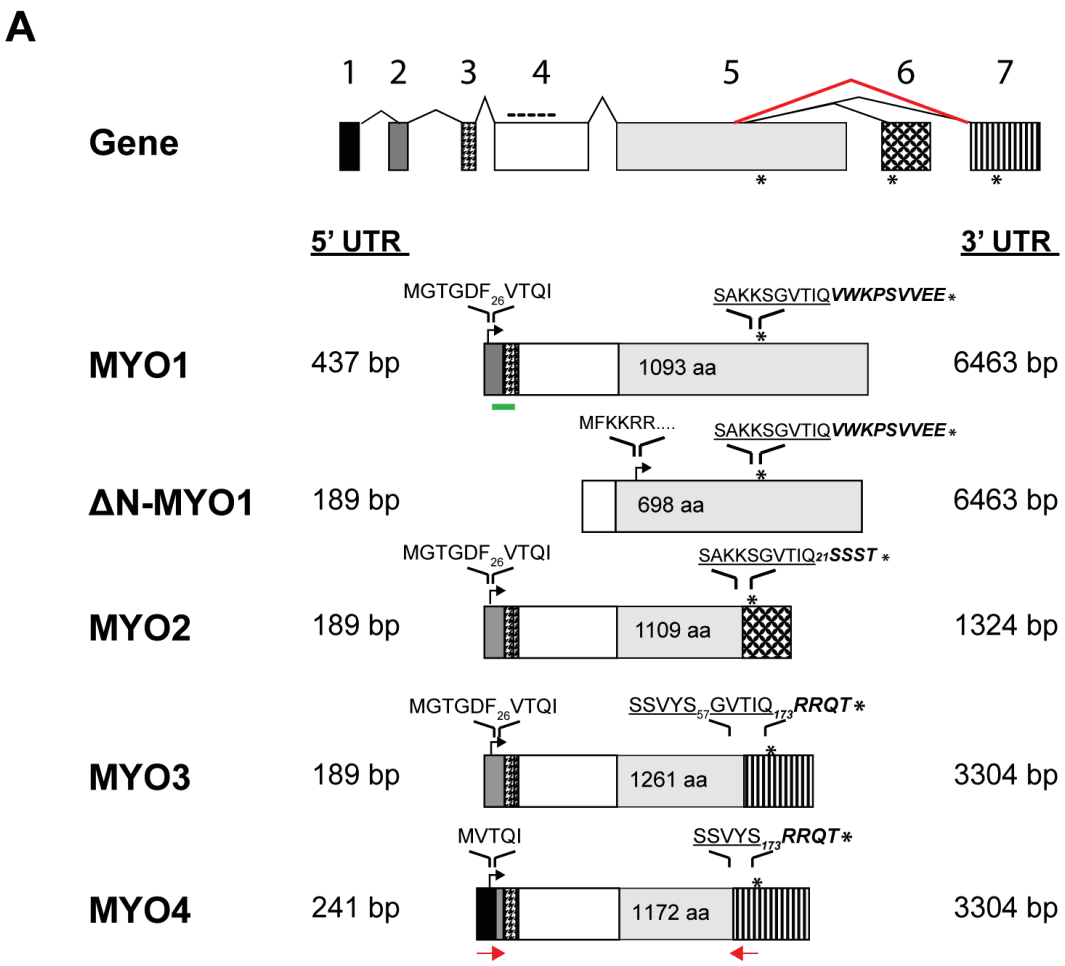
A
Gene
1 2 3 4 5 6 7
5' UTR
3' UTR
MYO1
437 bp
MGTGDF26VTQI
SAKKSGVTIQVWKPSVVEE*
1093 aa
6463 bp
ΔN-MYO1
189 bp
MFKKRR....
SAKKSGVTIQVWKPSVVEE*
698 aa
6463 bp
MYO2
189 bp
MGTGDF26VTQI
SAKKSGVTIQ21SSST*
1109 aa
1324 bp
MYO3
189 bp
MGTGDF26VTQI
SSVYS57GVTIQ173RRQT*
1261 aa
3304 bp
MYO4
241 bp
MVTQI
SSVYS173RRQT*
1172 aa
3304 bp
B
Control
PC3
BPH-1
MYO4
3.8 kb
MYO1
3.3 kb
GAPDH

Figure 7. Myopodin isoforms and validation of MYO4 expression. **(A)** Myopodin isoforms are generated via alternative splicing and promoter usage. The upper panel diagrams the arrangement of exons (rectangles) present in the myopodin gene and the location of splice sites. The red line represents the new splice site found in exon 5 for generation of the new MYO4 isoform. The dashed line above the fourth exon indicates the location of the alternate promoter used to express the ΔN-MYO1 mRNA. The lower panels indicate the arrangement of exons in the mRNAs encoding the five human myopodin isoforms, all of which share the conserved exon 5 sequence (light gray rectangle). Numbers in exon 5 indicate the total number of amino acid residues present in the isoform. The length of the 5' UTR and 3' UTR are indicated at both sides of each mRNA. The amino- and carboxy-terminal amino acid sequences present at the translational start (arrows) and stop (asterisks) sites are indicated above each mRNA. The sequences encoded by the carboxy-terminus of exon 5 are underlined followed by a number indicating the number of residues that separate this conserved sequence from the unique carboxy-terminal sequences of the isoforms (boldface). A forward primer targeting exon 1 and a reverse primer targeting exon 7 were used to confirm MYO4 expression (red arrows). **(B)** Semi-quantitative RT-PCR analysis of MYO4 expression in invasive PC3 cells and non-invasive BPH-1 cells. MYO1 was used as positive control of differential myopodin expression in cancerous and benign tumor cells. GAPDH was used as an internal control to ensure equal amount of RNA used in each reaction. PCR products of the predicted size (3.8 kb and 3.3 kb) were detected in the RT-PCR reactions to amplify MYO4 and MYO1, respectively.

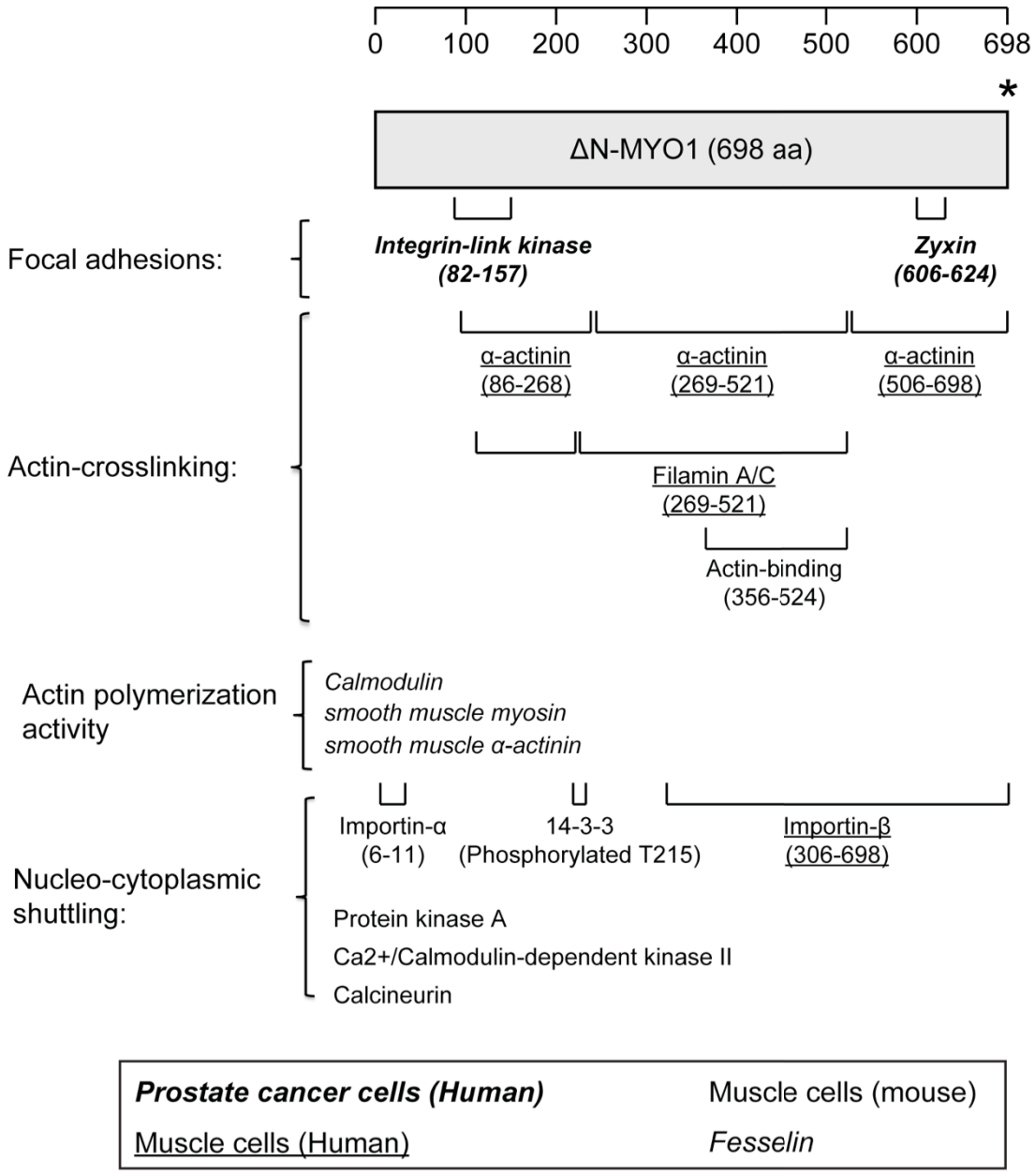

Figure 8. Interacting partners of human, mouse, and chicken myopodin. All known myopodin interacting partners bind to the conserved region of myopodin isoforms and are divided into three categories: focal adhesion-associated, actin-related (actin crosslinking or actin polymerization) or nucleo-cytoplasmic shuttling proteins. The number indicated below each interacting protein is the binding site within human ΔN-MYO1 and those proteins without numbers interact with myopodin but the sites remain to be identified. As indicated in the legend, different font styles represent the species or cell lines used by different research groups.

CHAPTER 2: MATERIALS AND METHODS

2.1. Cells, Antibodies, and Chemical Reagents

Cells. PC3 and NIH 3T3 cells were provided by David Hoskin (Dalhousie University). DU145 and BPH-1 cells were provided by Patrick Lee (Dalhousie University). All cells were routinely screened for mycoplasma contamination using VenorGeM Mycoplasm PCR-based Detection kit (Sigma; Cat. # MP0025). Cells were maintained in high glucose Dulbecco's modified Eagle's medium supplemented (Invitrogen) with heat-inactivated 10% fetal bovine serum (FBS) (Invitrogen) at 37°C in a 5% CO_2 atmosphere. Cell were subcultured every three days, counted, and seeded back at 0.8 x 10^6 cells per 15 cm dish (Corning Life Sciences). Cells grown under these conditions reached a confluency of ~60% prior to the subsequent trypsinization three days later.

Antibodies. The polyclonal rabbit anti-myopodin antibody (Abcam; Cat. # 50192) recognizes residues 566–585, which is located in the conserved region present in all myopodin isoforms. Monoclonal mouse (Cat. # M4439) or polyclonal rabbit anti-cmyc (Cat. # 3956) antibodies were purchased from Sigma. Anti-RhoA (Cytoskeleton; Cat. # ARH03), anti-Cdc42 (Cytoskeleton; Cat. # ACD03), anti-Rac1 (Cytoskeleton; Cat. # ARC03), anti-myosin regulatory light chain (Cell Signaling; Cat. # 9776), anti-myosin IIA (Cell Signaling; Cat. # 5144), anti-cofilin and phosphorylated cofilin (ECM Biosciences; Cat. # CP1151 and Cat. #1131), anti-LIMK and phosphorylated LIMK (ECM Biosciences; Cat. # LP2431 and Cat. # 1831), horseradish peroxidase-conjugated anti-rabbit antibody (Jackson ImmunoResearch), and horseradish peroxidase-conjugated anti-mouse antibody (Santa Cruz), were purchased from the indicated commercial sources.

Chemical reagents. Y-27632 (Sigma), blebbistatin (Sigma), puromycin (Invitrogen), neomycin (Invitrogen), Rac1/Cdc42 activator I (Cytoskeleton), Alexa555- and Alexa647-conjugated Phalloidin (Invitrogen), Sequabrene (Sigma), restriction enzymes (NEB biolabs), Matrigel (BD Bioscience) and NSC23766 (EMD Millipore), Trizol reagent (Invitrogen), Polyethyleneimine (Polysciences) were purchased from the indicated commercial sources.

2.2. Reverse-Transcription Polymerization Chain Reaction (RT-PCR)

Total RNA from cell lines was extracted using Trizol reagent according to the manufacturer's instructions followed by purification using the RNeasy Mini kit (Qiagen). The isolated RNA was treated with DNase (Qiagen) according to the manufacturer's on-column DNase instruction manual and used as template for cDNA synthesis using an oligo(dT) primer and Accuscript High-Fidelity Reverse Transcriptase (Agilent Biotechnologies). Two microliters of the cDNA reaction was used to amplify MYO4 cDNA with Pfu Ultra II HotStart DNA polymerase (Agilent Biotechnologies). The PCR reaction mixtures were denatured at 95°C for 30 sec, annealed at 56°C for 30 sec, and extended at 68°C for 30 sec/kb. These steps were repeated for 40 cycles followed by a final extension reaction for 5 min at 68°C. PCR products was resolved by agarose gel electrophoresis and the bands of interest were isolated using QiaQuick Gel Extraction kit (Qiagen) and cloned into the either pcDNA3 or pBMN plasmid vectors.

2.3. Molecular Cloning

MYO1, MYO2 and MYO3 in the pcDNA3.1/V5-His-TOPO vector were kindly provided by Jan Gettemans (Ghent University, Belgium) (De Ganck et al., 2008). These cDNAs were amplified using PfuUltra High Fidelity DNA polymerase (Agilent Biotechnologies) and subcloned into either pcDNA3 or the pBMN retroviral vector. ΔN-MYO1 was subcloned from the MYO1 template using a forward primer that removed the coding sequence for the 395 residues from the amino-terminus. The full-length myopodin (MYO1, MYO3, MYO4, and ΔN-MYO1) and truncated myopodin constructs (ΔN/ΔC-MYO and ΔC-MYO) were amplified using primers containing BamHI and SalI sites and subcloned into the BamHI and XhoI sites (SalI and XhoI generate compatible ends) in pBMN. MYO2 was cloned into pBMN using BclI and SalI sites because a BamHI sites exists within the MYO2 sequence. All the primers had a melting temperature within the range of 56-58°C. The PCR reaction mixtures were denatured at 95°C for 30 sec, annealed at 56°C for 30 sec, and extended at 72°C for 1 min/kb. These steps were repeated for 25 cycles followed by a 10 min final extension time at 72°C. The PCR products were resolved on agarose gels and imaged using a Kodak 4000-mm Pro CCD imager. The bands of interest were purified using the QIAquick Gel Extraction kit

(Qiagen), digested with the appropriate restriction enzymes (New England Biolabs) for 2 hr, purified again using the QIAquick PCR Purification kit, ligated to the vector for 1 hr at room temperature, and eventually transformed into MM294 or DH5α competent cells (Invitrogen). All new clones amplified from PCR reaction were sequenced by Molecular Cloning Laboratories (Mclab), San Franciso, CA, US.

2.4. Transfections

Phoenix cells are a retrovirus packaging cell line that stably express gag-pol and envelope proteins from ecotropic and amphotropic viruses, respectively, when maintained in culture under selective conditions using hygromycin (300 μg/ml) and diptheria toxin (1 μg/ml). Phoenix cells were transfected using polyethyleneimine (PEI). For each well of a 12-well plate, 0.5 μg of plasmid DNA and 1.5 μl of PEI transfection reagent were separately incubated in 50 μl of Opti-MEM I Reduced Serum Medium (Opti-MEM; Invitrogen) for 5 min and then combined and incubated for another 15 min. As PEI only works in the absence of serum, Phoenix cells were washed twice with PBS and cultured in serum-free medium prior to the addition of the DNA/transfection reagent mixture. The transfection medium was replaced with growth medium 4-6 hr later.

Lipofectamine LTX (Invitrogen) was used to transfect PC3 cells as these cells are not transfected efficiently by PEI. For each well of a 12-well plate, 1 μg of DNA was incubated with 200 μl of Opti-MEM, followed by the addition of 1 μl of Plus reagent for 5 min. After incubation, 1.5 μl of Lipofectamine LTX transfection reagent was added and further incubated for 30 min. The DNA/transfection reagent mixtures were added dropwise onto the cells cultured in the growth medium.

2.5. Western Blotting

Cells were lysed on ice for 20 min using RIPA buffer (10 mM Tris-HCl, 150 mM NaCl, 1 mM ethylenediaminetetraacetic acid, 1% Nonidet P40, 0.5% sodium deoxycholate and 0.1% sodium dodecyl sulfate, pH 8.0) containing a protease inhibitor cocktail (Pierce), and the lysate was sonicated using multiple short bursts with a stainless steel probe sonicator. Samples were centrifuged at 11 000g for 10 min at 4 °C, and the supernatant protein concentrations were determined using the Bradford protein assay (Bio-Rad). Concentrated protein sample buffer (5% sodium dodecyl sulfate, 0.25%

bromophenol blue and 50% glycerol) was added to the cell lysate (1:4 ratio), and supplemented with dithiothreitol (DTT; 50 mM final concentration) before boiling the lysates. An equal protein load of the cell lysates were fractionated by sodium dodecyl sulfate–polyacrylamide gel electrophoresis (SDS-PAGE), transferred electrophoretically onto polyvinylidene difluoride (PVDF) membranes and blocked for 1 hr at room temperature. The blocking solutions were either 5% skim milk or 5% bovine serum albumin (BSA) in TBST (50 mM Tris-HCl, 150 mM NaCl, 0.1% Tween 20), according to the manufacturer's instructions. Membranes were probed with primary antibodies in blocking solution and horseradish peroxidase-conjugated secondary antibodies. NOTE: Rac1, Cdc42, and RhoA primary antibodies were resuspended in TBST (not blocking solution) as suggested by the manufacturer. Blots were developed using ECL-Plus reagent (GE Healthcare) and visualized on a Kodak 4000-mm Pro CCD imager or Typhoon 9200 Scanner.

2.6. Retroviral Transduction System

Myopodin constructs in pBMN were introduced into Phoenix cells using PEI transfection reagent. After 48 hr, supernatants were collected and cell debris was removed by passage through 0.45 μm low protein-binding filters. Sequabrene (4 μg/ml), a cationic polymer that neutralizes the charge between virions and cells and increases infection efficiency, was then added to the viral supernatant. The virus-containing supernatant was immediately used for infection or was flash frozen in liquid nitrogen and stored in small aliquots at -80°C. Cells were infected with retroviruses carrying the indicated constructs for 24 hr and cultured for another 24 hr with fresh growth medium before selection with 1 μg/ml of puromycin (Invitrogen) for 3 days. Dead cells and debris were periodically removed by refeeding the monolayers with the selection medium.

2.7. Generation of Stable shRNA Knockdown Cells

Three shRNAs targeting the coding sequence of the protein of interest were designed using RNAi Central software (http://cancan.cshl.edu/RNAi_central/RNAi.cgi?type=shRNA). The shRNAs were individually cloned into the EcoRI and XhoI sites of plasmid pSMN (kindly provided by Dr. Craig McCormick). The shRNA constructs were transfected into PC3 cells to measure the knockdown efficiency, which

was assessed by western blotting. The construct displaying the maximum knockdown efficiency was selected and used to generate shRNA retroviruses using the retroviral transduction system except that cells were selected with 1 mg/ml neomycin (Invitrogen) for 5 days. The sequence of the selected RLC shRNA was 5'-TGCTGTTGACAGTGAGCGCTTGCTTGCTTTGATGAAGAAGTAGTGAAGCCAC AGATGTACTTCTTCATCAAAGCAAGCAAATGCCTACTGCCTCGGA-3.

2.8. Transwell Migration and Invasion Assays

Migration and invasion assays were performed using 24-well transwell units with 8 μm porous polycarbonate membranes (BD Falcon). The top chamber was seeded with 0.75×105 cells/well and was filled with Dulbecco's modified Eagle's medium supplemented with either 0.1% BSA or 10% FBS, whereas the bottom chamber was filled with Dulbecco's modified Eagle's medium containing 10% FBS or NIH 3T3 conditioned medium (CM) as indicated. NIH 3T3 CM was collected from cells after 24 hr of serum starvation. Y-27632 or NSC23766 were added to the top and bottom chambers at the indicated concentrations. Cells seeded on top of the insert membrane were incubated for 24 hr or 12 hr in the presence of FBS or NIH 3T3 CM, respectively. Following incubation, cells were removed from the top of the membrane with Q-tips and cells that had migrated through the filter to the bottom of the membrane were fixed with methanol and stained with Giemsa or 4´, 6-diamidino-2-phenylindole (DAPI) for 10min. Five random fields were imaged with a 20× objective on a Nikon Diaphot-TMD inverted microscope, using duplicate or triplicate filters for each sample, and the average number of cells per field that transmigrated through the membrane was quantified using ImageJ software. For invasion assays, the transwell filters were coated with a thin layer (40 μl) of Matrigel before seeding the cells. The rest of the experimental procedures were the same as in the migration assay. For invasion assays, both the numbers of cells that invaded and the percent cell invasion (i.e. number of cells invading through the Matrigel/number of cells migrating through the filters × 100) are presented.

2.9. Indirect Immunofluorescence Microscopy

PC3 cells (2 x 10^4 cells) were cultured on tissue culture treated 15 mm glass coverslips (Fisher Scientific) overnight, either with or without serum starvation. Cells

were fixed in 3.7% formaldehyde in phosphate-buffered saline (PBS) at room temperature for 20 min, then permeabilized with 0.25% Triton X-100 in PBS at room temperature for 10 min. Cells were blocked with 1% BSA in PBS and then incubated with the primary antibody overnight at 4°C or for 1 hr at room temperature. Dilutions of the myc antibody used for immunofluorescence were a dilution of 1:1000 (Sigma). Bound primary antibody was then visualized using the indicated anti-mouse or anti-rabbit fluorophore-conjugated secondary antibody at a dilution of 1:1000 (Molecular Probes). Filamentous actin was visualized using Alexa555- or Alexa633-conjugated phalloidin at a 1:40 dilution (Molecular Probes). Cells were viewed and photographed using a Zeiss Axiovert 200M fluorescence microscope (60x 1.25 NA oil- immersion objective lens on the fluorescence microscope fitted with a Hamamatsu ORCA-R2 digital camera) or Zeiss LSM 510 Meta confocal microscope. All confocal images were taken using a 100X 1.4 NA oil-immersion objective lens on a Zeiss LSM 510 Meta confocal microscope. Images were acquired using Zen software (Zeiss). Images were further processed using Photoshop CS5 (Adobe).

2.10. Bacterial Protein Expression and Purification

The bacterial expression plasmid pGEX-PBD expressing the GST-tagged p21-binding domain (PBD) of p21-activated kinase was kindly provided by Dr. Paola Marignani (Dalhousie University) and was used to detect activated Cdc42 and Rac1. The plasmid was transformed into the BL21-CP bacterial strain and bacterial colonies were expanded overnight at 37°C. Fifty milliliters of bacteria was diluted into 450 ml of Luria-Bertani (LB) broth the following day and the culture was grown to an OD600 of 0.6 (~3 hr after dilution) at 37°C, then induced with 0.1 mM IPTG for another 3 hr at 37°C. The bacterial culture was divided into 50 ml conical tubes and centrifuged at 4000 xg for 30 min at 4°C. Bacterial pellets were then stored at -80°C. Frozen cell pellets were thawed on ice for 15 min in the presence of 10 ml bacterial lysis buffer (50 mM Tris-HCl, 150 mM NaCl, 5 mM $MgCl_2$, 1 mM EDTA, 1 mM DTT, 1 mM PMSF, 1 μg/ml aprotinin, pH 7.5). To prevent protein degradation, all the protein purification steps were conducted at 4°C. After incubation with lysis buffer, the pellet was resuspended and sonicated three times with 30 sec bursts on ice. Triton X-100 (1% final concentration) was added to the

sonicated sample to increase the protein solubility and the sample was sonicated as described above. The lysate was cleared by centrifugation at 9300 xg for 30 min and the supernatant was transferred to a new tube and incubated with glutathione agarose beads (Thermo Scientific). After 3 hr incubation, the GST-PBD-coated beads were collected by centrifugation at 500 xg for 3 min, and then washed with bacterial wash buffer (50 mM Tris-HCl, 150 mM NaCl, 5 mM MgCl2, 1 mM DTT, 1 mM PMSF, 1 μg/ml aprotinin, pH 8.0). Expression of purified GST-PBD was confirmed by SDS-PAGE stained with 0.1% Coomassie Brilliant Blue R-250 (Sigma Aldrich).

2.11. Activated Rhoa, Cdc42, Rac1 Pulldown Assays

RhoA activity was examined using the RhoA activation assay kit (Cytoskeleton, Inc.; Cat # BK036) according to the manufacturer's instructions. Briefly, 0.4 $x10^5$ transduced PC3 cells in 10 cm dishes were starved for 2 days. Prior to the treatment with 10% FBS two days later, cells were roughly 60% confluent. Following FBS stimulation in DMEM for the indicated times, cell lysates were harvested using cell lysis buffer (50 mM Tris, 10 mM $MgCl_2$, 0.5M NaCl, 2% Igepal, pH 7.5). Ten microliters of the cell lysates were kept for protein concentration measurements while the rest of the lysates were snap frozen in liquid nitrogen. As GTP is easily hydrolysed into GDP, cell lysates were processed quickly and frozen within 10 minutes after lysis. Eight hundred micrograms of each lysate were incubated for 1 hr at 4°C with 50 μg of Rho binding domain (RBD)-coated glutathione agarose beads. After washing the beads with wash buffer (25 mM Tris, 30 mM $MgCl_2$, 40 mM NaCl, pH 7.5), the bound proteins were released from the beads by boiling with 30 μl 2x PSB and analyzed by western blotting using anti-RhoA antibody (Cytoskeleton). Cdc42 and Rac1 activity was examined using the identical assay except the glutathione beads were coated with GST-tagged PBD. The activated Cdc42 and Rac1 levels were detected by western blotting using anti-Cdc42 (Cytoskeleton) and anti-Rac1 (Cytoskeleton) antibodies, respectively.

2.12. Phospho-Specific Protein Microarray Analysis

The Cytoskeleton Phospho antibody microarray was purchased from Full Moon Biosystems, Inc. (Sunnyvale, CA). The microarray slides were coated with antibodies that recognize the phosphorylated and nonphosphorylated states of 141 actin regulators,

each of which has 6 replicates on the microarray slide. All reagents required for the assay were purchased from the company. The microarray experiment was conducted according to the manufacturer's instructions. Briefly, 2 x 10^6 mock- or myopodin-transduced cells were serum starved for 24 hr and then treated with 10% FBS for 1 hr prior to cell lysis using metal beads and extraction buffer (Full Moon Biosystems). Cell lysates were then biotinylated with 10 μg/μl biotin dissolved in N, N-dimethylformamide for 2 hr. During protein labeling, the antibody microarray slide was blocked with 3% milk at room temperature for 1 hr. The biotinylated cell lysates were added to the pre-blocked antibody-coated slides and incubated for 1 hr. Slides were then extensively washed with dH2O to remove the unbound proteins. Finally, Cy3-Streptavidin (Sigma) was used to detect the bound biotinylated proteins. The slides were imaged and analyzed by Full Moon Biosystems, Inc.

2.13. Live Imaging Analysis

PC3 cells stably expressing LifeAct-RFP (2 x 10^4 cells) were cultured on tissue culture treated 15 mm glass coverslips (Fisher Scientific) overnight and transfected with GFP-tagged myopodin construct using Lipofectamine LTX transfection reagent. Cells were serum-starved overnight and were then examined on a spinning disc confocal microscope system (3i Intelligent Imaging Innovations, Denver CO) equipped for live cell analysis. Cells were imaged for 90 min in HBSS buffer (0.137 M NaCl, 5.4 mM KCl, 0.25 mM Na_2HPO_4, 0.44 mM KH_2PO_4, 1.3 mM $CaCl_2$, 1.0 mM $MgSO_4$, 4.2 mM $NaHCO_3$). Briefly, the spining disk confocal microscope includes the Cell Observer Z1 microscope (Zeiss), an Evolve EMCCD camera (Photometric), and a CSU-X1 spinning-disk head (Yokagawa). Transfected PC3 cells were imaged every minute for 90 min within a temperature controlled (37°C) chamber and images were acquired with Slidebook (Version 5.0) imaging software.

2.14. Statistical Analysis

All results are expressed as the mean ± SEM (standard error of the mean) of three independent studies performed in duplicate, or as the mean ± SD (standard deviation) from a representative experiment (n = 3) conducted in triplicate. Statistical significance was performed by a two-tailed Student's t-test.

CHAPTER 3: MYOPODIN ISOFORMS ALTER THE CHEMOKINETIC RESPONSE OF PC3 CELLS BY MODULATING ACTIN BUNDLING ACTIVITY

3.1. Introduction

Myopodin was first identified as a clinical outcome prognosticator for invasive prostate cancer. Using the PCR-based differential subtraction chain method to search for gene deletions in prostate cancer determined >50% of prostate cancers tested have deletions in chromosome 4q25-26. Sequencing analysis revealed that this deleted region encodes myopodin (Lin et al., 2001). Analysis of a panel of prostate cancer tissues using a targeted PCR approach revealed that the majority of metastatic cancer cases had partial or complete deletions of the myopodin gene. Furthermore, complete inactivation of myopodin expression strongly correlates with prostate cancer relapse (Yu et al., 2006). This inverse correlation between myopodin expression and cancer aggressiveness is also noted in other cancer types. Hypermethylation-mediated silencing of myopodin expression is commonly found in bladder and colorectal cancers (Cebrian et al., 2008; Esteban et al., 2012). Downregulation of myopodin expression is not the only signature found in cancer patients. In normal cells, myopodin predominantly localizes to the nucleus. However, immunohistochemical staining of myopodin in non-invasive and invasive cancer cells revealed that if myopodin expression is not inactivated, myopodin redistributes to the cytoplasm (Cebrian et al., 2008; Yu et al., 2006). These findings suggest that aberrant subcellular localization of myopodin might also contribute to the early stage of cancer development.

Although the clinical reports all suggest that myopodin is a tumor suppressor, controversies about the *bona fide* role of myopodin in cancer cells remain unresolved. *In vivo* and *in vitro* studies substantiate the tumor suppressor function of ΔN-MYO1. Overexpression of myopodin suppresses matrigel invasion of PC3 cells and metastasis in xenografted SCID mice (Jing et al., 2004). However, the same research group has reported that overexpression of ΔN-MYO1 in PC3 cells suppresses or has no effect on cell migration (Yu and Luo, 2006; Yu and Luo, 2011). These inconsistent findings within a research group cast doubts on the role of myopodin as a tumor suppressor in cancer metastasis. Moreover, knockdown of all endogenous myopodin isoforms in PC3 prostate

cancer cells also reduces cell invasion and migration and enhances cell adhesions, suggesting that myopodin promotes, rather than suppresses, cancer metastasis (De Ganck et al., 2009).

The recent emergence of multiple myopodin splicing variants and differences in experimental approaches provide two possible explanations for these opposing findings. First, studies implicating myopodin as a tumor suppressor were based on ectopic expression of ΔN-MYO1 (De Ganck et al., 2009). Conversely, knockdown studies that reduce expression of all myopodin isoforms implicated myopodin as a tumour promoter (De Ganck et al., 2009). Compared to ΔN-MYO1, the new myopodin isoforms are much larger and contain a putative PDZ domain at the amino terminus. The PDZ domain is a highly versatile protein-protein or protein-lipid interaction domain and PDZ containing proteins are involved in almost every aspect of cellular activities (Ivarsson, 2012). It therefore seemed likely that the longer myopodin isoforms would be functionally distinct from ΔN-MYO1. Second, the two contradictory results were also obtained from different experimental conditions. When NIH3T3 CM was used as chemoattractant in transwell migration assays, ΔN-MYO1 functioned as a tumor suppressor (Jing et al., 2004). However, ΔN-MYO1 was discovered as a tumor promoter using FBS as the chemoattractant (De Ganck et al., 2009).

In vitro studies demonstrated that myopodin affects several mesenchymal traits of PC3 cells and cell migration and invasion. However, the molecular mechanisms of myopodin-regulated cell migration remain unclear. Previous studies with myopodin homologues from other species suggest that myopodin may remodel the actin cytoskeleton. *In vitro* biochemical studies revealed that fesselin, the chicken homologue of myopodin, binds to actin, promotes actin polymerization, and crosslink actin filaments in avian smooth muscle cells (Beall and Chalovich, 2001; Leinweber et al., 1999). However, the ~72% sequence similarity between human ΔN-MYO1 and fesselin makes it unclear if human myopodin also enhances actin polymerization and nucleation like fesselin. The actin bundling activity of myopodin was also reported in murine C2C12 myoblasts using GFP-tagged myopodin, although endogenous myopodin exhibits no such staining pattern (Weins et al., 2001). More recent studies with human ΔN-MYO1 indicate myopodin interacts and colocalizes with the actin crosslinkers α-actinin and filamin at the

sarcomeric Z-disc of skeletal muscle cells (Linnemann et al., 2010). ΔN-MYO1 was also reported to colocalize with uncharacterized actin filaments in prostate cancer cells (De Ganck et al., 2008). Although these studies established that ΔN-MYO1 localizes closely with other ABPs, none provided any insights into the effect of ΔN-MYO1 on actin cytoskeleton rearrangement or how these actin interactions might affect diverse biological events such as muscle cell differentiation or cell migration. Furthermore, there is no information on whether the different myopodin isoforms differentially associate with or remodel the actin cytoskeleton, or the effects of these isoforms on cell migration.

Using transwell migration assays, I determined that all of the myopodin isoforms could either promote or suppress the motility of PC3 cells, depending on the nature of the migratory stimulus. My results also indicate that myopodin exerts little effect on the invasion properties of PC3 cells but instead alters the non-directional, chemokinetic response of cells, which is controlled by both the N- and C-terminal regions of myopodin. Using immunofluorescene microscopy approaches, I also determined that the different myopodin isoforms induce distinct actin structures, either an actin meshwork or parallel actin bundles in the cell body. Truncation studies showed that the unique exons present in the myopodin isoforms are determinants of the induced actin structures and the presence of either type of actin structure confers a pro-migratory phenotype to PC3 cells. Based on these findings, I infer that the actin-binding activity of myopodin isoforms directly contributes to actin cytoskeletal rearrangements that drive cell migration.

3.2. Results

3.2.1. Validation of MYO4 Expression

Previous studies described the presence of numerous myopodin isoforms in human cancer cell lines and skeletal muscle tissues, including MYO1, ΔN-MYO1, MYO2, and MYO3 (Fig. 7A). Using AceView, a curated and comprehensive database of transcriptomes isolated from different organisms (Thierry-Mieg and Thierry-Mieg, 2006), we found another alternative splice variant, and I named it MYO4. The evidence of a 5' cap and a validated polyA tail supports the presence of MYO4 mRNA (see http://www.ncbi.nlm.nih.gov/IEB/Research/ Acembly/av.cgi? db=human &c=Gene&l =SYNPO2). To confirm the expression of the MYO4 transcript in my cell system, I

performed an RT-PCR reaction using a forward primer hybridizing to the unique 5' untranslated region (UTR) of MYO4 and a reverse primer specific to the 3' UTR that is common to MYO3 and MYO4. This primer set allowed me to distinguish MYO4 from MYO3 due to the unique exon 1 in MYO4. To clone MYO4 and to examine if MYO4 expression is downregulated in invasive cancer cells, equal amounts of RNA from benign prostatic hyperplasia cell line (BPH-1) and invasive PC3 prostatic carcinoma cell line were used to generate cDNA for MYO4 PCR amplification. PC3 cells are the most commonly used invasive prostate cancer cell line and express low levels of endogenous myopodin due to a hemizygous deletion, while BPH-1 cells are non-invasive prostate tumor cells that have normal myopodin expression levels. A 3.8 kilobase MYO4 product was successfully amplified from both invasive and non-invasive prostate cancer cell lines (Fig. 7B). As predicted from AceView, sequencing analysis showed that the MYO4 transcript is spliced differently from MYO3. MYO4 has a unique 241 bp exon at the 5' end and a unique splice site in exon 5 (Fig. 7A; red line), which is 186 bp upstream of the splice site in the exon 5 utilized by MYO2 and MYO3. Thus, the resulting MYO4 has a unique 31 residues at the amino-terminus and lacks 62 residues at the carboxy-terminus of the conserved sequence (Fig. 7A). Semi-quantitative PCR analysis demonstrated that MYO4, as well as the positive control MYO1, was expressed at a higher level in BPH-1 cells than in PC3 cells (Fig. 7B). These results are consistent with previous reports indicating that myopodin expression is down-regulated in invasive prostate cancer cells (Lin et al., 2001).

3.2.2. Opposing Effects of ΔN-MYO1 on PC3 Cancer Cell Migration under Different Chemoattractant Conditions

I sought to determine the relative contribution of different chemoattractant conditions and the effects of different myopodin isoforms on prostate cancer cell migration and invasion. As all the previous studies were conducted using PC3 cells, I chose PC3 cells to conduct my myopodin studies. To explore the effects of chemoattractants on prostate cancer cell migration, PC3 cells were seeded in Boyden chambers under different chemotactic stimuli. PC3 cells were either mock transduced or transduced with a retrovirus vector expressing the ΔN-MYO1 construct. Due to the

phenotypic heterogeneity of PC3 cells, cells were cultured under selective conditions for five days to obtain polyclonal, rather than monoclonal, transduced cells. Transduced cells were grown on transwell filters, with the upper chamber containing culture medium supplemented with 0.1% BSA and the lower chamber containing either CM or 10% FBS. These conditions are also denoted as 0.1% BSA/NIH 3T3 CM or 0.1% BSA/10% FBS, respectively. The effect of myopodin on PC3 cell migration was determined by the number of cells migrating through the pores to the lower surface of the filter. Cells that migrated through the filter were quantified by microscopic examination of stained filters.

The inherent migratory ability of mock-transduced PC3 cells was greatly influenced by the chemoattractant conditions, and myopodin could inhibit or enhance cell migration depending on these conditions. NIH 3T3 CM induced migration of mock-transduced PC3 cells more efficiently than FBS (Fig. 9A and B). Conditioned medium is such a strong chemoattractant that transwells were fixed at 12 hr post-seeding of cells. In contrast, only a small number of mock-transduced cells were able to traverse the transwells under FBS conditions after 24 hr. However, under the weak chemoattractant conditions (i.e. FBS), ectopic expression of ΔN-MYO1 increased cell migration >3-fold (Fig. 9A and B). Conversely, under conditions where PC3 cell migration was strongly stimulated by CM, ΔN-MYO1 inhibited PC3 cell migration by ~40% (Fig. 9A and B). Interestingly, the cells migrating through the transwells exhibited distinct cell shapes: under FBS conditions, PC3 cells exhibited a rounded morphology while in the presence of CM, PC3 cells were flattened and elongated (Figs. 9B & C). Importantly, the distinct cell morphology induced by FBS and CM was not affected by the presence of myopodin (Fig. 9B). Using DIC imaging and phalloidin staining of cells grown on culture dishes, I observed that the different chemoattractant conditions also induced similar cell morphologies under these culture conditions (Fig. 9C). These observations suggest that growth factors present in the different media may trigger distinct signaling pathways in PC3 cells, and that myopodin differentially regulates these signaling pathways involved in cell morphology and cell migration. The ΔN-MYO1 isoform can therefore function as a tumor promoter or suppressor, depending on the response of PC3 cells to different chemoattractant conditions.

3.2.3. ΔN-MYO1 Enhances the Chemokinetic Activity of PC3 Cells

Chemotaxis is the directional movement of cells in response to a chemical concentration gradient. In contrast, chemokinesis is the non-directional migration of cells in response to soluble factors in the absence of a gradient (Liu and Klominek, 2004). To further explore the mechanisms ΔN-MYO1 employs to regulate PC3 cell migration, I asked if the strong stimulatory effect of ΔN-MYO1 on PC3 cell migration in the presence of FBS reflected an enhanced response to a weak chemotactic or chemokinetic stimulus. Cells were cultured with 10% FBS or 0.1% BSA present in both the upper and lower wells of the Boyden chamber to remove the chemotactic gradient. Mock-transduced PC3 cells displayed the same migration phenotype under all culture conditions (Fig. 10A), indicating that FBS does not serve as a chemoattractant for PC3 cells. Furthermore, ΔN-MYO1 increased PC3 migration 3-4 fold in the absence (10% FBS at top chamber and 10% FBS at bottom chamber; denoted as 10% FBS/10% FBS) or presence of an FBS gradient (0.1% BSA/10% FBS), indicating that ΔN-MYO1 promotes PC3 cell migration by increasing the chemokinetic, not chemotactic, activity of the cells (Fig. 10A). Checkerboard transmigration assay further confirmed that myopodin enhanced the chemokinetic activity of PC3 cells (Fig. 10B). Varying the concentration of FBS in the upper and lower chambers of a transwell indicated that myopodin stimulated cell migration in the presence of both negative and positive gradients. Myopodin-stimulated cell migration was very sensitive to the presence of FBS since the lowest amount of FBS (i.e. 1.5%) achieved the maximal effects on myopodin in cell migration (Fig. 10B). Interestingly, cells cultured in the absence of FBS did not increase their migration in response to myopodin expression (Fig. 10A & B; 0.1% BSA/0.1% BSA). Enhanced PC3 cell migration in response to the chemokinetic effect of ΔN-MYO1 is therefore dependent on chemical factors present in FBS. Taken together, these results indicate that ΔN-MYO1 can differentially modulate the migration phenotype of PC3 cells in response to environmental cues by altering the chemokinetic activity of the cells.

3.2.4. ΔN-MYO1 is a Weak Suppressor of PC3 Cell Invasion under Different Chemokinetic Conditions

The above assays examined the migration phenotype of PC3 cells through the pores of transwell filters. To determine the effects of myopodin on cell invasion, these assays were repeated in the presence of matrigel to provide a three-dimensional extracellular matrix. As in the previous transwell migration assays, the effects of ΔN-MYO1 on the ability of PC3 cells to traverse the matrigel were dependent on the chemoattractant conditions. Mock-transduced PC3 cells were two-fold more invasive in the presence of CM than under FBS conditions (Fig. 11A). Moreover, ΔN-MYO1 increased the invasion of PC3 cells in response to FBS three-fold while inhibiting invasion in response to CM by 50% (Fig. 11A).

The number of cells invading to the bottom of the filter reflects both the migration phenotype of the cells and their ability to invade through the matrigel. To distinguish these two activities, the assays were repeated in the presence or absence of matrigel and the percent invasion was determined (i.e. number of cells invading through the matrigel/ number of cells migrating through the filters x 100). Interestingly, the percent invasion results indicated that myopodin serves as a weak tumor suppressor under both tested chemokinetic conditions (Fig. 11B). Even though FBS did not promote increased cell motility, almost 90% of the mock-transduced PC3 cells that were motile were also invasive under these conditions. Although ΔN-MYO1 enhanced overall cell migration in response to FBS, the percentage of invasive cells was ~20% lower compared to the mock-transduced PC3 cells (Fig. 11B; $p<0.05$). Under the CM condition, mock-transduced PC3 cells were highly motile but only 50% of these cells were able to traverse the matrigel. Ectopic expression of ΔN-MYO1 suppressed both PC3 cell migration and invasion in response to CM, reducing the percent invasion of PC3 cells by 25% (Fig. 11B; $p<0.05$), similar to what was observed under the FBS conditions. Ectopic expression of myopodin therefore consistently suppresses PC3 cell invasive ability through an extracellular matrix, albeit modestly, even under conditions which differentially affect PC3 chemokinetic activity.

3.2.5. All Human Myopodin Isoforms Affect Cell Migration but only Modestly Affect Cell Invasion

The majority of previous studies on myopodin used the ΔN-MYO1 isoform. To determine whether the different MYO isoforms exhibit similar effects on cell migration and invasion, the different isoforms were ectopically expressed in PC3 cells. All five isoforms, including the newest MYO4 isoform, were expressed in PC3 cells, as determined by western blotting using a polyclonal antibody raised against epitopes in the conserved sequence present in all myopodin isoforms (Fig. 12A). Consistent with previous reports (De Ganck et al., 2008), the apparent molecular masses of the larger MYO isoforms based on gel mobility are considerably larger than their sequence-predicted molecular masses (~120 kDa), suggesting these isoforms likely contain undefined post-translational modifications (Fig 12A). Expression of ΔN-MYO1 resulted in two protein products, one with an estimated molecular mass of 80 kDa, as previously reported for this isoform and consistent with the sequence-predicted size (Beall and Chalovich, 2001; Leinweber et al., 1999; Weins et al., 2001), and the other with an estimated mass of 110 kDa suggesting a post-translational modification (Fig. 12A). The higher molecular weight band of ΔN-MYO1 is also observed in fesselin and murine ΔN-MYO1 studies (Beall and Chalovich, 2001; Leinweber et al., 1999; Weins et al., 2001).

Although not presented in this thesis, I spent considerable time exploring the nature of this post-translational modification and successfully identified the regulatory region of the modification down to two amino acids. However, the exact modification site(s) and the type of modification remain undefined. Manipulation of the regulatory region allowed me to enrich the upper 110 kDa or lower 80 kDa bands and to examine the function of each myopodin species. I found that the post-translational modification of myopodin is essential for its function in promoting C2C12 differentiation but has no effect on PC3 cell migration. This data is consistent with fesselin studies showing that both 110 kDa and 80 kDa species can promote actin polymerization (Beall and Chalovich, 2001).

When examined using the transwell migration assay, all of the isoforms moderately suppressed PC3 cell migration under CM conditions but substantially enhanced cell migration under FBS conditions at levels similar to those observed with ΔN-MYO1 (Fig. 12B). Notably, the discrepancy between the protein expression levels of myopodin isoforms did not influence their effects on cell migration (Fig. 12A, B). The

various isoforms, however, differentially affected the percent cell invasion when transduced cells were examined using the matrigel invasion assay. All isoforms except MYO3 had a modest inhibitory effect (~20%) on cell invasion under FBS conditions, but only ΔN-MYO1 and MYO4 exerted a statistically significant inhibitory effect (~20%) under CM conditions (Fig. 12C). These results indicate that all myopodin isoforms can either promote or inhibit cell migration depending on the chemokinetic conditions, but these multiple isoforms exert little, if any, effect on PC3 cell invasion.

3.2.6. Myopodin Isoforms Differentially Induce Distinct Actin Structures in the Cell Body of PC3 Cells

Although myopodin is identified as an actin binding and actin bundling protein (Leinweber et al., 1999; Weins et al., 2001), there are almost no studies on the actin regulating activities of human myopodin and none have explored the relationship between myopodin effects on the actin cytoskeleton and cell migration. Furthermore, it remains to be investigated whether the multiple myopodin isoforms differentially affect actin cytoskeleton rearrangement. To address these questions, I assayed the effects of the myopodin isoforms on actin cytoskeleton architecture within PC3 cells. Since myopodin only modestly (~40%) suppressed the migration of PC3 cells in response to CM but displayed a much stronger stimulatory effect on cell migration in response to FBS (~3-5 fold increase), I focused my analysis of the effects of myopodin on the actin cytoskeleton using conditions that induce the much stronger latter phenotype.

To examine the subcellular localization of the different myopodin isoforms, a ten-residue myc epitope tag was fused to the amino-terminus of each isoform. Epitope tags were used because the quality of staining with commercially available antibodies was inadequate. The different myopodin isoforms conjugated with a FLAG epitope tag displayed the same staining pattern as the myc-tagged constructs, suggesting the epitope tags did not alter myopodin subcellular distribution. Localization of each myopodin isoform with respect to the cytoskeleton in PC3 cells was visualized using indirect immunofluorescence and phalloidin staining.

To avoid biased visual assessment, I imaged a minimum of sixty PC3 cells per infection, reconstructed the confocal Z-stacks, and examined the actin networks using

phalloidin staining. ΔN-MYO1, the most commonly studied isoform, is provided as an example to demonstrate the way I analyzed the actin structures (Fig. 13). Confocal sections of fixed ΔN-MYO1-expressing PC3 cells labeled for myopodin and actin revealed that myopodin colocalized with actin bundles between 60 nm and 120 nm from the bottom of the cells (Fig. 13A). These thick actin bundles were located in the cytoplasm and predominantly underneath the nucleus, as shown by the orthogonal views of the confocal Z stacks (Fig. 13B). Therefore, to quantitatively assay the effects of myopodin on actin cytoskeletal remodeling, cells with actin structures located beneath the nucleus and at 100 nm from the bottom of the cell body were counted in all subsequent experiments.

Qualitative analysis demonstrated that mock-transduced PC3 cells displayed F-actin staining around the cell periphery but the cell body was almost devoid of complex actin fibers (Fig. 14, top panels). Strikingly, PC3 cell lines expressing each of the myopodin isoforms had an abundance of complex actin structures underneath the nucleus in the cell body (Fig. 14, middle column). Expression of the myopodin isoforms also appeared to promote the formation of membrane protrusions. While mock-transduced cells displayed a diffuse staining of actin at the cell periphery, myopodin-expressing cells appeared to have more cortical filamentous actin and actin rich membrane protrusions (Fig. 14). The effect of myopodin on membrane protrusions will be discussed in full detail in Chapter 5.

Interestingly, the different myopodin isoforms also induced three morphologically distinct types of actin networks. First, MYO1 and ΔN-MYO1 typically formed actin meshworks composed of both thick F-actin bundles in the center of the meshwork and thinner F-actin bundles at the periphery. The actin structures in these meshworks were not oriented in a regular pattern, appearing instead as a tangled network of actin bundles (Fig. 14). In contrast, the second type of actin structures observed in PC3 cells expressing MYO3 or MYO4 were mostly long, thin, well-organized F-actin bundles oriented in parallel along the long axes of the cells (Fig. 14). Within PC3 cells expressing MYO3 and MYO4, I never observed the irregular thick actin bundles like those in cells expressing MYO1 or ΔN-MYO1 constructs. The third type of actin structures induced by MYO2 was undefined, amorphous actin structures. Long, thick actin bundles (Fig. 14;

MYO2, circle) or irregular short, thinner bundles (Fig. 14; MYO2, rectangle) were sometimes observed in MYO2-expressing cells. In addition, many cells expressing MYO2 also exhibited very short, amorphous actin bundles stained positively by phalloidin.

To quantitatively assess the effect of the myopodin isoforms on actin cytoskeleton dynamics, PC3 cells with visible actin structures in the cell body, regardless of the F-actin morphology, were counted. Less than 20% of mock-transduced PC3 cells had any actin structures in the cell body detectible by phalloidin staining (Fig. 15A). More than 80% of PC3 cells expressing MYO1 and ΔN-MYO1 constructs had prominent actin structures while ~50% of cells expressing MYO2, MYO3, or MYO4 exhibited actin bundle formation (Fig. 15A). As the actin structures induced by MYO2, MYO3, and MYO4 are much less prominent, it is possible that the number of cells with induced actin structures scoring was underestimated, as compared to MYO1 and ΔN-MYO1. Furthermore, although the concentration of actin-crosslinkers can affect bundle thickness (Stokes and DeRosier, 1991), that did not appear to be the explanation for the different myopodin actin structures since western blot analysis (see Fig. 15B) did not reveal a correlation between myopodin expression levels and the different actin structures. My findings demonstrate that myopodin isoforms differentially remodel the actin cytoskeleton in PC3 cells.

3.2.7. MYO Isoforms Differentially Colocalize with the Induced Actin Structures

Interestingly, although myopodin isoforms promote actin-rich membrane protrusions, each of the isoforms selectively colocalized with actin structures in the cell body. The fluorescence intensity profile along the traced lines in Fig. 13B showed that ΔN-MYO1 strongly colocalized with the actin cytoskeleton in the cell body, with little, if any, ΔN-MYO1 fluorescent signal detected at the actin-rich regions at the periphery of the cell or in the membrane protrusions (Fig. 13C; 35-45 μm region of the X-axis). Qualitatively, the same situation applied to all of the myopodin isoforms that displayed strong colocalization with actin structures in the cell body but not at the cell periphery (Fig. 14).

The different myopodin isoforms also differentially associated with the induced actin structures (Fig. 14). Two general types of myopodin staining pattern were observed: contiguous (type I) and punctuated (type II) staining along the F-actin bundles. Qualitatively, the contiguous type I staining pattern was associated with the thick, irregular actin meshwork typically induced by MYO1 and ΔN-MYO1 (Fig. 14, left column and merge column). It is also important to note that around the prominent type I contiguous staining of MYO1 and ΔN-MYO1, punctuated staining was observed at the periphery where actin bundles are thinner. In contrast, the type II staining pattern was very distinctive and always noticed along the thin, parallel actin bundles typically present in cells expressing MYO3 or MYO4. MYO2, which induced formation of amorphous structures, also exhibited an indefinable staining pattern. Although both contiguous and punctuated staining patterns were observed in cells expressing MYO2, the correlation of the MYO2 staining pattern and the bundle morphology did not hold true in MYO-2 expressing cells. In MYO2-expressing cells the punctuated staining pattern was sometimes found along thick actin bundles or the contiguous staining pattern was observed along thinner actin bundles.

To quantitatively assess the myopodin staining patterns with the actin structures, I counted cells displaying either predominantly contiguous staining or punctuated staining. Two rules were followed when quantifying the staining patterns: (1) if both contiguous and punctuated staining were present within a cell, the cell was scored positive for the contiguous staining pattern; (2) a cell was scored positive for the punctuated myopodin staining pattern if no contiguous staining pattern was observed in that cell (Fig. 15C). Quantification of these staining patterns revealed that ~80% of cells expressing MYO1 and ΔN-MYO1 displayed contiguous myopodin staining of the thick, disorganized F-actin meshwork with only ~20% of cells containing only the punctuated staining along thin, parallel F-actin bundles (Figs. 15D). In contrast, >90% of the cells expressing MYO3 and MYO4 exhibited the type II punctuated staining pattern (Figs. 15D). Approximately 50% of MYO2-expressing cells displayed each staining pattern, although the staining pattern did not correlate with the actin structures as with the other isoforms (Fig. 15D). Overall, these results indicate that the different myopodin isoforms differentially remodel and colocalize with the actin cytoskeleton.

3.2.8. Carboxy-termini of MYO Isoforms Regulate Myopodin Subcellular Localization with the Actin Cytoskeleton

Previous studies showed that the actin-binding domain of mouse myopodin is located in the central conserved region of myopodin that is present in all myopodin isoforms (Weins et al., 2001). Therefore, while this region might be responsible for the ability of human myopodin to colocalize with actin structures in cells, it seems unlikely to account for the differential effects of myopodin isoforms on actin remodeling. To map the regions responsible for the different cytoskeletal phenotypes of the MYO isoforms, I generated truncated constructs containing deletions of the unique termini present in the different isoforms and analyzed the effects on the actin architecture in cells (Fig. 16A). As MYO1 and ΔN-MYO1 both induced an irregular meshwork of thick actin bundles and exhibited a contiguous staining pattern along this network, the 395 N-terminal amino acids that distinguish these two isoforms appeared to be dispensable for myopodin function in actin cytoskeleton remodeling. To test this hypothesis, these residues were deleted from MYO3 to generate ΔN-MYO3 (Fig. 16A). Consistent with my speculation, cells expressing ΔN-MYO3 induced the formation of thin, parallel F-actin bundles and displayed the type II punctuated staining pattern along these filaments characteristic of full-length MYO3 (Fig. 16B).

Since the type I and II myopodin staining patterns appeared to correlate with the presence of the unique C-termini, I constructed a ΔC-MYO truncation of MYO3 by introducing a stop codon after the last amino acid residue encoded by exon 5 of myopodin gene (Fig. 16A). This construct removed the unique carboxy-termini present in the different isoforms. When examined qualitatively, cells expressing ΔC-MYO still induced actin structures in the cell body. However, the actin morphology induced by ΔC-MYO was not as distinctive as the typical MYO1 and MYO3 phenotype. I found that approximately half of the ΔC-MYO-expressing cells exhibited thick bundle formation and the other half exhibited thin bundle formation. As compared to the MYO3, MYO4, and ΔN-MYO3-induced bundles, the parallel actin bundles in ΔC-MYO-expressing cells did not traverse the entire cell body and the bundles were not as discernible. The ΔC-MYO-expressing cells that exhibited thick actin bundles were similar to those present in MYO1- and ΔN-MYO1-expressing cells. I also found that ΔC-MYO displayed either punctuated or contiguous staining patterns with respect to the actin cytoskeleton. ΔC-

MYO generally stained contiguously along the thick actin bundles while staining in a punctuated pattern in the cells with less prominent parallel actin bundles (Fig. 16B).

These qualitative results were confirmed quantitatively. As with MYO3, >80% of the cells expressing ΔN-MYO3 displayed thin, parallel actin fibers with the type II punctuated staining pattern (Fig. 17A). The dispensable nature of the amino-terminus in regard to the formation and staining of actin structures was further supported by the observation that MYO3 and MYO4, two isoforms with identical carboxyl-termini but different amino-termini, exhibited the same actin phenotype (Fig. 14). Western blot analysis showed that ΔN-MYO3 is expressed at a similar level as ΔN-MYO1 (see Fig. 18B), confirming that the different staining patterns are not due to different levels of protein. Notably, the removal of the amino-terminus also led to two forms of ΔN-MYO3 (120 kDa versus 150 kDa), further substantiating that the first 395 amino acids may suppress the undefined post-translational modifications. In contrast, deletion of the C-terminus eliminated the type I staining pattern typical of the MYO1 and ΔN-MYO1 and the type II staining pattern characterisitic of MYO3 and MYO4. Instead, the ΔC-MYO staining pattern resembled that of MYO2, with a mixture of types of actin bundles and contiguous and punctuated staining (Fig. 17A). Thus, I concluded that the unique carboxy-terminal sequences present in the different myopodin isoforms differentially regulate the effects on actin cytoskeleton remodeling and the pattern of colocalization of myopodin with the induced actin structures.

3.2.9. Myopodin-mediated Remodeling of the Actin Cytoskeleton is Directly Responsible for Increased PC3 Chemokinetic Activity

3.2.9.1. Multiple Regions of Myopodin Contribute to Actin Structure Formation and Enhanced PC3 Cell Migration

The observation that MYO1, MYO2 and MYO3 all have similar effects on PC3 cell migration suggests that the distinct actin structures induced by the different myopodin isoforms may all serve to promote PC3 chemokinetic activity. To test this hypothesis, I performed transwell migration assays using the truncation mutants, ΔN-MYO3 and ΔC-MYO, to determine whether these deletions affect the role of myopodin in cell migration. Results indicated that the ΔN-MYO3 construct increased PC3 cell

migration in response to FBS and modestly decreased migration in response to CM to approximately the same extent as the authentic myopodin isoforms (Fig. 17B). Thus, the presence or absence of the N-terminal PDZ domain and the ability of this region to regulate post-translation modification does not affect the ability of myopodin to regulate the cellular response to chemokinetic stimuli. Similarly, the ΔC-MYO construct, which mimicked the MYO2 construct by inducing a mixture of actin structures inside cells, had the same effect on PC3 cell migration as the full-length constructs (Fig. 17B). Therefore, removal of either the amino- or carboxy-termini of the myopodin isoforms did not affect the ability of myopodin to alter the chemokinetic response of PC3 cells.

Interestingly, while deletion of the carboxy-terminal 9 residues from MYO1 had no effect on cell migration (the ΔC-MYO construct in Fig. 17B), removal of the same sequence from ΔN-MYO1 (the ΔN/ΔC-MYO1 construct in Fig. 18A) significantly impaired the ability of this isoform to promote cell migration in the presence of FBS (Fig. 18C). Although this deletion is located outside of the characterized actin-binding domains, I speculated that the 9-residue carboxy-terminal sequence unique to MYO1 and ΔN-MYO1 might be an important regulatory site of ΔN-MYO1 function in actin network formation. Immunofluorescence staining revealed that the ΔN/ΔC-MYO1 construct failed to induce the formation of actin networks in transduced cells but myopodin was still detected in the cell body in a disseminated, punctate staining pattern (Fig. 18D). The nine unique carboxy-terminal amino acids of MYO1 and ΔN-MYO1 therefore do not affect myopodin localization to the cell body but are required for actin cytoskeleton remodeling in the absence of the extended amino-terminal region. Overall, the truncation results indicate that the conserved amino-termini present in the three long myopodin isoforms and the unique carboxy-terminus of MYO1 and ΔN-MYO1 individually contribute to both actin cytoskeleton remodeling and the chemokinetic effects of myopodin.

3.2.9.2. Myopodin Confers a Promigratory Property to PC3 Cells via its Actin Remodeling Activity

Since myopodin induces actin bundle formation, I speculated that the formation of these actin networks is directly linked to the mechanism by which myopodin enhances the migration of PC3 cells in response to FBS. As all the distinct actin cytoskeleton

networks induced by the different myopodin isoforms correlated with the increased migratory property of PC3 cells, only the most commonly studied isoform, ΔN-MYO1, was used in subsequent studies to probe the biological roles of the induced actin cytoskeletal networks on PC3 cell migration. Chemokinetic analysis demonstrated that myopodin has no effect on PC3 cell migration under starvation conditions (i.e. no FBS) while it enhances cell migration upon FBS stimulation (Fig. 10). Therefore, I examined whether FBS treatment induced the formation of actin networks in myopodin-expressing PC3 cells, which in turn might lead to increased cell migration.

ΔN-MYO1-transduced PC3 cells were starved for 24 hr prior to FBS addition and the effect of FBS on actin cytoskeleton dynamics was examined using immunocytochemical staining. Transwell migration assays were performed in parallel to ascertain the effect of FBS addition on PC3 cell motility. Under starvation conditions, ΔN-MYO1 had no effect on cell migration and few, if any, actin networks were observed in the myopodin-expressing PC3 cells (Fig. 19). Strikingly, within 30 min of FBS exposure, complex actin networks in the cell body were constructed and myopodin co-localized with the induced networks (Fig. 19A). As previously described (Fig. 10A), the addition of FBS also led to ~4-fold increase in cell migration (Fig. 17B). Mock-transduced and ΔN-MYO1-transduced PC3 cells were also examined at several time points (1 hr, 6 hr, and 24 hr) following FBS treatment. Myopodin-expressing PC3 cells were able to maintain the induced actin structures even 24 hr post FBS addition (Fig. 14), the time when transwell migration assays were quantified. However, mock-transduced cells failed to construct complex actin networks at any time after FBS addition, which may explain why mock-transduced PC3 cells are relatively unaffected by FBS stimulation. These results demonstrated a direct correlation between the enhanced chemokinetic activity of PC3 cells and the induction of complex actin networks in cells expressing myopodin.

3.2.9.3. Cytochalasin D Treatment Severely Disrupts Myopodin-induced PC3 Cell Chemokinetic Activity

The importance of the actin cytoskeleton meshwork induced by ΔN-MYO1 for enhanced PC3 cell migration was further evaluated using transwell migration assays in

the presence of different concentrations of cytochalasin D, an inhibitor of actin polymerization. Results indicated that cytochalasin D inhibited the ability of myopodin to promote cell migration in a dose-dependent manner (Fig. 20A). Although the migration of mock-transduced PC3 cells was inhibited by cytochalasin D treatment at doses of 40nM or higher, ΔN-MYO1-expressing PC3 cell migration was inhibited to an even greater extent under these treatment conditions. Most importantly, the lowest dose of cytochalasin D (20 nM) had no inhibitory effect on the migration of mock-transduced PC3 cells but the enhanced migration of cells expressing ΔN-MYO1 was signifcantly suppressed (Fig. 20A). Immunofluorescence microscopy further revealed that the 20 nM cytochalasin D treatment severely perturbed the actin cytoskeletal meshwork normally present in ΔN-MYO1-expressing cells (Fig. 20B). Under drug treatment, the actin cytoskeleton was stained diffusely around the cell periphery and in membrane protrusions with actin aggregates randomly distributed through the cell body. ΔN-MYO1 largely colocalized with these actin aggregates and to some extent with actin near the cell periphery (Fig. 20B). A similar study using nocodazole, a microtubule inhibitor, indicated that myopodin-enhanced cell migration is not dependent on microtubules. Although disrupting microtubules does inhibit cell migration, at each dose of nocodazole both mock-transduced and ΔN-MYO1-transduced PC3 cells displayed the same proportionate decrease in cell migration (Fig. 20C). In other words, cells expressing ΔN-MYO1 still migrated ~3-fold more than mock-transduced cells even though the overall extent of cell migration was inhibited by increasing doses of nocodazole.

Overall, inhibiting formation of the myopodin-induced actin meshwork by serum starvation, by partial inhibition of actin polymerization using cytochalasin D, and by terminal truncations of myopodin all eliminated or greatly reduced the ability of myopodin to enhance cell migration. Based on these results, I infer that myopodin-mediated remodeling of the actin cytoskeleton is directly responsible for the enhanced migration phenotype of myopodin in response to FBS stimulation.

3.2.10. Myopodin Isoforms Differentially Remodel the Actin Cytoskeleton in BPH-1 and DU145 Cells

The effect of myopodin isoforms on actin cytoskeleton remodeling was striking in malignant PC3 cells. However, it was unknown if myopodin isoforms also reorganize the actin cytoskeleton and affect cell migration in other cell types. Since myopodin may be a useful biomarker for invasive prostate cancer, the effects of myopodin on actin cytoskeleton rearrangement and cell migration were examined in two other prostate cell lines. The DU145 cell line was isolated from a brain metastasis derived from a case of invasive prostate cancer (Stone et al., 1978) while BPH-1 are non-invasive prostate hyperplasia. The expression level of myopodin is also downregulated in DU145 cells as in PC3 cells due to the hemizygous deletion of myopodin gene (Jing et al., 2004) while BPH-1 cells have higher myopodin expression levels than PC3 and DU145 cells (Fig. 7B; only PC3 cells and BPH-1 shown). DU145 and BPH-1 cell lines ectopically expressing myc-tagged myopodin constructs were generated using the retroviral transduction system and the effects of the myopodin isoforms on actin cytoskeleton rearrangement and cell migration were assessed in an identical manner as in PC3 cells.

Unlike PC3 cells, phalloidin staining indicated these two cell lines, even in the absence of myopodin, had prominent actin fibers in the cell body and actin-rich membrane protrusions (Fig. 21A). Nevertheless, the myopodin isoforms differentially remodeled and associated with the actin cytoskeleton in the cell body of both cell lines. MYO1 and ΔN-MYO1 rearranged the stress fibers normally present in DU145 and BPH-1 cells into amorphous, irregular actin networks (Fig. 21B; only MYO1 staining shown). In contrast, MYO3 and MYO4 organized the actin networks into long, thin parallel arrays of actin fibres that were generally positioned along the long axis of cells (Fig. 21B; only MYO3 staining shown). I did not observe any significant differences in the membrane protrusions between mock- and myopodin-expressing cells, as were observed in PC3 cells expressing myopodin (Fig. 21).

Immunofluorescence microscopy did reveal that myopodin isoforms not only remodeled the actin cytoskeleton, they also differentially associated with the actin structures. In DU145 and BPH-1 cells, MYO3 and MYO4 displayed the same punctuated staining pattern along the parallel F-actin fibers as was observed in PC3 cells (Fig. 14 & 21B). However, the staining pattern of MYO1 and ΔN-MYO1 in DU145 and BPH-1 cells was different from that in PC3 cells (Fig. 14 & 19B). MYO1 and ΔN-MYO1 both stained

strongly with the amorphous actin structures in the cell body that were distinct from what was observed within PC3 cells (Fig. 21B). Similar to the PC3 results, MYO2 exhibited an intermediate staining pattern with respect to the actin cytoskeleton, exhibiting either aggregated or punctuated staining patterns in both DU145 and BPH-1 cells. As in PC3 cells, the myopodin isoforms also did not colocalize ubiquitously with the actin cytoskeleton of DU145 and BPH-1. Myopodin predominantly localized to the cell body in BPH-1 cells. However, significant amounts of myopodin staining, for both the MYO1 and MYO3 staining pattern, were found along F-actin bundles at the cell periphery of DU145 cells (Fig. 21B, arrows).

Therefore, in three different prostate cancer cell lines, and despite differences in the types of actin structures, the different myopodin isoforms differentially induced and colocalized with actin structures in a consistent manner (i.e. MYO1 and ΔN-MYO1 are similar to each other but distinct from MYO3 and MYO4, which are similar to each other but distinct from MYO2). .

3.2.11. Myopodin Isoforms Exert Little Affect on BPH-1 and DU145 Cell Migration

Because myopodin can remodel the actin cytoskeleton in DU145 and BPH1 and the actin cytoskeleton is important for cell migration, I used transwell migration assays to further examine if the actin rearrangements induced by the myopodin isoforms also affected BPH-1 and DU145 cell migration. In contrast to PC3 cells, NIH 3T3 CM and FBS did not differentially affect BPH-1 or DU145 cell migration (Fig. 22A). Furthermore, BPH-1 and DU145 cells both migrated 3-5-fold better than PC3 cells under FBS stimulation (Fig. 22A). The myopodin isoforms modestly suppressed DU145 and BPH-1 cell migration under FBS conditions, although not all of the decreases in cell migration were statistically significant (Fig. 22B, C). In contrast, myopodin isoforms had little, if any, inhibitory effect in on DU145 or BPH-1 cell migration in the presence of CM (Fig. 20B, C). However, although not statistically significant, there was a trend for myopodin expression to modestly decrease migration of both cell types in response to CM. Overall, my results demonstrated that, although the different myopodin isoforms differentially remodel the actin cytoskeleton in mutilple cell types, the effects of myopodin on cell migration are cell-type specific and environmental stimuli-specific.

3.3. Discussion

Biomarkers that accurately predict whether localized prostate cancer will remain indolent or become invasive could help patients to make informed decisions regarding their treatment options and improve the quality of life of prostate cancer patients. Myopodin represents one such biomarker. Loss of myopodin expression strongly correlates with both increased invasive prostate cancer and with clinical prostate cancer relapse (Lin et al., 2001; Yu et al., 2006). Epigenetic silencing of myopodin gene expression is also a prognosticator of invasive bladder and colorectal cancers (Cebrian et al., 2008; Esteban et al., 2012). However, little is known about why myopodin loss correlates with tumour development, or the roles of recently identified myopodin isoforms in this process. There are also conflicting reports on whether myopodin is a tumor suppressor or promoter. The present study provides an explanation for these contradictory reports by revealing that myopodin modulates the cellular response to stimuli that differentially activate signaling pathways, resulting in either increased or decreased cell motility. Results also indicate that myopodin alters the chemokinetic response of PC3 cells to external stimuli, which is largely responsible for the effects of myopodin on cell invasion through the ECM. This first comparative study of the effects of the different myopodin isoforms on cell migration and invasion also revealed that all isoforms exert a similar effect on the cellular response to chemokinetic stimuli. Additionally, I determined for the first time that human myopodin isoforms induce actin cytoskeleton remodeling that directly correlates with the myopodin-stimulated chemokinetic activity of PC3 cells. Although all myopodin isoforms promote the chemokinetic activity of PC3 cells to the same extent, the different myopodin isoforms induced morphologically distinct actin networks in the cell body, suggesting the myopodin isoforms may not be functionally redundant. Although all myopodin isoforms promoted cell migration in response to FBS and inhibited migration in response to CM when assessed using transwell migration assays, it is possible that they exert different effects on cell migration in the complex, three-dimensional architecture of a tumour microenvironment. The differential effect of myopodin on actin cytoskeleton remodeling was also observed in DU145 and BPH-1 cell lines, emphasizing the ability of myopodin to restructure the actin cytoskeleton. However, the consequence of actin cytoskeleton

remodeling induced by myopodin on cell migration is dependent on both the type of cell and the environmental stimuli.

Myopodin Can Both Enhance and Suppress Cell Migration

The confusion over whether myopodin promotes or suppresses cell motility and invasion reflects the unexpected ability of myopodin to exert opposing effects on the cellular response to different external stimuli. This conclusion is supported by my observations that cell motility and cellular morphology are strikingly different in PC3 cells in the presence of CM and FBS (Fig. 9B & C), suggesting that these commonly employed stimuli activate different signaling pathways. FBS and CM have been frequently used interchangeably in publications. While PC3 cells are the most commonly used prostate cancer cell line, little attention has been paid to the chemotactic conditions used in transwell assays. One might think that PC3 cells are an outlier as it was the only one of the three prostate cell lines (PC3, DU145, and BPH-1) where myopodin induced an opposing effect on cell migration in response to the two different environmental stimuli (Fig. 22A). However, this seems unlikely because myopodin also enhances HEK293 cell migration and invasion under FBS conditions (Van Impe et al., 2003). My studies demonstrated the importance of recognizing that myopodin can alter the cellular response to different external stimuli that activate distinct signaling pathways during cell migration, resulting in myopodin exerting either a tumor suppressing or promoting effect on cells.

Based on publications from different myopodin research groups, I found the data to be very inconsistent, even within a research group. The Luo group supports the idea that myopodin is a tumor suppressor. They generally use CM as the chemoattractant for transwell migration assays and they select monoclonal ΔN-MYO1-expressing PC3 cells (Jing et al., 2004). Their results reported that myopodin has no effect on cell migration (Jing et al., 2004), and that myopodin suppresses cell migration (Yu and Luo, 2006; Yu and Luo, 2011). They also used FBS as a chemoattractant in one study and, unlike my results, reported that ΔN-MYO1 suppresses migration under these conditions (Yu and Luo, 2006). There is no discussion of the basis for their own contradictory results, and I am unsure why my results under FBS conditions differ from theirs. In contrast, the De

Ganck group, who supports myopodin as a tumor promoter, used polyclonal myopodin-expressing PC3 cells (De Ganck et al., 2009). PC3 cells are very heterogenous in their morphology and isolated monoclonal cells from this cell line differ in their functional characteristics under different culture conditions (Festuccia et al., 2000; Liu, 2000). Therefore, the data obtained from clonal selection of PC3 cells and different culture conditions should be evaluated carefully. I did note that each of the monoclonal myopodin-expressing PC3 cells used by the Luo group have differences in their cell migration ability, that could explain discrepancies in their data. In order to eliminate biased results, I ectopically expressed myopodin in PC3 cells and experiments were performed with the heterogeneous cell population under different culture conditions.

My data reconcile some of the confusion in the myopodin literature: cell lines, culture conditions and clonal selection may all contribute to discrepancies in the predicted roles of myopodin in tumor progression. It is now apparent that myopodin can dramatically alter the cellular response to different growth factors, presumably via its effects on diverse cellular signaling pathways, suggesting a complicated role for myopodin in cancer metastasis. The tumor microenvironment contains diverse chemical factors that can promote, inhibit, and coordinate the migration of both benign and cancerous cells. The plasticity of tumor cell morphology, similar to the different cell morphologies of PC3 cells under FBS or CM conditions (Fig. 9C), also allows cells to migrate efficiently in different tumor microenvironments (Friedl and Wolf, 2010). Here, I showed that myopodin can promote or decrease cell motility, either or both of which could provide an explanation for the role of myopodin as a tumor suppressor. For example, the coordinated, directional migration of epithelial cells is required to maintain the integrity of epithelium. If myopodin naturally functions to promote epithelial cell migration to maintain the healthy basal lamina that serves as barrier to cancer metastasis, then loss of myopodin expression would result in disruption of the epithelium. The function of myopodin as a tumor suppressor might, therefore, reflect roles in promoting and/or inhibiting cell migration. Since myopodin displayed a robust stimulatory effect on cell migration in response to FBS (~3-5 fold increase) as compared to CM, I focused the majority of my subsequent studies on analyzing the basis for the much stronger phenotype.

Chemotaxis Versus Chemokinesis

My results determined for the first time that myopodin alters the chemokinetic response of PC3 cells to an FBS stimulus. It was surprising that PC3 cells have such low intrinsic motility under FBS conditions (Fig. 9A) because various growth factors in FBS usually stimulate the migration of many cell types (Wells, 2000). Strikingly, the combination of FBS and myopodin significantly increased PC3 cell motility (Fig. 9A). It is likely that FBS activates some signaling pathways that can be altered by myopodin to drive cell movement. I further showed that myopodin promotes cell migration to the same extent in the presence of both positive and negative gradients of the external stimulus, indicating that myopodin enhances the chemokinetic, not the chemotactic, activity of PC3 cells. Chemotactic cells need to persistently establish a front-rear polarity axis and spatially restrict localization of polarity proteins for directional sensing in order to migrate along a gradient axis. In contrast, randomly migrating cells have a front-rear axis but fail to sense the direction of external cues to maintain persistent migration (Etienne-Manneville, 2008). My data suggest that myopodin activates the overall motility of PC3 cells but fails to polarize cells to migrate along a chemical gradient. This speculation is further supported by the fact that myopodin-regulated cell migration is independent of microtubules (Fig. 20C) as microtubules are crucial for cell polarization and directional cell movement (Kaverina and Straube, 2011). Although the checkerboard assay is widely used to differentiate chemotaxis and chemokinesis, one caveat is that the external stimulus can diffuse across the transwell porous membrane over time, leading to a loss of the chemical gradient. Live imaging of cells using an under-agarose cell migration assay that maintains the long-term chemical gradient has been used to deal with this issue in some studies (Heit and Kubes, 2003). However, this was not required in my studies since my results indicate that myopodin increases the chemokinetic activity of PC3 cells, a conclusion that would not be altered by diffusion of the external stimulus.

Myopodin Regulates Cell Invasion by Altering Cell Motility

The designation of myopodin as a tumor suppressor or promoter was also based on different approaches to data analysis of matrigel invasion assays (De Ganck et al.,

2009; Jing et al., 2004; Yu and Luo, 2006; Yu and Luo, 2011). Two general approaches to data analysis have been used: (1) direct quantification of the number of cells that traverse the matrigel-coated Boyden chambers, or (2) normalization of the number of cells invaded with the number of cells migrated (i.e. percent invasion). As shown in Fig. 11, two different conclusions could be drawn when I analyzed my results using these different approaches. The first approach, based on only quantifying the number of cells that traverse the matrigel-coated membrane, suggests that myopodin exerts opposing effects on cancer cell invasion in response to FBS or CM (Fig. 11A). However, when the effect of myopodin on cell migration is taken into account using percent invasion, myopodin always modestly suppressed the percent of invasive cells under both conditions (Fig. 11B). In the presence of CM, myopodin suppressed cell migration and invasion by ~40-50%, leading to an overall decrease in the percent cell invasion of ~25% (Fig. 11B). Under FBS conditions, myopodin led to an ~4-5-fold increase in cell migration but only an ~3.5-fold increase invasion, resulting in an overall ~25% decrease in the percent cell invasion (Fig. 11B). Myopodin therefore affected the percent cell invasion to approximately the same degree, regardless of whether it was promoting or inhibiting cell migration. Similar correlations between the percent inhibition of migration and invasion are evident in other studies (Yu and Luo, 2006; Yu and Luo, 2011). Since myopodin affected migration and invasion to approximately the same extent, the present results suggest that myopodin affects cell invasion primarily by altering cell motility.

Differential Effects of Myopodin Isoforms on Actin Cytoskeleton Remodeling

Human myopodin has been reported to colocalize with actin filaments in cells (De Ganck et al., 2008), and the mouse, rabbit and chicken homologues of myopodin promote actin polymerization and/or actin bundling (Beall and Chalovich, 2001; Leinweber et al., 1999; Weins et al., 2001). However, until recently, no studies have demonstrated that human myopodin affects actin structures, and no studies have reported that myopodin can bundle filamentous actin in a cell context. My results demonstrated that myopodin is able to induce the formation of thick or thin actin bundles within cells and myopodin is closely associated with the induced actin networks (Fig. 14). The type I disoriented actin meshwork induced by MYO1 and ΔN-MYO1 appeared to be composed of thick actin

filaments. In contrast, the type II actin network induced by MYO3 and MYO4 appeared as relatively thin, parallel F-actin fibres. The myopodin isoforms clearly colocalized preferentially with the induced F-actin structures, suggesting that myopodin may crosslink F-actin into bundles. This hypothesis is consistent with very recent *in vitro* biochemical assays that demonstrate human ΔN-MYO1 is an actin-bundling protein and possesses at least two independent actin binding sites (Linnemann et al., 2012).

Both types of myopodin-induced actin bundles, which are located between 60 nm to 120 nm from the ventral side of the cell, are spatially similar to ventral stress fibers or graded polarity actomyosin bundles, which are usually found beneath the nucleus and at the ventral side of the cell. Graded polarity bundles are composed of overlapping actin bundles that traverse the entire length of the cells while ventral stress fibers are usually shorter and appear along with dorsal and tranverse stress fibers. MYO3-induced actin bundles usually span the entire length of the cell, suggesting that the actin bundles induced by MYO3 are morphologically more similar to graded polarity bundles than to ventral stress fibers (Cramer et al., 1997). The punctuated MYO3 staining pattern along the bundles is also similar to myosin and α-actinin, which stain in an interdigitated pattern along the bundles (Langanger et al., 1986). Co-immunostaining of myopodin and myosin or α-actinin will be useful to determine how similar these thin, parallel actin bundles are to classical graded polarity actomyosin bundles.

The ΔN-MYO1-induced thick actin bundles, however, were very distinct from typical ventral stress fibers. Although the actin bundles are located at the ventral side of the cells, they are thick and not oriented along the longitudinal axis of cells. This morphology resembles the types of actin networks generated by higher concentrations of actin crosslinkers. For instance, low concentrations of filamin crosslink actin filaments at right angles forming orthogonal branches, higher concentrations lead to a mixture of thick parallel actin bundles embedded in an actin meshwork, and extremely high concentrations induce preferential formation of thick parallel bundles (Schmoller et al., 2009). Thus, one possible explanation for the different types of actin structures induced by myopodin is the different isoforms possess different degrees of actin crosslinking activity at a given myopodin concentration.

Yeast two hybrid assays demonstrated that a multimerization site (predominantly dimerization) is present in the second actin-binding site of myopodin (Linnemann et al., 2012). Differences in actin-binding affinity, actin bundling activity, or myopodin multimerization could, therefore, contribute to genesis of a contiguous staining pattern of myopodin along thick filaments versus punctuated staining along thin filaments. The ΔN-MYO1 and MYO1 isoforms may have higher binding affinity to actin filaments, leading to more myopodin binding per unit length of F-actin. As more myopodin is bound to the F-actin filament, the multiple actin-binding sites of myopodin could interact with more F-actin filaments. Under this scenario, the punctuated staining pattern of MYO3 and MYO4 is due to lower F-actin binding affinity and therefore less actin filaments are bundled. A second possibility is that all isoforms have the same affinity for F-actin but different actin-bundling activity. For example, ΔN-MYO1 and MYO1 may have all three actin-binding sites exposed while MYO3 has only 1 or 2 actin binding sites exposed. Thus, ΔN-MYO1 can crosslink more actin filaments than MYO3. The contiguous staining may then be attributed to the resolution limits of confocal microscopy that cannot resolve the individual punctuated staining along the thick actin bundles. A third possibility is the dimerization or multimerization domain of myopodin is exposed in ΔN-MYO1 and MYO1. Thus, myopodin multimers are present in close proximity and lead to contiguous staining. The above possibilities are not necessarily mutually exclusive, and it is conceivable that actin-binding affinity, actin bundling activity, or myopodin multimerization may all contribute to the nature of the myopodin-induced actin networks.

The amorphous MYO2-induced bundles suggest that the last exon of MYO2 may potentially inhibit its effect on actin cytoskeletal remodeling. MYO2 exhibited both contiguous and punctuated staining. It is possible that MYO2 affinity for actin filaments, bundling activity or multimerization activity is intermediate compared to ΔN-MYO1 and MYO3. Therefore, MYO2 fails to construct definable actin bundles. Furthermore, as myopodin was shown to promote actin polymerization, it is possible that MYO2 does not polymerize actin filaments as efficiently as the other isoforms, thus leading to shorter actin bundles. Electron microscopic analysis of the induced actin networks within cells coupled with immunogold staining of myopodin, or *in vitro* actin bundling assays using purified myopodin isoforms could confirm these speculations. Another possibility is that

the unique exons of the myopodin isoforms interact with different actin scaffolding proteins leading to distinct network formation. Additional yeast two-hybrid assays or co-immunoprecipitation assays using the unique myopodin exons might identify such interacting proteins and shed light on the molecular basis of these morphologically distinct actin bundles induced by the different myopodin isoforms.

Regardless of the distinct actin structures and staining patterns, all of the myopodin isoforms preferentially colocalized with the induced actin structures in the cell body, not with peripheral actin networks. The actin network in the cell body is triggered by overexpression or activation of RhoA (Ridley and Hall, 1992). Activation of RhoA enhances actomyosin contractibility and tail retraction for cell translocation. It is therefore possible that myopodin isoforms promote the formation of actomyosin bundles, leading to enhanced cell migration in response to FBS activation of cells. In addition, myopodin also promotes formation of membrane protrusions in PC3 cells (Fig. 14). Since Rho GTPases are important regulators of this process, analysis of the Rho signaling pathways is clearly warranted.

During cell migration, cross-talk between focal adhesion complex dynamics and the actin cytoskeletal network is also essential (Geiger et al., 2009). Thus, it is possible that myopodin alters the maturation of focal adhesions and therefore enhances cell migration. This speculation is supported by the recent observations that myopodin interacts with the focal adhesion-associated proteins ILK and zyxin (Yu and Luo, 2006; Yu and Luo, 2011). My analysis of Rho signaling pathways and focal adhesion dynamics are presented in Chapters 4 and 5, respectively.

Myopodin-induced Actin Networks Correlate with Enhanced Cell Migration

Three independent lines of evidence also indicated a direct correlation between the presence of the myopodin-induced actin networks and enhanced PC3 cell migration. First, the concomitant appearance of actin structures and enhanced chemokinetic activity of PC3 cells under FBS conditions in myopodin-expressing but not in mock-transduced cells suggest these two phenotypes are related (Fig. 19). Second, the importance of the induced structures was further corroborated by the findings that cytochalasin D suppressed actin structure formation and myopodin-stimulated cell migration (Fig. 20A,

C). Lastly, the ΔN/ΔC-MYO truncation construct that failed to promote PC3 cell migration also did not induce prominent actin structures. These results provide strong evidence in support of the conclusion that the myopodin-induced actin networks are a direct reflection of how myopodin promotes cell migration. However, it is unclear whether these actin structures are the cause or the consequence of the mechanism by which myopodin increases cell motility. For example, the demonstrated strong correlation between myopodin-induced actin bundles in the cell body and enhanced cell migration could indicate that myopodin, like tropomyosin, stabilizes the actin cytoskeleton in the cell body by inhibiting depolymerization of F-actin at the pointed end (Cooper, 2002). Conversely, during cell migration, myosin contraction results in the retrograde transfer of actin fibers present in filopodia and lamellipodia at the leading edge of the cell back toward the cell body. These fibers directly contribute to the formation of actin bundles and stress fibers in the cell body (Hotulainen and Lappalainen, 2006; Nemethova et al., 2008). Therefore, myopodin might promote cell migration by enhancing actin fiber formation at the leading edge, which results in the eventual integration of these fibers into actin networks in the cell body. Under this scenario, the low levels of myopodin staining at the cell periphery (Fig. 11C) would be more functionally relevant to cell migration than myopodin colocalization with the actin structures in the cell body. Again, these two possible roles for how myopodin induces actin bundles in the cell body and the involvement of these structures in cell migration may not be mutually exclusive.

The Unique Termini of the Myopodin Isoforms Influence the Formation of Actin Networks and Cell Migration

I also showed that the amino- and carboxy-termini of myopodin function in conjunction and exert different effects on formation of actin networks and cell migration. Removal of either the unique amino- or carboxy-termini of the different isoforms did not eliminate formation of the actin networks (Fig. 16) and had no effect on cell migration (Fig. 17). However, removal of both termini and strikingly, removal of just the nine unique amino acids present at the carboxy-terminus of ΔN-MYO1, dramatically impaired myopodin-induced cell migration and actin structure formation. Interestingly, the amino-termini could be removed with no affect on actin structures or cell migration, and while

deletion of the carboxy-terminus did not affect cell migration, it did have an observable effect on the induced actin network (Fig. 16). Cells expressing ΔC-MYO had a combination of shorter, parallel actin bundles with a punctuated myopodin staining pattern and thick irregular actin bundles with contiguous myopodin staining (Fig. 16B). The unique carboxy-termini of the myopodin isoforms might, therefore, regulate the actin binding or crosslinking activity of myopodin, leading to the formation of either disoriented or organized actin networks composed of actin fibers with different thicknesses. All previous publications focused on the the conserved region present in all myopodin isoforms, which has multiple protein-protein interaction sites (Weins et al., 2001; Yu and Luo, 2006; Yu and Luo, 2011). My truncation results imply that additional interaction motifs or regulatory domains are also present within the extended amino-termini of the long myopodin isoforms and in the short carboxy-terminal regions, and that these regions play an important role in myopodin-induced actin networks and cell migration.

It remains unclear why ΔC-MYO, but not ΔN/ΔC-MYO1, can still induce, albeit altered, actin structures in PC3 cells yet ΔN-MYO3 has no discernible phenotype. It is possible that the amino- and carboxy-termini of myopodin are two independent modules that are responsible for stepwise synthesis of actin bundles. For example, the 395 amino-terminal residues of myopodin might facilitate the ability of the actin binding sites in the conserved region to promote actin filament formation, with the unique exons at the carboxy-termini then influencing the nature and degree of filament crosslinking into actin bundles. However, if this were the case, then promotion of actin filament formation by the amino-terminus must be dispensible or capable of occuring in some other manner in order to explain the lack of a ΔN-MYO3 phenotype.

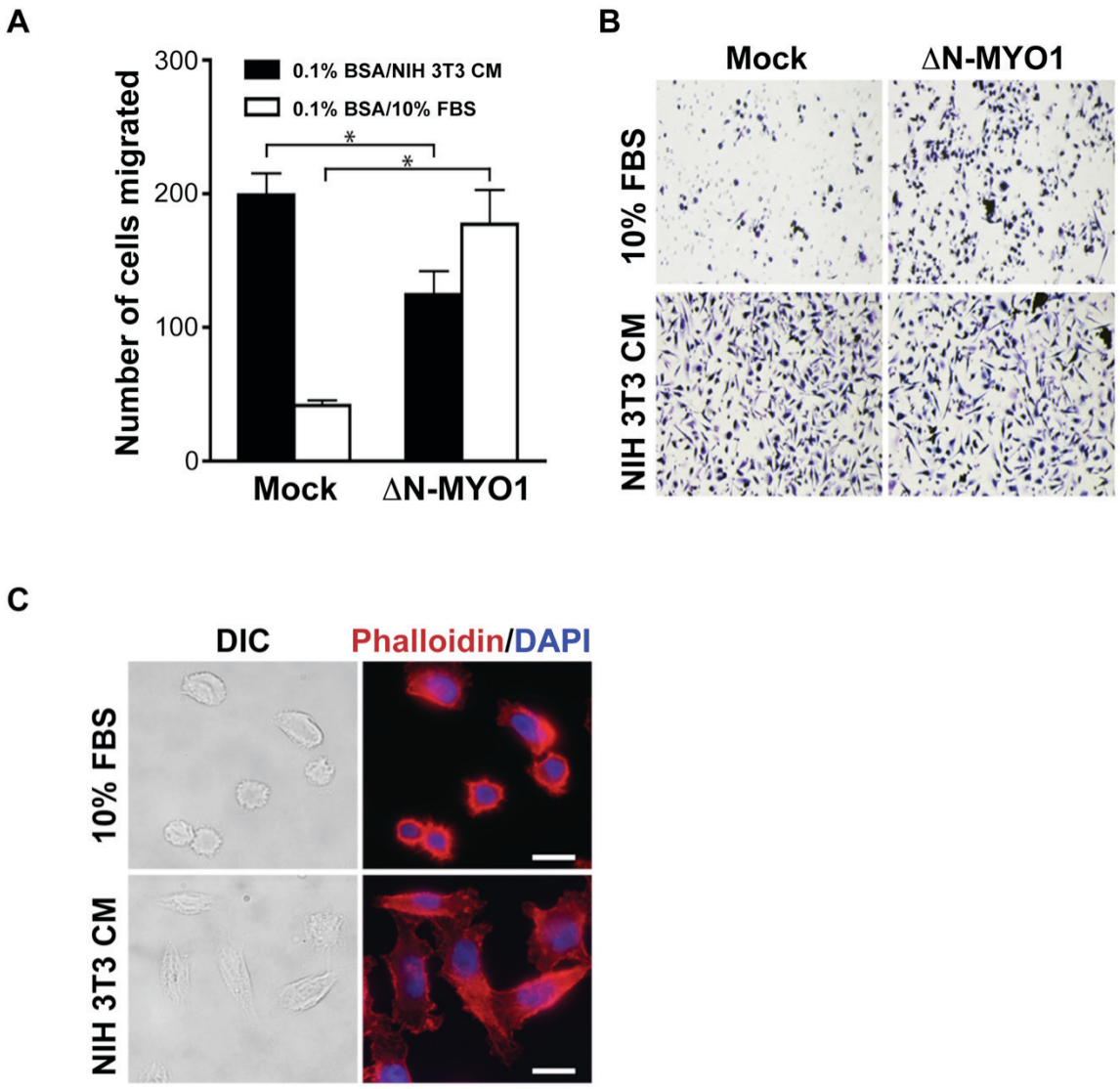

Figure 9. ΔN-MYO1 differentially alters the migration and morphology of PC3 cells in response to different chemoattractant conditions. (A) PC3 cells were transduced with retroviral vectors encoding ΔN-MYO1 or mock-transduced, cells were cultured with 0.1% BSA in the upper compartment and either 10% FBS (0.1% BSA/10% FBS) or NIH 3T3 CM (0.1% BSA/NIH 3T3 CM) in the lower compartment of the Boyden chambers, and the number of cells that migrated across the transwell membranes was quantified. Results are reported as the mean number of cells migrated per microscopic field ± SEM from three independent experiments performed in duplicate. Statistically significant differences between paired samples are indicated (*$P < 0.05$). **(B)** Representative images, at 10× final magnification, of Giemsa-stained ΔN-MYO1- and mock-transduced cells on the lower side of a transwell membrane from a representative experiment as described in panel A. **(C)** Mock-transduced PC3 cells under the indicated chemoattractant conditions were visualized by differential interference contrast (DIC) microscopy, and by fluorescence microscopy of DAPI and AlexaFluor555-conjugated phalloidin stained cells. Scale bar = 20 μm.

A

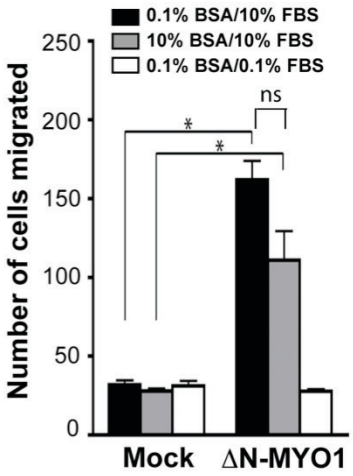

B

		Top chamber (%FBS)			
		0.1%*	1.50%	3%	10%
Bottom chamber (%FBS)	0.1%*	45.6 ± 7.10	183.2 ± 27.0	167.8 ± 10.8	123.0 ± 23.9
	1.50%	267.4 ± 15.5	**278.2 ± 16.0**	293.4 ± 49.1	182.0 ± 23.4
	3%	298.5 ± 26.1	255.8 ± 32.1	**287.0 ± 16.1**	158.0 ± 19.2
	10%	273.6 ± 23.4	263.6 ± 20.5	230.6 ± 30.9	191.8 ± 23.3

Figure 10. Myopodin affects the chemokinetic properties of PC3 cells. (A) PC3 cells were transduced with retroviral vectors encoding ΔN-MYO1 or mock-transduced, and the number of cells that migrated across transwell membranes in response to the indicated concentrations of 0.1% BSA and 10% FBS in the upper or lower compartments of the Boyden chambers was quantified. Results are reported as the mean number of cells migrated per microscopic field ± SEM from three independent experiments performed in duplicate. **(B)** The chemokinetic effect of myopodin on cell migration was assessed with a checkerboard transmigration assay at the indicated concentrations of attractant in the lower and upper chambers. Numbers are the mean number of cells ± SD that migrated across the membrane. (*$P < 0.05$; ns=not significant).

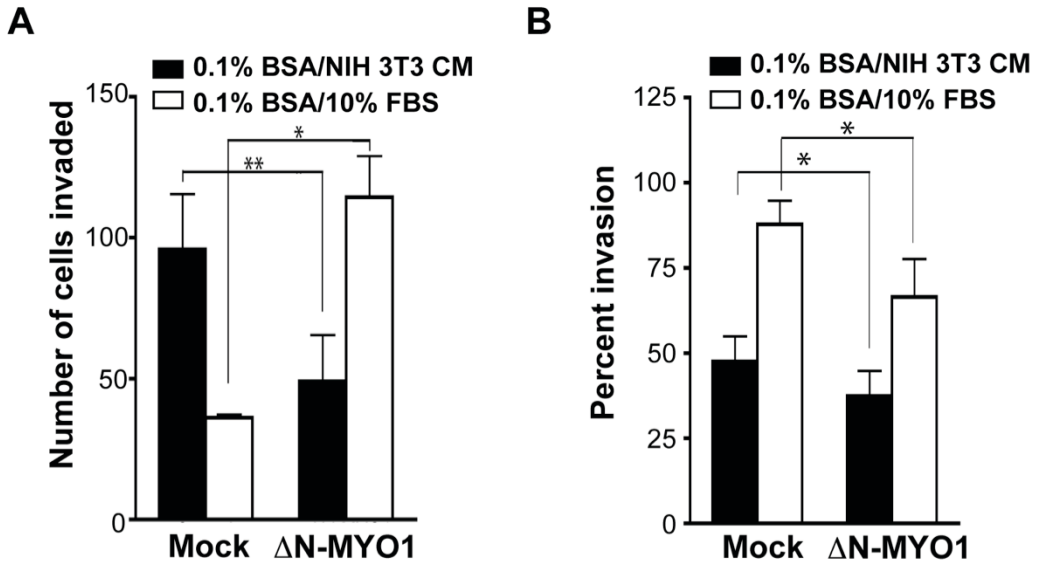

Figure 11. ΔN-MYO1 modestly inhibits the invasion of PC3 cells in response to different chemoattractant conditions. (A) As in Fig. 9, except filters were coated with matrigel to examine the effects of ΔN-MYO1 and the indicated chemoattractant conditions on PC3 cell invasion. **(B)** As in panel A, except membranes were either coated with matrigel to quantify cell invasion or not coated to assess cell migration, and results are reported as the percent invasion (number of cells invading through the matrigel/number of cells migrating through the filters × 100). For both panels, results are reported as the mean ± SEM from three independent experiments performed in duplicate. Statistically significant differences between paired samples are indicated (*$P < 0.05$; **$P < 0.01$).

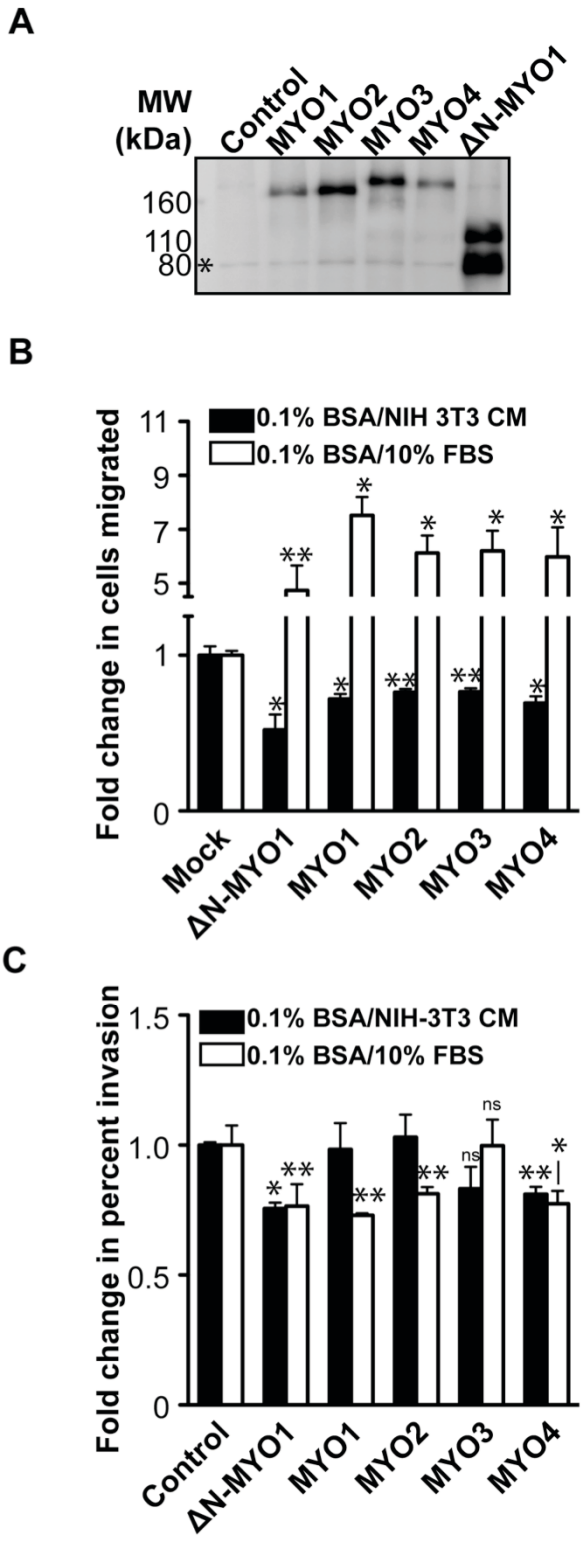
A
MW
(kDa)
Control
MYO1
MYO2
MYO3
MYO4
ΔN-MYO1
160
110
80
B
0.1% BSA/NIH 3T3 CM
0.1% BSA/10% FBS
Fold change in cells migrated
11
9
7
5
1
0
Mock
ΔN-MYO1
MYO1
MYO2
MYO3
MYO4
C
0.1% BSA/NIH-3T3 CM
0.1% BSA/10% FBS
Fold change in percent invasion
1.5
1.0
0.5
0
ns
Control
ΔN-MYO1
MYO1
MYO2
MYO3
MYO4

Figure 12. All myopodin isoforms exert similar differential effects on the migration and invasion of PC3 cells in response to different chemoattractant conditions. (A) PC3 cells were transduced with retrovirus vectors expressing the indicated myopodin isoforms or mock-transduced, and myopodin expression levels were determined by western blotting using a polyclonal anti-myopodin antibody. The migration of molecular mass standards is indicated on the left. The asterisk indicates a cross-reacting host cell protein. shRNA knockdown analysis demonstrated that this background band is not endogenous myopodin. **(B)** The migration of PC3 cells, mock-transduced or transduced with vectors expressing the indicated myopodin isoforms, through transwell membranes in response to the indicated migration stimulus (CM or FBS) was determined as described in Fig. 9. **(C)** The effect of myopodin isoforms on cell invasion under the indicated conditions was determined as in Fig. 11B. Results are reported as the mean fold change in cells migrated relative to mock-transduced cells (control) ± SEM from three independent experiments performed in duplicate. Statistically significant differences between paired samples are indicated (*$P < 0.05$; **$P < 0.01$; ns=not significant).

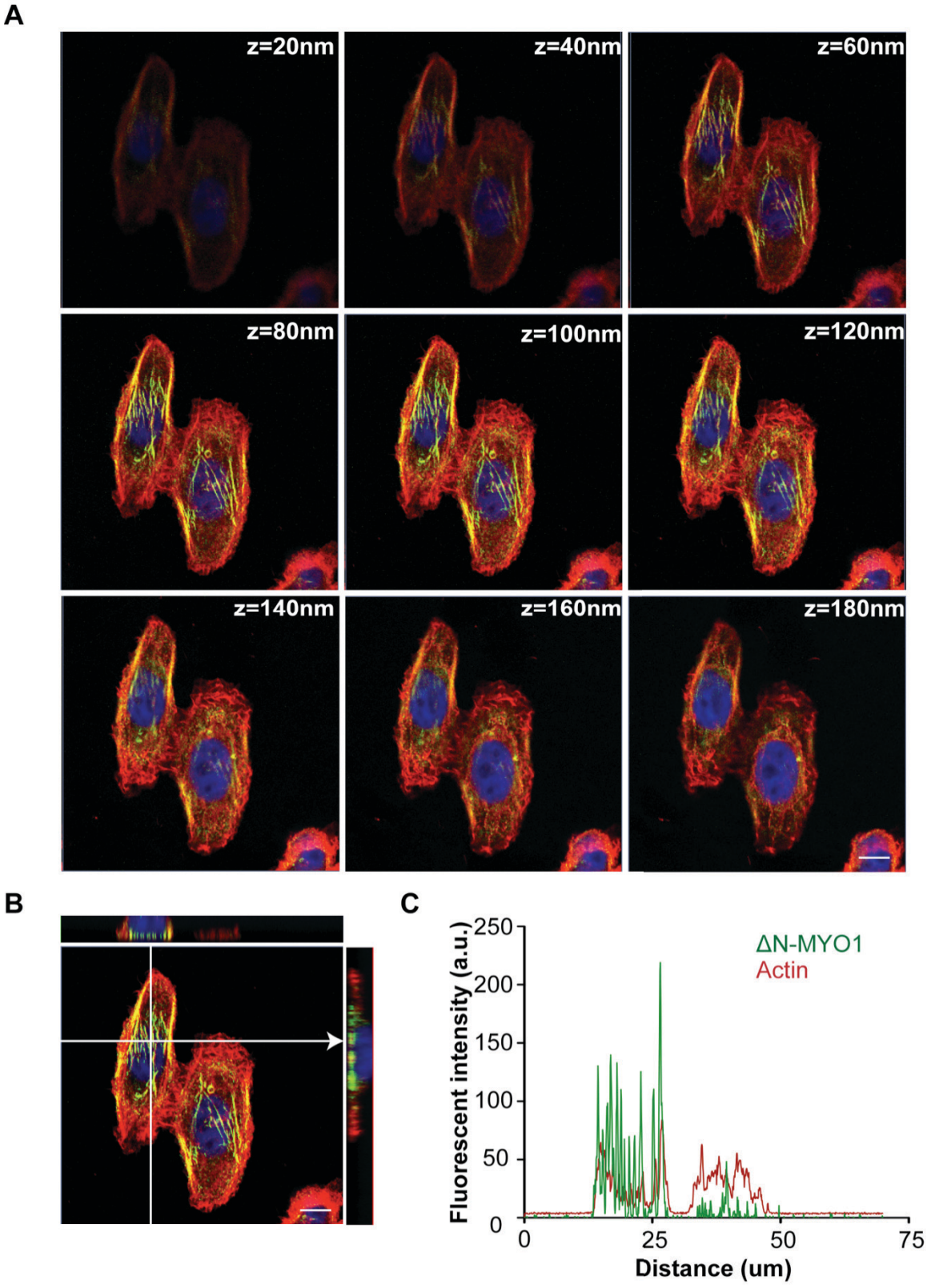
A
z=20nm
z=40nm
z=60nm
z=80nm
z=100nm
z=120nm
z=140nm
z=160nm
z=180nm
B
C
ΔN-MYO1
Actin
Fluorescent intensity (a.u.)
250
200
150
100
50
0
0
25
50
75
Distance (um)

Figure 13. Approaches to quantify cells with actin structures and to analyze subcellular localization of myopodin. (A) PC3 cells were transduced with a retrovirus vector expressing myc-tagged ΔN-MYO1. The subcellular localization of myopodin was detected using anti-myc primary antibody (green). The actin cytoskeleton and the nucleus were visualized using phalloidin (red) and DAPI (blue), respectively. Confocal sections of PC3 cells expressing ΔN-MYO1 construct between 20 nm (bottom) and 180 nm (top) exhibited prominent actin structures near the ventral side of cells. Scale bar=10 μm. **(B)** The orthogonal views of confocal images of ΔN-MYO1-expressing PC3 cells (imaged along the vertical and horizontal white lines) demonstrated the actin structures were located beneath the nucleus and in the cell body. Scale bar=10 μm. **(C)** Subcellular localization of the actin cytoskeleton and myopodin (imaged along the white line with arrowhead in panel B) was analyzed using ImageJ software. ΔN-MYO1 predominantly colocalized with the actin structures in the cell body with trace amounts of myopodin detected in the vicinity of actin structures at the cell periphery.

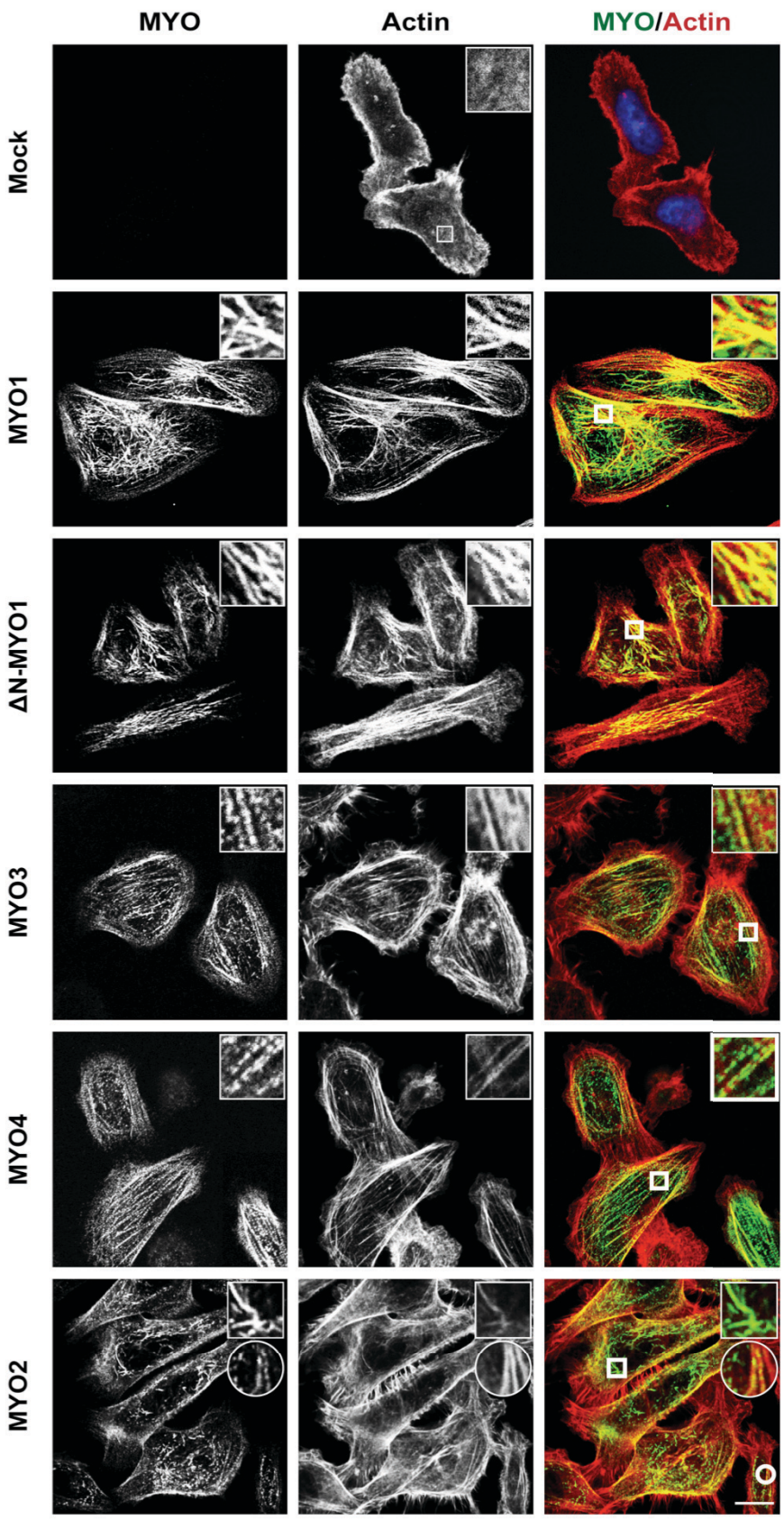
MYO
Actin
MYO/Actin
Mock
MYO1
ΔN-MYO1
MYO3
MYO4
MYO2

Figure 14. Myopodin isoforms differentially induce distinct actin networks and differentially colocalize with the actin structures. PC3 cells were transduced with the indicated retrovirus vectors expressing myc-tagged myopodin isoforms. Myc-tagged myopodin was immunostained with anti-myc antibody (green) and filamentous actin was stained with phalloidin (red). The 4 μm x 4 μm areas indicated in the images are magnified 420% in the insets. Scale bar=10 μm.

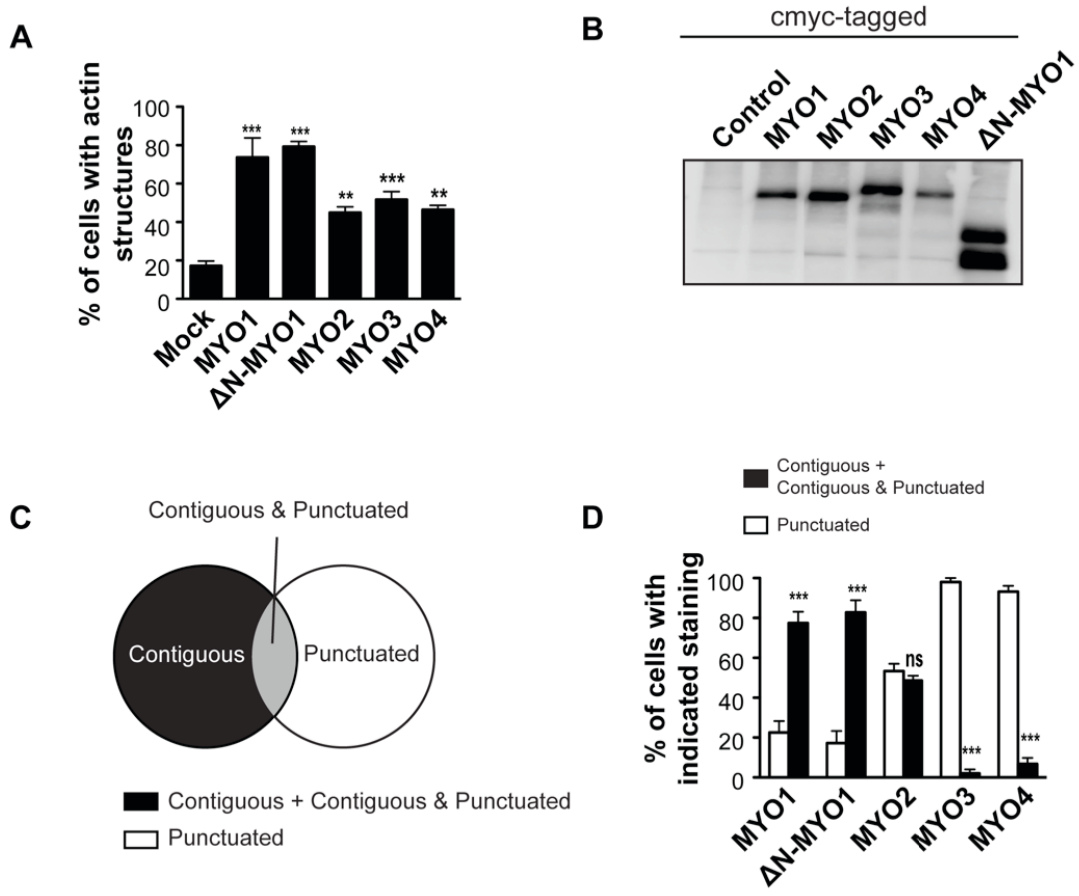

Figure 15. Quantification of the effect of myopodin isoforms on actin cytoskeleton architecture and myopodin staining patterns. (A) The effect of myopodin isoforms on actin cytoskeleton architecture is reported as percentage of cells with actin structures, which was derived from the equation: cells with both actin structures and myopodin staining/total cells with myopodin staining. A minimum of 60 cells was imaged and counted. Results are reported as the mean ± SEM from three independent experiments. **(B)** The expression levels of all myopodin isoforms within PC3 cells were determined by western blotting using a polyclonal anti-myopodin antibody. **(C)** Two commonly observed myopodin staining patterns: (1) contiguous myopodin staining along thick bundles in the center of the cell and (2) only punctuated staining along the thin bundles. Some cells displayed both patterns (intersection of the Venn diagram) with the punctuated staining on thin bundles around the perimeter of the cell. (D) Quantification of the staining pattern of myopodin isoforms in PC3 cells. Results are reported as mean percentage of cells with the indicated staining ± SEM from three independent experiments (***P < 0.001; **P<0.01; ns=not significant).

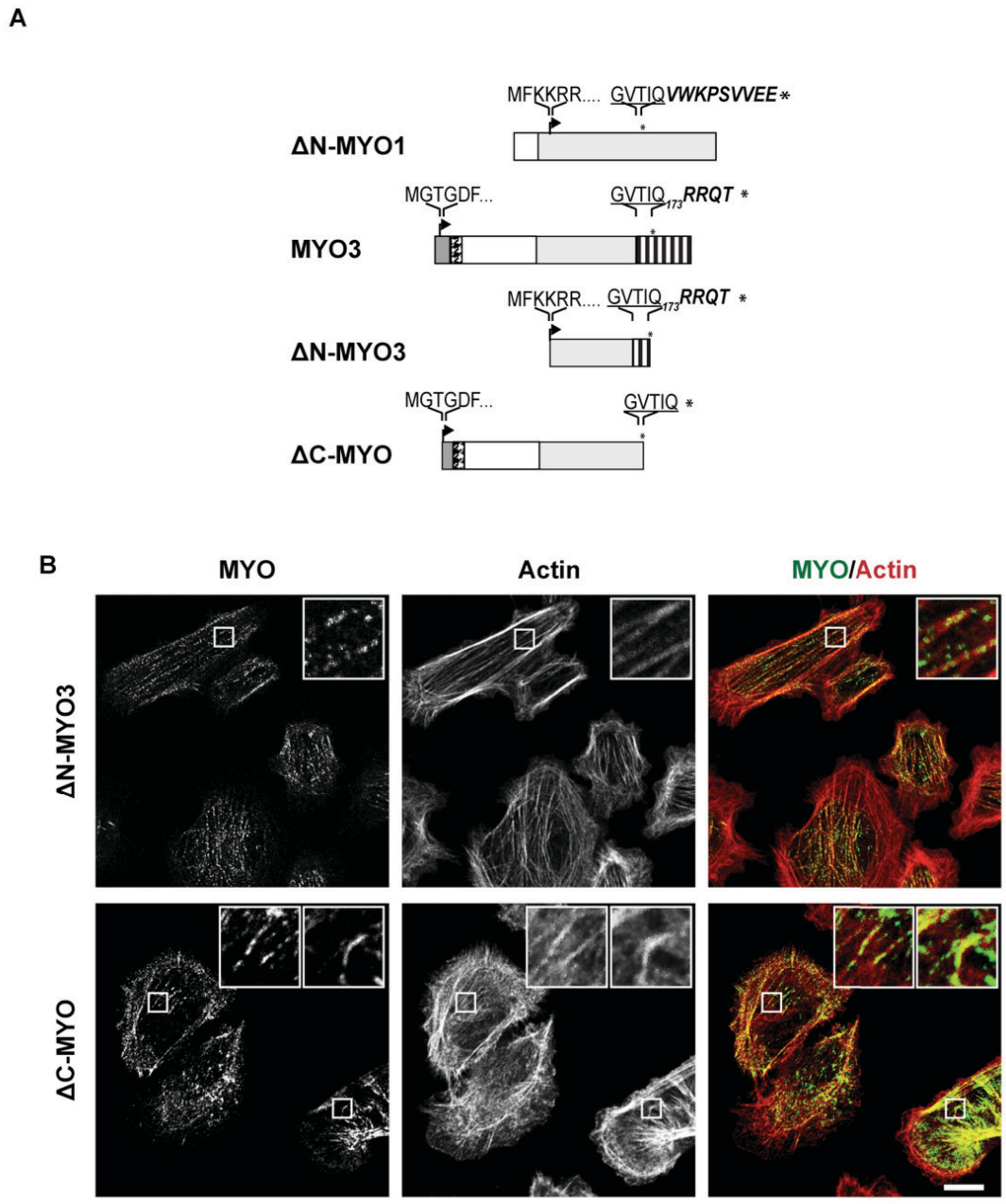

Figure 16. The carboxy-terminus of myopodin determines actin bundle thickness and staining pattern of myopodin isoforms with respect to the actin cytoskeleton. **(A)** Schematic diagram of the truncated myopodin mutants generated to identify the sequences responsible for the myopodin staining patterns and type of bundles formed. The amino-terminus of MYO3 was truncated to the methionine start codon of the ΔN-MYO1 isoform (ΔN-MYO3 construct). The unique carboxy-termini of the various isoforms were truncated back to the sequence conserved in all isoforms (underlined sequence; ΔC-MYO construct). **(B)** PC3 cells expressing ΔN-MYO3 and ΔC-MYO were immunostained as described in Fig. 14. The 4.5 μm x 4.5 μm areas indicated in the images are magnified 430% in the insets. Scale bar=10 μm.

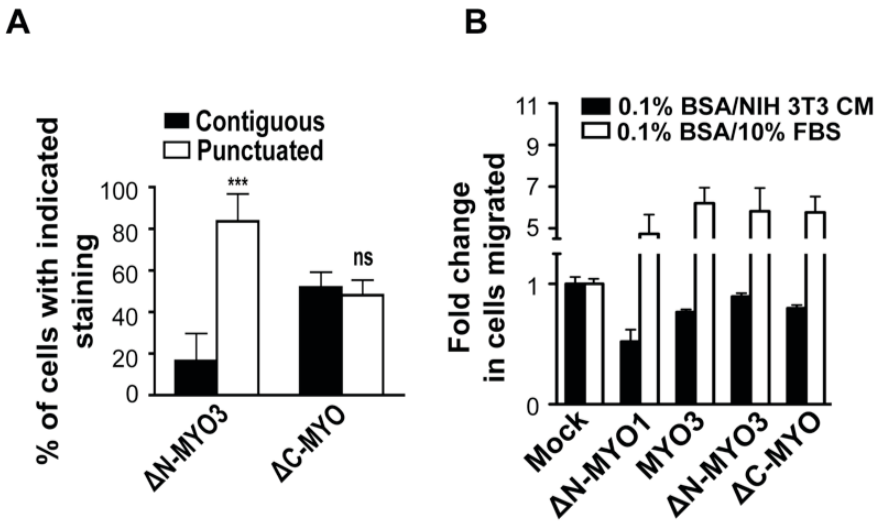

Figure 17. Deletions of the unique residues at either the amino or carboxy-termini of myopodin isoforms have no effect on myopodin-stimulated cell migration. (A) The staining pattern of ΔN-MYO3 and ΔC-MYO were quantified as described in Fig. 15C. Results are reported as percentage of cells with the indicated staining ± SEM from a three independent experiments (***P < 0.001; ns=not significant). **(B)** The migration of PC3 cells, mock-transduced or transduced with vectors expressing the indicated myopodin constructs, through transwell membranes in response to the indicated migration stimulus (CM or FBS) was determined as described in Fig. 9. Results are reported as the mean fold change in cells migrated relative to mock-transduced cells ± SD from a representative experiment (n = 3) conducted in triplicate.

A

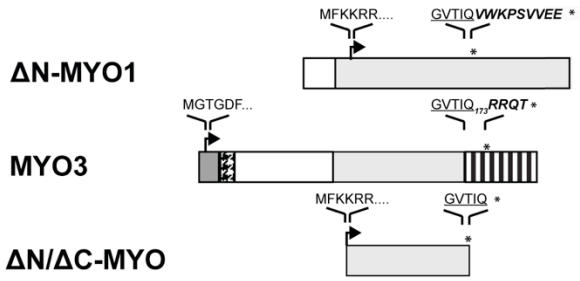
MFKKRR....
GVTIQVWKPSVVEE *
ΔN-MYO1
MGTGDF...
GVTIQ173RRQT *
MYO3
MFKKRR....
GVTIQ *
ΔN/ΔC-MYO

B

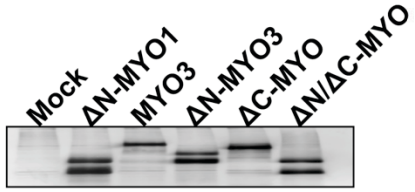
Mock
ΔN-MYO1
MYO3
ΔN-MYO3
ΔC-MYO
ΔN/ΔC-MYO

C

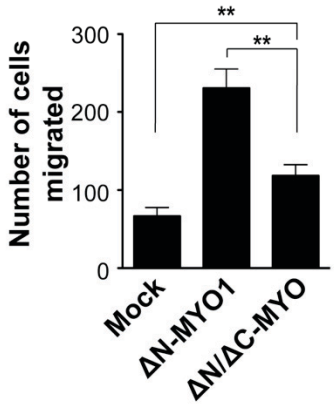
**
**
300
200
100
0
Number of cells migrated
Mock
ΔN-MYO1
ΔN/ΔC-MYO

D

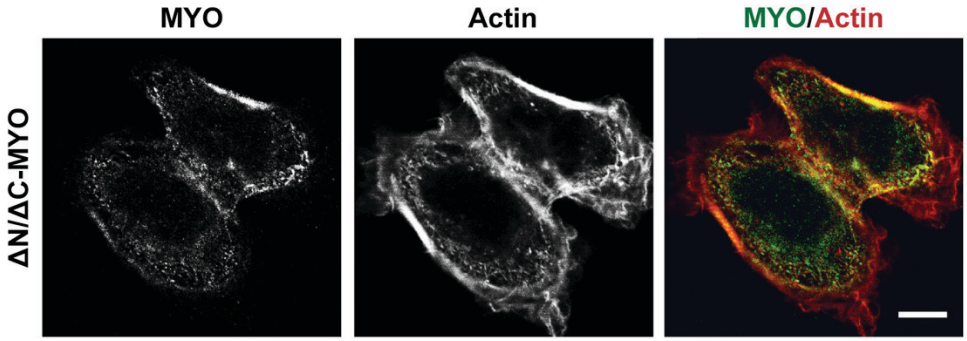
MYO
Actin
MYO/Actin
ΔN/ΔC-MYO

Figure 18. Both the amino- and carboxy-termini of myopodin isoforms are required for myopodin-stimulated cell migration. (A) Schematic diagram of the truncated myopodin mutant ΔN/ΔC-MYO, which starts from the methionine start codon of ΔN-MYO1 and was carboxy-terminally truncated to the sequence conserved in all isoforms (underlined sequence; ΔC-MYO construct). **(B)** Western blot detection of the ectopically expressed myopodin constructs in PC3 cells using a polyclonal anti-myopodin antibody. **(C)** The chemokinetic activity of PC3 cells expressing ΔN/ΔC-MYO, ΔN-MYO1 or control vector under FBS conditions was assessed using transwell migration assays as described in Fig. 9. Results are reported as the number of cells migrated across the filter ± SEM from three independent experiments conducted in triplicate (**P<0.01). **(D)** The effect of ΔN/ΔC-MYO1 on actin cytoskeleton architecture was assessed using immunofluorescence and phalloidin staining as described in Fig. 14. Scale bar=10 μm.

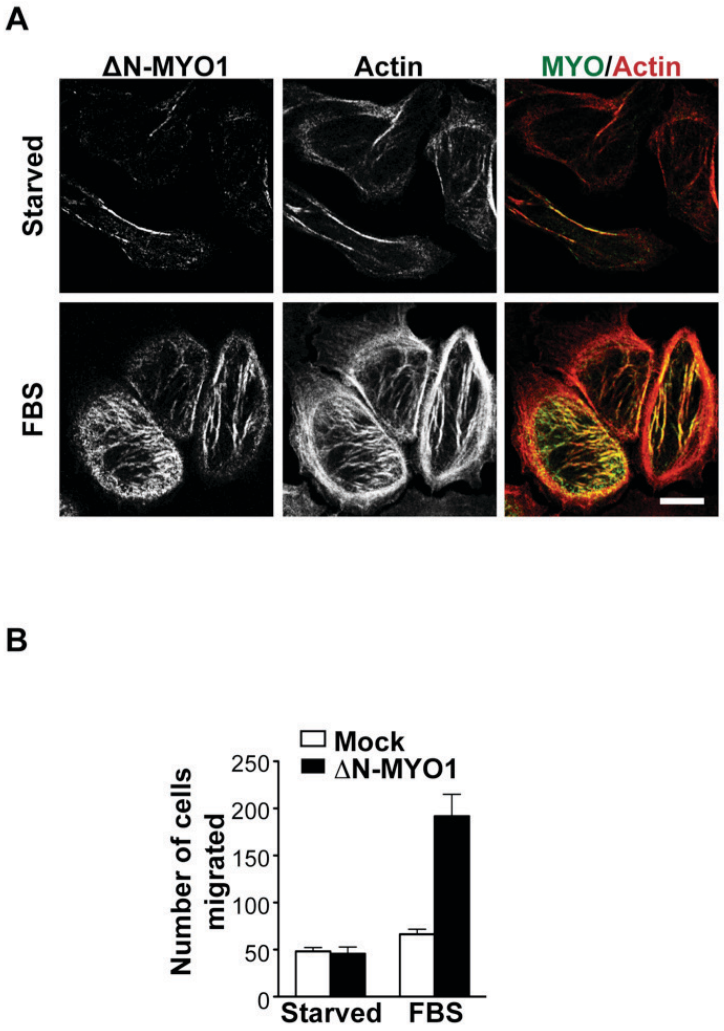

Figure 19. Myopodin induces prominent actin structures and enhances PC3 cell chemokinetic activity upon FBS stimulation. (A) PC3 cells expressing mock or ΔN-MYO1 constructs were synchronized under serum-starvation conditions overnight. PC3 cells were treated with serum-free medium or FBS for 30 min prior to fixation for immunofluorescence staining as described in Fig. 14. **(B)** The migratory ability of transduced PC3 cells was assessed as described in Fig. 9 in parallel with the immunofluorescence analysis in panel A. Results are reported as the number of cells migrated ± SD from a representative experiment (n = 3) conducted in triplicate. Scale bar=10 μm.

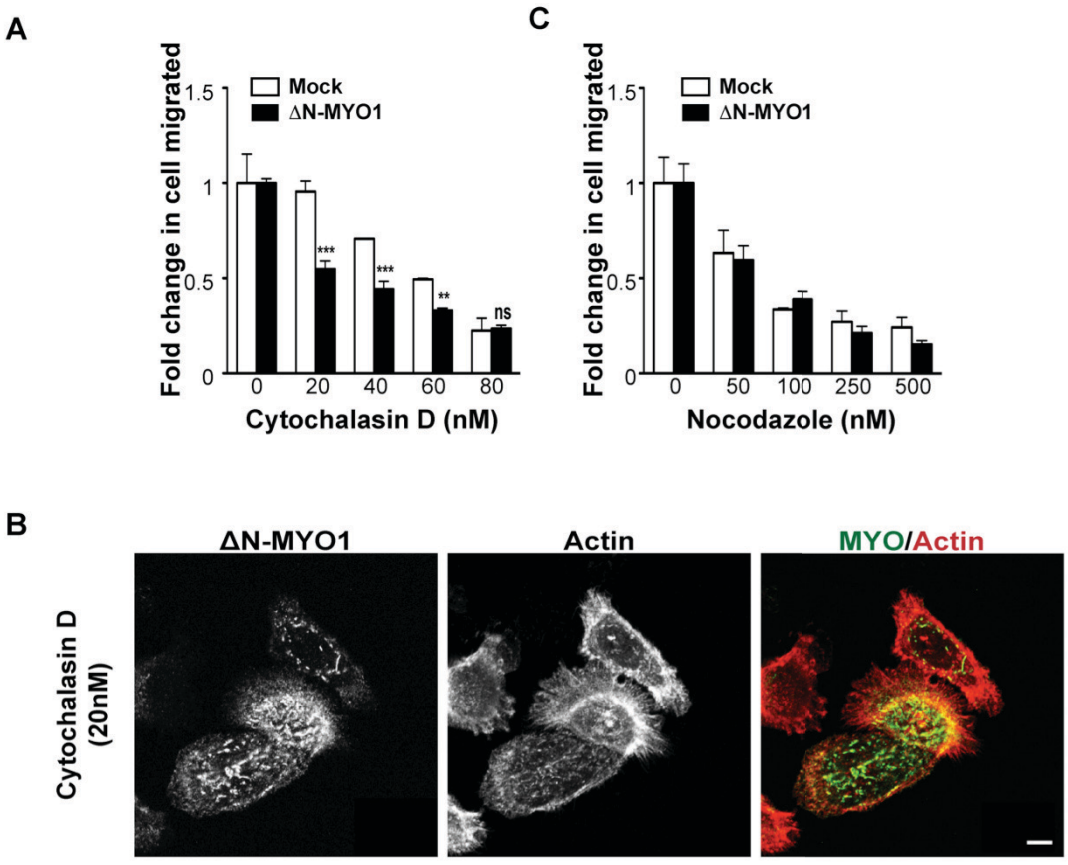

Figure 20. Myopodin-stimulated PC3 cell migration is dependent on the actin cytoskeleton but is independent of microtubules. Dose-responses curves of cytochalasin D, an actin polymerization inhibitor **(A)** and nocodazole, a microtubule inhibitor **(C)** were generated. PC3 cells were transduced with retroviral vectors expressing the indicated ΔN-MYO1- or mock-transduced, and the number of cells that migrated across transwell membranes of the Boyden chambers under FBS conditions was quantified as described in Fig. 9. Results are reported as the mean fold change in mock- and ΔN-MYO1-transduced cells migrated relative to the untreated transduced cells ± SEM from three independent experiments conducted in duplicate. **(B)** The effect of 20 nM cytochalasin D on PC3 cells expressing ΔN-MYO1 construct was visualized using phalloidin staining (red) and immunofluorescence staining of myopodin using anti-myc antibody (green) as described in Fig. 14. Scale bar=10 μm.

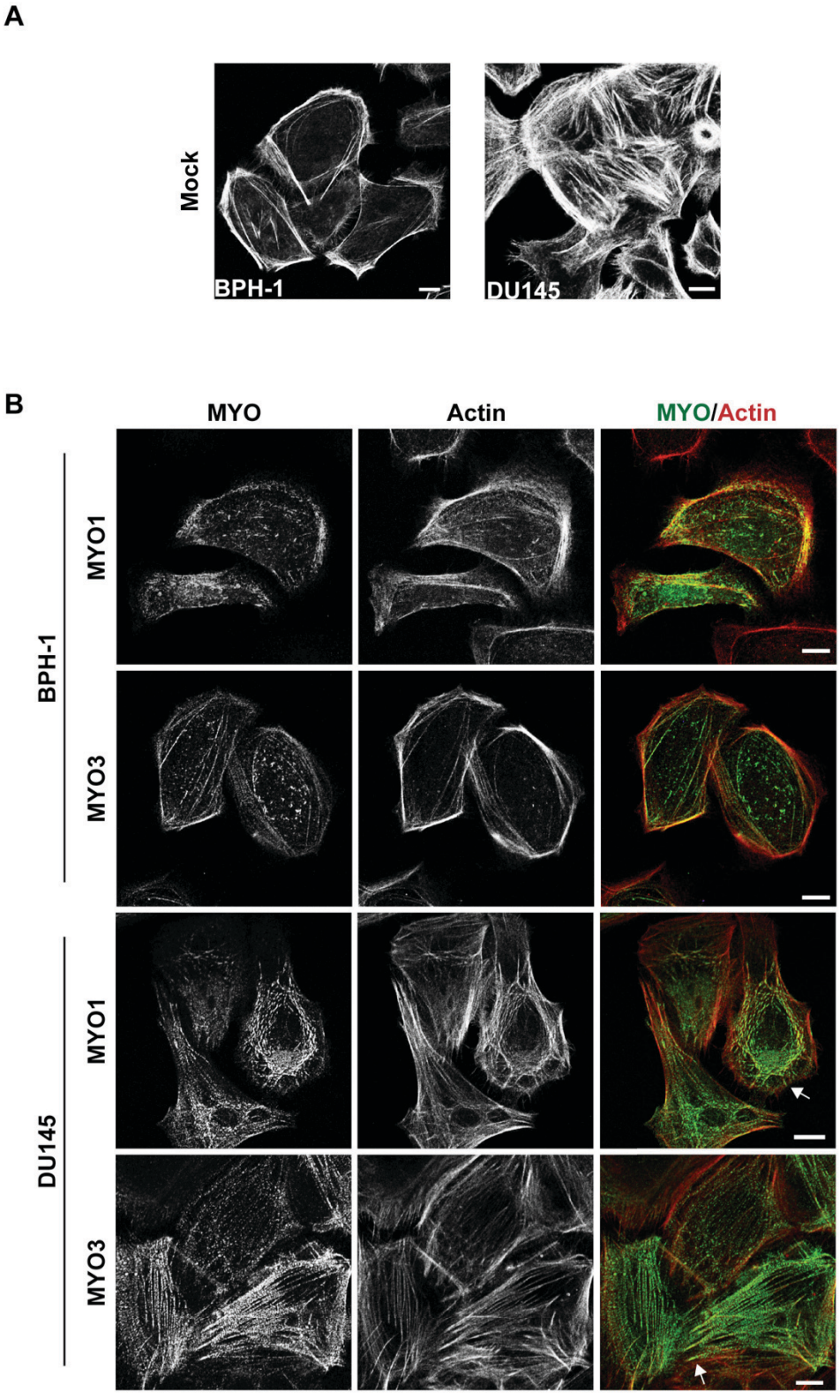
A
Mock
BPH-1
DU145
B
MYO
Actin
MYO/Actin
BPH-1
MYO1
MYO3
DU145
MYO1
MYO3

Figure 21. Myopodin isoforms differentially remodel and colocalize with the actin cytoskeleton of BPH-1 and DU145 cells. (A) Actin architectures of the parental BPH-1 and DU145 cells were visualized using phalloidin staining (white). **(B)** DU145 and BPH-1 cells were transduced with the indicated retrovirus vectors expressing myc-tagged myopodin isoforms. Myopodin was immunostained using anti-myc antibody (green) and the actin cytoskeleton was visualized using phalloidin staining (red). Strong myopodin staining at the cell periphery of DU145 cells is indicated with white arrows. Scale bar=10 μm.

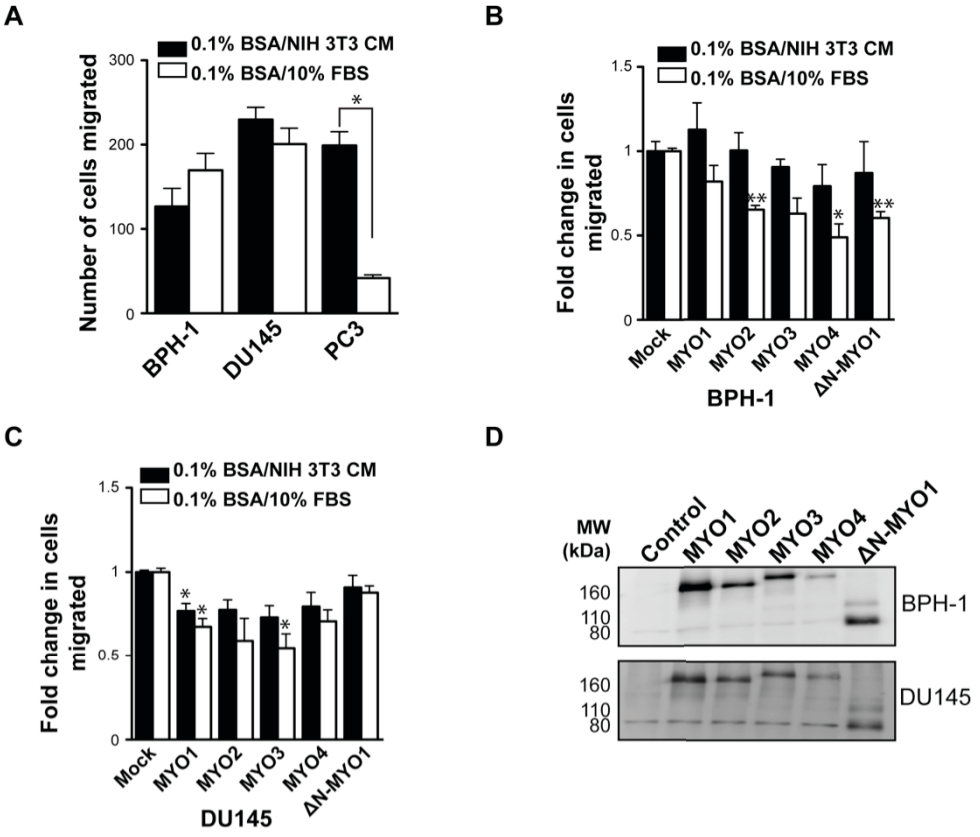

Figure 22. Myopodin isoforms have little, if any, effect on DU145 and BPH-1 cell migration. (A) The number of parental BPH-1, DU145, and PC3 cells that migrated across transwell membranes in response to the indicated conditions (FBS and CM) was quantified. Results are reported as the number of cells migrated across the filter ± SEM from three independent experiments conducted in duplicate (*P<0.05). The effects of myopodin isoforms on BPH-1 **(B)** and DU145 **(C)** cell migration were assessed as in Fig. 9 under the indicated conditions. Results are reported as the mean fold change in cells migrated relative to mock-transduced cells ± SEM from three independent experiments conducted in triplicate (**P<0.01; *P<0.05). **(D)** Expression levels of each isoform were confirmed by western blotting using polyclonal anti-myopodin antibody. The migration of molecular mass standards is indicated on the left.

CHAPTER 4: MYOPODIN ISOFORMS ENHANCE PC3 CHEMOKINETIC ACTIVITY VIA RHO-ROCK-DEPENDENT SIGNALING BUT INDEPENDENT OF NON-MUSCLE MYOSIN II

4.1. Introduction

Myopodin isoforms have opposing effects on PC3 cell migration under different chemokinetic conditions, suggesting myopodin differentially regulates the response of PC3 cells to distinct external stimuli. The striking effect of myopodin on cell migration and the formation of actin networks in the presence of FBS provided a great system to study the mechanism of myopodin-mediated cell migration. While disruption of myopodin-induced actin structures impaired cell migration, the molecular mechanisms behind these myopodin-mediated events were unclear.

One mechanism by which myopodin might induce formation of ventral stress fibers or graded polarity actomyosin bundles is by affecting actin crosslinking. Ventral stress fibers attach to FAs at both ends and are usually found along with dorsal and tranverse stress fibers, both of which directly contribute to the formation of ventral stress fibers (Fig. 4B) (Hotulainen and Lappalainen, 2006). Graded stress fibers are also located in the ventral area of the cell. In contrast to ventral stress fibers, graded stress fibers are usually longer and span the entire length of the cell (Fig. 4A) (Cramer et al., 1997). Both ventral and graded polarity stress fibers are bound by NM II and α-actinin, that localize in an interdigitated manner along the bundled actin filaments. Consequently, ventral and graded polarity stress fibers are also called actomyosin bundles. Since fesselin can interact with α-actinin and myosin, it is possible that human myopodin may have similar interaction sites and, therefore, be recruited to actomyosin bundles. It is also conceivable that the distinct contiguous and punctuated staining patterns of myopodin on actin bundles could reflect differences in myopodin interactions with these actin crosslinkers. Actin crosslinkers are also important for stress fiber formation and maintenance. For instance, the expression of a truncated α-actinin mutant disassembles stress fibers, even in the presence of functional NM II (Pavalko and Burridge, 1991; Schultheiss et al., 1992). Using its actin crosslinking activity, myopodin may therefore facilitate actin network formation by stabilizing actomyosin bundles. As several components of the Rho/ROCK pathway are involved in stress fiber formation, myopodin may induce actin

structures by modulating this pathway. Stress fiber formation can be induced by overexpression of RhoA (Paterson et al., 1990) and synaptopdin-long, one of the synaptopodin-1 family members, induces prominent stess fibers by suppressing RhoA degradation in kidney podocytes (Asanuma et al., 2006). In addition to possible direct effects on RhoA, similar to synaptopodin-1, several downstream effectors that regulate actin cytoskeleton remodeling are potential targets for myopodin. For instance, GTP-bound RhoA activates ROCK, a kinase that phosphorylates NM II and MLC phosphatase (Vicente-Manzanares et al., 2009), which in turn increases phosphorylation levels of NM II. Phosphorylation of Ser19 and Thr18 in the RLC subunit converts NM II from a compact, inactive structure to an open active structure that enables myosin to crosslink actin (Fig. 3). NM II ATPase activity is activated upon actin binding and phosphorylation of the RLC greatly enhances actin-activated ATPase activity, thereby allowing NM II to convert chemical energy into mechanical work by mediating contraction of actomyosin bundles to drive cell migration. Studies indicate that fesselin and myosin bind competitively to actin, and *in vitro* ATP hydrolysis assays show fesselin decreases avian myosin actin-activated ATPase activity (Schroeter and Chalovich, 2005). Like fesselin, human myopodin could regulate actomyosin contraction by competitively blocking myosin interaction with actin.

In addition to NM II activation, ROCK also activates LIMK. Cofilin, an actin depolymerizing and severing protein, is inactivated by LIMK phosphorylated of Ser3 in cofilin (Maciver, 1998; Yang et al., 1998). Therefore, if myopodin inhibits cofilin activity in the cell body, actin bundle formation would be increased. Lastly, in addition to RhoA that promotes formation of actin-rich lamellipodia, Rac1 and Cdc42 are well-documented Rho GTPases that promote filopodia and stress fiber, respectively (Vega and Ridley, 2008). Since I observed that myopodin-expressing PC3 cells frequently have actin-rich protrusions at the edge of cells (Fig. 14), myopodin could promote formation of these structrures and cell migration through Rac1 and/or Cdc42 signaling pathways.

Stress fibers can also directly affect actin cytoskeleton dynamics at the cell front and cell rear. Stress fibers in the cell body can distally promote formation of the lamellipodium and filopodia, two actin-rich structures critically involved in cell movement. During actin polymerization at the leading cell edge, high plasma membrane

tension leads to the retrograde flow of the polymerizing actin filaments. Although myosins are physically absent at the lamellipodia, tension generated by actomyosin contraction in the lamella is transmitted along the F-actin fibers resulting in FA maturation at the cell front (Giannone et al., 2007). Focal complexes can then bind tightly to actin filaments, converting the fast retrograde flow into slow retrograde slow and thereby promoting membrane protrusions and cell migration (Alexandrova et al., 2008) (Fig. 6B). On the other hand, actomyosin bundles in the cell body can also facilitate cell migration by promoting tail retraction (Small and Resch, 2005). Thus, cells need to disassemble stable adhesions to detach the cell rear from the ECM. Depending on the cell type, several mechanical (i.e. actomyosin contraction) or biochemical (actin polymerization and calpain-mediated proteolytic cleavgage of FAs) processes have been implicated in tail retraction (Guo and Wang, 2012; Huttenlocher et al., 1997; Mseka and Cramer, 2011). For instance, inhibition of calpain protease in Chinese hamster ovary (CHO) cells stabilizes FAs, decreases cell motility, and reduces tail retraction, suggesting that proteolytic cleavage of FAs may help for tail retraction. In NIH-3T3 fibroblasts, actomyosin contraction in the cell body provides mechanical force to promote cell body translocation and tail retraction. This is supported by the observation that localized inhibition of NM II ATPase activity in the cell body using blebbistatin or ROCK inhibitor results in elongated cells and tails that resist retraction (Guo and Wang, 2012). The formation of prominent actin stress fibers in the cell body and enhanced migration of myopodin-expressing cells could reflect myopodin affects on any of these processes.

As is clear from the above discussion, a complex interplay between numerous cell factors and processes regulates cytoskeleton remodeling and cell migration, and the Rho GTPases are particularly important signaling molecules in these events. Here, I investigated the potential signaling networks regulated by myopodin using predominantly ΔN-MYO1, but also MYO3 to determine whether an observed effect correlated with the distinct actin remodeling activities of these two isoforms. I found that the actin structures induced by these myopodin isoforms are not only morphologically, but are also biochemically, distinct. Nonetheless, both myopodin isoforms promote RhoA activation and ROCK activity. Furthermore, pharmacological inhibition or siRNA knockdown of

NM II failed to impair the ability of myopodin to promote cell migration, suggesting that myopodin-induced cell migration was independent of NM II activity.

4.2. Results

4.2.1. Myopodin Isoforms Differentially Induce Biochemically Distinct Actin Networks

Previous immunofluorescence staining revealed that myopodin isoforms differentially induced distinct actin bundles and differentially colocalized with the bundles in the cell body. To examine if the induced actin structures are biochemically similar to the previously characterized stress fibers (i.e. ventral and graded polarity actomyosin bundles), co-immunofluorescence staining for myosin and myopodin was conducted. ΔN-MYO1- and MYO3-expressing cells were used as the representatives of each actin bundle type to examine if the induced actin bundles stain with the signature pattern of typical actomyosin bundle, namely, an interdigitated pattern of myosin along the actin filaments. Immunofluorescent staining of myosin and myopodin was conducted as described previously.

Consistent with the previous phalloidin staining (Fig. 14), ΔN-MYO1 exhibited a contiguous staining pattern along relatively irregular, short, thick actin bundles (Fig. 23A; left column). Although ΔN-MYO1 exhibited prominent contiguous staining of the thick actin bundles in the central region of cells, some punctuated staining was also observed at the cell periphery where actin bundles were thinner. Co-immunofluorescence staining of myopodin and myosin revealed that ΔN-MYO1 did not stain in an interdigitated pattern with NM II along the thick bundles in the cell body (Fig. 23A). Instead, NM II appeared to be completely excluded from these actin structures (Fig. 23A; inset). This conclusion was supported by analyzing the relative fluorescence intensity of NM IIA and ΔN-MYO1 along a plane through the contiguously stained actin bundles (white line in the insets of Fig. 23B). NM IIA appeared to cluster at the region where ΔN-MYO1 was depleted. The fluorescence intensity profile plot showed an inverse correlation of NM IIA and ΔN-MYO1 fluorescence, particularly in the cell body, indicating very low levels of colocalization. Interestingly, ΔN-MYO1 did stain in an interdigitated pattern with NM II on the thinner actin bundles at the cell periphery (Fig. 23A; arrow), suggesting ΔN-

MYO1 localization to actin bundles might exclude NM II association at the same location.

In contrast to ΔN-MYO1, MYO3-induced actin bundles that seemed to be typical stress fibers. MYO3 exhibited a distinct punctuated staining pattern along thin, long, parallel, actin bundles that spanned the entire length of the transduced PC3 cells (Fig. 23A). More importantly, NM IIA co-localized with MYO3 on these bundles in an interdigitated pattern. Quantitative analysis of the fluorescence intensity of myopodin and myosin along a plane through the cell perpendicular to the parallel actin bundles further supported the observation that MYO3 and NM II colocalize on these bundles (Fig. 23B; right panel). Taken together, these results indicate that the different myopodin isoforms induce two distinct types of actin structures that are both morphologically and biochemically distinct.

4.2.2. Myopodin-Mediated Cell Migration is RhoA-Dependent

The small Rho GTPase RhoA is known to be one of the key regulators of stress fiber formation (Chrzanowska-Wodnicka and Burridge, 1996). As PC3 cells ectopically expressing myopodin proteins displayed complicated actin bundle networks in the cell body, I speculated that myopodin might activate RhoA to promote stress fiber formation. To assess the amount of active RhoA within mock- and myopodin-expressing cells, the GST-tagged Rho binding domain (RBD) of rhotekin was used as bait to pull down active RhoA. Since myopodin only enhanced the chemokinetic activity of PC3 cells under FBS conditions, mock- and ΔN-MYO1-transduced PC3 cells were cultured under serum-free conditions for 48 hours to inhibit myopodin activity and reduce the basal levels of activated Rho GTPases. PC3 cells were then treated with FBS for the indicated times to examine the effect of myopodin on RhoA activation. In parallel, the effect of myopodin on PC3 cell migration in the presence of NIH 3T3 CM was similarly assessed.

I found that ΔN-MYO1 differentially regulated RhoA activation of PC3 cells in response to the different extracellular stimuli. Under serum-starved conditions, low levels of active RhoA were detected in both mock- and ΔN-MYO1-expressing PC3 cells (Fig. 24A). This data is consistent with my observation that mock-transduced cells and myopodin-expressing cells had low cell motility in the absence of FBS (Fig. 10A). As

serum contains various growth factors that can activate Rho GTPases (Van Aelst and D'Souza-Schorey, 1997), the level of RhoA-GTP within mock-transduced PC3 cells increased by 4-fold over the 10 min timecourse of FBS treatment (Fig. 24A). Although RhoA increased 4-fold under FBS conditions, FBS still failed to serve as a chemokinetic stimulus to PC3 cells (Fig. 10A). Strikingly, ΔN-MYO1 amplified the effect of FBS on RhoA activation by 11-fold within 10 min after FBS stimulation (Fig. 24A). The effect of ΔN-MYO1 on RhoA activation was also observed at the earlier 6 min time point (Fig. 24A). To further strengthen the connection between myopodin-stimulated RhoA activation and enhanced cell cell migration, I performed transwell migration assays in the presence of C3 transferase, a Rho inhibitor. Within the range of 0.3-0.5 μg/ml of C3 transferase, the effects of ΔN-MYO1 on cell migration were modestly inhibited (~25%) and at statistically significant levels (Fig. 24B). It should be noted that 2-10 μg/ml is the commonly used dose range to efficiently knockdown RhoA activity (Sakai et al., 2013; Simpson et al., 2004). However, my dose-response curve of C3 transferase showed a statistically significant difference within the lower dose range but the high doses also inhibited mock-transduced cell migration, suggesting that the mock-transduced cell may also be dependent on RhoA activity.

The activated RhoA pulldown assay revealed that ΔN-MYO1 also regulated RhoA activation upon CM treatment although in a converse manner to what was observed in FBS stimulated cells. CM strongly stimulated RhoA activation in PC3 cells, increasing the levels of RhoA-GTP by ~8-9 fold within 3-6 min of CM treatment (Fig. 24A). However, this robust activation was not sustained over time as active RhoA levels decreased to 5.6-fold after 10 minutes of CM treatment. Most importantly, RhoA activation by CM was strongly inhibited by expression of ΔN-MYO1 (Fig. 24A). These results agreed with my observations that CM is a potent stimulus of PC3 cell migration and that myopodin partially suppresses this promigratory effect (Fig. 9).

Overall, these results confirmed my prediction that the different external stimuli used in transwell migration assays differentially activate signaling pathways in PC3 cells, particularly the RhoA pathway, and that the different effects of myopodin on PC3 cell migration in response to these stimuli reflects myopodin alterations of the RhoA signaling response of PC3 cells.

4.2.3. Myopodin Isoforms have Minimal Effects on Rac1 activation

Since myopodin upregulates cell migration and RhoA activation, I wondered if myopodin also affected the activation status of the other two Rho GTPases. To study the roles of Rac1 and Cdc42 in myopodin-mediated cell migration, I conducted active Rac1 and Cdc42 pulldown assays using the GST-tagged p21-binding domain (PBD) as bait. PC3 cells were starved for 48 h prior to FBS activation as in the RhoA activation assay. The Rac1 pull-down assay was validated in the presence of commercial Rac1/Cdc42 activator (the catalytic domain of CNF bacterial toxins), which increased Rac1 activation by >3-fold within 2 min (Fig. 25A). FBS treatment stimulated Rac activation, but only by ~2-3 fold and only at the last time point (Fig. 25A; t=9 min). PC3 cells expressing ΔN-MYO1 did not show a higher level of Rac activation than mock-transduced cells, but they did respond faster to the FBS stimulus, achieving the highest amount of Rac1-GTP level after 6 min post-stimulation (Fig. 25A; t=6 min). Faster activation of Rac1 in PC3 cells expressing ΔN-MYO1 was observed in two independent experiments. Although Rac-GTP levels in MYO3-expressing PC3 cells were slightly higher than mock-transduced cells in some experiments and at some time points (Fig. 25A), these results were not reproducible. Furthermore, transwell assays conducted in the presence of a Rac inhibitor (NSC23766) impaired both mock- and ΔN-MYO1-transduced PC3 cell migrationto the same level (Fig. 21B). Therefore, Rac1 has little, if any, affect on the enhanced migration phenotype of PC3 cells expressing myopodin.

Similar experiments were conducted to examine if myopodin altered Cdc42 activation. In contrast to Rac1 and RhoA GTPases, serum starved mock-transduced PC3 cells exhibited higher levels of active Cdc42 than cells expressing the myopodin constructs (Fig. 21C). Moreover, FBS activation lead to a decrease in Cdc42-GTP levels in both mock-transduced and myopodin-transduced cells, such that all these cells expressed similar low levels of active Cdc42 (Fig. 21C). It seems highly unlikely that Cdc42 activation is responsible for the myopodin-induced phenotypes. One caveat to this conclusion is that the positive control Rac/Cdc42 activator failed to activate Cdc42 in three separate experiments. Optimizing this assay or using another positive control is necessary to validate whether myopodin expression alters Cdc42 activation.

4.2.4. Myopodin-stimulated Cell Migration is Dependent on the ROCK Signaling Pathway

Since RhoA activation is increased in myopodin-expressing cells and ROCK is a downstream effector of RhoA, I used Y-27632, a pharmacologic inhibitor of ROCK, to explore the relative contribution of this pathway to the chemokinetic effects of myopodin. The activity of ROCK inhibitor was confirmed by western blotting to detect the phosphorylation status of the NM II RLCs, a target for ROCK phosphorylation. ROCK inhibitor effectively inhibited phosphoryaltion of both Ser19 and Thr18 in the RLCs (Fig. 26A). Interestingly, I found that CM-stimulated cell migration was almost completely ROCK-dependent since Y-27632 treatment reduced cell migration to almost the level of inherent PC3 migration in the absence of an external stimulus. Under FBS conditions, the ROCK inhibitor had no affect on PC3 cell migration, suggesting the basal level of PC3 cell migration under FBS conditions is independent of ROCK activity. However, myopodin-enhanced cell migration in response to FBS stimulation was decreased by ~40% following Y-27632 treatment (Fig. 26B), suggesting that myopodin-induced cell migration is at least partially ROCK-dependent. I also generated a Y-27632 dose response curve using both ΔN-MYO1 and MYO3 to confirm the general dependence of myopodin-induced cell migration on ROCK activity (Fig. 26C). From the range of 2.5-10 uM Y-27632, mock-transduced PC3 cell migration was unaffected. However, ΔN-MYO1- and MYO3-stimulated cell migration decreased up to 40%. Myopodin can therefore regulate PC3 cell migration via manipulating the Rho-ROCK response of PC3 to different chemokinetic conditions.

4.2.5. Myopodin Stimulates Cell Migration in a Myosin-independent Manner

GTP-bound RhoA activates ROCK, which in turn phosphorylates RLC of NM II thereby enhancing myosin crosslinking and contraction activity. As myopodin isoforms promoted cell migration in a RhoA/ROCK-dependent manner and induced actin bundles, it seemed likely that myopodin might also activate NM II activity. Furthermore, *in vitro* biochemical studies demonstrated that fesselin is able to inhibit myosin ATPase activity (Schroeter and Chalovich, 2005), suggesting that myopodin may potentially regulate NM II ATPase activity. However, the inhibition of myosin contraction by fesselin seems

counterintuitive to a similar role for myopodin in promoting cell migration, which is generally facilitated by actomyosin contraction. Nonetheless, it is possible that in the presence of other interacting proteins within the cell, myopodin might promote, rather than suppress, myosin contraction. Hence, I examined if myopodin-expressing cells had higher levels of phosphorylated NM II RLCs or promoted myosin ATPase activity.

Mock and ΔN-MYO1-transduced PC3 cells were cultured in growth media and harvested for western blot analysis using phospho-specific antibodies. Of note, I did not synchronize PC3 cells with serum-free medium. If myopodin promoted actin bundle formation by enhancing phosphorylation of RLCs, this effect should be maintained under normal culture conditions because the induced actin bundles were still readily detectable in non-synchronized cells. Although ΔN-MYO1-stimulated cell migration required ROCK activity, no enhancement of RLC phosphorylation levels relative to mock-transduced cells was detected for either the Ser19 or Thr18 residues of RLC (Fig. 27). The specificity of the antibodies that recognize the phosphorylated Ser19 or Thr18/Ser19 residues of RLC was corroborated using Y-27632 treatment, which decreased the phosphorylation levels of RLC by 60-80% in either mock- or ΔN-MYO1-transduced PC3 cells (Fig. 27).

The importance of NM II phosphorylation to myopodin-induced cell migration was further tested using ML-7, an inhibitor that suppresses myosin light chain kinase (MLCK), which phosphorylates NM II in parallel to ROCK. Unlike ROCK inhibitor that had no effect on inherent PC3 cell migration, increasing doses of ML-7 inhibited mock-transduced PC3 cell migration, suggesting that the inherent migration ability of PC3 cells is based on NM II activity (Fig. 28A). Similar to mock-transduced cells, PC3 cells expressing myopodin also had lower motility. However, the ~3-fold increase in the number of myopodin-expressing cells relative to mock-transduced cells that migrated through the transwell was maintained at all doses of ML-7, indicating that myopodin-induced cell migration is independent of myosin phosphorylation levels.

To examine if myopodin-stimulated cell migration was dependent on myosin ATPase activity, blebbistatin, an inhibitor that specifically suppresses myosin ATPase activity but has no effect on RLC phosphorylation, was added to the top and bottom of Boyden chambers. As expected, blebbistatin had no effect on RLC phosphorylation

levels (Fig. 27). As with the ML-7 inhibitor of RLC phosphorylation, blebbistatin inhibited the migration of ΔN-MYO1- and MYO3-transduced cells to approximately the same extent (65-75% at 10 μM of blebbistatin) (Fig. 28B). The effectiveness of the blebbistatin treatment was confirmed based on the appearance of large membrane protrusions (Fig. 28C), which are typically associated with blebbistatin inhibition of NM II ATPase activtiy (Kuo et al., 2011). NM II ATPase activity is therefore required for inherent PC3 cell motility but not for enhanced myopodin-induced migration.

Lastly, I generated stable PC3 cell lines expressing shRNA constructs to deplete endogenous levels of RLC. Western blotting confirmed the shRNA knockdown of RLC levels by 60-70% compared to cells transduced with a scrambled shRNA (Fig. 29A). NM II facilitates cell body translocation and tail retraction (Guo and Wang, 2012) and promotes retraction of the leading edge (Giannone et al., 2007). As a result, depletion of NM II leads to tails that resist retraction and to larger membrane protrusions. Consistent with these previous reports, I found that mock-transduced PC3 cells expressing RLC shRNA had larger membrane protrusions, and an increased proportion of the cells contained long extended tails indicative of a tail retraction defect (Fig. 29B; left column). Interestingly, while little, if any, morphological differences were observed between mock- and ΔN-MYO1-transduced PC3 cells (Fig. 29B; top row), cells expressing both myopodin and RLC shRNA constructs exhibited even more pronounced membrane protrusions (Fig.29B; middle row). Myopodin may thus function to promote membrane protrusion formation under low levels of myosin activity. In addition, in contrast to mock-transduced PC3 cells whose tail and membrane protrusions were frequently found at opposing ends of the cell, the membrane protrusions in myopodin-expressing cells were formed around the cells without polarity (Fig. 29B; arrow). Consistent with the ML-7 and blebbistatin findings, transwell migration assays with the shRNA-transduced cells indicated that knockdown of endogenous RLC decreased both mock- and myopodin transduced cells to the same degree (~50%) (Fig. 29C), indicating the inherent motility of PC3 cells, but not myopodin-enhanced cell migration, is dependent on NM II. Thus, using two different inhibitors that target NM II activity from distinct pathways and shRNA knockdown analysis, I demonstrated that myopodin-induced cell migration is independent of the levels of myosin phosphorylation levels and ATPase activity.

4.2.6. Myopodin Promotes Tail Retraction in a ROCK-dependent Manner

During serum starvation, I noticed a substantial difference in the morphology of mock- and ΔN-MYO1-transduced PC3 cells. Many of the mock-transduced cells appeared to have a tadpole shape with long slender tails and a rounded head (sometimes with membrane protrusions) at opposing ends of the cell (Fig. 30A; arrows). The long tails are indicative of a tail retraction defect. In contrast, ΔN-MYO1-expressing cells exhibited an elongated cell shape but rarely had long tails (Fig. 30A). This distinct morphology was abolished following FBS stimulation as most of the mock- and ΔN-MYO1-transduced cells rounded up within 1 hr of FBS treatment (Fig. 30A). Although not shown here, the rounded morphology was induced within 10 min after FBS addition and persisted for more than 1 day. By 48 hr post-FBS treatment, the mock-transduced PC3 cells reverted to the polarized morphology while ΔN-MYO1-expressing cells maintained an elongated or rounded cell morphology.

To assess the affect of myopodin on tail retraction quantitatively, cells with long tails and and the total number of cells in random microscopic fields were counted. As a rule of quantification, cells with a tail retraction defect were those with only one slender tail that stretched more than one body length (see inset of Fig. 30B as an example). Quantitatively, ΔN-MYO1 decreased the number of PC3 cells with a tail retraction defect by 80% under starvation conditions (Fig. 30B). Upon FBS treatment, <10% of mock-transduced cells had a tail retraction defect and <2% of myopodin-expressing cells displayed such a defect. By 28 hr post-FBS stimulation, the tail retraction defect reappeared in mock-transduced cells, due presumably to depletion of the growth stimulatory factors in the serum, while the vast majority of myopodin-expressing cells still exhibited no tail retraction defect. These results indicate that serum starvation induces a tail retraction defect in PC3 cells and myopodin is able to rescue this defect.

As myopodin promotes cell migration in a RhoA/ROCK-dependent pathway and this pathway is known to promote tail retraction (Worthylake et al., 2001), I wondered if myopodin-stimulated tail retraction is dependent on ROCK activity. To test this hyopthesis, I treated mock- and ΔN-MYO1-transduced PC3 cells with 10 μM ROCK inhibitor for 24 hr, the dose that had no effect on mock-transduced cell migration but

impaired cell migration in ΔN-MYO1-expressing cells by ~40% (Fig. 26B). Regardless of the presence or absence of myopodin, Y-27632-treated cells were flattened and had more membrane protrusions around the perimeter of cells compared to untreated cells (Fig. 31A). This is consistent with reports showing that inhibiting ROCK activity promotes the formation of FAs and multiple competing membrane protrusions (Worthylake and Burridge, 2003). Importantly, both ΔN-MYO1-expressing cells and mock-transduced cells exhibited a tail retraction defects under Y-27632 treatment (Fig. 31A; arrow).

The loss of actin bundle formation in serum-starved cells expressing myopodin (Fig. 19) correlates with the appearance of a tail retraction defect in these cells, suggesting these two phenotypes might be causally linked. To determine whether there was a similar correlation between loss of actin bundles and the tail retraction defect in ΔN-MYO1-expressing cells treated with ROCK inhibitor, these cells were examined by fluorescence microscopy. As previously noted (Fig. 31A), after a 24 hr treatment with ROCK inhibitor the majority of cells appeared flattened with multiple membrane protrusions (Fig. 31B; arrowhead) and elongated tails (Fig. 31B; arrow). Myopodin accumulated around the slender tail area and was stained diffusely in the cell body. As shown by phalloidin staining, the myopodin-induced actin bundles were largely disrupted and the thick, irregular actin structures typical of ΔN-MYO1-expressing cells were absent from the cell body (Fig. 31B). The correlation between actin bundle formation and tail retraction was also evident in some cells that appeared not to respond to Y-27632 treatment (Fig. 31B; cell at top right corner). Taken together, these data indicate that myopodin promotes cell migration and tail retraction in a ROCK-dependent manner, and there is a direct correlation between these phenotypes and myopodin-induced actin bundle formation.

4.2.7. Myopodin does not Affect Cofilin or LIMK Phosphorylation Levels.

The above findings demonstrated that myopodin-stimulated cell migration was not inhibited by decreasing myosin activity, suggesting ROCK might induce cell migration through alternative pathways, such as the LIMK/cofilin pathway. The activities of LIMK and cofilin are regulated by their phosphorylation status. ROCK phosphorylates

LIMK at Ser323 (Maekawa et al., 1999), which in turn phosphorylates cofilin at Ser3 (Yang et al., 1998), leading to inactivation of cofilin-mediated actin disassembly. Thus, it is possible that myopodin inactivates cofilin-mediated actin disassembly thereby promoting actin structure formation. To test this speculation, mock- and ΔN-MYO1-expressing cells were synchronized under serum-starved conditions prior to FBS stimulation and then were harvested at the indicated time points. In both mock- and ΔN-MYO1-expressing cells, the total protein and phosphorylation levels of LIMK and cofilin were sustained at the same level from starvation to 3 hr post-FBS stimulation (Fig. 32). These data suggest that myopodin-induced actin structure formation is dependent on ROCK-activity but is independent of enhanced LIMK activity or decreased cofilin-mediated actin depolymerization.

4.3 Discussion

Myopodin isoforms differentially regulate cell migration under distinct extracellular stimuli. Under FBS conditions, myopodin isoforms promoted cell migration by 3-5 fold but suppressed cell migration by 40% in the presence of CM. Several lines of evidence in Chapter 3 implied that PC3 chemokinetic activity under FBS conditions is dependent on the formation of myopodin-induced actin structures. Although all isoforms promoted cell migration, they induced morphologically distinct actin structures. Here, I demonstrated that the MYO3-induced thin actin bundles and ΔN-MYO1-induced thick actin meshwork were biochemically distinct. Co-immunofluorescence staining revealed that MYO3 interdigitates with NM II along the thin, parallel actin bundles while the ΔN-MYO1-induced thick actin bundles were devoid of detectible myosin staining. Although ΔN-MYO1 did not colocalize with myosin on the thick actin bundles, active RhoA pulldown assays demonstrated that ΔN-MYO1 differentially regulated the RhoA pathway under different culture conditions. Consistent with myopodin effects on cell migration, myopodin stimulated or inhibited RhoA activation in the presence of FBS or CM, respectively. However, myopodin had little effect on global Rac1 and Cdc42 activation. Pharmacological inhibition of ROCK, a downstream effector of activated RhoA, also impaired myopodin-induced PC3 chemokinetic activity. While RhoA and ROCK were both activated by myopodin expression, inhibition of NM II ATPase activity or

knockdown of NM II had no effect on myopodin-enhanced cell migration. Furthermore, myopodin could rescue the tail retraction defect of PC3 cells that appears under specific culture conditions. ROCK inhibitor treatment diminished formation of the myopodin-induced actin structures and the effect of myopodin on tail retraction, suggesting ΔN-MYO1 promoted PC3 cell tail retraction in a ROCK-dependent manner. I also showed that the induced actin structures in ΔN-MYO1-expressing cells were not due to lower levels of cofilin depolymerizing activity. Taken together, my data suggest that ΔN-MYO1 enhanced PC3 chemokinetic activity via RhoA/ROCK-dependent but myosin- and cofilin-independent pathways.

Biochemically Distinct Myopodin-induced Actin Networks

MYO1 and ΔN-MYO1 predominantly induced an irregular, thick actin meshwork while MYO3 and MYO4 induced parallel, thin actin bundles (Fig. 14). The interdigitated staining of MYO3 and NM II along the thin bundles (Fig. 23) is similar to myosin staining along stress fibers. However, ΔN-MYO1 induced thick actin bundles that were devoid of NM II and showed contiguous myopodin staining (Fig. 23), a pattern distinct from all canonical stress fibers in the cell body. Within ΔN-MYO1-expressing cells, interdigitated myopodin and myosin staining was evident on the thinner actin bundles present at the perimeter of the cell (Fig. 23A, B). Alpha-actinin is another signature protein found along stress fibers with myosin. As ΔN-MYO1 interacts with α-actinin and the interacting motif is located within the conserved region of myopodin (Fig. 8), ΔN-MYO1 and MYO3 might both colocalize with α-actinin as in sarcomeric muscle cells (Linnemann et al.). I attempted to determine if ΔN-MYO1 specifically eliminated myosin from the thick bundles and colocalized along these bundles with α-actinin. Unfortunately, I was unsuccessful in staining α-actinin in PC3 cells using two different commercial antibodies. It is possible that PC3 cells, like HEK293 cells (Asanuma et al., 2005), have no endogenous α-actinin.

Several possibilities could explain myosin depletion from the ΔN-MYO1-induced actin structures. Stress fibers in the cell body are derived from dorsal stress fibers and transverse stress fibers (Kovac et al., 2012). Elongating dorsal stress fibers from FAs are crosslinked by α-actinin and have no myosin while transverse stress fibers contain

myosin and tropomyosin (Hotulainen and Lappalainen, 2006). When dorsal stress fibers and transverse coincide, NM II displaces α-actinin and is integrated into the elongating actin bundles, forming actomyosin bundles with a periodic α-actinin and myosin pattern (Hotulainen and Lappalainen, 2006). The mutually exclusive staining patterns of MYO3 and ΔN-MYO1 with myosin are consistent with fesselin studies showing that fesselin and myosin competitively bind to F-actin filaments, and that fesselin can also bind weakly with myosin (Schroeter and Chalovich, 2005). The interdigitated staining of myosin and MYO3 may therefore be attributed to both weak interactions of myopodin with myosin and displacement of myosin from actin bundles. ΔN-MYO1 and MYO3 might also be integrated into α-actinin crosslinked bundles in a similar fashion as myosin. Because myosin and myopodin bind competitively to F-actin, it is possible that the contiguous staining pattern of ΔN-MYO1 results from high concentrations of ectopically expressed protein. This seems unlikely as MYO3 was expressed at a similar level as MYO1, yet both isoforms differentially lead to punctuated and contiguous staining, respectively (Fig. 15B). One possibility is the unique exon of ΔN-MYO1 enhances its affinity for F-actin and therefore outcompetes myosin binding to F-actin filaments, leading to the contiguous ΔN-MYO1 staining pattern.

Myosin integration into stress fibers is also dependent on tropomyosin isoform 4 (TM4), one of the tropomyosin family members (Tojkander et al., 2011). Most tropomyosin isoforms are needed to maintain the stability of actin bundles, and siRNA knockdown of most tropomyosin isoforms compromises stress fiber formation (Tojkander et al., 2011). However, cells depleted of TM4 retain actin bundles that are morphologically abnormal and devoid of NM II (Tojkander et al., 2011). Live imaging analysis shows that the recruitment of NM II requires the presence of TM4-decorated actin fibers. Recent studies demonstrate that synaptopodin-1 is able to rescue the defects of stress fiber formation in *Drosopohila* oocytes with the tropomyosin gene deleted (Wong et al., 2012). Both synaptopodin-1 and tropomyosin are also involved in similar pathways to promote stress fiber formation, such as inhibition of RhoA degradation (Wong et al., 2012). Thus, like synaptopodin-1, myopodin might spatially and functionally replace TM4 and therefore impair TM-4-specific myosin recruitment to thick actin bundles.

Myopodin-stimulated Cell migration is Dependent on RhoA/ROCK Signaling

ΔN-MYO1-stimulated cell migration involved activation of RhoA (Fig. 24) and ROCK (Fig. 26). RhoA is well documented to promote actin bundle formation and cell migration (Kovac et al., 2012; Ridley and Hall, 1992). While synaptopodin-1 promotes actin bundle formation by inhibiting Smurf-1-mediated RhoA degradation (Asanuma et al., 2006), myopodin exploited a different RhoA-dependent strategy to promote actin structure formation. Under FBS conditions, ΔN-MYO1 promoted RhoA activation by 3-fold (Fig. 24A) but had no effect on total RhoA expression levels (Fig. 24A), indicating ΔN-MYO1 promoted RhoA activation instead of RhoA stabilization. Using ROCK inhibitor (Y-27632), I further demonstrated that myopodin-stimulated cell migration was dependent on the RhoA/ROCK signaling pathway (Fig. 26C). High levels of RhoA activity within myopodin-expressing cells could also activate other RhoA-dependent but ROCK-independent activities. For example, RhoA can lead to activation of formin nucleation activity (Rose et al., 2005). The larger membrane protrusions present in myopodin-expressing cells with low myosin activity (e.g. shRNA knockdown of NM II) (Fig. 29B) imply a potential role of myopodin in actin assembly at the leading cell edge. If so, then the RhoA-dependent activity of myopodin might also reflect affects of myopodin on membrane protrusions (Kurokawa and Matsuda, 2005).

The involvement of myopodin in altering the RhoA response of cells to external migration stimuli was confirmed in cells stimulated with CM. PC3 cells became highly motile under CM where myopodin suppressed, rather than promoted, cell migration (Fig. 9A). The elongated cell morphology and enhanced migration in response to CM was almost completely ROCK-dependent, as ROCK inhibition strongly inhibited PC3 cell migration by 75% (Fig. 26). Most importantly, ΔN-MYO1 suppressed CM-stimulated RhoA activation by at least 50% (Fig. 25A), clearly demonstrating that ΔN-MYO1 differentially regulates RhoA/ROCK signaling pathways under distinct external stimuli.

Despite the robust activation of RhoA by myopodin, treatments with C3 transferase or ROCK inhibitor suggested RhoA activation is not the full story. Knockdown of RhoA activity by C3 transferase modestly inhibited cell migration by ~15-20% (Fig. 24B) while the maximum decrease in myopodin-induced cell migration by

ROCK inhibitor was 40%. The partial inhibition of cell migration by ROCK inhibitor was not due to inefficient ROCK inhibition since the inhibitor almost eliminated phosphoryation of RLC, a downstream target of ROCK (Fig. 26C). These results suggested that other signaling pathways are involved in myopodin-stimulated cell migration. Active Rac1 and Cdc42 GTPase pulldown assays suggested these two key GTPases involved in lamellipodia and filopodia formation are not responsible for the RhoA-independent effects of myopodin because myopodin did not stimulate their activation (Fig. 25). FBS was a good stimulus for Rac1 activation, increasing the levels of Rac1-GTP in mock-transduced PC3 cells by 3-fold within 9 min post-FBS treatment (Fig. 25A). However, ΔN-MYO1-expressing cells showed similar levels of Rac1 activation, although myopodin-expressing cells might have responded slightly faster than mock-transduced cells, and pharmacological inhibition of Rac1 had no effect on myopodin-stimulated cell migration (Fig. 25B).

While this global analysis suggested myopodin-stimulated cell migration is independent of Rac1 and Cdc42 activation, this conclusion needs to be further supported by a spatio-temporal analysis of Rho GTPases. Many Rho GTPases are activated spatio-temporally, therefore myopodin may regulate these Rho GTPases at the spatial and temporal levels. For instance, recent studies indicate that Rac1, Cdc42 and RhoA are all activated at different compartments of the leading edge to promote actin assembly, protrusions, and retraction (Machacek et al., 2009). Although global Rac1 and Cdc42 activation was not affected by myopodin, it is possible that myopodin regulates the activation of these Rho GTPases at spatio-temporal levels to control cell migration. Many Rho GTPases are activated spatio-temporally (Machacek et al., 2009). It will be useful to examine the Rho, Cdc42, and Rac1 GTPase activation status at different actin-rich compartments using Raichu fluorescence resonance energy transfer (FRET) biosensors (Nakamura et al., 2006). This probe is designed to examine Rho GTPase activation status in situ. For example, the Raichu-RhoA probe construct consists of RhoA and Rho-binding domain (RBD), which are sandwiched by yellow fluorescent protein (YFP) and cyan fluorescent protein (CFP). As only RhoA-GTP, but not RhoA-GDP, binds to RBD, RhoA activation results in the intramolecular binding of activated RhoA

and RBD brings CFP and YFP into close proximity and therefore results in an increase of FRET from CFP to YFP (Yoshizaki et al., 2003).

Myopodin-stimulated Cell Migration is Independent of the level of NM II Activity

The correlation between RhoA activation by FBS and the concurrent induction of actin bundle formation and cell migration suggested a plausible mechanism for myopodin-induced cell migration. Under this scenario, myopodin activates RhoA/ROCK leading to myosin phosphorylation and activation, resulting in stress fiber formation and cell migration (see pathway in Fig. 2B). The actin crosslinking and contraction activities of myosin are well documented to drive cell migration (Vicente-Manzanares et al., 2009). Myosin contraction provides mechanical forces required for focal adhesion maturation at the leading edge, cell body translocation, and tail retraction. Surprisingly, although the overall level of cell migration is NM II-dependent, three lines of evidence suggested that myopodin-enhanced cell migration is independent of NM II activity. First, MYO3- and ΔN-MYO1-transduced cells exhibited more prominent actin structures compared to mock-transduced cells but equivalent levels of phosphorylated RLC (Fig. 27; only ΔN-MYO1 shown), suggesting that myopodin isoforms do not activate myosin activity. Second, inhibiting NM II activity using ML-7 or blebbistatin suppressed the migration of both mock-transduced and myopodin-transduced cells to the same extent, meaning myopodin-expressing cells still migrated ~3-4 fold more efficiently than mock-transduced cells (Fig. 28A, B). Third, global reduction of NM II activity by RLC shRNA also inhibited both mock- and ΔN-MYO1-transduced PC3 cell migration to the same extent as in ML-7 and blebbistatin treatments. Therefore, inherent PC3 cell migration, but not myopodin-induced PC3 chemokinetic activity, is affected by the levels of NM II activity.

Under conditions of limited myosin activity, membrane protrusions in ΔN-MYO1-expressing PC3 cells were striking (Fig. 29B). Interestingly, RLC-depleted myopodin-expressing cells with substantial membrane protrusions still migrated ~3-4 times better RLC-depleted mock-transduced cells (Fig. 29), suggesting that myopodin may promote PC3 chemokinetic activity by promoting membrane protrusions. Actin assembly within lamellipodia and filopodia drives formation of membrane protrusions.

Subsequently, the actin network at the leading edge is integrated into actomyosin bundles within lamella by myosin contraction (Hotulainen and Lappalainen, 2006). Therefore, myopodin may promote formation of actin filaments and membrane protrusions at the leading edge, with actomyosin contraction recruiting these filaments to form stress fibers. Thus, thick bundle formation in the cell body might be an incidental effect of myosin-mediated contraction but not the direct effect of myopodin on cell migration.

ΔN-MYO1 Rescued Tail Retraction Defect of PC3 Cells

Serum-starvation revealed that ΔN-MYO1 was able to rescue a tail retraction defect that manifests itself in PC3 cells under these conditions (Fig. 30A). Immunofluorescence microscopy and transwell migration assays showed that myopodin-stimulated cell migration, tail retraction and actin bundle formation were all sensitive to ROCK inhibition. Therefore, myopodin-enhanced PC3 chemokinetic activity may result from ROCK-dependent actin bundle formation and tail retraction (Fig. 31). Furthermore, myosin inhibition studies indicated myopodin promotes tail retraction in a myosin-independent manner. In many cell types, cell body translocation and tail retraction are both dependent on RhoA/ROCK and myosin activity (Guo and Wang, 2012; Ridley and Hall, 1992; Smith et al., 2003). However, ROCK inhibition of monocytes, but not myosin inhibition with ML-7 or BDM (another inhibitor that suppresses myosin ATPase activity), leads to accumulation of integrins at resistive tails and impairs cell migration (Worthylake et al., 2001). As with myopodin, the tail retraction of monocytes is therefore also RhoA/ROCK-dependent but myosin-independent. Several other mechanisms also promote tail retraction, such as actin depolymerizaton-based force or calpain-mediated proteolysis of adhesion proteins (Franco et al., 2004; Mseka and Cramer, 2011). For instance, in chick fibroblasts, actomyosin bundles are needed for cell polarization but not tail retraction. Instead, actin depolymerization triggers tail retraction, breaks the symmetry of cells, and drives cell migration (Mseka and Cramer, 2011). It remains to be investigated whether these alternative mechanisms to promote tail retraction have any relevance to myopodin activity.

As myopodin-mediated cell migration requires RhoA/ROCK but not myosin, I also examined other effectors of RhoA/ROCK signaling pathway. As compared to mock-

transduced PC3 cells, LIMK and cofilin phosphorylation level was not altered in myopodin-expressing cells, suggesting that myopodin-induced actin structures are not due to inactivation of cofilin depolymerizing activity (Fig. 32). Investigation of other affectors or effectors of RhoA or Rho/ROCK signalling may provide further insights into how myopodin promotes cell migration. For instance, phosphorylated ERM (ezrin, radixin, and moesin) proteins, a group of proteins that act as membrane-actin cytokskeleton linkers, recruit and activate RhoA and ROCK to mark the posterior part of the cell, which facilitates cell migration by establishing front-rear asymmetry in migrating lymphocytes (Lee et al., 2004).

Here, I demonstrated that myopodin promotes membrane protrusions and tail retraction under limiting NM II conditions. It remains unknown exactly how myopodin affects these two spatially segregated events. Myopodin-induced actin bundles could facilitate cell migration in a similar fashion as actomyosin bundles, which induce membrane protrusions at the leading edge by promoting FA maturation and tail retraction at the cell rear. Similarly, the low levels of myopodin at the leading edge could enhance F-actin polymerization and membrane protrusions while the induced actin bundles in the cell body and periphery facilitate tail retraction. The role of myopodin at the leading cell edge is explored in more detail in Chapter 5.

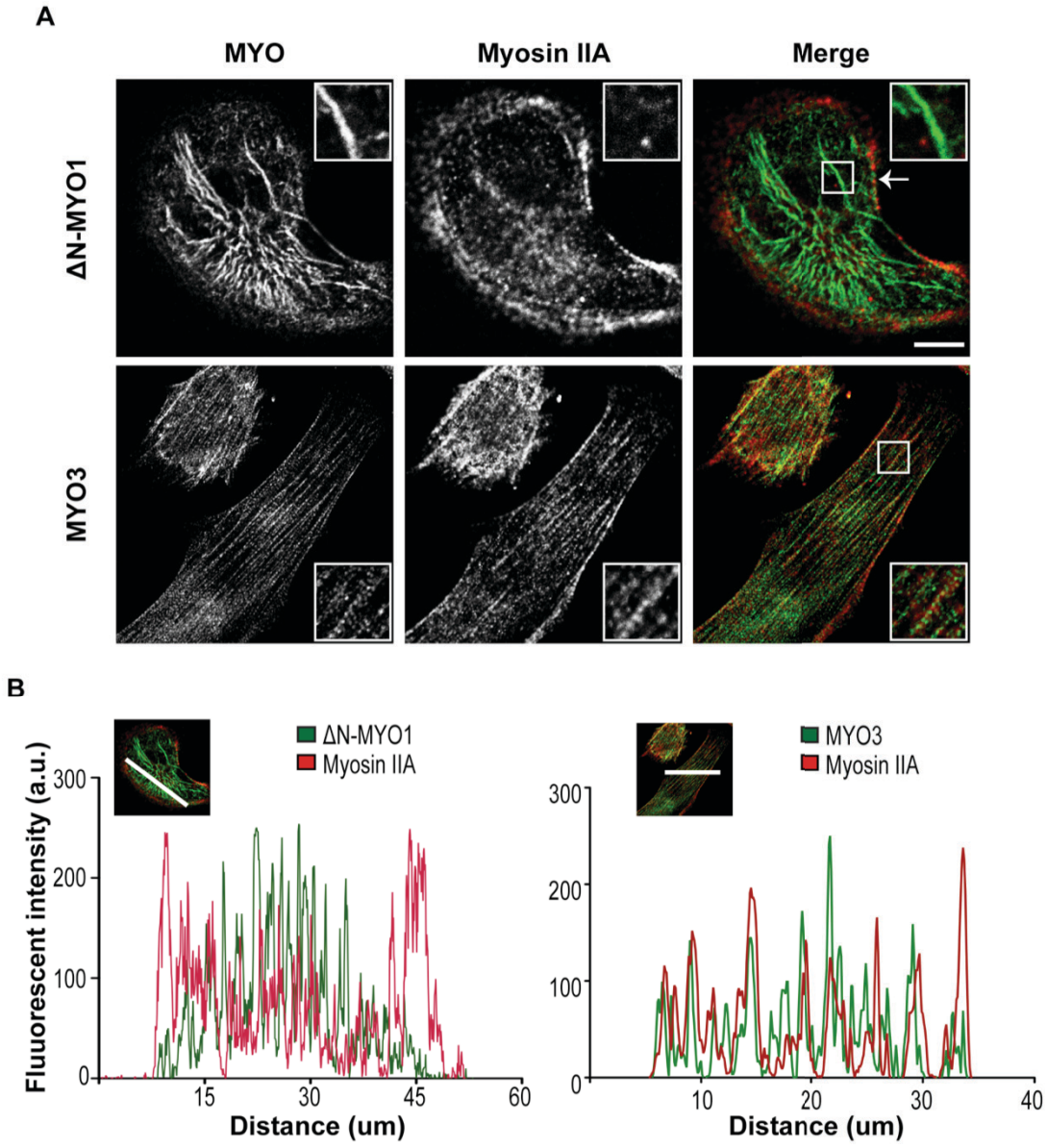

Figure 23. Myopodin isoforms induce two morphologically and biochemically distinct actin networks in PC3 cells. (A) PC3 cells expressing myc-tagged ΔN-MYO1- or MYO3 constructs were fixed and stained with anti-myc (green) and anti-myosin (red) antibodies. Thick actin bundles showing contiguous staining of ΔN-MYO1 were devoid of detectible myosin staining (top row; inset). Myopodin colocalized with myosin on thin actin bundles in an interdigitated pattern at the perimeter of ΔN-MYO1-expressing cells (arrow) or in MYO3-expressing cells (bottom row; inset). The 6 μm x 6 μm areas indicated in the images are magnified 150% in the insets. Scale bar=10 μm. **(B)** Fluorescence intensities of ΔN-MYO1 (left; green) and MYO3 (right; green) and myosin (red) along the plane indicated by the white lines in the insets were analyzed using ImageJ software.

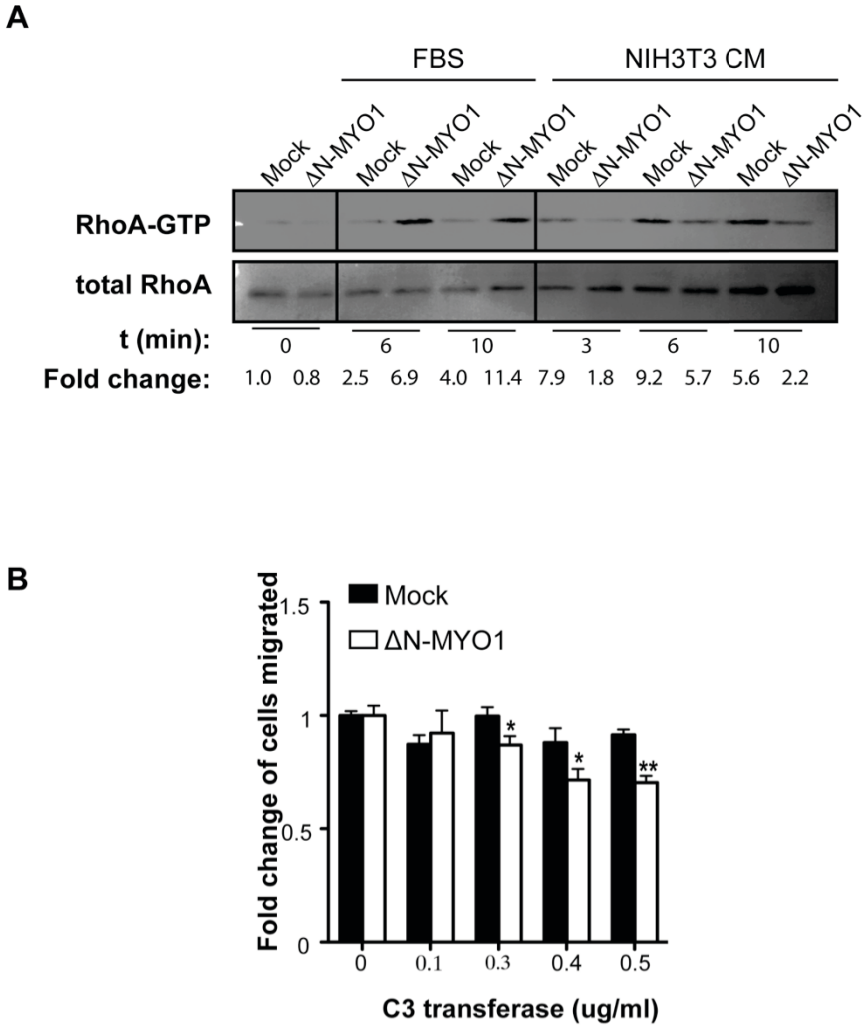

Figure 24. Myopodin differentially regulates cell migration via effects on Rho activation. (A) The levels of RhoA-GTP present in mock-transduced and ΔN-MYO1-transduced PC3 cells, following serum-starvation and subsequent stimulation with 10% FBS or NIH 3T3 CM for the indicated times, were determined using the Rho activation assay kit and western blotting using anti-RhoA antibody. The fold change in Rho-GTP levels, relative to starved mock- or ΔN-MYO1-transduced cells at t = 0, was determined by densitometric quantitation of the western blot using ImageJ software. **(B)** Dose-response titration of the Rho inhibitor, C3 transferase. PC3 cells were transduced with retroviral vectors expressing the indicated ΔN-MYO1 construct or mock-transduced, and the number of cells that migrated across transwell membranes under FBS conditions was quantified as described in Fig. 9. Results are reported as the mean fold change in inhibitor-treated cells migrated relative to untreated transduced cells ± SEM from three independent experiments conducted in duplicate (**P<0.01; *P<0.05).

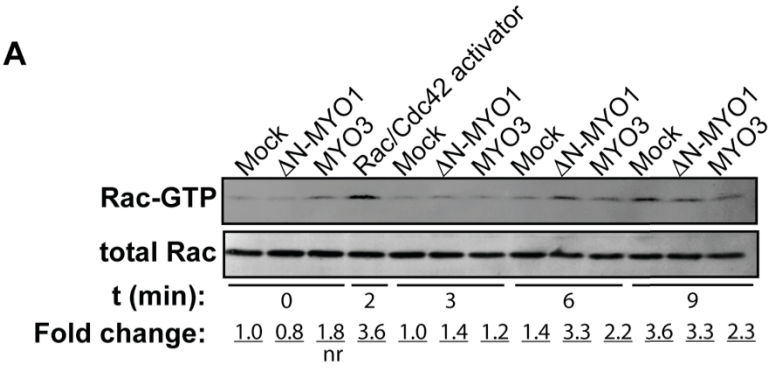
A
Mock
ΔN-MYO1
MYO3
Rac/Cdc42 activator
Rac-GTP
total Rac
t (min):
0
2
3
6
9
Fold change:
1.0 0.8 1.8 3.6 1.0 1.4 1.2 1.4 3.3 2.2 3.6 3.3 2.3
nr

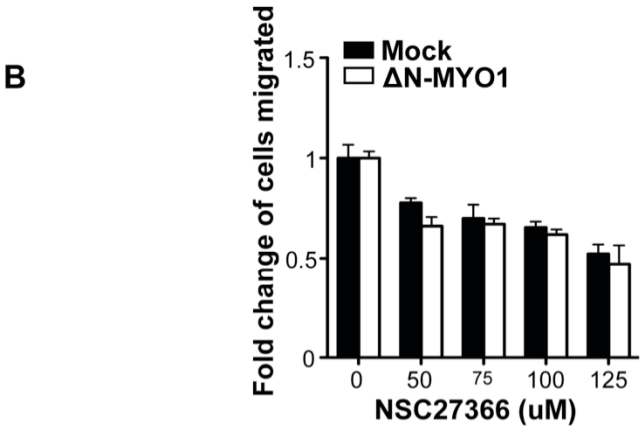
B
Mock
ΔN-MYO1
Fold change of cells migrated
1.5
1
0.5
0
0
50
75
100
125
NSC27366 (uM)

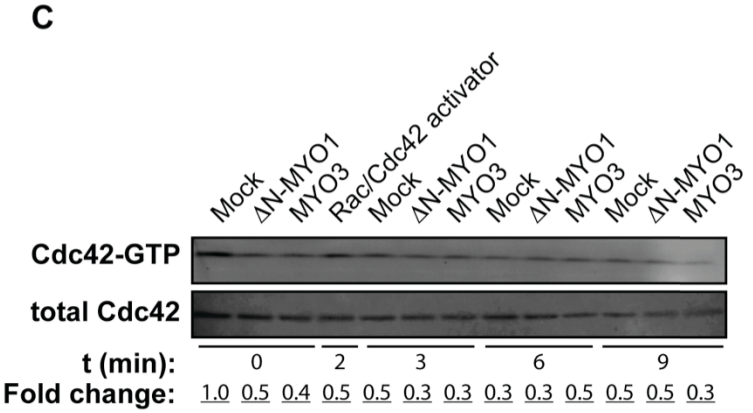
C
Mock
ΔN-MYO1
MYO3
Rac/Cdc42 activator
Cdc42-GTP
total Cdc42
t (min):
0
2
3
6
9
Fold change:
1.0 0.5 0.4 0.5 0.5 0.3 0.3 0.3 0.3 0.5 0.5 0.5 0.3

Figure 25. Myopodin has little, if any, effect on Cdc42 and Rac1 activation. Following serum-starvation and subsequent stimulation for the indicated times with 10% FBS, the levels of Rac-GTP **(A)** and Cdc42-GTP **(C)** in mock- and ΔN-MYO1-transduced PC3 cells were analyzed using Rac and Cdc42 pulldown assays and western blotting using anti-Rac1 and anti-Cdc42 antibodies. The fold change in active Cdc42 and Rac1 levels was determined as described in Fig. 24. (nr=not reproducible). **(B)** Dose-response curve of the Rac inhibitor NSC27366 in PC3 cells expressing mock- and ΔN-MYO1 constructs. The number of cells that migrated through the transwell membrane in the presence of different amounts of NSC27366 was quantified. Results are reported as the mean fold change in mock- or ΔN-MYO1-tranduced cells migrated in the presence of different NSC27366 doses relative to the corresponding untreated cells ± SEM from three independent experiments conducted in triplicate.

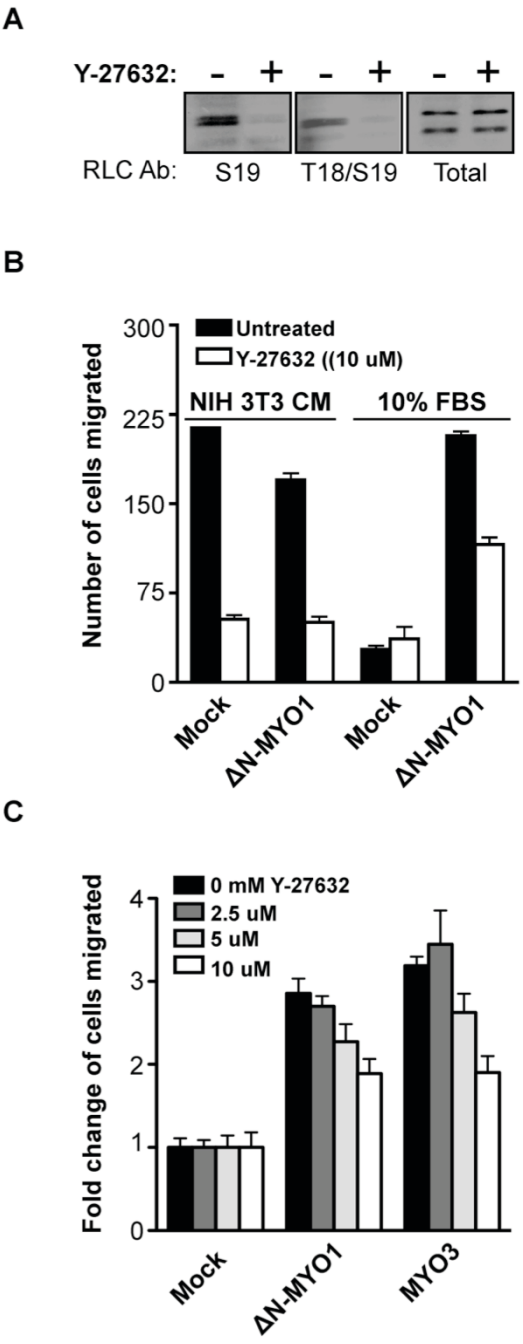
A
Y-27632: - + - + - +
RLC Ab: S19 T18/S19 Total
B
Untreated
Y-27632 ((10 uM)
NIH 3T3 CM
10% FBS
Number of cells migrated
300
225
150
75
0
Mock
ΔN-MYO1
Mock
ΔN-MYO1
C
0 mM Y-27632
2.5 uM
5 uM
10 uM
Fold change of cells migrated
4
3
2
1
0
Mock
ΔN-MYO1
MYO3

Figure 26. Myopodin differentially regulates cell migration via effects on ROCK-dependent signaling. (A) The effect of 10 μM Y-27632 treatment on inhibiting ROCK-dependent myosin regulatory light chain (RLC) phosphorylation was determined by western blotting using phospho-specific antibodies against Ser19 (S19) or Thr18 and Ser19 (T18/S19) residues in RLC, or a polyclonal antibody against RLC to detect total RLC levels. **(B)** Mock-transduced and ΔN-MYO1-transduced PC3 cells were analyzed for migration using transwell assays, as described in Fig. 9, in the presence or absence of 10 μM ROCK inhibitor (Y-27632) and in the presence of the indicated migration stimulus (CM or FBS). Results are reported as the mean number of cells migrated per microscopic field relative to mock-transduced cells ± SD from a representative experiment (n = 3) conducted in triplicate. **(C)** Mock-transduced and ΔN-MYO1- or MYO3-transduced PC3 cells were analyzed for migration using transwell assays and FBS as a migration stimulus, as described in Fig. 9, and in the presence or absence of the indicated concentrations of ROCK inhibitor (Y-27632). Results are reported as the mean fold change in cells migrated relative to mock-transduced cells ± SD from a representative experiment (n = 3) conducted in triplicate.

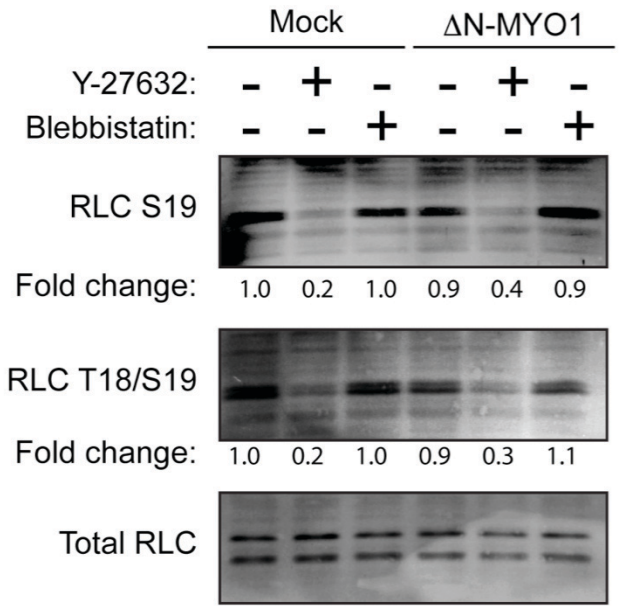

Figure 27. ΔN-MYO1 has no effect on the phosphorylation levels of RLC. The effect of 10 μM Y-27632 and 5 μM blebbistatin treatments on RLC phosphorylation was determined by western blotting using phospho-specific antibodies against Ser19 (S19) or Thr18 and Ser19 (T18/S19) residues in RLC, or a polyclonal antiserum against RLC to detect total RLC levels. The fold change in RLC phosphorylation levels was determined as described in Fig. 24.

A

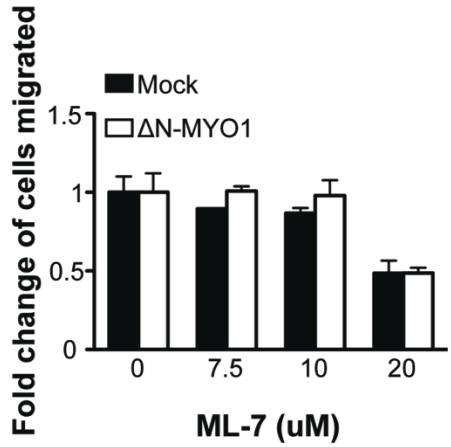
Mock
ΔN-MYO1
Fold change of cells migrated
1.5
1
0.5
0
0
7.5
10
20
ML-7 (uM)

B

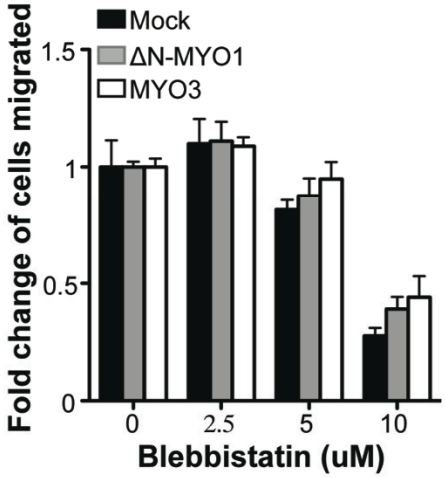
Mock
ΔN-MYO1
MYO3
Fold change of cells migrated
1.5
1
0.5
0
0
2.5
5
10
Blebbistatin (uM)

C

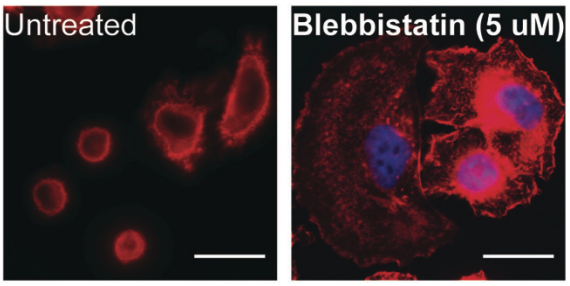
Untreated
Blebbistatin (5 uM)

Figure 28. Myopodin-stimulated cell migration is independent of myosin activity. **(A)** The effect of myosin light chain kinase inhibitor, ML-7, on myopodin-induced cell migration was examined using transwell migration assays as described in Fig. 9. Dose response curves were generated for ML-7-treated or untreated PC3 cells expressing ΔN-MYO1 or control vector under FBS conditions. Results are reported as the mean fold change in cells migrated in the presence of ML-7 relative to untreated transduced cells ± SEM from three independent experiments conducted in triplicate. **(B)** The myosin ATPase inhibitor, blebbistatin, was used to examine if myosin-generated tension is required for myopodin-stimulated cell migration. Dose response curves were generated for blebbistatin-treated or untreated PC3 cells expressing ΔN-MYO1, MYO3 or control vector. Results are reported as the mean fold change in cells migrated in response to FBS and in the presence of blebbistatin relative to untreated transduced cells ± SEM from three independent experiments conducted in duplicate. **(C)** The effectiveness of blebbistatin was confirmed based on changes in cellular morphology. PC3 cells were treated with 5 μM of blebbistatin, and phalloidin (red) and DAPI (blue) staining were used to visualize the actin cytoskeleton and the nucleus within the blebbistatin-treated cells. Scale bar=10 μm.

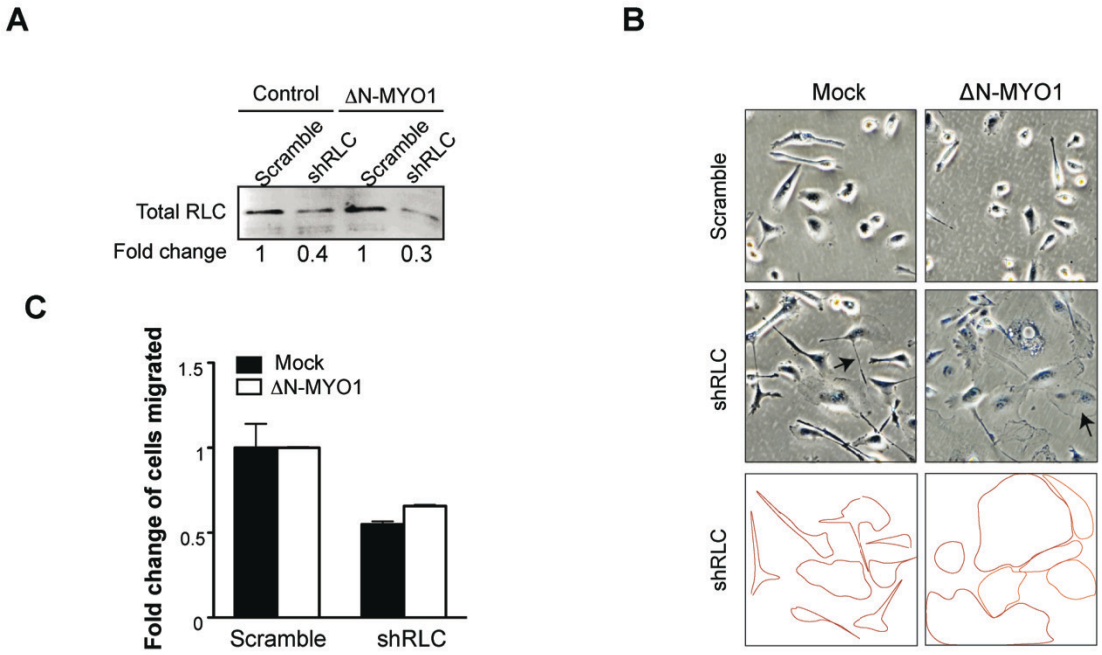

Figure 29. Knockdown of endogenous RLC has no effect on myopodin-stimulated cell migration. (A) Cells were transduced with retrovirus vectors expressing a scrambled shRNA or shRNA that targets RLC, then transduced with a control retrovirus vector or vector expressing ΔN-MYO1. The knockdown efficiency of RLC within mock- and ΔN-MYO1-transduced PC3 cells was confirmed by western blot analysis. **(B)** Morphological changes induced by scrambled or RLC shRNAs in PC3 cells expressing either mock- or ΔN-MYO1 constructs were imaged using brightfield microscopy. The cell perimeter of mock- or ΔN-MYO1-transduced cells expressing RLC shRNA constructs are traced by red lines in the lower panels. **(C)** The effect of RLC knockdown by shRNA on mock- and ΔN-MYO1-transduced PC3 cell migration was assessed using transwell migration assays under FBS conditions as described in Fig. 9. Results are presented as the mean fold change in shRNA-knockdown cells migrated relative to scramble knockdown transduced cells ± SEM from three independent experiments conducted in triplicate.

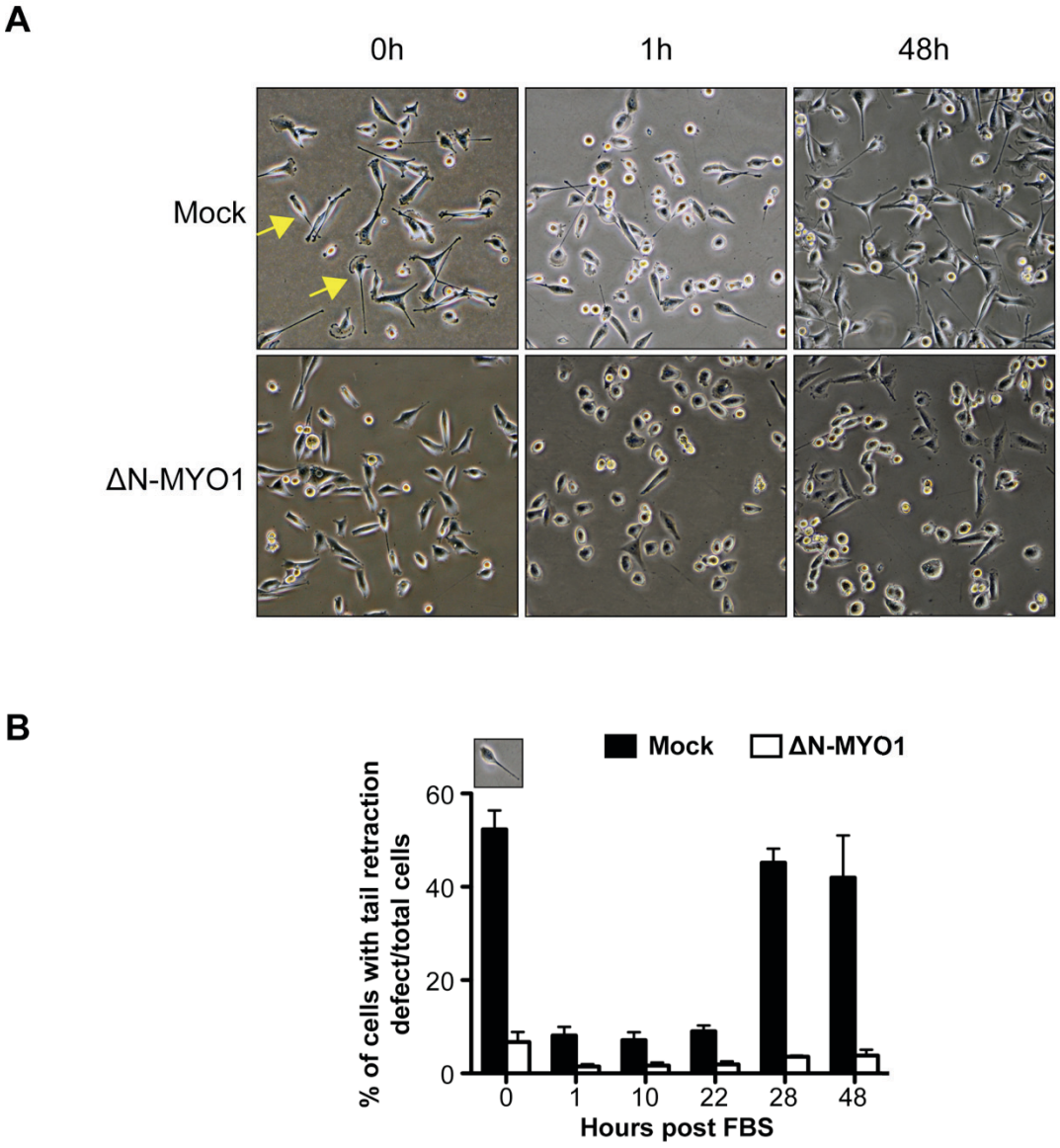

Figure 30. ΔN-MYO1 promotes tail retraction in PC3 cells. (A) Mock- and ΔN-MYO1-transduced PC3 cells were starved overnight prior to FBS stimulation. Morphological changes of transduced PC3 cells were visualized using brightfield microscopy at the indicated times post-FBS addition. Examples of cells scored positive for a tail retraction defect are indicated with arrows. **(B)** The number of cells with a tail retraction defect (example shown in inset) was quantified. A minimum of 750 cells were counted (~50 cells/field and 5 fields/well in triplicate) and results are reported as percentage of cells with a tail retraction defect over total cells counted ± SD from single a experiment conducted in triplicate.

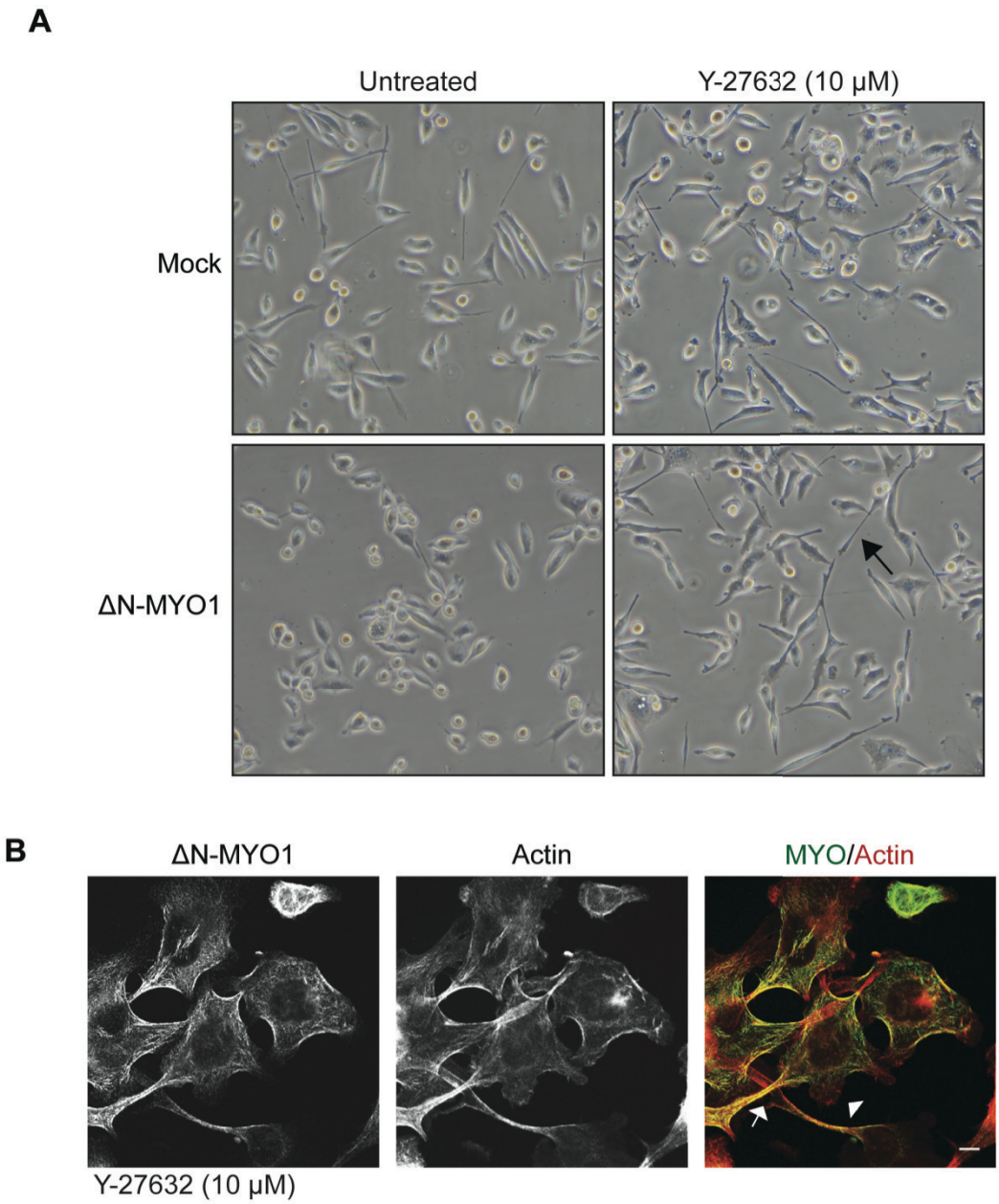

Figure 31. ΔN-MYO1 promotes tail retraction in a ROCK-dependent manner. (A) Mock- and ΔN-MYO1-expressing PC3 cells in growth medium were treated with PBS or 10 μM Y-27632 overnight. Morphological changes were visualized using brightfield microscopy. An example of a tail retraction defect is indicated with the arrow. **(B)** ΔN-MYO1-expressing PC3 cells were treated with 10 μM of Y-27632 for 24 hr and immunostained with anti-myc antibody (green) and phalloidin (red). The membrane protrusions and tails are indicated with a white arrowhead or arrow, respectively.

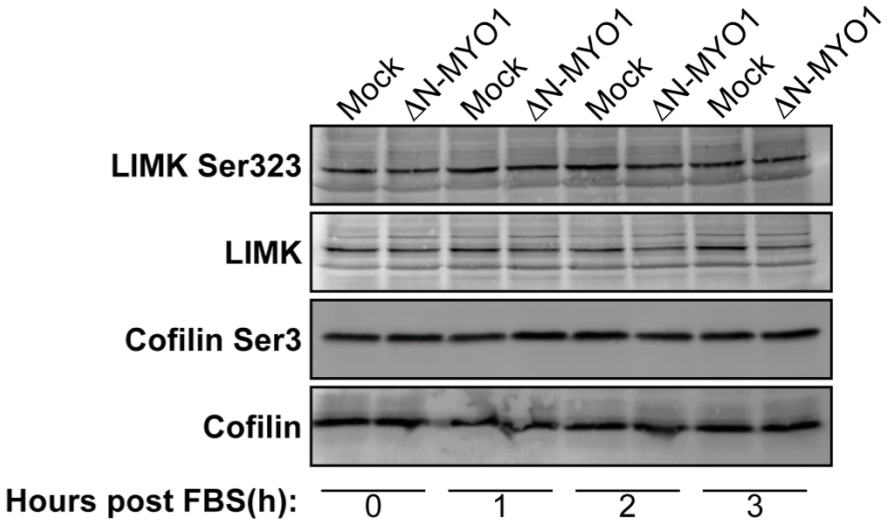

Figure 32. ΔN-MYO1 does not promote LIMK and cofilin activation. PC3 cells expressing mock or ΔN-MYO1 constructs were starved overnight, treated with FBS for the indicated times, harvested, and analyzed by western blotting using phospho-specific antibodies against Ser323 of LIMK and Ser3 of cofilin, or antibodies against total LIMK and cofilin.

CHAPTER 5: MYOPODIN POSTIVELY REGULATES MEMBRANE PROTRUSIONS IN PC3 CELLS

5.1. Introduction

Although myopodin-enhanced cell migration is independent of the level of myosin activity in cells, depletion of myosin RLCs bestowed striking morphological changes on ΔN-MYO1-transduced PC3 cells and led to substantial membrane protrusions, as compared to mock-transduced cells (Fig. 29C). These observations revealed a potential role for myopodin in the formation of membrane protrusions. The formation of membrane protrusions is driven by actin polymerization and focal adhesion formation and maturation. Since myopodin can interact with α-actinin and FA-associated proteins, such as zyxin and ILK (Yu and Luo, 2006; Yu and Luo, 2011), and since fesselin can enhance actin polymerization (Beall and Chalovich, 2001), myopodin might promote focal adhesion dynamics and actin assembly, and therefore, membrane protrusions.

Focal adhesions are multiprotein complexes that connect the actin cytoskeleton to the ECM. Based on morphology, subcellular localization, lifespan, and protein composition profile, FAs can be divided into nascent adhesions, adhesion complexes, and mature adhesions. Nascent adhesions (<0.25 μm) are formed within the lamellipodium and their formation is dependent on actin polymerization (Alexandrova et al., 2008; Choi et al., 2008). The maturation of nascent adhesions into more stable focal adhesions requires actin crosslinkers but is independent of myosin ATPase activity. In contrast, focal complexes (<1 μm) are formed at the base of lamellipodia. The formation of focal complexes is Rac-dependent and their maintenance is dependent on myosin contraction (Giannone et al., 2007; Rottner et al., 1999). Both of these types of adhesions are very dynamic and appear as small, circular structures at the leading cell edge (Huttenlocher and Horwitz, 2011). The conversion of focal complexes into elongated, mature adhesions (>1 μm) requires stress fiber templates as well as tension exerted by myosin ATPase activity (Oakes et al., 2012). The emergence of early stable focal adhesions is followed by reduced retrograde flow of F-actin at the leading edge and increased membrane protrusions. Further studies showed that these early focal adhesions function as a

molecular clutch to convert the centripetal flow of F-actin into forward movement of the leading edge (Alexandrova et al., 2008) (Fig. 6B).

Depending on cell type, membrane protrusions comprise filopodia and/or lamellipodia. Lamellipodia are composed of a densely packed Arp2/3 complex-nucleated branched actin network (Mullins et al., 1998). The thickness of a lamellipodium from the leading edge to the lamellum is usually ~1-5 μm (Small et al., 2002). The treadmilling actin network within lamellipodia is highly dynamic and is composed of Arp2/3 complexes and cofilin. In contrast, the assembled actin network in the lamellum is more stable than that in the lamellipodium and is made up of actin bundles. Tropomyosin and myosin, but not Arp2/3 complexes, are detected within the lamellum (DesMarais et al., 2002; Ponti et al., 2004). Productive, directional cell movement requires cooperation between the lamellum and the lamellipodium (Ponti et al., 2004). Filopodia are composed of parallel actin bundles perpendicular to the leading edge, and actin nucleation at the tips of filopodia is mediated by formin. At the base of filopodia, parallel actin bundles are embedded in the lamellipodium and even in the lamellum (Chhabra and Higgs, 2007). The origin of filopodia remains controversial, as some believe that filopodia are derived from actin cytoskeleton rearrangement of Arp2/3 complex-nucleated actin filaments while others suggest that filopodia are nucleated *de novo* by formin (Yang and Svitkina, 2011).

Forward cell migration involves both protrusion and retraction of the membrane at the leading edge. The rate of membrane protrusion and retraction are the same, but the duration of membrane protrusion is about four-fold higher than that of edge retraction, leading to a net forward membrane protrusion (Giannone et al., 2007). Membrane retraction is regulated by myosin contraction, which is required for FA maturation near the leading edge. However, the mechanical force generated by myosin is sometimes strong enough to break actin networks near the cell front, leading to the integration of F-actin filaments into the lamellum (Giannone et al., 2007; Nemethova et al., 2008). On the other hand, myosin can also promote stress fiber formation from Arp2/3 complex-nucleated actin filaments and formin-nucleated dorsal stress fibers in lamellipodia within osteosarcoma cells (Hotulainen and Lappalainen, 2006), or from parallel actin bundles within the filopodia of fish fibroblasts (Nemethova et al., 2008). Hence, actin filaments

generated in lamellipodia and filopodia directly contribute to the formation of actomyosin bundles in lamella. Actomyosin bundles in the lamellum move centripetally and either coalesce into ventral stress fibers or disassemble. Since myopodin promotes membrane protrusions (Fig. 29C), it is conceivable that myopodin enhances cell migration by promoting actin assembly at the leading cell edge. Under this scenario, the myopodin-induced actin bundles in the cell body (Fig. 14) arise due to myosin contraction and fracture of the myopodin-induced actin bundles.at the leading edge, followed by integration of these F-actin filaments into large bundles in the lamellum and cell body. Moreover, the observation that myopodin-enhanced cell migration is independent of NM II activity would imply that the functionally relevant role of myopodin is actin bundle formation at the leading edge, and that the NM II-dependent formation of actin bundles in the cell body of myopodin-expressing cells is a bystander effect and not directly responsible for the migration phenotype.

Several results reported in the previous chapters are consistent with the above hypothesis. I noted that myopodin-expressing cells under normal growth conditions appeared to have more protrusions at the cell periphery than mock-transduced cells (Fig. 14). These membrane protrusions became much more obvious when NM II contraction was inhibited (Fig. 29), and there was at least partial disruption of the myopodin-induced actin bundles in the cell body in cells treated with ROCK inhibitor (Fig. 31), which inhibits NM II RLC phosphorylation (Fig. 27). In addition, although myopodin predominantly localized with the actin bundles in the cell body, low levels of myopodin staining were also observed at the cell periphery (Fig. 14). A myosin-independent, actin assembly function of myopodin at the leading cell edge might therefore be the mechanism underlying the migration-stimulatory effects of myopodin.

To directly test the above hypothesis, I used the myosin ATPase inhibitor blebbistatin to show that inhibition of myosin contraction increased the amount of myopodin localized to the leading edge. At the same time, larger membrane protrusions were observed, just as in myopodin-expressing PC3 cells stably depleted of NM II RLCs. Synchronized PC3 cells expressing myopodin under FBS chemokinetic conditions also exhibited pronounced membrane protrusions, and the formation of these protrusions was abolished by the Arp2/3 complex inhibitor CK666, suggesting that myopodin-stimulated

membrane protrusions are lamellipodia-dependent. Staining focal adhesions using paxillin antibody also revealed that the large membrane protrusions of myopodin-expressing cells, but not mock-transduced PC3 cells, contained elongated mature adhesions that formed along the ends of the myopodin-induced actin bundles, although myopodin-induced protrusions were not dependent on FA maturation. Live cell imaging of myopodin-expressing PC3 cells further supported that myopodin was present within filopodia and lamellipodia when myosin contraction was suppressed. Taken together, this data provided important insights into the role of myopodin in enhancing membrane protrusions, linking this role of myopodin to a possible mechanism of enhanced cell migration by myopodin.

5.2. Results

5.2.1. Myopodin Promotes the Formation of Membrane Protrusions Under Conditions of Low Myosin Activity

Myopodin-transduced PC3 cells stably expressing RLC shRNA construct displayed substantial membrane protrusions (Fig. 29C). To examine if the same phenotype was also observed in cells under transient inhibition of NM II activity, I synchronized mock- and ΔN-MYO1-transduced PC3 cells using serum-free media and then activated myopodin chemokinetic function using FBS. FBS-stimulated PC3 cells were treated with a high dose (75-100 μM) of blebbistatin, which is required for high-level suppression of myosin ATPase activity (Shutova et al., 2012). Parallel cultures were treated with 1.5% DMSO, the solvent for blebbistatin. Consistent with my previous findings, many cells exhibited a rounded morphology following FBS stimulation (Fig. 33A; left panels). Of note, I also noticed that more DMSO-treated mock- or ΔN-MYO1-expressing cells exhibited a rounded cell shape than cells treated with 10% FBS but no DMSO, suggesting that 1.5% DMSO alters cell morphology. However, the effects of DMSO were reversible as most cells reverted to normal morphology following removal of DMSO (Fig. 33A).

In the presence of 75 μM blebbistatin, mock-transduced cells displayed long, spider-like membrane projections (Fig. 33A; middle column). In contrast, ΔN-MYO1-expressing PC3 cells were surrounded by extensive, sheet-like membrane protrusions.

These distinct morphological changes in mock- and myopodin-transduced cells rapidly regressed after removal of blebbistatin. Upon removal of blebbistatin, mock-transduced PC3 cells lost their spider-like extensions and sheet-like protrusions became evident as the cells flattened out (Fig. 33A; right column). The extensive sheet-like protrusions in ΔN-MYO1-expressing cells declined and cells tended to exhibit an elongated cell body, although with still noticeable membrane protrusions. Therefore, myopodin augments the formation of membrane protrusions following either stable knockdown (Fig. 29) or transient inhibition (Fig. 33) of myosin activity.

The affect of myopodin on membrane protrusions was also evident at lower doses (5-10 μM) of blebbistatin, although the effects were not as prominent as those induced by 75 μM treatment (Fig. 38). When myopodin-expressing PC3 cells were treated with 10 μM blebbistatin under FBS conditions for an hour and analyzed by immunofluorescence microscopy, the myopodin-induced thick actin bundles remained prominent within the cell body (Fig. 33B). However, as indicated in the orthogonal view of confocal sections, myopodin appeared to stain slightly more prominently near the edges of the induced membrane protrusions when myosin activity was modestly inhibited (Fig. 33B; arrow; see Fig. 13B for comparison). Thus, under conditions of partial or complete inhibition of NM II activity, myopodin induces prominent membrane protrusions and can be detected in these protrusions.

5.2.2. Myopodin Promotes Lamellipodia Formation Under FBS Chemokinetic Conditions

As inhibition of myosin activity revealed a role for myopodin in the formation of membrane protrusions, I wondered if myopodin also promoted membrane protrusions under FBS chemokinetic conditions. Mock- and ΔN-MYO1-transduced PC3 cells were synchronized by serum-starvation followed by FBS stimulation, and the affect of FBS on transduced PC3 cell morphology was observed using brightfield microscopy over a 24 hr timecourse. Strikingly, within 30 min of FBS stimulation, myopodin-expressing cells exhibited prominent membrane protrusions (Fig. 34A), although the extent of membrane protrusion was not as robust as in blebbistatin-treated myopodin-expressing PC3 cells. In contrast, mock-transduced cells appeared as rounded or ellipsoid shapes and displayed few, if any, membrane protrusions (Fig. 34A).

Because the protrusions in myopodin-expressing cells morphologically resembled lamellipodia at the leading cell edge, I examined whether the induced protrusions were dependent on factors that drive lamellipodia formation. Hence, the Arp2/3 complex inhibitor CK666, which prevents the transition of Arp2/3 complexes into their active conformation (Nolen et al., 2009), was used to assay if myopodin-induced membrane protrusions were dependent on the Arp2/3 complex-nucleated actin network. Consistent with previous findings, 30 min of FBS stimulation induced substantial membrane protrusions in PC3 cells expressing myopodin (Fig. 34B). Strikingly, the large membrane protrusions were severely perturbed by 20 μM CK666 treatment, implying the myopodin-induced membrane protrusions are dependent on functional Arp2/3 complexes. It is unlikely that the disappearance of membrane protrusions was due to toxicity issues as previous studies showed that even 80 μM of CK666 had no effect on cellular mitosis (Nolen et al., 2009).

The reliance on Arp2/3 complexes for myopodin-induced membrane protrusions was also examined by confocal immunofluorescence microscopy, staining for the subcellular localization of myopodin, actin, and myosin. After 30 min of FBS stimulation, most of the myopodin-expressing cells had created large, sheet-like membrane protrusions, as revealed by phalloidin staining of actin. These protrusions contained actin-rich rims ~1 μm thick along the edge of the protrusions (Fig. 35; red arrow in bottom panel), a characteristic staining pattern of lamellipodia. At this timepoint, myopodin predominantly colocalized with the thick actin bundles that formed in the cell body, although low levels of myopodin were also apparent in a punctate staining pattern throughout the lamellum (the region behind the actin-rich rim) and to a lesser extent in the region corresponding to the lamellipodium (Fig. 35; red arrow). NM IIA staining was detected strongly in the cell body, within the lamellum and at the lamellipodium-lamellum boundary. As previously shown (Fig. 23), NM IIA in the cell body did not colocalize with the myopodin-induced actin bundles and the punctuated myopodin and myosin staining pattern at the cell periphery rarely overlapped, further suggesting myopodin and myosin are mutually excluded.

The sheet-like protrusions and actin-rich rims present in untreated, myopodin-expressing cells were replaced in the CK666-treated cells by smaller actin-rich

protrusions (Fig. 35, right column). These protrusions appeared to contain parallel actin bundles, and myopodin colocalized along the actin bundles and out toward the tips of the protrusions (Fig. 35; yellow arrow). NM IIA, a marker of lamella, was also enriched along the actin bundles but was localized nearer the base of the protrusions (Fig. 35; yellow arrow). In addition, myopodin-transduced PC3 cells treated with CK666 appeared to have fewer actin bundles in the cell body, suggesting that the Arp2/3 nucleated actin network might contribute to bundle formation in the cell body (Fig. 35; right column). Taken together, these results indicate that myopodin promotes lamellipodia formation in an Arp2/3 dependent manner, and that when lamellipodia formation is inhibited, myopodin can still induce formation of smaller protrusions and colocalizes with the parallel actin bundles in these protrusions.

5.2.3. Myopodin Promotes Focal Adhesion Maturation

Since the formation of nascent adhesions and subsequent FA maturation are essential for formation of membrane protrusions (Alexandrova et al., 2008), I examined whether the protrusion formation in myopodin-expressing cells could be attributed to altered FA dynamics under chemokinetic conditions. Mock- and ΔN-MYO1-transduced PC3 cells were stimulated with FBS following serum starvation, and transduced cells were fixed at the indicated times and stained for myopodin, actin, and FAs using paxillin, a commonly used focal adhesion marker and one of the earliest proteins recruited to nascent focal adhesions (Zaidel-Bar et al., 2003). Consistent with previous findings (Fig. 19), mock- and ΔN-MYO1-expressing cells under starvation conditions became flattened and elongated and had no prominent actin bundles in the cell body (Fig. 36). Focal adhesions in mock- and myopodin-transduced cells were stained in a punctate manner throughout the cells with no apparent difference in focal adhesion number or size (Fig. 36). By 20 min post-FBS addition, myopodin-induced actin bundles became visible and FAs became elongated and colocalized with the induced actin bundles (Fig. 36; bottom row inset). FAs of ΔN-MYO1-transduced PC3 cells oriented centripetally and were larger than those in mock-transduced cells, whose FAs were also enriched near the cell periphery. At this timepoint, the membrane protrusions in mock- and ΔN-MYO1-expressing cells appeared to be quite similar.

Differences in the size and morphology of membrane protrusions and FAs between mock- and ΔN-MYO1-transduced cells became striking between 30 min to 1 hr post-FBS stimulation (Fig. 37) By 30 min post-FBS stimulation, prominent actin bundles were observed in the cell body of myopodin-expressing cells. Mock-transduced cells maintained the punctate staining pattern of FAs around the cell periphery, although the size of FAs at these later time points was slightly larger than those observed at 20 min post-FBS treatment (Figs. 36 and 37). Regardless of their size, FAs in mock-transduced cells were localized almost exclusively to the cell periphery, suggesting that FBS treatment failed to promote the formation of elongated, mature FAs in mock-transduced cells. This observation was anticipated by the inability of FBS to promote PC3 cell migration (Chapter 3 results). In contrast, after 30 min of FBS treatment, myopodin-expressing cells exhibited numerous dot-like FAs at the cell periphery but also elongated FAs oriented centripetally within the lamellum and the cell body (Fig. 37). By 1 hr post-FBS treatment, the small, nascent focal adhesions or focal complexes near the cell perimeter were dramatically decreased and there was a corresponding increase in the presence of elongated, mature FAs in toward the cell body. Myopodin-expressing cells contained actin bundles that resembled dorsal stress fibers in the lamellum and the elongated FAs lay along the stress fiber template. Myopodin-induced cell migration therefore corresponds with lamellipodia and dorsal stress fiber formation and FA maturation.

5.2.4. Inhibition of Myosin Activity Abolished the Formation of Elongated FAs in Myopodin-expressing Cells

As myosin contraction is known to promote FA maturation, I examined whether inhibiting myosin activity disrupts tension-dependent FA maturation within myopodin-expressing cells. Mock- and ΔN-MYO1-expressing cells were starved, stimulated with FBS in the presence of blebbistatin (5 μM or 75 μM), and fixed at 30 min post-FBS stimulation, the time point when actin bundles became evident and many FAs became mature in untreated myopodin-expressing cells (Fig. 37). At the low dose of blebbistatin, mock-transduced PC3 cells exhibited fewer and slightly smaller punctate FAs around the cell periphery compared to untreated, mock-transduced cells (Figs. 37 and 38). Consistent

with previous findings (Fig. 33B), when myosin activity was modestly inhibited, myopodin-induced actin structures were still prominent within 30 min of FBS stimulation and stronger myopodin staining was detected within the lamellum and cell body (Fig. 38). Myopodin-induced actin bundles were oriented perpendicular or parallel to leading edge (Fig. 38A inset; arrowhead and arrow, respectively). FAs in blebbistatin-treated, ΔN-MYO1-expressing cells were larger within the lamellipodium and the lamellum compared to mock-transduced cells, and oriented centripetally (Fig. 38A). However, the quantity of elongated mature FAs in the cell body was significantly decreased compared to myopodin-expressing cells not treated with a low dose of blebbistatin (Fig. 37; 30 min post-FBS stimulation). The size of the sheet-like membrane protrusions in myopodin-expressing cells in the presence of 5 μM blebbistatin was similar to, or slightly larger than, those present in untreated cells (Fig. 37, 38A), suggesting that myopodin-induced membrane protrusions do not require myosin-dependent FA maturation.

The high dose of blebbistatin (75 μM) abrogated FA maturation, and small, nascent focal adhesions or focal complexes were present throughout the cell body. At this higher dose, mock-transduced PC3 cell exhibited numerous, spider-like membrane protrusions (Fig. 38B) as shown previously by brightfield microscopy (Figs. 33A and 38B), and small, immature FAs were observed in the cell body (Fig. 38B). In marked contrast, myopodin-expressing cells under a high dose of blebbistatin exhibited even more pronounced formation of sheet-like membrane protrusions resembling lamellipodia. These protrusions were filled with a layer of diffuse actin network that was largely devoid of myopodin staining. The diffuse actin network was frequently rimed by large actin bundles, either in toward the cell body or out near the cell periphery. The peripheral actin bundles were in the form of long, filopodia-like protrusions filled with apparently parallel actin bundles. Myopodin colocalized with the actin-rich bundles at the base of membrane protrusions and with the parallel actin bundles in the filopodia-like protrusions (Fig. 38B, arrow & inset). The effect of myopodin on membrane protrusions was further supported by the observation that cells expressing lower levels of myopodin lacked the striking membrane protrusions (Fig. 38B; arrowhead). As inhibiting myosin activity impaired FA maturation but failed to disrupt, or even assisted, myopodin-induced

membrane protrusions, myopodin-induced membrane protrusions and cell migration is not based on myopodin promotion of FA maturation.

5.2.5. Myopodin Colocalized with the Actin Networks at the Leading Cell Edge in the Early Stage of FBS Stimulation

The formation of nascent adhesions requires actin dynamics in lamellipodia and subsequent maturation of nascent adhesions into focal complexes requires the presence of crosslinked actin filaments (Choi et al., 2008). As myopodin is an actin-binding protein and interacts with α-actinin (Leinweber et al., 1999; Linnemann et al., 2010; Schroeter et al., 2008), I speculated that myopodin might affect the formation of actin bundles and thus the formation of early FAs at the leading edge. To test this hypothesis, I synchronized myopodin-expressing PC3 cells using serum-starvation and stimulated the transduced cells with FBS. Unlike previously, I fixed the myopodin-transduced cells prior to the formation of the thick actin bundles in the cell body and examined whether myopodin colocalized with actin fibers at the cell periphery. During starvation, myopodin was stained diffusely within the cell body and occasionally strongly at the cell periphery (Fig. 36). Within 15 min post-FBS stimulation, actin-rich lamellipodia were observed in myopodin-expressing cells and myopodin staining was detectible within the lamellipodium (Fig. 39; arrow). Numerous actin bundles also appeared perpendicular to the leading edge and myopodin colocalized along these bundles (Fig. 39; inset). One end of these bundles was located within the actin-rich lamellipodium while the other end appeared to be connected to the myopodin-rich actin bundles that were oriented parallel to the leading edge, resembling transverse stress fibers. These observations indicated myopodin expression promotes actin bundle formation at the leading edge, possibly providing actin templates for nascent adhesion maturation into focal complexes followed by membrane protrusions.

5.2.6. Myopodin Promotes both Filopodia and Lamellipodia Formation

The effect of myopodin on membrane protrusions was also examined by live imaging of myopodin-expressing PC3 cells. To visualize dynamic interaction between myopodin and the actin cytoskeleton using spinning disk confocal microscopy, PC3 cells

stably expressing the LifeAct-RFP (red fluorescent protein) construct were generated. LifeAct-RFP is a RFP tagged 17-amino acid peptide from *Saccharomyces cerevisae* that binds specifically to filamentous actin (Riedl et al., 2008). GFP-tagged ΔN-MYO1 plasmids were transfected into PC3 cells stably expressing RFP-tagged LifeAct and examined for the effects of myopodin on actin cytoskeleton architecture. Of note, these cells appeared perfectly normal under brightfield microscopy. I also noted that LifeAct-RFP was not very photostable, so the last few time points in each experiment had reduced LifeAct signal, and myopodin-induced actin bundle formation was a little slower in these cells. However, the myopodin-induced actin bundle formation and restrictive subcellular localization of myopodin within the cell body remained the same. To confirm that actin cytoskeleton remodeling was mediated by myopodin, four separate cells were imaged in the experiments reported here, two of which expressed detectible levels of myopodin while the other two were either low expressors or were not transfected.

Similar to immunostained PC3 cells, myopodin-expressing PC3 cells had few, if any, actin bundles in the cell body under starvation conditions (Fig. 40, t=0 timepoint). Within 45 min post-FBS stimulation, prominent stress fibers were observed in the cell body. Although it was difficult to tell from individual frames, images from a series of timepoints showed that F-actin at the cell periphery flowed centripetally to the cell body, implying that myopodin-induced actin bundles in the cell body were derived from the cell periphery. During the timecourse of FBS stimulation, the leading edge of the myopodin-transfected and untransfected cells exhibited membrane protrusion and retraction. Qualitatively, myopodin-expressing cells appeared to have slightly longer or more persistent membrane protrusions. The subsequent inhibition of myosin activity with blebbistatin stopped the retraction of membrane protrusions in both mock- and myopodin-transduced cells and resulted in the formation of actin-rich filopodia-like projections. Some of these actin-rich projections were observed in mock-transduced cells, but they stopped growing when they reached ~1.5 μm in length. In contrast, blebbistatin-treated, myopodin-expressing cells exhibited numerous long actin projections (up to 5 μm) and myopodin was frequently found within the shaft of these projections (Fig. 40; 75 min) and around the cell periphery. The long filopodia-like projections subsequently bent towards one another and waves of diffuse myopodin and actin encompassed the

projections, creating a lamellipodia-like membrane protrusion (Fig. 40; inset and arrows). The live imaging analysis therefore suggested that myopodin first promotes filopodia formation followed by lamellipodia formation.

5.3 Discussion

Depletion of NM II RLCs in myopodin-expressing PC3 cells led to formation of substantial membrane protrusions (Fig. Fig. 29), revealing a potential role for myopodin in membrane protrusions. The affect of myopodin at the leading edge was also evident under transient inhibition of myosin activity using blebbistatin treatment (Fig. 33) and FBS stimulation (Fig. 34), both of which induced prominent sheet-like protrusions at the cell periphery. Using FBS chemokinetic conditions and blebbistatin, I demonstrated that myopodin-stimulated membrane protrusions were independent of tension-mediated adhesion maturation but correlated with the presence of nascent adhesions or focal complexes. Immunofluorescence staining of cells at the early times post-FBS stimulation and prior to membrane protrusion formation showed that myopodin colocalized with the actin bundles at the leading cell edge, which are essential for stabilization and growth of nascent adhesions and focal complexes. Live imaging analysis also showed that myopodin flowed centripetally in toward the cell body following FBS stimulation. Subsequent inhibition of NM II activity with blebbistatin led to the formation of membrane protrusions and the appearance of myopodin within the shaft of induced filopodia and within lamellipodia. My data indicate that myopodin promotes membrane protrusions by stimulating actin bundle formation at the leading edge, which coincides with FA formation or stabilization, and that the actin bundles within the cell body are an incidental effect of myosin contraction.

Under non-synchronized, normal growth conditions, myopodin predominantly localizes with the induced actin bundles in the cell body and only trace amounts of myopodin are found at the cell periphery. The majority of my earlier research efforts therefore focused on characterizing mypodin interactions with these actin networks in the cell body. Although I frequently observed actin-rich membrane protrusions in myopodin-expressing cells (Fig. 14), the membrane protrusions were not very prominent in non-synchronized cells and it was difficult to examine the effects quantitatively. The

inhibitory affect of serum-starvation on myopodin-induced chemokinetic activity (discussed in Chapter 3) suggested a means to synchronize cells and examine the kinetics of myopodin function. Using synchronization with serum-free medium and subsequent FBS stimulation, I was able to detect a striking and uniform phenotype in the majority of myopdin-expressing PC3 cells that involved membrane protrusions at the leading edge. This synchronization approach, coupled with inhibitor studies and live cell imaging, provided a major conceptual breakthrough in our understanding of how myopodin promotes cell migration and the genesis of the actin bundles in the cell body. Actin-rich protrusions are responsible for generating actin bundles in the cell body because myosin contraction constantly recruits Arp2/3 complex-nucleated and formin-nucleated actin networks into the lamellum for the formation of stress fibers (Hotulainen and Lappalainen, 2006). Immunofluorescence and live imaging analyses of myopodin-expressing cells suggest that myopodin-induced actin bundles are derived from the leading edge, and subsequently integrated into the actin network of the cell body.

Focal adhesion formation and maturation and actin assembly drives membrane protrusions (Alexandrova et al., 2008). Myopodin-expressing cells with substantial membrane protrusions exhibited elongated FA but mock-transduced cells that had few membrane protrusions failed to promote FA maturation (Figs. 36 and 37). This observation suggested that myopodin might promote membrane protrusions by stimulating FA formation or maturation. However, the elimination of elongated mature adhesions (>1 μm FA size) by blebbistatin (Fig. 38) did not impair the membrane protrusions, suggesting that the formation of early FAs, but not tension-mediated FA maturation, is important for myopodin-stimulated membrane protrusions. Blebbistatin-treated cells expressing myopodin exhibited more dot-like, small adhesions at the leading edge and in the lamellum than observed in mock-transduced cells (Fig. 38). These results suggested that myopodin might promote the formation, or inhibit the disassembly of nascent adhesions or focal complexes. Different signals trigger the formation of nascent adhesions and focal complexes although they can both grow into mature FAs. The formation of nascent adhesions requires dynamic actin assembly within lamellipodia and their growth requires a crosslinked actin structure (a template along which the FA grows) but is independent of myosin contraction (Choi et al., 2008). Formation of focal

complexes at the base of lamellipodia is dependent on Rac activation (Rottner et al., 1999), and their maturation requires myosin activity as well as a stress fiber template (Oakes et al., 2012). It remains unknown whether myopodin stimulates the formation of focal complexes or nascent adhesions, as they are difficult to distinguish based on size under confocal microscopy. Furthermore, blebbistatin treatment transforms Rac-activated focal complexes into smaller FAs that are indistinguishable from nascent adhesions (Choi et al., 2008). On the other hand, when nascent adhesions become mature behind the lamellipodia, it is impossible to tell if the adhesion complex developed from a nascent adhesion or the dot-like structure is a newly formed focal complex. Our understanding of how nascent and focal complexes forms is still in its infancy, and it remains unclear whether focal complexes and the more stable form of nascent adhesions are identical. Additional live imaging analysis of the appearance FAs within myopodin-expressing cells might shed light on the origin of these dot-like FAs.

Compositional change and growth are two important features of FA maturation, both of which require a stress fiber template (Oakes et al., 2012). When dorsal stress fiber assembly at the leading edge is impaired by depletion of formin or α-actinin, the compositional change of FAs is perturbed and their lifespan is shortened (Oakes et al., 2012). Thus, the stress fiber template is important for the compositional changes characteristic of FA maturation and inhibits disassembly of FAs. FAs that have been through compositional change but not FA growth can still remodel the ECM when myosin activity is inhibited up to 80%. However, FAs fail to transmit the force to remodel the ECM when myosin activity is inhibited more than 80% or dorsal stress fiber assembly is impaired (Oakes et al., 2012). These data suggest that a nominal amount of tension and parallel actin structures are both required for force transmission through the ECM. As myopodin-expressing cells contained more dot-like adhesions near the cell periphery when FA maturation was suppressed with blebbistatin (Fig. 38), it is possible that myopodin may enhance membrane protrusions by promoting formation of stress fiber templates, which in turn leads to the compositional change characteristic of FA maturation or inhibition of FA disassembly.

Actin assembly and actin crosslinkers, such as α-actinin, are important for stress fiber formation, and therefore, the growth of nascent adhesions and focal complexes

(Choi et al., 2008). *In vitro* assays demonstrated that human and mouse myopodin can crosslink actin filaments (Linnemann et al., 2012; Weins et al., 2001), and fesselin can promote actin nucleation and elongation (Beall and Chalovich, 2001). The colocalization of myopodin with actin bundles at the cell periphery (Figs. 38, 39, and 40) suggests myopodin might facilitate FA formation by increasing actin polymerization within the lamllipodium and/or by crosslinking actin filaments, thereby promoting nascent adhesion formation. Fesselin studies also showed that the effect of fesselin on actin polymerization is attenuated in the presence of α-actinin (Pham and Chalovich, 2006). Therefore, it is possible that when myopodin colocalizes with α-actinin along the bundles, myopodin may function as an actin crosslinker but when myopodin localizes by itself on the filaments, it functions as an actin polymerizing factor. Additional effort should be placed on trying to detect α-actinin in cells, which could then be used in co-immunofluroescence assays to examine myopodin and α-actinin localization on peripheral actin structures.

Cell migration involves cycles of membrane protrusion, cell body translocation, and tail retraction. Upon serum starvation and FBS stimulation, the affect of myopodin on membrane protrusions was striking within the first two hours (Figs. 33 and 34) but these effects diminished over time. This observation explains why under normal culture conditions, the differences in membrane protrusions between mock- and ΔN-MYO1-expressing cells were less prominent (Fig. 14). One possibility for diminished membrane protrusions is that at the early timepoint, the machinery in the cell body responsible for cell body translocation and tail retraction, such as the actin bundles, is not fully assembled, and therefore membrane protrusions continue to expand but the cell body and the cell rear remain stationary. When actin bundles are integrated into the cell body at the later timepoints, the bundles actuate cell body translocation, and the rest of the cell is able to couple the cell rear with the protruding cell front to promote cell migration.

The affect of myopodin on membrane protrusions was also evident in murine C2C12 muscle cells and in 3D culture. Compared to mock-transducd C2C12 cells, the murine MYO1 homologue induced formation of many discrete lamellipodia at the leading edge (Fig. 41A; arrow). Interestingly, myopodin was closely associated with the leading cell edge in C2C12 cells, even without synchronization or blebbistatin treatment. This further supports the conclusion that myopodin effects at membrane protrusions are

not an artifact of the FBS stimulus or pharmacological inhibition. Myopodin-expressing cells cultured in 3D matrigel also exhibited dramatic filopodia formation (between 15 μm-25μm in length) while mock-transduced cells had few, if any, membrane protrusions (Fig. 41B). It is unclear why myopodin induced only filopodia, but not lamellipodia, under these 3D culture conditions. It seems likely that different signaling pathways are activated under 3D culture conditions, as the physical properties of the ECM directly modulate the cellular morphology and mode of migration (Petrie and Yamada, 2013). Elongated and amoeboid modes of cell migration are commonly observed in 3D culture, which are dependent on Rac1 or RhoA activity, respectively (Petrie and Yamada, 2013; Sahai and Marshall, 2003). The morphology of mock-transduced PC3 cells resembles amoeboid cell morphology under FBS conditions, which had rounded cell morphology and few protrusions. However, the filopodia-like extensions from the myopodin-expressing cells within 3D culture were not typical amoeboid cell morphology. These long, slender, actin-rich protrusions resemble the overexpression phenotype of the formin family members, FMNL3 and mDia2, which localize to the tips of filopodia and stimulate formation of long filopodia in Jurkat cells (Harris et al., 2010). Whether myopodin localizes in the shaft of the induced filopodia in 3D culture remains to be investigated.

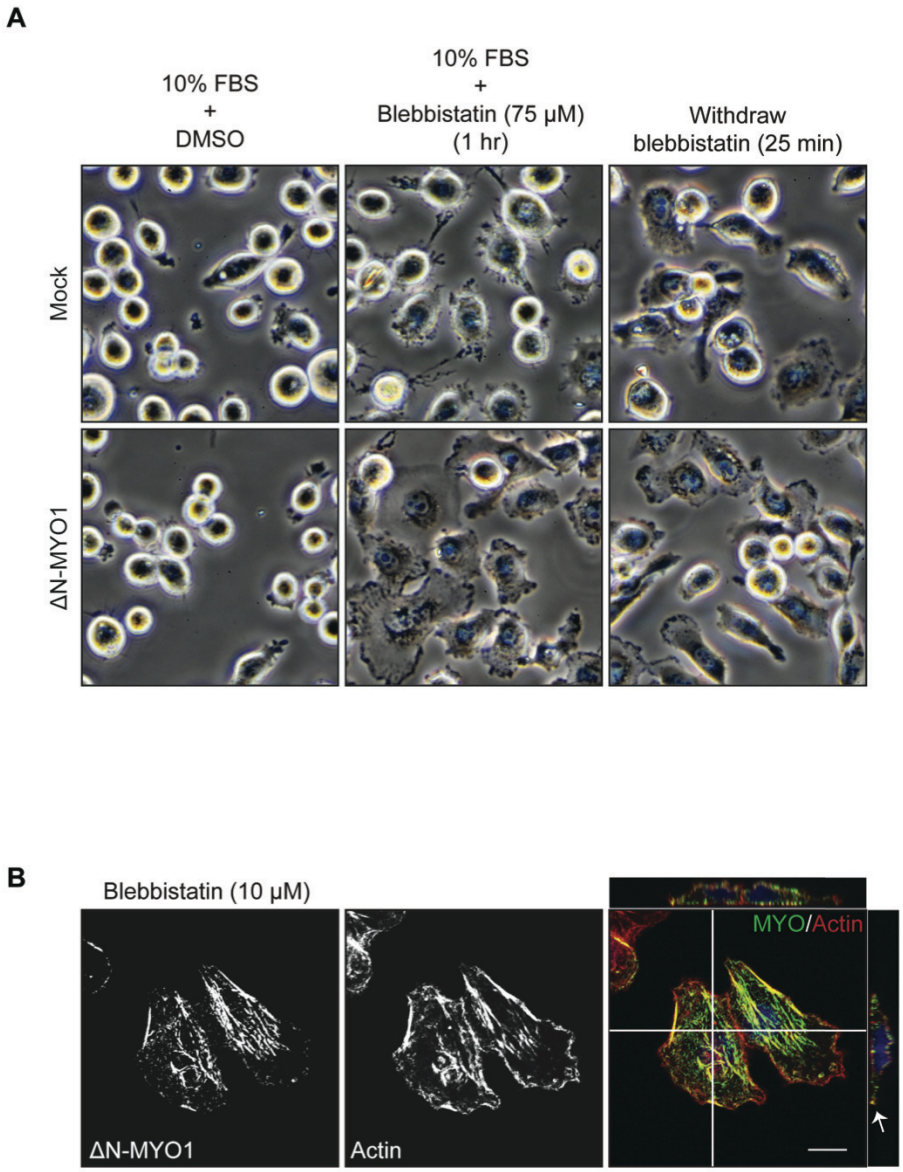

Figure 33. ΔN-MYO1 promotes the formation of membrane protrusions and localizes to the protrusions in PC3 cells at low myosin activity. (A) Mock- and ΔN-MYO1-transduced PC3 cells were starved overnight prior to FBS stimulation. Transduced PC3 cells were treated using FBS with either DMSO control or 75 μM blebbistatin, which was subsequently replaced with fresh FBS medium. Morphological changes of transduced PC3 cells were visualized using brightfield microscopy at 1 hr post-blebbistatin (75 μM) addition and at 25 min post-blebbistatin withdrawal. **(B)** ΔN-MYO1-transduced PC3 cells were treated with 10 μM blebbistatin in growth medium for 1 hr and immunostained with anti-myc antibody (green), phalloidin (red), and DAPI (blue). The orthogonal views of confocal images of ΔN-MYO1-expressing PC3 cells (imaged along the vertical and horizontal white lines) demonstrated that stronger myopodin staining was found at the leading cell edge and membrane protrusions (arrow). Scale bar=10 μm.

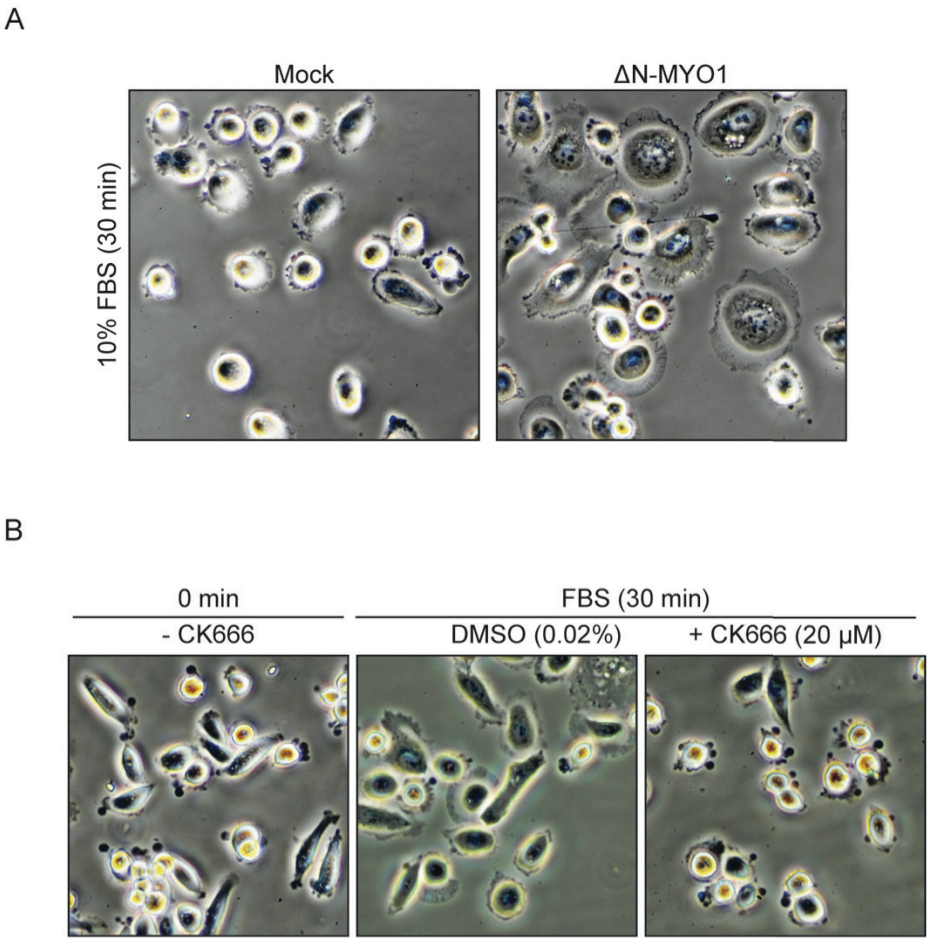

Figure 34. ΔN-MYO1 promotes lamellipodia formation under FBS chemokinetic conditions. (A) Mock- and ΔN-MYO1-expressing PC3 cells were starved overnight, stimulated with 10% FBS for 30 min and the effect of myopodin on membrane protrusions was imaged using brightfield microscopy. **(B)** ΔN-MYO1-transduced PC3 cells were treated as described in panel (A) except 20 μM of the Arp2/3 complex inhibitor CK666 and DMSO control were used to examine the genesis of the membrane protrusions.

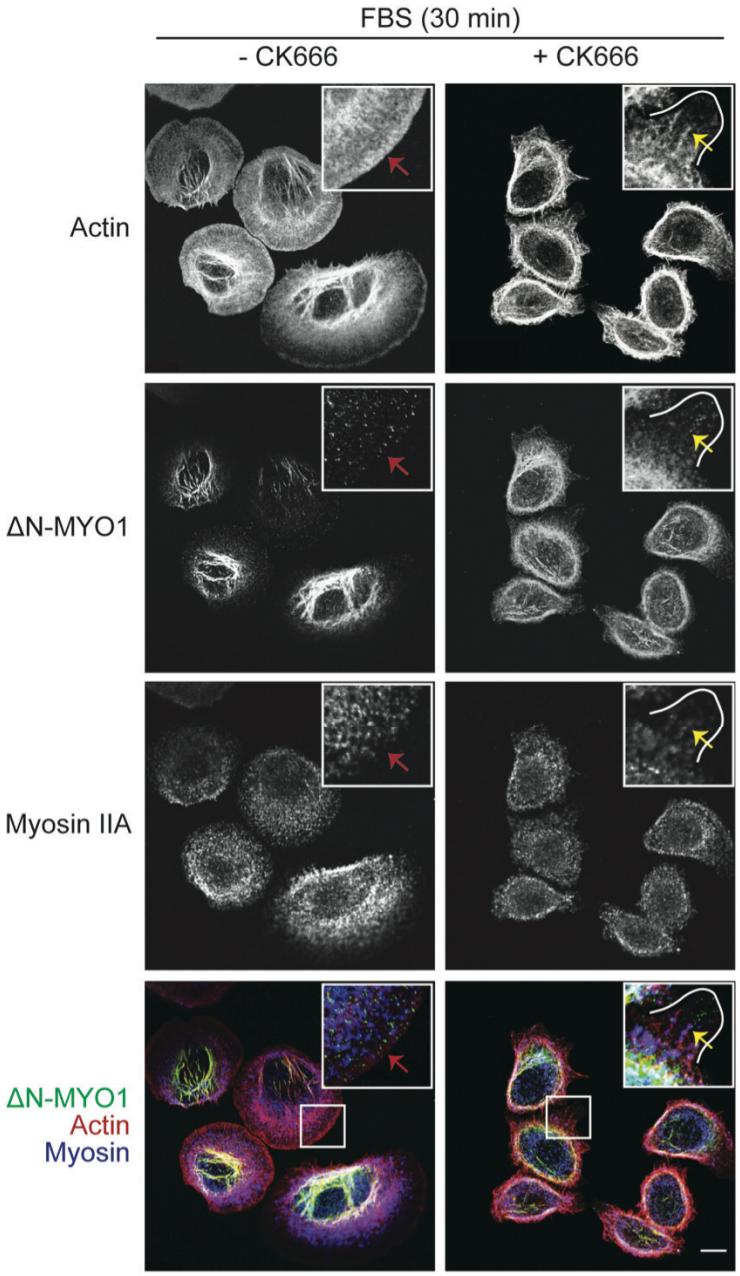

Figure 35. ΔN-MYO1 promotes the formation of an actin-rich rim at the cell periphery in an Arp2/3 complex-dependent manner. Mock- and ΔN-MYO1-expressing PC3 cells were treated as described in Fig. 34B and immunostained with phalloidin (red), anti-myc (green), and anti-myosin (blue) antibodies. The actin-rich rim in FBS-stimulated cells, the actin bundles in CK666-treated cells, and the boundary of membrane protrusions are indicated with a red arrow, yellow arrow, or white line, respectively. The 16.7 μm x 16.7 μm areas indicated in the images are magnified 250% in the insets. Scale bar=10 μm.

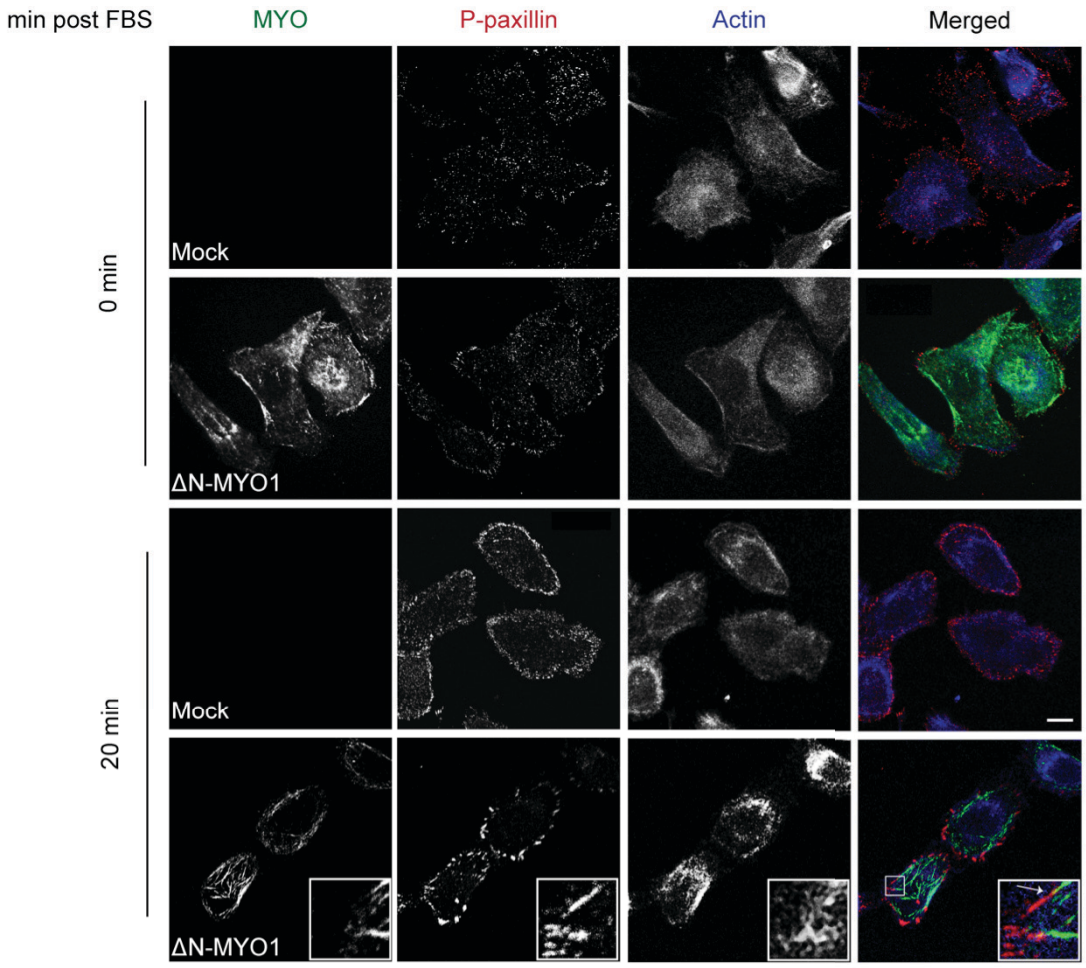

Figure 36. ΔN-MYO1 promotes mature focal adhesion formation. Mock- and ΔN-MYO1-expressing PC3 cells were starved and treated with FBS at the indicated time, and immunostained with phalloidin (blue), anti-myc (green), and focal adhesion marker phospho-specific paxillin (red) antibodies. Colocalization of myopodin-induced actin bundles with focal adhesions is indicated with the white arrow. The 7.7 μm x 7.7 μm area indicated in the images are magnified 425% in the insets. Scale bar=10 μm.

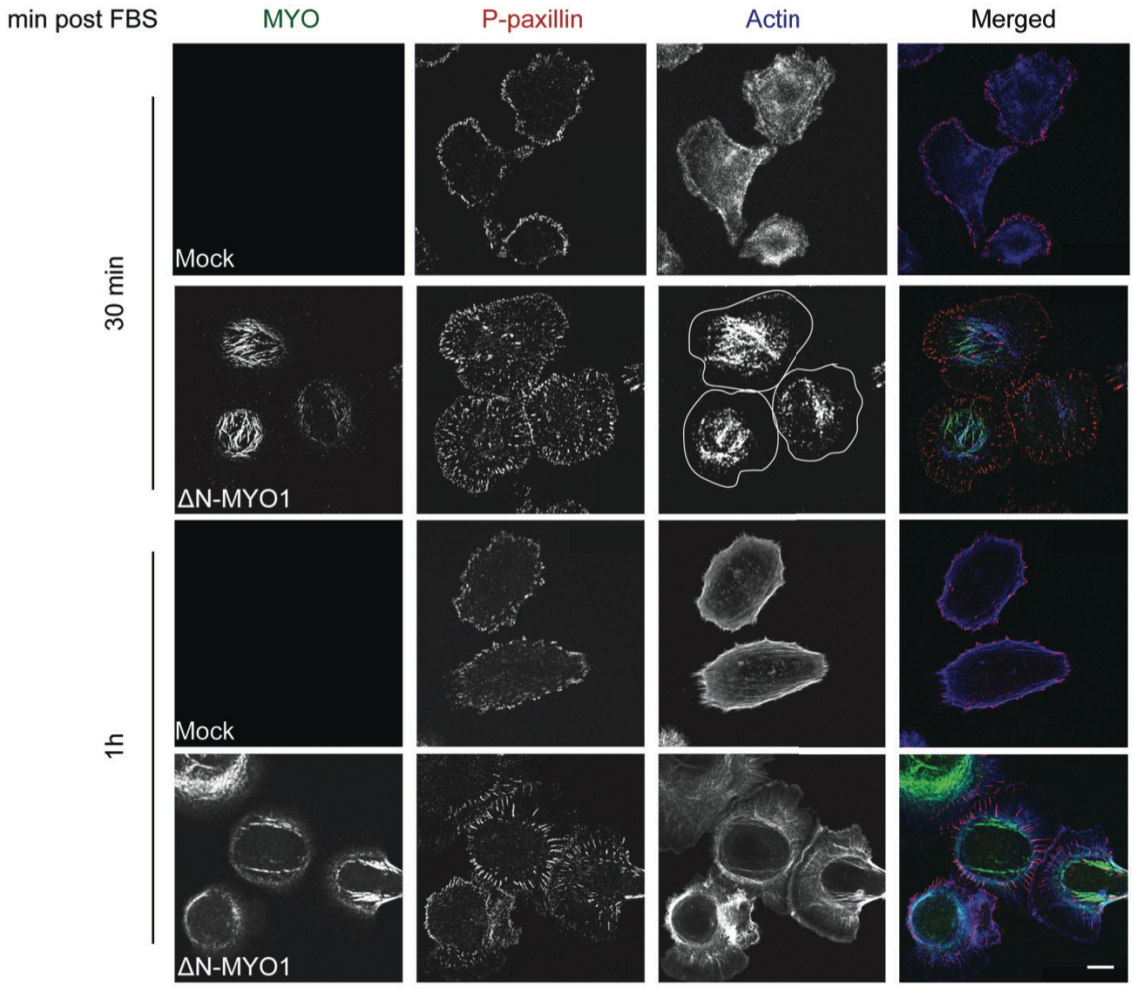

Figure 37. ΔN-MYO1 promotes the formation of mature focal adhesions and membrane protrusions. The effect of ΔN-MYO1 on FA dynamics at the indicated timepoint was analyzed as described in Fig. 36. Scale bar=10 μm.

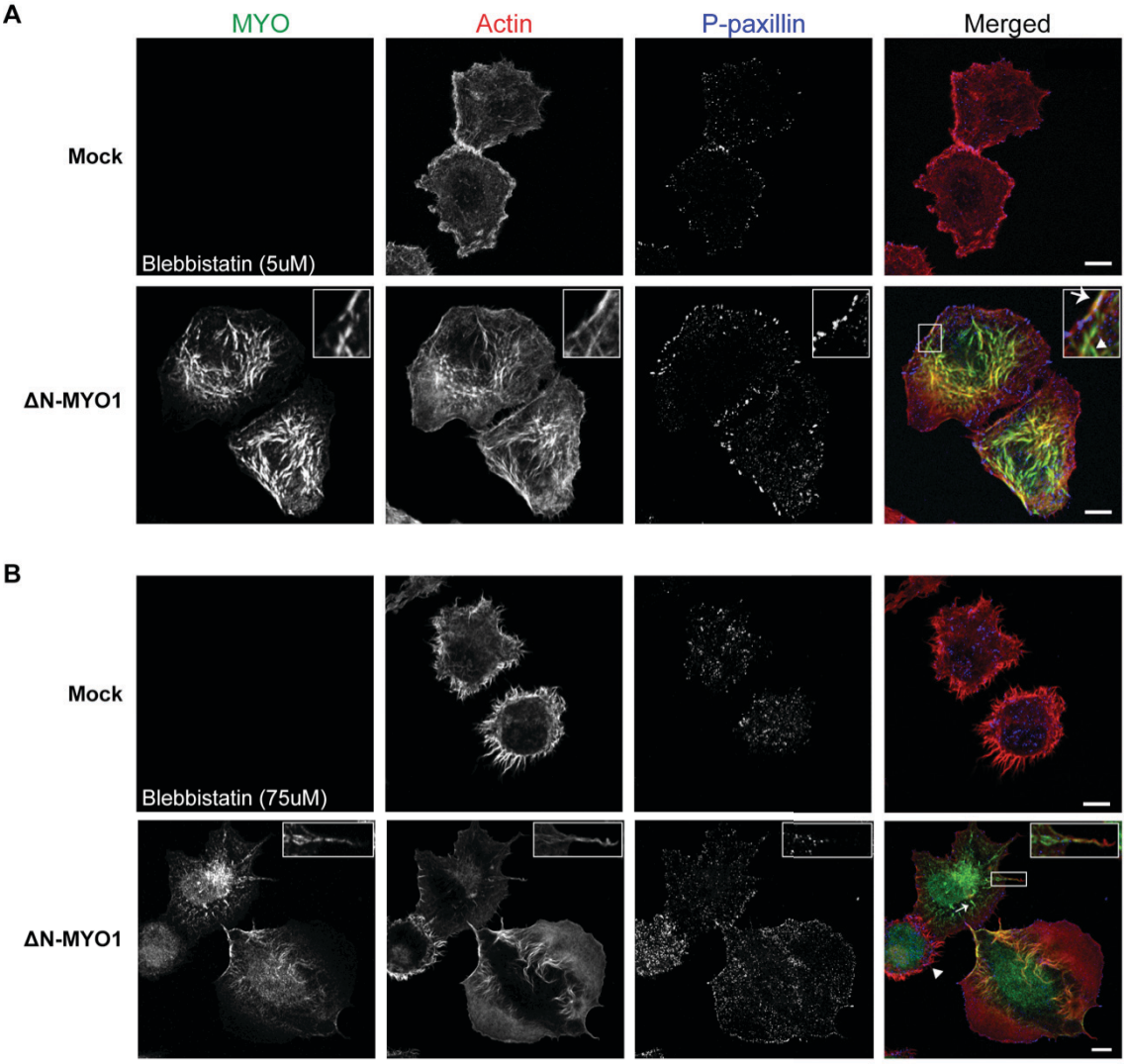

Figure 38. ΔN-MYO1-enhanced membrane protrusions are not dependent on myosin-mediated focal adhesion maturation. Mock- and ΔN-MYO1-transduced PC3 cells were starved overnight followed by FBS stimulation in the presence of 5 μM **(A)** or 75 μM **(B)** blebbistatin for an hour and immunostained with phalloidin (red), anti-myc (green), and anti-phosphorylated paxillin (blue) antibodies. **(A)** At low myosin activity, myopodin colocalized with the actin structures along the leading cell edge (arrow), with actin bundles perpendicular to the leading edge (arrowhead), and actin bundles in the cell body. The 8.4 μm x 10 μm areas indicated in the images are magnified 250% in the insets. Scale bar=10 μm. **(B)** At near complete suppression of myosin activity, myopodin colocalized with parallel actin bundles within lamella (arrow) and filopodia (inset). A cell with low myopodin expression level also lacked extensive membrane protrusions (arrowhead). The 17.8 μm x 6.8 μm areas indicated in the images are magnified 250% in the insets. Scale bar=10 μm.

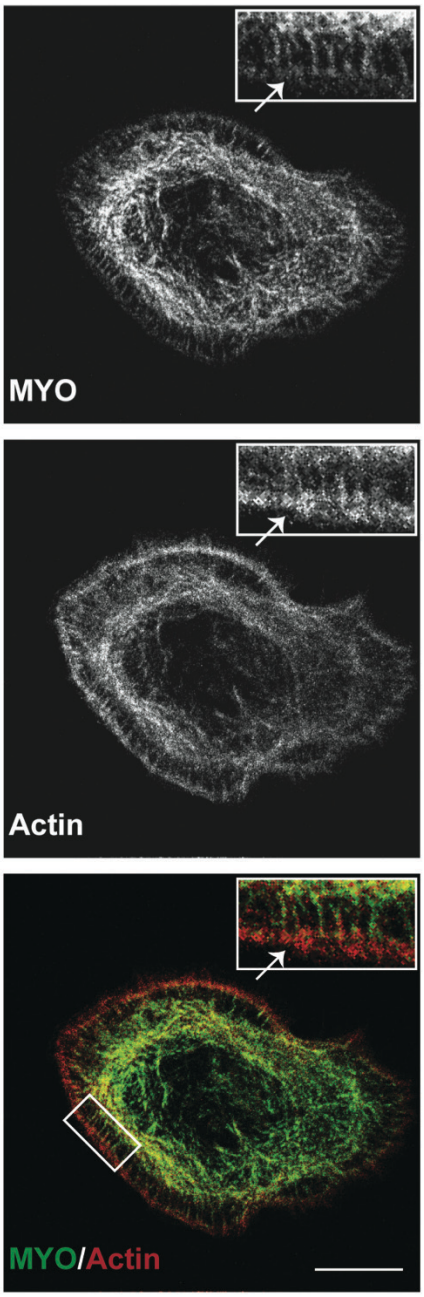

Figure 39. ΔN-MYO1 colocalizes with actin structures in the lamellipodium and dorsal stress fibers prior to prominent actin bundle formation in the cell body. Mock- and ΔN-MYO1-expressing PC3 cells were synchronized with serum-free media overnight and stimulated with FBS for 15 min, the timepoint before actin bundles in the cell body and membrane protrusions became prominent. Transduced cells were immunostained with phalloidin (red) and anti-myc (green) antibody. Myopodin colocalized with the actin structures within the actin-rich lamellipodium and the lamellum (arrows). The 8.1 μm x 4 μm areas indicated in the images are magnified 250% in the insets. Scale bar=10 μm.

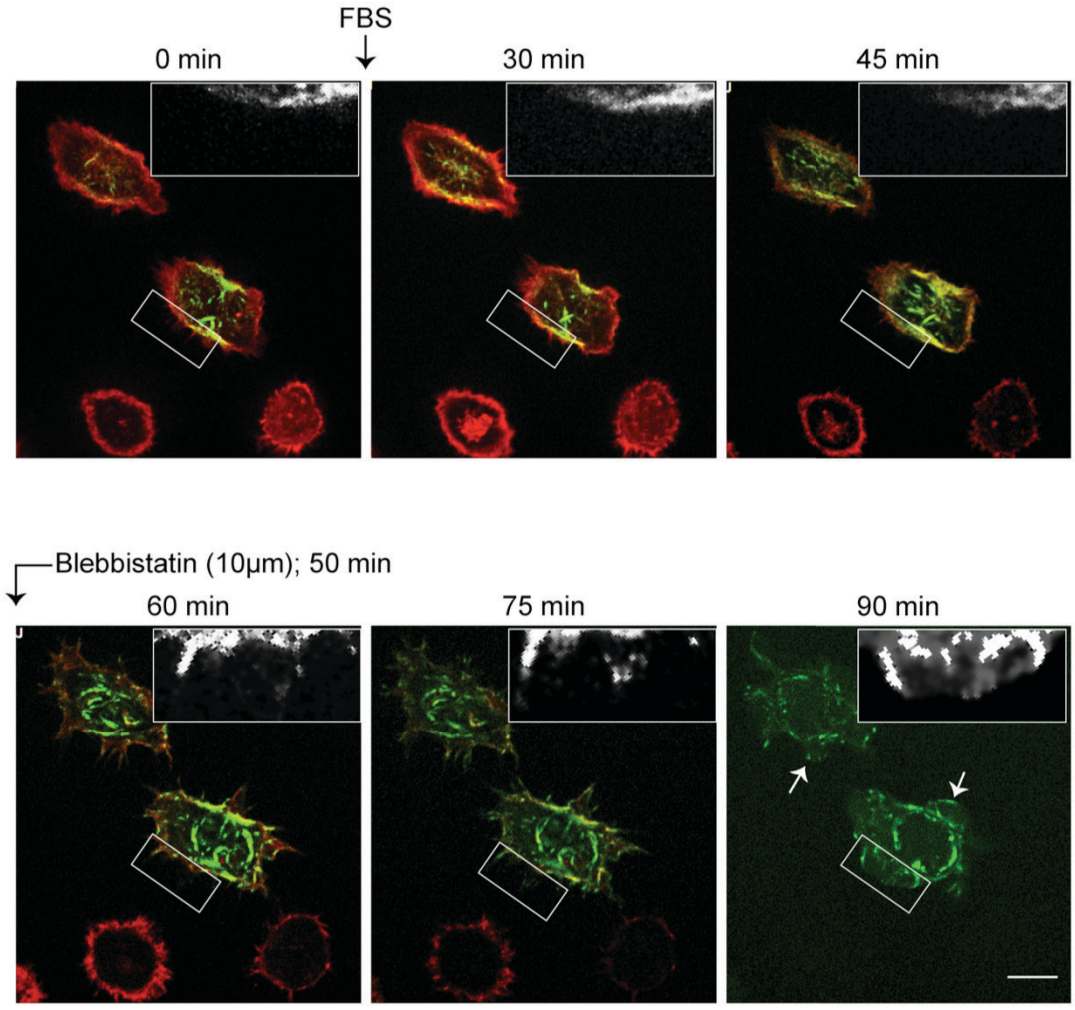

Figure 40. Live imaging analysis of ΔN-MYO1-stimulated filopodia and lamellipodia formation. Spinning disk confocal microscopic analysis of the dynamic interaction between myopodin and the actin cytoskeleton using GFP-tagged ΔN-MYO1 (green) and PC3 cells stably expressing LifeAct-RFP (red), a marker of F-actin filaments. After transfecting myopodin into PC3 cells, cells were starved overnight. Four cells were imaged, two of which expressed myopodin and the other two were either untransfected or low myopodin expressors. The time post-FBS addition is indicated above each frame. After prominent actin bundles were formed in the cell body (45 min post-FBS addition), 10 μM blebbistatin was added. The dynamics between myopodin and the actin cytoskeleton were imaged for another 40 min. Several areas of myopodin-induced filopodia and lamellipodia formation are also indicated (arrows; white box). The formation of filopodia and lamellipodia at the cell periphery are magnified 250% in the insets. Notably, the LifeAct-RFP is not as photostable as GFP and therefore RFP signals diminished at the later timepoints. Scale bar= 10 μm.

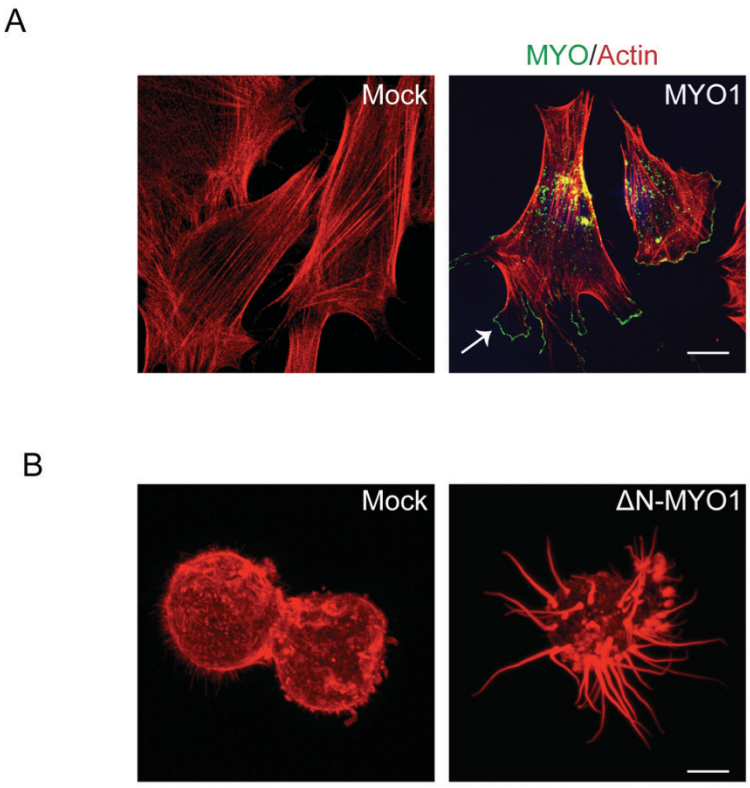

Figure 41. Myopodin promotes membrane protrusions in C2C12 myoblasts and in 3D culture. (A) Control vector and murine MYO1 homologues were stably expressed in C2C12 myoblasts. Myopodin localization and actin cytoskeleton structures were visualized using anti-myc (green) and phalloidin staining (red), respectively. Myopodin was stained strongly along the leading edge (arrow). **(B)** Mock- and ΔN-MYO1-expressing cells were cultured under 5.0 mg/ml three-dimensional matrigel matrix. Transduced cells were stained with phalloidin (red) and imaged with confocal microscopy. Scale bar= 10μm.

CHAPTER 6: CONCLUSIONS

Myopodin was discovered as an invasive cancer biomarker more than a decade ago, but only a handful of studies have examined how myopodin affects cancer cell metastasis. This project was very challenging in the beginning because of controversial and inconsistent results in the literature on the role of myopodin in cancer cell metastasis, and the subsequent emergence of multiple splicing variants of myopodin. My initial goals were to try to reconcile the contradictory data on whether myopodin is a tumour promoter or tumour suppressor, and to investigate whether different myopodin isoforms exert different effects on prostate cancer cell migration and invasion.

In Chapter 3, my studies with two different chemoattractants demonstrated that myopodin can both increase or decrease cell migration in response to different stimuli, suggesting myopodin may have diverse effects on cell migration in the complex signaling milieu of a tumor microeonvironment. I further showed that all myopodin isoforms exert similar affects on cancer cell migration with only modest direct affects on cell invasion. I subsequently determined that myopodin isoforms differentially affect actin cytoskeleton dynamics. Interestingly, although all myopodin isoforms confer a promigratory phenotype to PC3 cells in response to FBS stimulation, they induce biochemically and morphologically distinct actin structures within PC3 cells, and the formation of these different structures directly correlated with the enhanced chemokinetic activity of PC3. These are the first studies to document the effects of myopodin on actin cytoskeleton rearrangement *in vivo* and the relationship between myopodin-regulated actin dynamics and enhanced cell migration.

Based on my discoveries of the differential response of PC3 cells to different migration stimuli and the involvement of myopodin in actin cytoskeleton remodeling, I decided to investigate the nature of the signaling pathways involved in these processes. My results in Chapter 4 indicate that ΔN-MYO1 promotes cell migration in response to FBS via the RhoA/ROCK signaling pathway, the pathway that regulates actin bundle formation in the cell body. I further showed that myopodin promotes actin bundle formation and rescued a PC3 tail retracton defect in a ROCK-dependent manner. Since ROCK inhibition abrogated myopodin-induced actin bundle formation while only partially inhibiting myopodin-stimulated cell migration, the induced actin bundles are

likely not the only factor that contributes to PC3 chemokinetic activity. Myosin is the most studied downstream effector of the RhoA/ROCK signaling pathway, but pharmacological inhibition and shRNA knockdown of NM II activity had no affect on myopodin-stimulated cell migration. Therefore, although myopodin-induced formation of actin bundles is somehow linked to the pro-migratory phenotype of myopodin, the mechanism behind this phenotype is not linked to the levels of NM II activity in cells.

Although the most obvious change in the cytoskeleton I observed in PC3 cells expressing myopodin was the appearance of large actin bundles in the cell body, I also noted what appeared to be an increase in actin-rich protrusions at the cell periphery. I therefore decided to investigate in more detail the mechanisms responsible for formation of these spatially and structurally distinct actin structures. My results in Chapter 5 indicate that myopodin functions at the cell periphery to promote formation of Arp2/3 complex-dependent membrane protrusions and affects FA dynamics. When Arp2/3 complex activity was inhibited, the myopodin-induced formation of smaller membrane protrusions containing parallel actin bundles became apparent. Neither type of myopodin-induced membrane protrusion was affected by inhibiting NM II activity, although FA maturation was decreased. Timecourse studies and live imaging further revealed that the myopodin-induced actin structures at the cell periphery are subsequently integrated into stress fibers in the lamellum in an NM II-dependent manner. These studies revealed for the first time that myopodin can promote membrane protrusions via its effects on actin dynamics at the cell periphery.

Based on all of my results, I developed a working model of how myopodin promotes PC3 cell migration in response to FBS stimulation (Fig. 42). This model explains how decreased myosin activity can lead to prominent membrane protrusions but has no effect on myopodin-stimulated cell migration, and suggests that myopodin promotes PC3 chemokinetic activity by enhancing membrane protrusions. The model also integrates the formation of membrane protrusions at the leading edge with the appearance of actin bundles in the cell body and the ability of myopodin to promote tail retraction.

In the absence of FBS, PC3 cells expressing myopodin have low levels of RhoA-GTP, no stress fibers, and myopodin is distributed throughout the cell. FBS stimulation

activates the function of myopodin in actin cytoskeleton remodeling. Since fesselin has been shown to promote actin polymerization (Pham and Chalovich, 2006; Schroeter and Chalovich, 2004), myopodin may similarly promote actin polymerization at the leading edge resulting in increased numbers of branched and/or parallel actin filaments. Fesselin has also been shown to crosslink actin, and a similar crosslinking activity by human myopodin would lead to actin bundle formation at the leading edge. Membrane tension would result in the retrograde flow of these polymerizing filaments and actin bundles. However, actin polymerization in lamellipodia is a signal for the formation of nascent adhesions and actin crosslinking activity is a signal for FA maturation and stabilization (Oakes et al., 2012). My results are consistent with this viewpoint, since myopodin-expressing cells showed increased membrane protrusions and increased numbers of nascent FAs or focal complexes that matured into FAs over time (Figs. 38 and 39). Formation and maturation of these nascent adhesions and their interaction with the pointed ends of the growing actin filaments would provide a traction point, allowing the growing actin filaments to initiate membrane protrusions. Thus, multiple roles of myopodin may contribute to membrane protrusions at the leading edge, directly by increasing actin polymerization and crosslinking and indirectly by enhancing FA formation and stabilization.

At later timepoints post-FBS stimulation, myopodin-induced actin bundles appear at the lamellipodium-lamellum boundary in association with FAs (Fig. 42B). Within the lamellum, NM II constantly recruits actin filaments from the leading edge in toward the cell body. The increased numbers of actin filaments or bundles generated by myopodin at the leading edge would therefore result in increased stress fiber formation. Since myopodin is associated with the actin filaments at the leading edge by its binding and/or crosslinking activity, the recruitment of actin bundles by myosin contraction would also recruit myopodin into the lamellum. Live cell imaging results are consistent with this model, since I found that the actin bundles in the cell body are derived from the cell periphery (Fig. 41).

Eventually, large actin bundles and stress fibers with associated myopodin appear and concentrate in the cell body, either by continued NM II-dependent retrograde flow or as the cell moves forward (Fig. 42C). The relevance of these bundles in the cell body to

the myopodin-enhanced migration phenotype is still unclear. Inhibiting NM II activity with low doses of blebbistatin did not reduce the stimulatory effect of myopodin on cell migration, but it also did not inhibit the formation of actin bundles in the cell body (Fig. 40A). Longer timecourses are needed to see if the typical actin bundles and stress fibers in the cell body were also formed under these conditions. High doses of blebbistatin did inhibit actin bundle formation in the cell body (Fig. 40B), but these doses were not assessed for their effects on cell migration and it is likely that such doses would eliminate inherent PC3 cell migration, confounding analysis of the pro-migratory role of myopodin. The formation of myopodin-induced actin bundles in the cell body also correlates with the ability of myopodin to suppress a tail retraction defect in PC3 cells evident under serum-starvation conditions (Fig. 30A). However, myopodin does not promote cell migration under these conditions (Fig. 10A). In contrast, ROCK inhibitor does suppress, at least partially, the pro-migratory phenotype of myopodin-expressing cells (Fig. 26C) and this coincides with a loss of actin bundles in the cell body (Fig. 31B) and a loss of myopodin-induced tail retraction (Fig. 31). Whether these three events are functionally related is still unclear.

This working model also provides a possible explanation for the apparent NM II-independent manner in which myopodin promotes cell migration. Cells need myosin contraction to move but the pro-migratory phenotype of myopodin-expressing cells is unaffected by inhibiting NM II activity. The fact the PC3 cells still migrate, albeit at reduced levels, when NM II was inhibited by low doses of blebbistatin, by ML-7 treatment to inhibit MLCK-mediated phosphorylation of NM II RLCs, or by shRNA knockdown of NM II (Figs. 28 and 29) implies cells retained some low level of functional NM II. It therefore seems likely that myopodin functions upstream of NM II, presumably by promoting membrane protrusions at the leading edge. If this is true, then we must assume that the rate-limiting event in PC3 cell migration is not the level of NM II activity in cells but the rate or extent of actin filament and bundle formation at the leading edge.

It remains unclear how, exactly, myopodin promotes actin polymerization. Several classes of actin nucleators have been discovered, including Arp2/3 complexes, formins, and Spire (Campellone and Welch, 2010). All of these actin nucleators promote

actin polymerization by enhancing actin nucleus formation. *In vitro* biochemical studies revealed that fesselin can also accelerate actin polymerization by ~50-fold, eliminating the actin nucleation lag phase of actin assembly and enhancing the rate of actin elongation (Beall and Chalovich, 2001). This data suggested a potential role for myopodin in actin nucleation. However, no detailed molecular and structural studies on myopodin have been conducted to examine the mechanism of myopodin-stimulated actin polymerization. Formin homodimers can form a ring structure to encircle actin monomers (Xu et al., 2004) and Spire has several G-actin binding WH2 domains next to one another (Quinlan et al., 2005) to promote actin nucleation. A motif scan of myopodin revealed no typical WH2 domains and previous studies showed that the actin-binding site of myopodin does not have a typical actin-binding motif (Weins et al., 2001). Therefore, it remains to be determined if myopodin possesses non-canonical actin monomer binding sites or forms higher order structures to bring actin monomers into close proximity. Additional *in vitro* studies of the actin polymerization activity of human myopodin and further definition of the G-actin binding sites in myopodin might be useful for analyzing myopodin function in membrane protrusion formation.

The predicted disordered structure of myopodin (Khaymina et al., 2007) presumably facilitates interaction with numerous protein partners and suggests that myopodin is a multi-functional protein. In addition to polymerization, it seems likely that myopodin also affects actin bundling. Actin crosslinkers play an important role in actin cytoskeleton organization. For instance, actin bundles are crosslinked by fascin into tight, stiff bundles, allowing actin bundles to create membrane protrusions (Nakamura et al., 2011). *In vitro* biochemical studies revealed that myopodin can also bundle actin filaments (Linnemann et al., 2012). Indeed, what appeared to be crosslinked actin bundles associated with myopodin along their length were frequently found in filopodia when myosin activity was inhibited (Figs 38 & 40). This data suggested that myopodin might strengthen actin bundle stiffness and thereby promote membrane protrusions. The presence of crosslinked actin bundles is also important for growth and stabilization of FAs (Choi et al., 2008; Oakes et al., 2012), which can promote membrane protrusions (Alexandrova et al., 2008). Alpha-actinin is the only actin crosslinker currently known that is indispensible for the growth of nascent FA (Choi et al., 2008). Myopodin

colocalizes with actin bundles perpendicular to the leading edge, its presence induces FA formation (Figs. 38 and 39), and it interacts with focal adhesion-associated proteins (e.g. ILK) (Yu and Luo, 2011), suggesting myopodin may be another actin crosslinker that promotes focal adhesion formation and membrane protrusions. Photobleaching analysis and living imaging of FA dynamics may provide further insights into the direct or indirect effects of myopodin on FA formation and disassembly.

Many proteins involved in actin assembly are multifunctional proteins and their functions are regulated by the presence of other proteins or buffer conditions. For instance, the effect of Ena/VASP on actin assembly varies under different ionic strength conditions. Under low ionic strength, Ena/VASP functions as an anti-capping protein and a processive actin polymerase (Hansen and Mullins, 2010). However, this function requires the presence of profilin at higher ionic strength buffer. Similarly, the actin polymerization activity of fesselin is inhibited by α-actinin and calcium-bound calmodulin. Furthermore, calcium-bound calmodulin inhibits myopodin binding to G-actin but not F-actin, suggesting that the actin polymerizing and F-actin binding activities of myopodin are regulated independently (Pham and Chalovich, 2006; Schroeter and Chalovich, 2004). At this point, it is not possible to conclude whether myopodin functions to promote actin polymerization and/or actin crosslinking, two activities that may be spatially or temporally regulated by its surrounding context. Myopodin mutants defective in either of these functions would be very helpful to resolve the contribution of these two potential activities to membrane protrusions and cell migration.

Although it is well accepted that Arp2/3 complexes nucleate the branched actin network within lamellipodia, the genesis of filopodia remains controversial. Some believe that Arp2/3 complex-nucleated actin filaments converge to form parallel actin bundles for filopodia formation, while others suggest that filopodia are nucleated *de novo* by formins (Yang and Svitkina, 2011). The supporting evidence for *de novo* nucleation of filopodia is that filopodia remain evident in Arp2/3-depleted cells (Steffen et al., 2006). Myopodin-expressing cells exhibited substantial membrane protrusions but inhibiting Arp2/3 complex formation with CK666 impaired, but did not eliminate, myopodin-stimulated protrusions (Fig. 35). These results imply that Arp2/3-nucleated actin networks are involved in, but are not necessary for, myopodin-induced membrane protrusion

formation. However, two alternate possibilities can also explain the formation of membrane protrusions at low levels of Arp2/3. First, it is possible that 20 μM CK666 does not completely eliminate Arp2/3 activity and that the residual Arp2/3 complexes nucleate actin filaments to promote formation of small protrusions. Second, it is possible that other unidentified actin-polymerizing factors, besides Arp2/3 complexes, can promote actin nucleation; myopodin could be one such factor. This could also provide an explanation for why filopodia can be formed in Arp2/3-depleted cells.

Most of my project focused on the positive role of myopodin on cell migration following FBS stimulation as these conditions confered a striking and consistent phenotype. Importantly, studies of myopodin under FBS conditions provided several new insights into how myopodin can regulate cell migration under distinct environmental conditions and in different cell lines. First, I discovered that myopodin could differentially regulate RhoA activation in the presence of different migration stimuli (Fig. 24A). Second, I was able to show that myopodin isoforms are able to differentially remodel the actin cytoskeleton within PC3 cells, DU145 cells, and BPH-1 cells (Fig. 21). Third, my results indicate that ΔN-MYO1 is able to promote membrane protrusions in PC3 cells in three-dimensional or two-dimensional culture conditions and also within C2C12 myoblast cells (Fig. 41). The FBS stimulation model therefore provided a useful system to study myopodin function in actin cytoskeleton dynamics.

I recognize that there are several limitations in extrapolating my results to an explanation of how myopodin affects prostate cance cell invasion. For example, it is unlikely that FBS stimulation mimics the complex signaling environment found in a tumour microenvironment. Analysis of a single cell type in isolation and in two-dimensional cell culture also does not reflect the complex intracellular interactions that occur between multiple cell types in the three-dimensional tissue environment. However, the first two caveats are the limitations of almost all cell culture approaches, and my preliminary 3D analysis in matrigel confirmed that myopodin has profound effects on the formation of cellular protrusions (Fig. 41). Perhaps the greatest restriction to extrapolating my results to the *in vivo* situation is the reliance of my studies on ectopic, overexpression of myopodin. However, siRNA knockdown of endogenous myopodin isoforms in PC3 cells showed reduced cell migration in response to FBS stimulation (De

Ganck et al., 2009), consistent with my results showing that ectopic expression of myoposin increases PC3 cell migration under the same stimulus. Future studies might want to exploit the Tet-inducible expression system to control and synchronize the levels of myopodin expression (Loew et al., 2010).

My PhD project obtained a macroscopic view of myopodin-stimulated cell migration mechanisms. I also investigated the signaling pathways regulated by myopodin, focusing on the Rho GTPase pathways. In conclusion, I would like to present some additional analysis I conducted using high throughput screening to examine the effects of myopodin expression on several pathways and proteins involved in regulating cytoskeleton dynamics. I conducted a phosphorylation antibody microarray screen to identify potential signaling pathways regulated by myopodin. Since I determined that myopodin affects actin dynamics, I selected an antibody microarray that includes 141 phospho-specific antibodies that recognize proteins involved in actin cytoskeleton rearrangement. The screen identified several interesting targets (Fig. 43A) and the hits that showed the same trend within two out of three independent experiments, although the extent varied, are listed in Figs. 43B and 43C.

Interestingly, the endogenous level of several key proteins involved in regulating cytoskeleton dynamics was significantly elevated in myopodin-expressing compared to mock-transduced cells (Fig. 43B). These proteins were ezrin, focal adhesion kinase (FAK), LIM kinase (LIMK1/2), MEK1, Src, and VASP (Fig. 43B). After normalization to the total protein amount, the phosphorylation levels of several additional signaling proteins were also either upregulated (positive value) or downregulated (negative value) in myopodin-expressing cells (Fig. 43C). These proteins included proteins involved in actin assembly (VASP, WAVE1, LIMK), focal adhesion-associated proteins (FAK, Src), Rho GTPase signaling pathways (GAP and Rho/Rac GEF-2), and membrane-associated proteins (ezrin, PI3K). VASP can function as an anti-capping protein or an actin polymerase, depending on the conditions (Hansen and Mullins, 2010). Increased VASP levels could facilitate actin polymerization under FBS conditions by its anti-capping or actin polymerization activity. However, phosphorylation of VASP at Ser157 has no effect on its recruitment to focal adhesions, oligomerization, or interaction with profilin but attenuates VASP's ability to polymerize actin and interact with actin filaments (Harbeck

et al., 2000). Why increased VASP levels but also increased VASP phosphorylation might help myopodin effect changes actin cytoskeleton rearrangement and cell migration needs to be investigated. It is possible that the increase in the total amount of VASP facilitates actin polymerization.

Another hit, WAVE1, is one of the NPFs that promote Arp2/3 actin nucleation activity (Machesky et al., 1999). WAVE1 is inhibited by a multiprotein complex composed of Nap1/Nap125, Sra-1/Pir21, HSPC300, and Abi (Steffen et al., 2004). Phosphorylation of WAVE1 at Tyr125 by Src does not release WAVE1 from the inhibitory complex but it does enhance WAVE1-inhibitory complex binding of Arp2/3 complexes, thereby suppressing Arp2/3-mediated stress fiber formation (Ardern et al., 2006). It is therefore possible that the robust effect of myopodin at the leading edge turns off other alternative pathways that promote actin assembly.

Myopodin promotes activation of RhoA GTPase in PC3 cells (Fig. 24A), so it was interesting to see an enhanced phosphorylation level of Rho/Rac guanine nucleotide exchange factor-2 (GEF-2) in the Full Moon screen. GEF-2 increases GTP-bound GTPase levels. Rho/Rac GEF2 is commonly known as GEF-H1, which is a microtubule-localized GEF. Interaction between microtubules and GEF-H1 inhibits its guanine nucleotide exchange function. When GEF-H1 dissociates from microtubules, the exchange factor can lead to RhoA activation and stress fiber formation (Krendel et al., 2002). The p21-activated kinase-1 (PAK), which is activated by Cdc42 or Rac1, phosphorylates GEF-H1 at Ser885, leads to increased binding of 14-3-3 to GEF-H1 and therefore relocates 14-3-3 to microtubules (Zenke et al., 2004). Interestingly, 14-3-3 also interacts with murine myopodin, suggesting a potential link between the upregulation of GEF-H1 phosphorylation levels and myopodin-stimulated cell migration. One possiblity is that the interaction between myopodin, 14-3-3 and phosphorylated GEF-H1 dissociates GEF-H1 from microtubules. GEF-H1 would then be free to activate RhoA within myopodin-transduced cells.

Another hit in the Full Moon screen was GTPase activation protein (GAP), which promotes hydrolysis of GTP to GDP by GTPases. GAP is phosphorylated at Ser387 by Aurora B, which activates its latent GAP activity that is important for cytokinesis. (Minoshima et al., 2003). However, no studies have examined the effect of GAP

phosphorylation on cell migration. Since the phosphorylation level of GAP at Ser387 within myopodin-expressing cells was lower than mock-transduced cells, it is possible that myopodin suppresses GAP phosphorylation levels and therefore maintains a high Rho-GTP level.

The effect of myopodin on the formation of nascent adhesions and nascent complexes was also evident in the Full Moon screen. Phosphorylation levels of focal adhesion kinase (FAK) were decreased. FAK is one of the earliest FA proteins recruited to the nascent adhesions. FAK is autophosphorylated at Tyr397 upon integrin clustering, and this autophosphorylation promotes its kinase activity, allowing Src binding and p130Cas activation that can modulate the activity of multiple GEFs and therefore affect Rho GTPase activity (Fonseca et al., 2004; Roca-Cusachs et al., 2012).

Some of the hits from the Full Moon screen may well be spurious. For example, according to the Full Moon screen, the total amount of LIMK was increased while the phosphorylation levels were slightly decreased in myopodin-expressing cells. However, my results did not confirm this hit; LIMK phosphorylation levels were not decreased when assessed by phospho-specific western blotting (Fig. 32). Thus, thorough and careful validation of the phosphorylation screen to rule out false positive results is necessary and determining the relevance of any of these hits requires further investigation.

In summary, downregulation of myopodin gene expression is frequently found in diverse invasive cancers, suggesting myopodin plays a critical role in cancer metastasis. My current studies demonstrated that myopodin has a robust effect on cell migration in response to FBS stimulation, providing a reproducible and consistent system to examine the effects of myopodin on actin cytoskeleton dynamics and cell migration. More importantly, my project highlights that the complexities of signaling factors in the tumor microenvironment need to be considered when evaluating how myopodin loss might correlate with invasive tumour development.

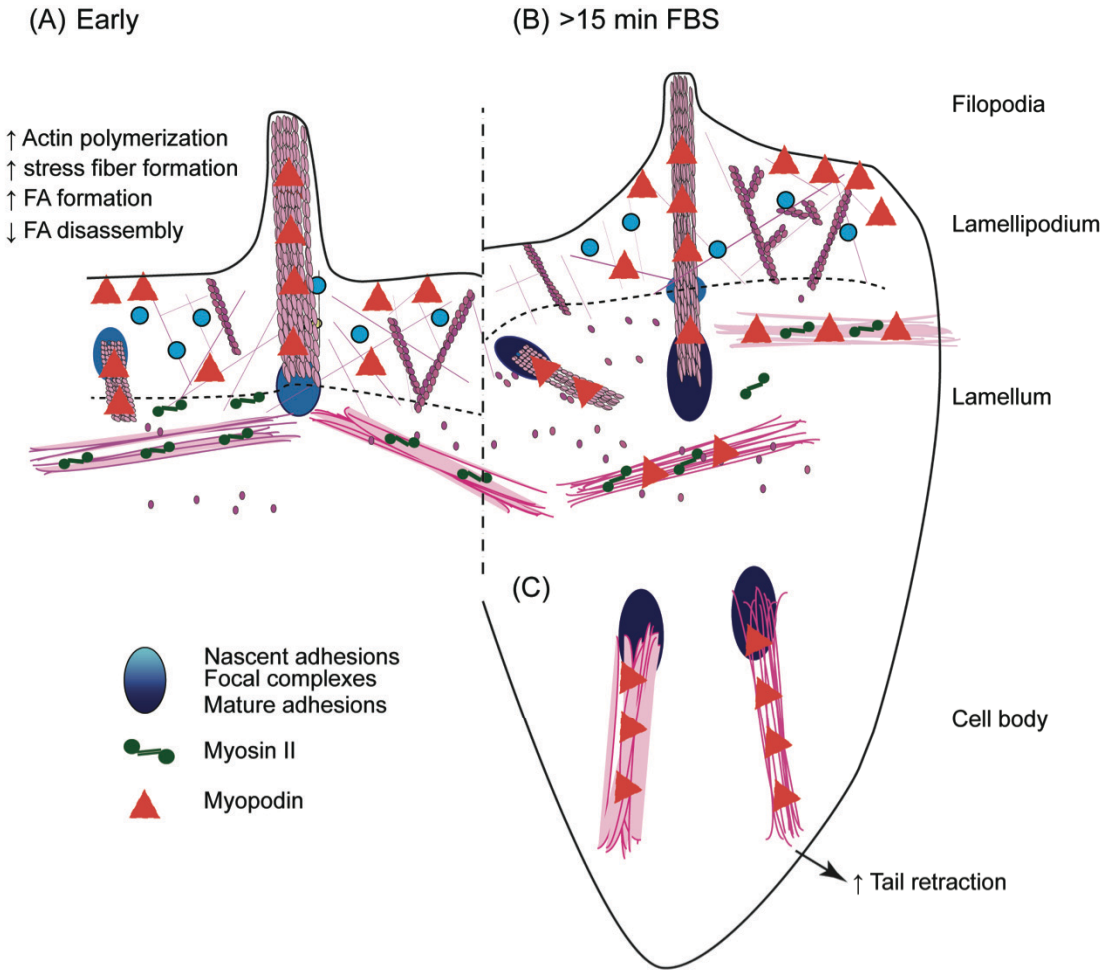

Figure 42. Model of myopodin-stimulated PC3 cell migration. (A) At the early stage of FBS stimulation, myopodin promotes the formation of actin bundles at the leading cell edge, presumably by increasing the rate of actin polymerization and/or actin crosslinking activity. The enhanced actin dynamics and bundle formation within the lamellipodium allows the formation and growth of nascent adhesions and prevents the disassembly of FAs. Mature FAs can then convert the retrograde flow of F-actin into forward protrusions. **(B)** While membrane protrusions advance (>15 min post-FBS addition), the actin filaments end up in the lamellum, the region that has abundant myosin. Myosin can pull on the actin bundles and integrates the actin network from the cell front in toward the cell body. At the same time, myosin promotes the growth of FAs. Notably, the effect of myopodin is within the leading edge illustrated in panel **(A)**, and therefore inhibition of myosin has no effect on myopodin-stimulated cell migration but enhances membrane protrusions. **(C)** Myopodin-crosslinked actin bundles eventually end up in the cell body as the cell advances. As myopodin and myosin competitively bind to actin filaments, the enrichment of myopodin on actin bundles outcompetes the binding of myosin, leading to the formation of actin bundles that are devoid of myosin. The actin bundles in the cell body can subsequently rescue the tail retraction defect of PC3 cells in RhoA/ROCK-dependent manner. FAs with different size and shade of blue are indicated in the figure legend.

A

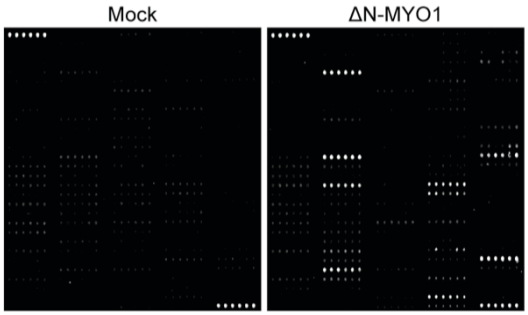

B

Protein list	Signal fold change (T-C)/C
Ezrin	4.12
FAK	3.01
LIMK1/2	1.44
MEK1	1.71
Src	3.29
VASP	1.66

C

	Ratio Analysis (Phospho vs non-phospho)
Ezrin (P-Tyr478)	-0.23
FAK (P-Ser397)	-0.45
LIMK (P-Thr508)	-0.21
Src (P-Tyr418)	-0.86
PI3K p85-subunit alpha-gamma (P-Tyr467/Tyr199)	-0.22
GTPase activation protein (Phos-Ser387)	-0.52
Rho/Rac guanine nucleotide exchange factor 2 (P-Ser885)	0.31
VASP (P-Ser157)	0.65
WAVE1 (P-Tyr125)	0.40

Figure 43. Identification of potential signaling pathways regulated by ΔN-MYO1. **(A)** Cell lysates of mock- and ΔN-MYO1-expressing PC3 cells were collected and the protein levels were analyzed using Full Moon Cytoskeleton Phosphorylation Microarray slides as described in Materials and Methods. Representative images of microarray results from mock- (left) and myopodin-expressing cells (right) are shown. Each antibody has six replicate dots, and the top left and bottom right lanes on each slide are the positive controls. Total protein levels **(B)** or the phosphorylated protein levels **(C)** upregulated or downregulated in myopodin-expressing cells are listed. Only results that were consistent from two out of three independent experiments are listed. These results were quantitatively analyzed by Full Moon Biosystem, Inc. Signal fold change of total protein amount was calculated from the equation = (protein levels in myopodin-expressing cells – proteins levels in mock-transduced cells)/protein levels in mock-transduced cells. **(C)** Ratio of phosphorylated over non-phosphorylated proteins was analyzed and the ratio difference between mock- and ΔN-MYO1-expressing cells is listed. Positive and negative values indicate an increase or a decrease in total protein levels or phosphorylation levels in myopodin-expressing cells, respectively.

BIBLIOGRAPHY

Abercrombie, M., J.E. Heaysman, and S.M. Pegrum. 1970. The locomotion of fibroblasts in culture. II. "RRuffling". *Experimental cell research*. 60:437-444.

Alberts, B., J.H. Wilson, and T. Hunt. 2008. Molecular biology of the cell. Garland Science, New York. xxxiii, 1601, 1690 p. pp.

Alexandrova, A.Y., K. Arnold, S. Schaub, J.M. Vasiliev, J.J. Meister, A.D. Bershadsky, and A.B. Verkhovsky. 2008. Comparative dynamics of retrograde actin flow and focal adhesions: formation of nascent adhesions triggers transition from fast to slow flow. *PloS one*. 3:e3234.

Alvarez-Mugica, M., V. Cebrian, J.M. Fernandez-Gomez, F. Fresno, S. Escaf, and M. Sanchez-Carbayo. Myopodin methylation is associated with clinical outcome in patients with T1G3 bladder cancer. *J Urol*. 184:1507-1513.

Amann, K.J., and T.D. Pollard. 2001. Direct real-time observation of actin filament branching mediated by Arp2/3 complex using total internal reflection fluorescence microscopy. *Proceedings of the National Academy of Sciences of the United States of America*. 98:15009-15013.

Anderson, T.W., A.N. Vaughan, and L.P. Cramer. 2008. Retrograde flow and myosin II activity within the leading cell edge deliver F-actin to the lamella to seed the formation of graded polarity actomyosin II filament bundles in migrating fibroblasts. *Molecular biology of the cell*. 19:5006-5018.

Applewhite, D.A., M. Barzik, S. Kojima, T.M. Svitkina, F.B. Gertler, and G.G. Borisy. 2007. Ena/VASP proteins have an anti-capping independent function in filopodia formation. *Molecular biology of the cell*. 18:2579-2591.

Ardern, H., E. Sandilands, L.M. Machesky, P. Timpson, M.C. Frame, and V.G. Brunton. 2006. Src-dependent phosphorylation of Scar1 promotes its association with the Arp2/3 complex. *Cell motility and the cytoskeleton*. 63:6-13.

Asanuma, K., K. Kim, J. Oh, L. Giardino, S. Chabanis, C. Faul, J. Reiser, and P. Mundel. 2005. Synaptopodin regulates the actin-bundling activity of alpha-actinin in an isoform-specific manner. *The Journal of clinical investigation*. 115:1188-1198.

Asanuma, K., E. Yanagida-Asanuma, C. Faul, Y. Tomino, K. Kim, and P. Mundel. 2006. Synaptopodin orchestrates actin organization and cell motility via regulation of RhoA signalling. *Nat Cell Biol*. 8:485-491.

Balcer, H.I., K. Daugherty-Clarke, and B.L. Goode. 2010. The p40/ARPC1 subunit of Arp2/3 complex performs multiple essential roles in WASp-regulated actin nucleation. *The Journal of biological chemistry*. 285:8481-8491.

Bamburg, J.R., and B.W. Bernstein. 2010. Roles of ADF/cofilin in actin polymerization and beyond. *F1000 biology reports*. 2:62.

Barzik, M., T.I. Kotova, H.N. Higgs, L. Hazelwood, D. Hanein, F.B. Gertler, and D.A. Schafer. 2005. Ena/VASP proteins enhance actin polymerization in the presence of barbed end capping proteins. *The Journal of biological chemistry*. 280:28653-28662.

Beall, B., and J.M. Chalovich. 2001. Fesselin, a synaptopodin-like protein, stimulates actin nucleation and polymerization. *Biochemistry*. 40:14252-14259.

Bear, J.E., T.M. Svitkina, M. Krause, D.A. Schafer, J.J. Loureiro, G.A. Strasser, I.V. Maly, O.Y. Chaga, J.A. Cooper, G.G. Borisy, and F.B. Gertler. 2002. Antagonism between Ena/VASP proteins and actin filament capping regulates fibroblast motility. *Cell*. 109:509-521.

Beli, P., D. Mascheroni, D. Xu, and M. Innocenti. 2008. WAVE and Arp2/3 jointly inhibit filopodium formation by entering into a complex with mDia2. *Nat Cell Biol*. 10:849-857.

Blanchoin, L., T.D. Pollard, and S.E. Hitchcock-DeGregori. 2001. Inhibition of the Arp2/3 complex-nucleated actin polymerization and branch formation by tropomyosin. *Current biology : CB*. 11:1300-1304.

Bogenrieder, T., and M. Herlyn. 2003. Axis of evil: molecular mechanisms of cancer metastasis. *Oncogene*. 22:6524-6536.

Burridge, K., and K. Wennerberg. 2004. Rho and Rac take center stage. *Cell*. 116:167-179.

Campellone, K.G., and M.D. Welch. 2010. A nucleator arms race: cellular control of actin assembly. *Nature reviews. Molecular cell biology*. 11:237-251.

Carlier, M.F., V. Laurent, J. Santolini, R. Melki, D. Didry, G.X. Xia, Y. Hong, N.H. Chua, and D. Pantaloni. 1997. Actin depolymerizing factor (ADF/cofilin) enhances the rate of filament turnover: implication in actin-based motility. *J Cell Biol*. 136:1307-1322.

Carlier, M.F., and D. Pantaloni. 1997. Control of actin dynamics in cell motility. *Journal of molecular biology*. 269:459-467.

Cebrian, V., M. Alvarez, A. Aleman, J. Palou, J. Bellmunt, P. Gonzalez-Peramato, C. Cordon-Cardo, J. Garcia, J.M. Piulats, and M. Sanchez-Carbayo. 2008. Discovery of myopodin methylation in bladder cancer. *J Pathol*. 216:111-119.

Chan, A.Y., M. Bailly, N. Zebda, J.E. Segall, and J.S. Condeelis. 2000. Role of cofilin in epidermal growth factor-stimulated actin polymerization and lamellipod protrusion. *J Cell Biol*. 148:531-542.

Chan, C., C.C. Beltzner, and T.D. Pollard. 2009. Cofilin dissociates Arp2/3 complex and branches from actin filaments. *Current biology : CB*. 19:537-545.

Chhabra, E.S., and H.N. Higgs. 2006. INF2 Is a WASP homology 2 motif-containing formin that severs actin filaments and accelerates both polymerization and depolymerization. *The Journal of biological chemistry*. 281:26754-26767.

Chhabra, E.S., and H.N. Higgs. 2007. The many faces of actin: matching assembly factors with cellular structures. *Nat Cell Biol*. 9:1110-1121.

Choi, C.K., M. Vicente-Manzanares, J. Zareno, L.A. Whitmore, A. Mogilner, and A.R. Horwitz. 2008. Actin and alpha-actinin orchestrate the assembly and maturation of nascent adhesions in a myosin II motor-independent manner. *Nat Cell Biol*. 10:1039-1050.

Chrzanowska-Wodnicka, M., and K. Burridge. 1996. Rho-stimulated contractility drives the formation of stress fibers and focal adhesions. *J Cell Biol*. 133:1403-1415.

Conrad, P.A., K.A. Giuliano, G. Fisher, K. Collins, P.T. Matsudaira, and D.L. Taylor. 1993. Relative distribution of actin, myosin I, and myosin II during the wound healing response of fibroblasts. *J Cell Biol*. 120:1381-1391.

Cooper, J.A. 2002. Actin dynamics: tropomyosin provides stability. *Current biology : CB*. 12:R523-525.

Cramer, L.P., M. Siebert, and T.J. Mitchison. 1997. Identification of novel graded polarity actin filament bundles in locomoting heart fibroblasts: implications for the generation of motile force. *J Cell Biol*. 136:1287-1305.

Crowley, E., and A.F. Horwitz. 1995. Tyrosine phosphorylation and cytoskeletal tension regulate the release of fibroblast adhesions. *J Cell Biol*. 131:525-537.

De Ganck, A., V. De Corte, E. Bruyneel, M. Bracke, J. Vandekerckhove, and J. Gettemans. 2009. Down-regulation of myopodin expression reduces invasion and motility of PC-3 prostate cancer cells. *Int J Oncol*. 34:1403-1409.

De Ganck, A., V. De Corte, A. Staes, K. Gevaert, J. Vandekerckhove, and J. Gettemans. 2008. Multiple isoforms of the tumor suppressor myopodin are simultaneously transcribed in cancer cells. *Biochem Biophys Res Commun*. 370:269-273.

DesMarais, V., I. Ichetovkin, J. Condeelis, and S.E. Hitchcock-DeGregori. 2002. Spatial regulation of actin dynamics: a tropomyosin-free, actin-rich compartment at the leading edge. *Journal of cell science*. 115:4649-4660.

Eden, S., R. Rohatgi, A.V. Podtelejnikov, M. Mann, and M.W. Kirschner. 2002. Mechanism of regulation of WAVE1-induced actin nucleation by Rac1 and Nck. *Nature*. 418:790-793.

Esteban, S., P. Moya, A. Fernandez-Suarez, M. Vidaurreta, P. Gonzalez-Peramato, and M. Sanchez-Carbayo. 2012. Diagnostic and prognostic utility of methylation and protein expression patterns of myopodin in colon cancer. *Tumour biology : the journal of the International Society for Oncodevelopmental Biology and Medicine*. 33:337-346.

Etienne-Manneville, S. 2008. Polarity proteins in migration and invasion. *Oncogene*. 27:6970-6980.

Faul, C., A. Dhume, A.D. Schecter, and P. Mundel. 2007. Protein kinase A, Ca2+/calmodulin-dependent kinase II, and calcineurin regulate the intracellular trafficking of myopodin between the Z-disc and the nucleus of cardiac myocytes. *Mol Cell Biol*. 27:8215-8227.

Faul, C., S. Huttelmaier, J. Oh, V. Hachet, R.H. Singer, and P. Mundel. 2005. Promotion of importin alpha-mediated nuclear import by the phosphorylation-dependent binding of cargo protein to 14-3-3. *J Cell Biol*. 169:415-424.

Festuccia, C., G.L. Gravina, A. Angelucci, D. Millimaggi, and M. Bologna. 2000. Culture conditions modulate cell phenotype and cause selection of subpopulations in PC3 prostate cancer cell line. *Anticancer Res*. 20:4367-4371.

Fink, A.L. 2005. Natively unfolded proteins. *Current opinion in structural biology*. 15:35-41.

Fonseca, P.M., N.Y. Shin, J. Brabek, L. Ryzhova, J. Wu, and S.K. Hanks. 2004. Regulation and localization of CAS substrate domain tyrosine phosphorylation. *Cellular signalling*. 16:621-629.

Fradelizi, J., V. Noireaux, J. Plastino, B. Menichi, D. Louvard, C. Sykes, R.M. Golsteyn, and E. Friederich. 2001. ActA and human zyxin harbour Arp2/3-independent actin-polymerization activity. *Nat Cell Biol*. 3:699-707.

Franco, S.J., M.A. Rodgers, B.J. Perrin, J. Han, D.A. Bennin, D.R. Critchley, and A. Huttenlocher. 2004. Calpain-mediated proteolysis of talin regulates adhesion dynamics. *Nat Cell Biol*. 6:977-983.

Friedl, P., and K. Wolf. 2010. Plasticity of cell migration: a multiscale tuning model. *J Cell Biol*. 188:11-19.

Geiger, B., J.P. Spatz, and A.D. Bershadsky. 2009. Environmental sensing through focal adhesions. *Nat Rev Mol Cell Biol*. 10:21-33.

Gentry, B.S., S. van der Meulen, P. Noguera, B. Alonso-Latorre, J. Plastino, and G.H. Koenderink. 2012. Multiple actin binding domains of Ena/VASP proteins determine actin network stiffening. *European biophysics journal : EBJ*. 41:979-990.

Giannone, G., B.J. Dubin-Thaler, O. Rossier, Y. Cai, O. Chaga, G. Jiang, W. Beaver, H.G. Dobereiner, Y. Freund, G. Borisy, and M.P. Sheetz. 2007. Lamellipodial actin mechanically links myosin activity with adhesion-site formation. *Cell*. 128:561-575.

Gournier, H., E.D. Goley, H. Niederstrasser, T. Trinh, and M.D. Welch. 2001. Reconstitution of human Arp2/3 complex reveals critical roles of individual subunits in complex structure and activity. *Molecular cell*. 8:1041-1052.

Guo, W.H., and Y.L. Wang. 2012. A three-component mechanism for fibroblast migration with a contractile cell body that couples a myosin II-independent propulsive anterior to a myosin II-dependent resistive tail. *Molecular biology of the cell*. 23:1657-1663.

Hannigan, G.E., C. Leung-Hagesteijn, L. Fitz-Gibbon, M.G. Coppolino, G. Radeva, J. Filmus, J.C. Bell, and S. Dedhar. 1996. Regulation of cell adhesion and anchorage-dependent growth by a new beta 1-integrin-linked protein kinase. *Nature*. 379:91-96.

Hansen, S.D., and R.D. Mullins. 2010. VASP is a processive actin polymerase that requires monomeric actin for barbed end association. *J Cell Biol*. 191:571-584.

Harbeck, B., S. Huttelmaier, K. Schluter, B.M. Jockusch, and S. Illenberger. 2000. Phosphorylation of the vasodilator-stimulated phosphoprotein regulates its interaction with actin. *The Journal of biological chemistry*. 275:30817-30825.

Harris, E.S., T.J. Gauvin, E.G. Heimsath, and H.N. Higgs. 2010. Assembly of filopodia by the formin FRL2 (FMNL3). *Cytoskeleton*. 67:755-772.

Heit, B., and P. Kubes. 2003. Measuring chemotaxis and chemokinesis: the under-agarose cell migration assay. *Science's STKE : signal transduction knowledge environment*. 2003:PL5.

Higgs, H.N., and T.D. Pollard. 2000. Activation by Cdc42 and PIP(2) of Wiskott-Aldrich syndrome protein (WASp) stimulates actin nucleation by Arp2/3 complex. *J Cell Biol*. 150:1311-1320.

Hirata, H., H. Tatsumi, and M. Sokabe. 2008. Mechanical forces facilitate actin polymerization at focal adhesions in a zyxin-dependent manner. *Journal of cell science*. 121:2795-2804.

Hoffman, L.M., C.C. Jensen, A. Chaturvedi, M. Yoshigi, and M.C. Beckerle. 2012. Stretch-induced actin remodeling requires targeting of zyxin to stress fibers and recruitment of actin regulators. *Molecular biology of the cell*. 23:1846-1859.

Hoffman, L.M., C.C. Jensen, S. Kloeker, C.L. Wang, M. Yoshigi, and M.C. Beckerle. 2006. Genetic ablation of zyxin causes Mena/VASP mislocalization, increased motility, and deficits in actin remodeling. *J Cell Biol*. 172:771-782.

Honda, M., K. Takiguchi, S. Ishikawa, and H. Hotani. 1999. Morphogenesis of liposomes encapsulating actin depends on the type of actin-crosslinking. *Journal of molecular biology*. 287:293-300.

Hotulainen, P., and P. Lappalainen. 2006. Stress fibers are generated by two distinct actin assembly mechanisms in motile cells. *J Cell Biol*. 173:383-394.

Huttenlocher, A., and A.R. Horwitz. 2011. Integrins in cell migration. *Cold Spring Harbor perspectives in biology*. 3:a005074.

Huttenlocher, A., S.P. Palecek, Q. Lu, W. Zhang, R.L. Mellgren, D.A. Lauffenburger, M.H. Ginsberg, and A.F. Horwitz. 1997. Regulation of cell migration by the calcium-dependent protease calpain. *The Journal of biological chemistry*. 272:32719-32722.

Ichetovkin, I., W. Grant, and J. Condeelis. 2002. Cofilin produces newly polymerized actin filaments that are preferred for dendritic nucleation by the Arp2/3 complex. *Current biology : CB*. 12:79-84.

Ivarsson, Y. 2012. Plasticity of PDZ domains in ligand recognition and signaling. *FEBS Lett*. 586:2638-2647.

Jing, L., L. Liu, Y.P. Yu, R. Dhir, M. Acquafondada, D. Landsittel, K. Cieply, A. Wells, and J.H. Luo. 2004. Expression of myopodin induces suppression of tumor growth and metastasis. *Am J Pathol*. 164:1799-1806.

Jung, H.S., S. Komatsu, M. Ikebe, and R. Craig. 2008. Head-head and head-tail interaction: a general mechanism for switching off myosin II activity in cells. *Molecular biology of the cell*. 19:3234-3242.

Kachroo, N., and V.J. Gnanapragasam. 2013. The role of treatment modality on the utility of predictive tissue biomarkers in clinical prostate cancer: a systematic review. *Journal of cancer research and clinical oncology*. 139:1-24.

Kaverina, I., and A. Straube. 2011. Regulation of cell migration by dynamic microtubules. *Seminars in cell & developmental biology*. 22:968-974.

Kelleher, J.F., S.J. Atkinson, and T.D. Pollard. 1995. Sequences, structural models, and cellular localization of the actin-related proteins Arp2 and Arp3 from Acanthamoeba. *J Cell Biol*. 131:385-397.

Khaymina, S.S., J.M. Kenney, M.M. Schroeter, and J.M. Chalovich. 2007. Fesselin is a natively unfolded protein. *Journal of proteome research*. 6:3648-3654.

Kim, A.S., L.T. Kakalis, N. Abdul-Manan, G.A. Liu, and M.K. Rosen. 2000. Autoinhibition and activation mechanisms of the Wiskott-Aldrich syndrome protein. *Nature*. 404:151-158.

Kovac, B., J.L. Teo, T.P. Makela, and T. Vallenius. 2012. Assembly of non-contractile dorsal stress fibers requires alpha-actinin-1 and Rac1 in migrating and spreading cells. *Journal of cell science*.

Kozma, R., S. Ahmed, A. Best, and L. Lim. 1995. The Ras-related protein Cdc42Hs and bradykinin promote formation of peripheral actin microspikes and filopodia in Swiss 3T3 fibroblasts. *Mol Cell Biol*. 15:1942-1952.

Krause, M., J.E. Bear, J.J. Loureiro, and F.B. Gertler. 2002. The Ena/VASP enigma. *Journal of cell science*. 115:4721-4726.

Krendel, M., F.T. Zenke, and G.M. Bokoch. 2002. Nucleotide exchange factor GEF-H1 mediates cross-talk between microtubules and the actin cytoskeleton. *Nat Cell Biol*. 4:294-301.

Kuo, J.C., X. Han, C.T. Hsiao, J.R. Yates, 3rd, and C.M. Waterman. 2011. Analysis of the myosin-II-responsive focal adhesion proteome reveals a role for beta-Pix in negative regulation of focal adhesion maturation. *Nat Cell Biol*. 13:383-393.

Kurokawa, K., and M. Matsuda. 2005. Localized RhoA activation as a requirement for the induction of membrane ruffling. *Molecular biology of the cell*. 16:4294-4303.

Lammers, M., S. Meyer, D. Kuhlmann, and A. Wittinghofer. 2008. Specificity of interactions between mDia isoforms and Rho proteins. *The Journal of biological chemistry*. 283:35236-35246.

Lammers, M., R. Rose, A. Scrima, and A. Wittinghofer. 2005. The regulation of mDia1 by autoinhibition and its release by Rho*GTP. *The EMBO journal*. 24:4176-4187.

Langanger, G., M. Moeremans, G. Daneels, A. Sobieszek, M. De Brabander, and J. De Mey. 1986. The molecular organization of myosin in stress fibers of cultured cells. *J Cell Biol*. 102:200-209.

Lappalainen, P., and D.G. Drubin. 1997. Cofilin promotes rapid actin filament turnover in vivo. *Nature*. 388:78-82.

Lebensohn, A.M., and M.W. Kirschner. 2009. Activation of the WAVE complex by coincident signals controls actin assembly. *Molecular cell*. 36:512-524.

Lebrand, C., E.W. Dent, G.A. Strasser, L.M. Lanier, M. Krause, T.M. Svitkina, G.G. Borisy, and F.B. Gertler. 2004. Critical role of Ena/VASP proteins for filopodia formation in neurons and in function downstream of netrin-1. *Neuron*. 42:37-49.

Lee, J.H., T. Katakai, T. Hara, H. Gonda, M. Sugai, and A. Shimizu. 2004. Roles of p-ERM and Rho-ROCK signaling in lymphocyte polarity and uropod formation. *J Cell Biol*. 167:327-337.

Leinweber, B.D., R.S. Fredricksen, D.R. Hoffman, and J.M. Chalovich. 1999. Fesselin: a novel synaptopodin-like actin binding protein from muscle tissue. *Journal of muscle research and cell motility*. 20:539-545.

Liang, J., G. Ke, W. You, Z. Peng, J. Lan, M. Kalesse, A.M. Tartakoff, F. Kaplan, and T. Tao. 2008. Interaction between importin 13 and myopodin suggests a nuclear import pathway for myopodin. *Mol Cell Biochem*. 307:93-100.

Lin, F., Y.P. Yu, J. Woods, K. Cieply, B. Gooding, P. Finkelstein, R. Dhir, D. Krill, M.J. Becich, G. Michalopoulos, S. Finkelstein, and J.H. Luo. 2001. Myopodin, a synaptopodin homologue, is frequently deleted in invasive prostate cancers. *Am J Pathol*. 159:1603-1612.

Linnemann, A., P. Vakeel, E. Bezerra, Z. Orfanos, K. Djinovic-Carugo, P.F. van der Ven, G. Kirfel, and D.O. Furst. 2012. Myopodin is an F-actin bundling protein with multiple independent actin-binding regions. *Journal of muscle research and cell motility*.

Linnemann, A., P.F. van der Ven, P. Vakeel, B. Albinus, D. Simonis, G. Bendas, J.A. Schenk, B. Micheel, R.A. Kley, and D.O. Furst. The sarcomeric Z-disc component myopodin is a multiadapter protein that interacts with filamin and alpha-actinin. *Eur J Cell Biol*. 89:681-692.

Linnemann, A., P.F. van der Ven, P. Vakeel, B. Albinus, D. Simonis, G. Bendas, J.A. Schenk, B. Micheel, R.A. Kley, and D.O. Furst. 2010. The sarcomeric Z-disc component myopodin is a multiadapter protein that interacts with filamin and alpha-actinin. *Eur J Cell Biol*. 89:681-692.

Liu, A.Y. 2000. Differential expression of cell surface molecules in prostate cancer cells. *Cancer Res*. 60:3429-3434.

Liu, Z., and J. Klominek. 2004. Chemotaxis and chemokinesis of malignant mesothelioma cells to multiple growth factors. *Anticancer research*. 24:1625-1630.

Loew, R., N. Heinz, M. Hampf, H. Bujard, and M. Gossen. 2010. Improved Tet-responsive promoters with minimized background expression. *BMC biotechnology*. 10:81.

Machacek, M., L. Hodgson, C. Welch, H. Elliott, O. Pertz, P. Nalbant, A. Abell, G.L. Johnson, K.M. Hahn, and G. Danuser. 2009. Coordination of Rho GTPase activities during cell protrusion. *Nature*. 461:99-103.

Machesky, L.M., and A. Hall. 1997. Role of actin polymerization and adhesion to extracellular matrix in Rac- and Rho-induced cytoskeletal reorganization. *J Cell Biol*. 138:913-926.

Machesky, L.M., R.D. Mullins, H.N. Higgs, D.A. Kaiser, L. Blanchoin, R.C. May, M.E. Hall, and T.D. Pollard. 1999. Scar, a WASp-related protein, activates nucleation of actin filaments by the Arp2/3 complex. *Proceedings of the National Academy of Sciences of the United States of America*. 96:3739-3744.

Maciver, S.K. 1998. How ADF/cofilin depolymerizes actin filaments. *Current opinion in cell biology*. 10:140-144.

Maekawa, M., T. Ishizaki, S. Boku, N. Watanabe, A. Fujita, A. Iwamatsu, T. Obinata, K. Ohashi, K. Mizuno, and S. Narumiya. 1999. Signaling from Rho to the actin cytoskeleton through protein kinases ROCK and LIM-kinase. *Science*. 285:895-898.

McGough, A., B. Pope, W. Chiu, and A. Weeds. 1997. Cofilin changes the twist of F-actin: implications for actin filament dynamics and cellular function. *J Cell Biol*. 138:771-781.

Miki, H., S. Suetsugu, and T. Takenawa. 1998. WAVE, a novel WASP-family protein involved in actin reorganization induced by Rac. *The EMBO journal*. 17:6932-6941.

Millius, A., N. Watanabe, and O.D. Weiner. 2012. Diffusion, capture and recycling of SCAR/WAVE and Arp2/3 complexes observed in cells by single-molecule imaging. *Journal of cell science*. 125:1165-1176.

Minoshima, Y., T. Kawashima, K. Hirose, Y. Tonozuka, A. Kawajiri, Y.C. Bao, X. Deng, M. Tatsuka, S. Narumiya, W.S. May, Jr., T. Nosaka, K. Semba, T. Inoue, T. Satoh, M. Inagaki, and T. Kitamura. 2003. Phosphorylation by aurora B converts MgcRacGAP to a RhoGAP during cytokinesis. *Developmental cell*. 4:549-560.

Mockrin, S.C., and E.D. Korn. 1980. Acanthamoeba profilin interacts with G-actin to increase the rate of exchange of actin-bound adenosine 5'-triphosphate. *Biochemistry*. 19:5359-5362.

Mseka, T., M. Coughlin, and L.P. Cramer. 2009. Graded actin filament polarity is the organization of oriented actomyosin II filament bundles required for fibroblast polarization. *Cell motility and the cytoskeleton*. 66:743-753.

Mseka, T., and L.P. Cramer. 2011. Actin depolymerization-based force retracts the cell rear in polarizing and migrating cells. *Current biology : CB*. 21:2085-2091.

Mullins, R.D., J.A. Heuser, and T.D. Pollard. 1998. The interaction of Arp2/3 complex with actin: nucleation, high affinity pointed end capping, and formation of branching networks of filaments. *Proceedings of the National Academy of Sciences of the United States of America*. 95:6181-6186.

Mundel, P., H.W. Heid, T.M. Mundel, M. Kruger, J. Reiser, and W. Kriz. 1997. Synaptopodin: an actin-associated protein in telencephalic dendrites and renal podocytes. *J Cell Biol*. 139:193-204.

Nakamura, F., T.P. Stossel, and J.H. Hartwig. 2011. The filamins: organizers of cell structure and function. *Cell adhesion & migration*. 5:160-169.

Nakamura, T., K. Kurokawa, E. Kiyokawa, and M. Matsuda. 2006. Analysis of the spatiotemporal activation of rho GTPases using Raichu probes. *Methods in enzymology*. 406:315-332.

Nemethova, M., S. Auinger, and J.V. Small. 2008. Building the actin cytoskeleton: filopodia contribute to the construction of contractile bundles in the lamella. *J Cell Biol*. 180:1233-1244.

Neuhaus, J.M., M. Wanger, T. Keiser, and A. Wegner. 1983. Treadmilling of actin. *Journal of muscle research and cell motility*. 4:507-527.

Nezami, A.G., F. Poy, and M.J. Eck. 2006. Structure of the autoinhibitory switch in formin mDia1. *Structure*. 14:257-263.

Nicholson-Dykstra, S.M., and H.N. Higgs. 2008. Arp2 depletion inhibits sheet-like protrusions but not linear protrusions of fibroblasts and lymphocytes. *Cell motility and the cytoskeleton*. 65:904-922.

Nikolopoulos, S.N., and C.E. Turner. 2001. Integrin-linked kinase (ILK) binding to paxillin LD1 motif regulates ILK localization to focal adhesions. *The Journal of biological chemistry*. 276:23499-23505.

Niwa, R., K. Nagata-Ohashi, M. Takeichi, K. Mizuno, and T. Uemura. 2002. Control of actin reorganization by Slingshot, a family of phosphatases that dephosphorylate ADF/cofilin. *Cell*. 108:233-246.

Nolen, B.J., N. Tomasevic, A. Russell, D.W. Pierce, Z. Jia, C.D. McCormick, J. Hartman, R. Sakowicz, and T.D. Pollard. 2009. Characterization of two classes of small molecule inhibitors of Arp2/3 complex. *Nature*. 460:1031-1034.

Oakes, P.W., Y. Beckham, J. Stricker, and M.L. Gardel. 2012. Tension is required but not sufficient for focal adhesion maturation without a stress fiber template. *J Cell Biol*. 196:363-374.

Otomo, T., D.R. Tomchick, C. Otomo, S.C. Panchal, M. Machius, and M.K. Rosen. 2005. Structural basis of actin filament nucleation and processive capping by a formin homology 2 domain. *Nature*. 433:488-494.

Pankov, R., E. Cukierman, B.Z. Katz, K. Matsumoto, D.C. Lin, S. Lin, C. Hahn, and K.M. Yamada. 2000. Integrin dynamics and matrix assembly: tensin-dependent translocation of alpha(5)beta(1) integrins promotes early fibronectin fibrillogenesis. *J Cell Biol*. 148:1075-1090.

Paterson, H.F., A.J. Self, M.D. Garrett, I. Just, K. Aktories, and A. Hall. 1990. Microinjection of recombinant p21rho induces rapid changes in cell morphology. *J Cell Biol*. 111:1001-1007.

Paul, A.S., and T.D. Pollard. 2008. The role of the FH1 domain and profilin in formin-mediated actin-filament elongation and nucleation. *Current biology : CB*. 18:9-19.

Pavalko, F.M., and K. Burridge. 1991. Disruption of the actin cytoskeleton after microinjection of proteolytic fragments of alpha-actinin. *J Cell Biol*. 114:481-491.

Pelham, R.J., Jr., and Y. Wang. 1997. Cell locomotion and focal adhesions are regulated by substrate flexibility. *Proceedings of the National Academy of Sciences of the United States of America*. 94:13661-13665.

Pellegrin, S., and H. Mellor. 2007. Actin stress fibres. *Journal of cell science*. 120:3491-3499.

Petrie, R.J., and K.M. Yamada. 2013. At the leading edge of three-dimensional cell migration. *Journal of cell science*.

Pham, M., and J.M. Chalovich. 2006. Smooth muscle alpha-actinin binds tightly to fesselin and attenuates its activity toward actin polymerization. *Journal of muscle research and cell motility*. 27:45-51.

Pollitt, A.Y., and R.H. Insall. 2009. WASP and SCAR/WAVE proteins: the drivers of actin assembly. *Journal of cell science*. 122:2575-2578.

Ponti, A., M. Machacek, S.L. Gupton, C.M. Waterman-Storer, and G. Danuser. 2004. Two distinct actin networks drive the protrusion of migrating cells. *Science*. 305:1782-1786.

Pruyne, D., M. Evangelista, C. Yang, E. Bi, S. Zigmond, A. Bretscher, and C. Boone. 2002. Role of formins in actin assembly: nucleation and barbed-end association. *Science*. 297:612-615.

Qualmann, B., and M.M. Kessels. 2009. New players in actin polymerization--WH2-domain-containing actin nucleators. *Trends in cell biology*. 19:276-285.

Quinlan, M.E., J.E. Heuser, E. Kerkhoff, and R.D. Mullins. 2005. Drosophila Spire is an actin nucleation factor. *Nature*. 433:382-388.

Revenu, C., R. Athman, S. Robine, and D. Louvard. 2004. The co-workers of actin filaments: from cell structures to signals. *Nature reviews. Molecular cell biology*. 5:635-646.

Ridley, A.J., and A. Hall. 1992. The small GTP-binding protein rho regulates the assembly of focal adhesions and actin stress fibers in response to growth factors. *Cell*. 70:389-399.

Ridley, A.J., H.F. Paterson, C.L. Johnston, D. Diekmann, and A. Hall. 1992. The small GTP-binding protein rac regulates growth factor-induced membrane ruffling. *Cell*. 70:401-410.

Riedl, J., A.H. Crevenna, K. Kessenbrock, J.H. Yu, D. Neukirchen, M. Bista, F. Bradke, D. Jenne, T.A. Holak, Z. Werb, M. Sixt, and R. Wedlich-Soldner. 2008. Lifeact: a versatile marker to visualize F-actin. *Nature methods*. 5:605-607.

Roca-Cusachs, P., T. Iskratsch, and M.P. Sheetz. 2012. Finding the weakest link: exploring integrin-mediated mechanical molecular pathways. *Journal of cell science*. 125:3025-3038.

Rohatgi, R., L. Ma, H. Miki, M. Lopez, T. Kirchhausen, T. Takenawa, and M.W. Kirschner. 1999. The interaction between N-WASP and the Arp2/3 complex links Cdc42-dependent signals to actin assembly. *Cell*. 97:221-231.

Romero, S., C. Le Clainche, D. Didry, C. Egile, D. Pantaloni, and M.F. Carlier. 2004. Formin is a processive motor that requires profilin to accelerate actin assembly and associated ATP hydrolysis. *Cell*. 119:419-429.

Rose, R., M. Weyand, M. Lammers, T. Ishizaki, M.R. Ahmadian, and A. Wittinghofer. 2005. Structural and mechanistic insights into the interaction between Rho and mammalian Dia. *Nature*. 435:513-518.

Rottner, K., A. Hall, and J.V. Small. 1999. Interplay between Rac and Rho in the control of substrate contact dynamics. *Current biology : CB*. 9:640-648.

Safer, D., M. Elzinga, and V.T. Nachmias. 1991. Thymosin beta 4 and Fx, an actin-sequestering peptide, are indistinguishable. *The Journal of biological chemistry*. 266:4029-4032.

Sahai, E., and C.J. Marshall. 2003. Differing modes of tumour cell invasion have distinct requirements for Rho/ROCK signalling and extracellular proteolysis. *Nat Cell Biol*. 5:711-719.

Sakai, N., J. Chun, J.S. Duffield, T. Wada, A.D. Luster, and A.M. Tager. 2013. LPA1-induced cytoskeleton reorganization drives fibrosis through CTGF-dependent fibroblast proliferation. *FASEB journal : official publication of the Federation of American Societies for Experimental Biology*.

Sanchez-Carbayo, M., K. Schwarz, E. Charytonowicz, C. Cordon-Cardo, and P. Mundel. 2003. Tumor suppressor role for myopodin in bladder cancer: loss of nuclear expression of myopodin is cell-cycle dependent and predicts clinical outcome. *Oncogene*. 22:5298-5305.

Sander, E.E., J.P. ten Klooster, S. van Delft, R.A. van der Kammen, and J.G. Collard. 1999. Rac downregulates Rho activity: reciprocal balance between both GTPases determines cellular morphology and migratory behavior. *J Cell Biol*. 147:1009-1022.

Sarmiento, C., W. Wang, A. Dovas, H. Yamaguchi, M. Sidani, M. El-Sibai, V. Desmarais, H.A. Holman, S. Kitchen, J.M. Backer, A. Alberts, and J. Condeelis. 2008. WASP family members and formin proteins coordinate regulation of cell protrusions in carcinoma cells. *J Cell Biol*. 180:1245-1260.

Schafer, C., S. Born, C. Mohl, S. Houben, N. Kirchgessner, R. Merkel, and B. Hoffmann. 2010. The key feature for early migratory processes: Dependence of adhesion, actin bundles, force generation and transmission on filopodia. *Cell adhesion & migration*. 4:215-225.

Schmoller, K.M., O. Lieleg, and A.R. Bausch. 2009. Structural and viscoelastic properties of actin/filamin networks: cross-linked versus bundled networks. *Biophysical journal*. 97:83-89.

Schonichen, A., and M. Geyer. 2010. Fifteen formins for an actin filament: a molecular view on the regulation of human formins. *Biochimica et biophysica acta*. 1803:152-163.

Schroder, F.H., J. Hugosson, M.J. Roobol, T.L. Tammela, S. Ciatto, V. Nelen, M. Kwiatkowski, M. Lujan, H. Lilja, M. Zappa, L.J. Denis, F. Recker, A. Berenguer, L. Maattanen, C.H. Bangma, G. Aus, A. Villers, X. Rebillard, T. van der Kwast, B.G. Blijenberg, S.M. Moss, H.J. de Koning, A. Auvinen, and E. Investigators. 2009. Screening and prostate-cancer mortality in a randomized European study. *N Engl J Med*. 360:1320-1328.

Schroeter, M., and J.M. Chalovich. 2004. Ca2+-calmodulin regulates fesselin-induced actin polymerization. *Biochemistry*. 43:13875-13882.

Schroeter, M.M., B. Beall, H.W. Heid, and J.M. Chalovich. 2008. The actin binding protein, fesselin, is a member of the synaptopodin family. *Biochem Biophys Res Commun*. 371:582-586.

Schroeter, M.M., and J.M. Chalovich. 2005. Fesselin binds to actin and myosin and inhibits actin-activated ATPase activity. *Journal of muscle research and cell motility*. 26:183-189.

Schultheiss, T., J. Choi, Z.X. Lin, C. DiLullo, L. Cohen-Gould, D. Fischman, and H. Holtzer. 1992. A sarcomeric alpha-actinin truncated at the carboxyl end induces the breakdown of stress fibers in PtK2 cells and the formation of nemaline-like bodies and breakdown of myofibrils in myotubes. *Proceedings of the National Academy of Sciences of the United States of America*. 89:9282-9286.

Sellers, J.R., E. Eisenberg, and R.S. Adelstein. 1982. The binding of smooth muscle heavy meromyosin to actin in the presence of ATP. Effect of phosphorylation. *The Journal of biological chemistry*. 257:13880-13883.

Shutova, M., C. Yang, J.M. Vasiliev, and T. Svitkina. 2012. Functions of nonmuscle myosin II in assembly of the cellular contractile system. *PloS one*. 7:e40814.

Simpson, K.J., A.S. Dugan, and A.M. Mercurio. 2004. Functional analysis of the contribution of RhoA and RhoC GTPases to invasive breast carcinoma. *Cancer Res*. 64:8694-8701.

Small, J.V. 1981. Organization of actin in the leading edge of cultured cells: influence of osmium tetroxide and dehydration on the ultrastructure of actin meshworks. *J Cell Biol*. 91:695-705.

Small, J.V., and G.P. Resch. 2005. The comings and goings of actin: coupling protrusion and retraction in cell motility. *Current opinion in cell biology*. 17:517-523.

Small, J.V., T. Stradal, E. Vignal, and K. Rottner. 2002. The lamellipodium: where motility begins. *Trends in cell biology*. 12:112-120.

Smith, A., M. Bracke, B. Leitinger, J.C. Porter, and N. Hogg. 2003. LFA-1-induced T cell migration on ICAM-1 involves regulation of MLCK-mediated attachment and ROCK-dependent detachment. *Journal of cell science*. 116:3123-3133.

Sousa, A.D., and R.E. Cheney. 2005. Myosin-X: a molecular motor at the cell's fingertips. *Trends in cell biology*. 15:533-539.

Spillane, M., A. Ketschek, S.L. Jones, F. Korobova, B. Marsick, L. Lanier, T. Svitkina, and G. Gallo. 2011. The actin nucleating Arp2/3 complex contributes to the formation of axonal filopodia and branches through the regulation of actin patch precursors to filopodia. *Developmental neurobiology*. 71:747-758.

Steffen, A., J. Faix, G.P. Resch, J. Linkner, J. Wehland, J.V. Small, K. Rottner, and T.E. Stradal. 2006. Filopodia formation in the absence of functional WAVE- and Arp2/3-complexes. *Molecular biology of the cell*. 17:2581-2591.

Steffen, A., K. Rottner, J. Ehinger, M. Innocenti, G. Scita, J. Wehland, and T.E. Stradal. 2004. Sra-1 and Nap1 link Rac to actin assembly driving lamellipodia formation. *The EMBO journal*. 23:749-759.

Stokes, D.L., and D.J. DeRosier. 1991. Growth conditions control the size and order of actin bundles in vitro. *Biophysical journal*. 59:456-465.

Stone, K.R., D.D. Mickey, H. Wunderli, G.H. Mickey, and D.F. Paulson. 1978. Isolation of a human prostate carcinoma cell line (DU 145). *International journal of cancer. Journal international du cancer*. 21:274-281.

Takenawa, T., and S. Suetsugu. 2007. The WASP-WAVE protein network: connecting the membrane to the cytoskeleton. *Nature reviews. Molecular cell biology*. 8:37-48.

Thierry-Mieg, D., and J. Thierry-Mieg. 2006. AceView: a comprehensive cDNA-supported gene and transcripts annotation. *Genome biology*. 7 Suppl 1:S12 11-14.

Tojkander, S., G. Gateva, and P. Lappalainen. 2012. Actin stress fibers--assembly, dynamics and biological roles. *Journal of cell science*. 125:1855-1864.

Tojkander, S., G. Gateva, G. Schevzov, P. Hotulainen, P. Naumanen, C. Martin, P.W. Gunning, and P. Lappalainen. 2011. A molecular pathway for myosin II recruitment to stress fibers. *Current biology : CB*. 21:539-550.

Tu, Y., Y. Huang, Y. Zhang, Y. Hua, and C. Wu. 2001. A new focal adhesion protein that interacts with integrin-linked kinase and regulates cell adhesion and spreading. *J Cell Biol*. 153:585-598.

Umemoto, S., A.R. Bengur, and J.R. Sellers. 1989. Effect of multiple phosphorylations of smooth muscle and cytoplasmic myosins on movement in an in vitro motility assay. *The Journal of biological chemistry*. 264:1431-1436.

Van Aelst, L., and C. D'Souza-Schorey. 1997. Rho GTPases and signaling networks. *Genes & development*. 11:2295-2322.

Van Impe, K., V. De Corte, L. Eichinger, E. Bruyneel, M. Mareel, J. Vandekerckhove, and J. Gettemans. 2003. The Nucleo-cytoplasmic actin-binding protein CapG lacks a nuclear export sequence present in structurally related proteins. *J Biol Chem*. 278:17945-17952.

Vega, F.M., and A.J. Ridley. 2008. Rho GTPases in cancer cell biology. *FEBS Lett*. 582:2093-2101.

Vicente-Manzanares, M., X. Ma, R.S. Adelstein, and A.R. Horwitz. 2009. Non-muscle myosin II takes centre stage in cell adhesion and migration. *Nature reviews. Molecular cell biology*. 10:778-790.

Vicente-Manzanares, M., J. Zareno, L. Whitmore, C.K. Choi, and A.F. Horwitz. 2007. Regulation of protrusion, adhesion dynamics, and polarity by myosins IIA and IIB in migrating cells. *J Cell Biol*. 176:573-580.

Vignjevic, D., S. Kojima, Y. Aratyn, O. Danciu, T. Svitkina, and G.G. Borisy. 2006. Role of fascin in filopodial protrusion. *J Cell Biol*. 174:863-875.

Watanabe, N., T. Kato, A. Fujita, T. Ishizaki, and S. Narumiya. 1999. Cooperation between mDia1 and ROCK in Rho-induced actin reorganization. *Nat Cell Biol*. 1:136-143.

Wear, M.A., A. Yamashita, K. Kim, Y. Maeda, and J.A. Cooper. 2003. How capping protein binds the barbed end of the actin filament. *Current biology : CB*. 13:1531-1537.

Weber, K., and U. Groeschel-Stewart. 1974. Antibody to myosin: the specific visualization of myosin-containing filaments in nonmuscle cells. *Proceedings of the National Academy of Sciences of the United States of America*. 71:4561-4564.

Wegner, A. 1976. Head to tail polymerization of actin. *Journal of molecular biology*. 108:139-150.

Wehrle-Haller, B. 2012. Structure and function of focal adhesions. *Current opinion in cell biology*. 24:116-124.

Weins, A., K. Schwarz, C. Faul, L. Barisoni, W.A. Linke, and P. Mundel. 2001. Differentiation- and stress-dependent nuclear cytoplasmic redistribution of myopodin, a novel actin-bundling protein. *J Cell Biol*. 155:393-404.

Wells, A. 2000. Tumor invasion: role of growth factor-induced cell motility. *Adv Cancer Res*. 78:31-101.

Wilt, T.J., M.K. Brawer, K.M. Jones, M.J. Barry, W.J. Aronson, S. Fox, J.R. Gingrich, J.T. Wei, P. Gilhooly, B.M. Grob, I. Nsouli, P. Iyer, R. Cartagena, G. Snider, C. Roehrborn, R. Sharifi, W. Blank, P. Pandya, G.L. Andriole, D. Culkin, T. Wheeler, and G. Prostate Cancer Intervention versus Observation Trial Study. 2012. Radical prostatectomy versus observation for localized prostate cancer. *N Engl J Med*. 367:203-213.

Wong, J.S., E. Iorns, M.N. Rheault, T.M. Ward, P. Rashmi, U. Weber, M.E. Lippman, C. Faul, M. Mlodzik, and P. Mundel. 2012. Rescue of tropomyosin deficiency in Drosophila and human cancer cells by synaptopodin reveals a role of tropomyosin alpha in RhoA stabilization. *The EMBO journal*. 31:1028-1040.

Worthylake, R.A., and K. Burridge. 2003. RhoA and ROCK promote migration by limiting membrane protrusions. *The Journal of biological chemistry*. 278:13578-13584.

Worthylake, R.A., S. Lemoine, J.M. Watson, and K. Burridge. 2001. RhoA is required for monocyte tail retraction during transendothelial migration. *J Cell Biol*. 154:147-160.

Wu, C., and S. Dedhar. 2001. Integrin-linked kinase (ILK) and its interactors: a new paradigm for the coupling of extracellular matrix to actin cytoskeleton and signaling complexes. *J Cell Biol*. 155:505-510.

Xu, Y., J.B. Moseley, I. Sagot, F. Poy, D. Pellman, B.L. Goode, and M.J. Eck. 2004. Crystal structures of a Formin Homology-2 domain reveal a tethered dimer architecture. *Cell*. 116:711-723.

Yam, P.T., C.A. Wilson, L. Ji, B. Hebert, E.L. Barnhart, N.A. Dye, P.W. Wiseman, G. Danuser, and J.A. Theriot. 2007. Actin-myosin network reorganization breaks symmetry at the cell rear to spontaneously initiate polarized cell motility. *J Cell Biol*. 178:1207-1221.

Yamashiro-Matsumura, S., and F. Matsumura. 1986. Intracellular localization of the 55-kD actin-bundling protein in cultured cells: spatial relationships with actin, alpha-actinin, tropomyosin, and fimbrin. *J Cell Biol*. 103:631-640.

Yanagida-Asanuma, E., K. Asanuma, K. Kim, M. Donnelly, H. Young Choi, J. Hyung Chang, S. Suetsugu, Y. Tomino, T. Takenawa, C. Faul, and P. Mundel. 2007. Synaptopodin protects against proteinuria by disrupting Cdc42:IRSp53:Mena signaling complexes in kidney podocytes. *Am J Pathol*. 171:415-427.

Yang, C., L. Czech, S. Gerboth, S. Kojima, G. Scita, and T. Svitkina. 2007. Novel roles of formin mDia2 in lamellipodia and filopodia formation in motile cells. *PLoS biology*. 5:e317.

Yang, C., and T. Svitkina. 2011. Filopodia initiation: focus on the Arp2/3 complex and formins. *Cell adhesion & migration*. 5:402-408.

Yang, N., O. Higuchi, K. Ohashi, K. Nagata, A. Wada, K. Kangawa, E. Nishida, and K. Mizuno. 1998. Cofilin phosphorylation by LIM-kinase 1 and its role in Rac-mediated actin reorganization. *Nature*. 393:809-812.

Yoshigi, M., L.M. Hoffman, C.C. Jensen, H.J. Yost, and M.C. Beckerle. 2005. Mechanical force mobilizes zyxin from focal adhesions to actin filaments and regulates cytoskeletal reinforcement. *J Cell Biol*. 171:209-215.

Yoshizaki, H., Y. Ohba, K. Kurokawa, R.E. Itoh, T. Nakamura, N. Mochizuki, K. Nagashima, and M. Matsuda. 2003. Activity of Rho-family GTPases during cell division as visualized with FRET-based probes. *J Cell Biol*. 162:223-232.

Yu, Y.P., and J.H. Luo. 2006. Myopodin-mediated suppression of prostate cancer cell migration involves interaction with zyxin. *Cancer Res*. 66:7414-7419.

Yu, Y.P., and J.H. Luo. 2011. Phosphorylation and interaction of myopodin by integrin-link kinase lead to suppression of cell growth and motility in prostate cancer cells. *Oncogene*. 30:4855-4863.

Yu, Y.P., G.C. Tseng, and J.H. Luo. 2006. Inactivation of myopodin expression associated with prostate cancer relapse. *Urology*. 68:578-582.

Zaidel-Bar, R., C. Ballestrem, Z. Kam, and B. Geiger. 2003. Early molecular events in the assembly of matrix adhesions at the leading edge of migrating cells. *Journal of cell science*. 116:4605-4613.

Zenke, F.T., M. Krendel, C. DerMardirossian, C.C. King, B.P. Bohl, and G.M. Bokoch. 2004. p21-activated kinase 1 phosphorylates and regulates 14-3-3 binding to GEF-H1, a microtubule-localized Rho exchange factor. *The Journal of biological chemistry*. 279:18392-18400.

Zhang, Y., K. Chen, Y. Tu, A. Velyvis, Y. Yang, J. Qin, and C. Wu. 2002. Assembly of the PINCH-ILK-CH-ILKBP complex precedes and is essential for localization of each component to cell-matrix adhesion sites. *Journal of cell science*. 115:4777-4786.

APPENDIX A: LETTER OF COPYRIGHT PERMISSION

OXFORD UNIVERSITY PRESS LICENSE
TERMS AND CONDITIONS

Feb 28, 2013

This is a License Agreement between FuiBoon Kai ("You") and Oxford University Press ("Oxford University Press") provided by Copyright Clearance Center ("CCC"). The license consists of your order details, the terms and conditions provided by Oxford University Press, and the payment terms and conditions.

All payments must be made in full to CCC. For payment instructions, please see information listed at the bottom of this form.

License Number	3097770859089
License date	Feb 28, 2013
Licensed content publisher	Oxford University Press
Licensed content publication	Carcinogenesis
Licensed content title	Myopodin isoforms alter the chemokinetic response of PC3 cells in response to different migration stimuli via differential effects on Rho-ROCK signaling pathways:
Licensed content author	FuiBoon Kai, Kaitlyn Tanner, Caroline King, Roy Duncan
Licensed content date	11/01/2012
Type of Use	Thesis/Dissertation
Institution name	
Title of your work	ROLES OF MYOPODIN IN ACTIN CYTOSKELETON REMODELING AND CANCER CELL MIGRATION
Publisher of your work	n/a
Expected publication date	Mar 2013
Permissions cost	0.00 USD
Value added tax	0.00 USD
Total	0.00 USD
Total	0.00 USD
Terms and Conditions	

STANDARD TERMS AND CONDITIONS FOR REPRODUCTION OF MATERIAL FROM AN OXFORD UNIVERSITY PRESS JOURNAL

1. Use of the material is restricted to the type of use specified in your order details.

2. This permission covers the use of the material in the English language in the following territory: world. If you have requested additional permission to translate this material, the terms and conditions of this reuse will be set out in clause 12.

3. This permission is limited to the particular use authorized in (1) above and does not allow you to sanction its use elsewhere in any other format other than specified above, nor does it

apply to quotations, images, artistic works etc that have been reproduced from other sources which may be part of the material to be used.

4. No alteration, omission or addition is made to the material without our written consent. Permission must be re-cleared with Oxford University Press if/when you decide to reprint.

5. The following credit line appears wherever the material is used: author, title, journal, year, volume, issue number, pagination, by permission of Oxford University Press or the sponsoring society if the journal is a society journal. Where a journal is being published on behalf of a learned society, the details of that society must be included in the credit line.

6. For the reproduction of a full article from an Oxford University Press journal for whatever purpose, the corresponding author of the material concerned should be informed of the proposed use. Contact details for the corresponding authors of all Oxford University Press journal contact can be found alongside either the abstract or full text of the article concerned, accessible from www.oxfordjournals.org Should there be a problem clearing these rights, please contact journals.permissions@oxfordjournals.org

7. If the credit line or acknowledgement in our publication indicates that any of the figures, images or photos was reproduced, drawn or modified from an earlier source it will be necessary for you to clear this permission with the original publisher as well. If this permission has not been obtained, please note that this material cannot be included in your publication/photocopies.

8. While you may exercise the rights licensed immediately upon issuance of the license at the end of the licensing process for the transaction, provided that you have disclosed complete and accurate details of your proposed use, no license is finally effective unless and until full payment is received from you (either by Oxford University Press or by Copyright Clearance Center (CCC)) as provided in CCC's Billing and Payment terms and conditions. If full payment is not received on a timely basis, then any license preliminarily granted shall be deemed automatically revoked and shall be void as if never granted. Further, in the event that you breach any of these terms and conditions or any of CCC's Billing and Payment terms and conditions, the license is automatically revoked and shall be void as if never granted. Use of materials as described in a revoked license, as well as any use of the materials beyond the scope of an unrevoked license, may constitute copyright infringement and Oxford University Press reserves the right to take any and all action to protect its copyright in the materials.

9. This license is personal to you and may not be sublicensed, assigned or transferred by you to any other person without Oxford University Press's written permission.

10. Oxford University Press reserves all rights not specifically granted in the combination of (i) the license details provided by you and accepted in the course of this licensing transaction, (ii) these terms and conditions and (iii) CCC's Billing and Payment terms and conditions.

11. You hereby indemnify and agree to hold harmless Oxford University Press and CCC, and their respective officers, directors, employs and agents, from and against any and all claims arising out of your use of the licensed material other than as specifically authorized pursuant to this license.

12. Other Terms and Conditions:

v1.4

If you would like to pay for this license now, please remit this license along with your payment made payable to "COPYRIGHT CLEARANCE CENTER" otherwise you will be invoiced within 48 hours of the license date. Payment should be in the form of a check or money order referencing your account number and this invoice number RLNK500967334.
Once you receive your invoice for this order, you may pay your invoice by credit card. Please follow instructions provided at that time.

Make Payment To:
Copyright Clearance Center
Dept 001
P.O. Box 843006
Boston, MA 02284-3006

For suggestions or comments regarding this order, contact RightsLink Customer Support: customercare@copyright.com or +1-877-622-5543 (toll free in the US) or +1-978-646-2777.

Gratis licenses (referencing $0 in the Total field) are free. Please retain this printable license for your reference. No payment is required.

NATURE PUBLISHING GROUP LICENSE
TERMS AND CONDITIONS

Feb 28, 2013

This is a License Agreement between FuiBoon Kai ("You") and Nature Publishing Group ("Nature Publishing Group") provided by Copyright Clearance Center ("CCC"). The license consists of your order details, the terms and conditions provided by Nature Publishing Group, and the payment terms and conditions.

All payments must be made in full to CCC. For payment instructions, please see information listed at the bottom of this form.

License Number	3097780101698
License date	Feb 28, 2013
Licensed content publisher	Nature Publishing Group
Licensed content publication	Nature Reviews Molecular Cell Biology
Licensed content title	Non-muscle myosin II takes centre stage in cell adhesion and migration
Licensed content author	Miguel Vicente-Manzanares, Xuefei Ma, Robert S. Adelstein and Alan Rick Horwitz
Licensed content date	Nov 1, 2009
Volume number	10
Issue number	11
Type of Use	reuse in a thesis/dissertation
Requestor type	academic/educational
Format	print and electronic
Portion	figures/tables/illustrations
Number of figures/tables/illustrations	1
High-res required	no
Figures	Figure 1: Domain structure of NM II
Author of this NPG article	no
Your reference number	
Title of your thesis / dissertation	ROLES OF MYOPODIN IN ACTIN CYTOSKELETON REMODELING AND CANCER CELL MIGRATION
Expected completion date	Mar 2013
Estimated size (number of pages)	180
Total	0.00 USD
Terms and Conditions	

Terms and Conditions for Permissions

Nature Publishing Group hereby grants you a non-exclusive license to reproduce this material for this purpose, and for no other use, subject to the conditions below:

1. NPG warrants that it has, to the best of its knowledge, the rights to license reuse of this material. However, you should ensure that the material you are requesting is original to Nature Publishing Group and does not carry the copyright of another entity (as credited in the published version). If the credit line on any part of the material you have requested indicates that it was reprinted or adapted by NPG with permission from another source, then you should also seek permission from that source to reuse the material.

2. Permission granted free of charge for material in print is also usually granted for any electronic version of that work, provided that the material is incidental to the work as a whole and that the electronic version is essentially equivalent to, or substitutes for, the print version. Where print permission has been granted for a fee, separate permission must be obtained for any additional, electronic re-use (unless, as in the case of a full paper, this has already been accounted for during your initial request in the calculation of a print run). NB: In all cases, web-based use of full-text articles must be authorized separately through the 'Use on a Web Site' option when requesting permission.

3. Permission granted for a first edition does not apply to second and subsequent editions and for editions in other languages (except for signatories to the STM Permissions Guidelines, or where the first edition permission was granted for free).

4. Nature Publishing Group's permission must be acknowledged next to the figure, table or abstract in print. In electronic form, this acknowledgement must be visible at the same time as the figure/table/abstract, and must be hyperlinked to the journal's homepage.

5. The credit line should read:
   Reprinted by permission from Macmillan Publishers Ltd: [JOURNAL NAME] (reference citation), copyright (year of publication)
   For AOP papers, the credit line should read:
   Reprinted by permission from Macmillan Publishers Ltd: [JOURNAL NAME], advance online publication, day month year (doi: 10.1038/sj.[JOURNAL ACRONYM].XXXXX)

   Note: For republication from the *British Journal of Cancer*, the following credit lines apply.
   Reprinted by permission from Macmillan Publishers Ltd on behalf of Cancer Research UK: [JOURNAL NAME] (reference citation), copyright (year of publication) For AOP papers, the credit line should read:
   Reprinted by permission from Macmillan Publishers Ltd on behalf of Cancer Research UK: [JOURNAL NAME], advance online publication, day month year (doi: 10.1038/sj.[JOURNAL ACRONYM].XXXXX)

6. Adaptations of single figures do not require NPG approval. However, the adaptation

should be credited as follows:

Adapted by permission from Macmillan Publishers Ltd: [JOURNAL NAME] (reference citation), copyright (year of publication)

Note: For adaptation from the *British Journal of Cancer*, the following credit line applies.
Adapted by permission from Macmillan Publishers Ltd on behalf of Cancer Research UK: [JOURNAL NAME] (reference citation), copyright (year of publication)

7. Translations of 401 words up to a whole article require NPG approval. Please visit http://www.macmillanmedicalcommunications.com for more information.
Translations of up to a 400 words do not require NPG approval. The translation should be credited as follows:

Translated by permission from Macmillan Publishers Ltd: [JOURNAL NAME] (reference citation), copyright (year of publication).

Note: For translation from the *British Journal of Cancer*, the following credit line applies.
Translated by permission from Macmillan Publishers Ltd on behalf of Cancer Research UK: [JOURNAL NAME] (reference citation), copyright (year of publication)

We are certain that all parties will benefit from this agreement and wish you the best in the use of this material. Thank you.

Special Terms:

v1.1

If you would like to pay for this license now, please remit this license along with your payment made payable to "COPYRIGHT CLEARANCE CENTER" otherwise you will be invoiced within 48 hours of the license date. Payment should be in the form of a check or money order referencing your account number and this invoice number RLNK500967346.
Once you receive your invoice for this order, you may pay your invoice by credit card. Please follow instructions provided at that time.

Make Payment To:
Copyright Clearance Center
Dept 001
P.O. Box 843006
Boston, MA 02284-3006

For suggestions or comments regarding this order, contact RightsLink Customer Support: customercare@copyright.com or +1-877-622-5543 (toll free in the US) or +1-978-646-2777.

Gratis licenses (referencing $0 in the Total field) are free. Please retain this printable license for your reference. No payment is required.
